SOIL-STRUCTURE INTERACTION AND IMPERFECT TRENCH INSTALLATIONS

AS APPLIED TO DEEPLY BURIED CONDUITS

Except where reference is made to the work of others, the work described in this dissertation is my own or was done in collaboration with my advisory committee. This dissertation does not include proprietary or classified information.

_____

Junsuk Kang

Certificate of Approval:

_____	_____
J. Michael Stallings Professor Civil Engineering	Chai H. Yoo, Chair Professor Civil Engineering
_____	_____
Frazier Parker Professor Civil Engineering	George T. Flowers Interim Dean Graduate School

SOIL-STRUCTURE INTERACTION AND IMPERFECT TRENCH INSTALLATIONS AS APPLIED TO DEEPLY BURIED CONDUITS

Junsuk Kang

A Dissertation

Submitted to

the Graduate Faculty of

Auburn University

in Partial Fulfillment of the

Requirements for the

Degree of

Doctor of Philosophy

Auburn, Alabama
May 10, 2007

SOIL-STRUCTURE INTERACTION AND IMPERFECT TRENCH INSTALLATIONS

AS APPLIED TO DEEPLY BURIED CONDUITS

Junsuk Kang

Permission is granted to Auburn University to make copies of this dissertation at its discretion, upon request of individuals or institutions and at their expense. The author reserves all publication rights.

_____
Signature of Author

_____
Date of Graduation

VITA

Junsuk Kang, son of Taehee Kang and Heeja Kang (Park), was born on July 25, 1972, in Seoul, Korea. He graduated from Hanyoung High School in Seoul, Korea in 1991. In March 1991 he entered Korea University and received the degree of Bachelor of Science (Civil and Environmental Engineering) in February 1998. He served as a military engineer in the Korean Army from January 1994 to March 1996. He entered graduate studies at Korea University in March 1998 and received the degree of Master of Science (Civil and Environmental Engineering) in February 2000. He was then employed as a Planning Engineer by Hyundai Engineering & Construction Company in Seoul, Korea. He came as a graduate student to Auburn University, Alabama, in pursuit of the degree of Doctor of Philosophy in August 2003.

DISSERTATION ABSTRACT

SOIL-STRUCTURE INTERACTION AND IMPERFECT TRENCH INSTALLATIONS AS APPLIED TO DEEPLY BURIED CONDUITS

Junsuk Kang

Doctor of Philosophy, May 10, 2007
(M.S., Korea University, 2000)
(B. S., Korea University, 1998)

228 Typed Pages

Directed by Chai H. Yoo

The imperfect trench installation method is used to reduce earth pressure on deeply buried conduits. Few quantitative refinements to the imperfect trench installation method, however, have been added since the fundamental mechanics of the reverse arching action was proposed by Marston and Spangler. There have been limited research results published regarding primarily qualitative aspects of earth load reduction for imperfect trench conditions. It was found during the course of this study that significant frictional forces develop along the sidewalls of buried conduits and adjacent sidefills in imperfect trench installations. Current American Association of State Highway and

Transportation Officials provisions do not consider these frictional forces, but they cannot be neglected in imperfect trench installations as their effect is dominant.

The objectives of this study were to study the soil-structure interaction for deeply buried roadway conduits (concrete pipes, corrugated polyvinyl chloride (PVC) pipes, corrugated steel pipes, and box culverts) and the efficiency of the imperfect trench method for their installations. This research identifies variables that significantly affect earth loads, as well as the effects of bedding and sidefill treatments. The soil-structure interaction was computed using the finite element method with soil response simulated with the Duncan soil model and Selig soil parameters. The geometry of the soft material zone that induces the reverse arching action was optimized to maximize the earth load reduction for imperfect trench installations. The optimization process was based on parametric studies of the geometry and location of the soft material zone, combined with bedding and sidefill treatments. Predictor equations for earth load, maximum wall stress, and deflection of the conduits were formulated that incorporate the proposed optimum soft material zone geometry and installation techniques. Parametric studies revealed that the optimum geometry of the soft material zone in the proposed imperfect trench installations could reduce the maximum wall stress or vertical earth load by 69-85%.

ACKNOWLEDGMENTS

The author is grateful for the financial support provided by the Alabama Department of Transportation Project No. 930-592, the Huff Eminent Scholar Fund, and the Highway Research Center, Auburn University. The author would like to thank his Advisory Committee, particularly Dr. Chai H. Yoo, for providing primary ideas and methodologies for this research.

Special thanks are due to all of his family members who have made all sacrifices for his study. Their great love and prayer were essential for him to complete this long and arduous study.

And the greatest thanks are due to my God for His salvation in my Lord Jesus Christ. May this study be to His glory.

Style manual or journal used: Journal of Geotechnical and Geoenvironmental Engineering, ASCE

Computer software used: ABAQUS version 6.4; AutoCAD 2000; CANDE-89; MAPLE 8; MathType 2002; Microsoft Excel 2003; Microsoft Word 2003; MSC/NASTRAN 2005; SPIDA

TABLE OF CONTENTS

LIST OF TABLES xiii

LIST OF FIGURES xiv

CHAPTER 1. INTRODUCTION 1

1.1 Objectives and Scope 5

1.2 Organization 7

CHAPTER 2. LITERATURE REVIEW 9

2.1 Introduction 9

2.2 Imperfect Trench Installation 14

CHAPTER 3. SOIL-STRUCTURE MODELING 20

3.1 Introduction 20

3.2 Soil Models and Parameters 22
3.2.1 Duncan Soil Model and Parameters 22
3.2.2 Selig Bulk Modulus and Parameters 33

3.3 Finite Element Modeling 35
3.3.1 Modeling Techniques 35
3.3.2 Verification of Modeling Techniques 39

CHAPTER 4. SOIL-STRUCTURE INTERACTION FOR DEEPLY BURIED CONCRETE ROUND PIPES 50

4.1 Introduction 50

4.2 Background 51

4.3 Soil-Structure Interaction 54

4.3.1 Effects of Bedding and Sidefill Treatment 54
4.3.2 Arching Factors 56

4.4 Imperfect Trench Installation 59

4.5 Predictor Equations 64

4.6 Displacement of Soft Material Zone 66

CHAPTER 5. SOIL-STRUCTURE INTERACTION FOR BURIED CORRUGATED PVC PIPES 68

5.1 Introduction 68

5.2 Background 70
5.2.1 Vertical Arching Factors 70
5.2.2 Deflections 72

5.3 Soil-Structure Interaction 74
5.3.1 Corrugated PVC Pipe versus Concrete Pipe 74
5.3.2 Finite Element Modeling 74
5.3.3 Effects of Sidefill Material Properties 75
5.3.4 Effects of Interface Conditions and Time-Dependent Properties 77

5.4 Imperfect Trench Installation 80
5.4.1 Optimization of Soft Zone Geometry 80
5.4.2 Imperfect Trench Installation versus Embankment Installation 84

5.5 Predictor Equations 89
5.5.1 Arching Factor, Deflection, and Maximum Wall Stress 89
5.5.2 Reduction Rates 92

CHAPTER 6. SOIL-STRUCTURE INTERACTION FOR BURIED CORRUGATED STEEL PIPES 97

6.1 Introduction 97

6.2 Background 100
6.2.1 Vertical Arching Factors 100
6.2.2 Deflections 100
6.2.3 Buckling 101

6.3 Soil-Structure Interaction 102
6.3.1 Finite Element Modeling 102
6.3.2 Effects of Sidefill Material Properties 102

6.3.3 Effects of Interface Conditions 104

6.4 Buckling Analyses 107

6.5 Imperfect Trench Installation 110
6.5.1 Optimization of Soft Zone Geometry 110
6.5.2 Imperfect Trench Installation versus Embankment Installation 114

6.6 Predictor Equations 120
6.6.1 Arching Factor, Deflection, and Maximum Wall Stress 120
6.6.2 Reduction Rates 123

CHAPTER 7. SOIL-STRUCTURE INTERACTION FOR BURIED BOX CULVERTS 128

7.1 Introduction 128

7.2 Background 129

7.3 Soil-Structure Interaction 131
7.3.1 Effects of Foundation Stiffness, Sidefill Treatment, and Interface Condition 131
7.3.2 Soil-Structure Interaction Factors 134

7.4 Imperfect Trench Installation 139
7.4.1 Effects of Soft Zone Geometry and Interface Conditions 139
7.4.2 Predictor Equations 143
7.4.3 Height of Soft Zone 148

CHAPTER 8. SUMMARY AND CONCLUSIONS 150

8.1 Summary and Conclusions 150

8.2 Recommendations for Future Study 155

REFERENCES 156

APPENDICES 165

APPENDIX 1. MARSTON AND SPANGLER'S THEORY 166

APPENDIX 2. TYPICAL INPUT FOR SPIDA 176

APPENDIX 3. TYPICAL INPUT FOR CANDE-89 192

APPENDIX 4. SURVEY RESULTS 196

APPENDIX 5. SPECIAL HIGHWAY DRAWINGS OF ALDOT PROJECT 930-592 199

APPENDIX 6. SPECIAL HIGHWAY DRAWING OF HIGHWAY RESEARCH CENTER, AUBURN UNIVERSITY 202

APPENDIX 7. VERTICAL STRESS DISTRIBUTIONS OF SOIL ABOVE THE STRUCTURE 204

LIST OF TABLES

Table 2.1. Standard Embankment Installation Soils and Minimum Compaction Requirements (AASHTO LRFD 2004a) 12
Table 3.1. Summary of the hyperbolic parameters 30
Table A1.1. Values of C_c in terms of H/B_c 170
Table A1.2. Design values of settlement ratio 170

LIST OF FIGURES

Fig. 1.1. Pressure transfer within a soil-structure system: (a) embankment installation; (b) trench installation; and (c) imperfect trench installation (F_v = generated friction forces or shear stresses)..... 3
Fig. 2.2. AASHTO standard embankment installations (AASHTO LRFD 2004a)..... 11
Fig. 2.3. Various types of conduit installations 13
Fig. 2.4. Mechanism of imperfect trench installation 15
Fig. 3.1. Hyperbolic stress-strain curve 24
Fig. 3.2. Transformed hyperbolic stress-strain curve 24
Fig. 3.3. Hyperbolic axial strain-radial strain curve 28
Fig. 3.4. Transformed hyperbolic axial strain-radial strain curve..... 28
Fig. 3.5. Hydrostatic compression test..... 34
Fig. 3.6. Linear transformation of hyperbola for bulk modulus 34
Fig. 3.7. Schematic finite element model: (a) embankment installation and (b) imperfect trench installation (B_c = width of the pipe; t = pipe wall thickness)..... 36
Fig. 3.8. Comparison of radial pressure distributions in AASHTO standard embankment installation (parameters: inside diameter of pipe= 1.8 m; backfill height= 6 m; sidefill= AASHTO type 3)..... 42
Fig. 3.9. Finite element modeling versus field test by the Ohio Research Institute for Transportation and Environment (ORITE): (a) verification of modeling techniques and (b) effects of interface conditions (parameters: pipe diameter = 0.8 m; fill height = 12 m)..... 43

Fig. 3.10. Comparison of radial earth pressures by ABAQUS, MSC/NASTRAN, and CANDE-89 (parameters: pipe diameter = 2 m; fill height = 24.4 m; interface condition= full-bonded) 44
Fig. 3.11. Multi-plate corrugated steel pipe during construction (Sargand and Moreland 2004) 45
Fig. 3.12. Slotted joint (Sargand and Moreland 2004) 46
Fig. 3.13. FEM vs. field tests by the Ohio Research Institute for Transportation and the Environment (ORITE) (*D*= 6.4m, JTL= joint travel length, AU= Auburn University) 47
Fig. 3.14. Comparison of earth pressures and shear distributions (in kPa unit) from CANDE-89, ABAQUS, and MSC/NASTRAN 48
Fig. 4.1. Radial pressure distributions on pipe wall in AASHTO standard embankment installations (parameters: inside diameter of pipe= 1.8 m; backfill height= 12 m) ... 55
Fig. 4.2. Vertical arching factor (*VAF*) and horizontal arching factor (*HAF*) versus backfill height: (a) AASHTO type 3 standard embankment installation and (b) AASHTO type 4 standard embankment installation..... 57
Fig. 4.3. Notation for imperfect trench installations and geometries of soft zone: (a) notation; (b) soft zone geometry I (proposed); and (c) soft zone geometry II (existing) (B_t = thickness of soft material below invert) 59
Fig. 4.4. Shearing stress development along the sidewall (parameters: inside diameter of pipe =1.8 m; backfill height=32 m; sidefill= AASHTO type 3)..... 61
Fig. 4.5. Comparison of radial pressure distributions of embankment installation, soft zone geometry I, and soft zone geometry II (parameters: inside diameter of pipe =1.8 m; backfill height=32 m; sidefill= AASHTO type 3) 61
Fig. 4.6. Reduction rates (R_v, R_h) versus soft zone geometry I and geometry II: (a) effects of height of soft zone and (b) effects of width of soft zone (parameters: inside diameter of pipe =1.8 m; backfill height=32 m; sidefill= AASHTO type 3)..... 63
Fig. 4.7. Reduction rates (R_v, R_h) versus modulus of elasticity of material in soft zone geometry I 65

Fig. 4.8. Vertical displacement at the top of the soft material zone versus modulus elasticity of lightweight material (E_s) (parameters: pipe diameter= 1.8 m, fill height= 32 m) 67
Fig. 5.1. Pressure transfer within a soil-pipe system: (a) rigid pipe in embankment installation; (b) flexible pipe in embankment installation; and (c) rigid or flexible pipe in imperfect trench installation (F_v = generated friction forces or shear stresses) 69
Fig. 5.2. Effects of the properties of backfill material: (a) *VAF* versus *H/D* and (b) *HAF* versus *H/D*..... 76
Fig. 5.3. Finite element analyses versus current design equations: (a) *VAF* versus *H/D* (short-term) and (b) *VAF* versus *H/D* (long-term) (parameters: pipe diameter = 0.6 m) (continued) 78
Fig. 5.3. Finite element analyses versus current design equations: (c) deflection versus *H/D* (short-term) and (d) deflection versus *H/D* (long-term) (parameters: pipe diameter = 0.6 m; deflection lag factor (D_L) = 1; bedding factor (K_b) = 0.1) 79
Fig. 5.4. Notation for imperfect trench installations and geometries of soft zone: (a) notation; (b) soft zone geometry I (proposed); and (c) soft zone geometry II (tried by Spangler (1950a) and Vaslestad et al. (1993)) 81
Fig. 5.5. Optimization process of soft zone geometry I: (a) height of soft zone (H_s) with W / D = 1.125 and B_s / D = 0.125 and (b) width of soft zone (W) with H_s / D = 0.25 and B_s / D = 0.125 (R_{ms} = reduction rate of maximum wall stress) (continued) 82
Fig. 5.5. Optimization process of soft zone geometry I: (c) bedding thickness of soft zone (B_s) with H_s / D = 0.25 and W / D = 1.125 (R_{ms} = reduction rate of maximum wall stress)..... 83
Fig. 5.6. Imperfect trench installations versus embankment installation: (a) radial earth pressure and (b) frictional stress (parameters: pipe diameter = 0.6 m; short-term material properties; fill height = 15 m; modulus of elasticity of the lightweight material = 345 kPa) (continued)..... 86

Fig. 5.6. Imperfect trench installations versus embankment installation: (c) axial force and (d) bending moment (parameters: pipe diameter = 0.6 m; short-term material properties; fill height = 15 m; modulus of elasticity of the lightweight material = 345 kPa) (continued) 87
Fig. 5.6. Imperfect trench installations versus embankment installations: (e) pipe wall stress (parameters: pipe diameter = 0.6 m; short-term material properties; fill height = 15 m; modulus of elasticity of the lightweight material = 345 kPa) 88
Fig. 5.7. Predictor equations of arching factors, deflection, and soil-structure interaction multiplier (F_{ms}) for maximum wall stress: (a) *VAF* and (b) *HAF* (*D* = pipe diameter; *r* = radius of gyration of corrugation; *ST* = short-term material properties; *LT* = long-term material properties; modulus of elasticity of the lightweight material = 345 kPa) (continued) 90
Fig. 5.7. Predictor equations of arching factors, deflection, and soil-structure interaction multiplier (F_{ms}) for maximum wall stress: (c) deflection and (d) F_{ms} (*D* = pipe diameter; *r* = radius of gyration of corrugation; *ST* = short-term material properties; *LT* = long-term material properties; modulus of elasticity of the lightweight material = 345 kPa) 91
Fig. 5.8. Predictor equations of reduction rates: (a) *VAF* and (b) *HAF* (*ST* = short-term material properties; *LT* = long-term material properties; σ_{ms} = maximum wall stress) (continued) 94
Fig. 5.8. Predictor equations of reduction rates: (c) deflection and (d) maximum wall stress (*ST* = short-term material properties; *LT* = long-term material properties; σ_{ms} = maximum wall stress) 95
Fig. 6.1. Pressure transfer within a soil-pipe system: (a) corrugated steel pipe in embankment installation and (b) corrugated PVC pipe in embankment installation (F_v = generated friction forces or shear stresses; interface condition= full-bonded) 97
Fig. 6.3. Variations of vertical arching factor (*VAF*) 104
Fig. 6.4. Effects of interface conditions for total vertical earth load (W_e) (parameters: pipe diameter = 2.4 m; fill height = 29 m) 105

Fig. 6.5. Vertical deflection (parameters: deflection lag factor (D_L) = 1; bedding factor (K_B) = 0.1) 106
Fig. 6.6. Pipe-spring model..... 107
Fig. 6.7. Comparison of critical buckling stresses between AASHTO, AISI, and pipe-spring model (D = pipe diameter; r = radius of gyration of corrugation)..... 109
Fig. 6.8. Notation for imperfect trench installations and geometries of soft zone: (a) notation; (b) soft zone geometry I (proposed); and (c) soft zone geometry II..... 110
Fig. 6.9. Optimization process of soft zone geometry I: (a) height of soft zone (H_s) with W= D +152mm and B_s/D= 0.125 and (b) thickness of soft zone below invert (B_s) with H_s/D= 0.25 and W= D +152mm (R_{ms} = reduction rate of maximum wall stress; modulus of elasticity of the lightweight material = 345 kPa) (continued)..... 112
Fig. 6.9. Optimization process of soft zone geometry I: (c) width of soft zone (W) with H_s/D= 0.25 and B_s/D= 0.125 (R_{ms} = reduction rate of maximum wall stress; modulus of elasticity of the lightweight material = 345 kPa)..... 113
Fig. 6.10. Imperfect trench installations versus embankment installations: (a) radial earth pressure (parameters: pipe diameter = 2.4 m; fill height = 29 m; modulus of elasticity of the lightweight material = 345 kPa) (continued) 115
Fig. 6.10. Imperfect trench installations versus embankment installations: (b) frictional stress and (c) axial force (parameters: pipe diameter = 2.4 m; fill height = 29 m; modulus of elasticity of the lightweight material = 345 kPa) (continued)..... 116
Fig. 6.10. Imperfect trench installations versus embankment installation: (d) bending moment and (e) pipe wall stress (parameters: pipe diameter = 2.4 m; fill height = 29 m; modulus of elasticity of the lightweight material = 345 kPa)..... 117
Fig. 6.11. Effects of interface properties in ITI: (a) *VAF* versus *H/D* and (b) *HAF* versus *H/D* (parameters: modulus of elasticity of the lightweight material = 345 kPa; proposed soft zone geometry I as shown in Fig. 6.8(b)) (continued) 118
Fig. 6.11. Effects of interface properties in ITI: (c) total vertical earth load (W_e) versus interface properties for pipe diameter = 2.4 m and fill height = 29 m (parameters:

modulus of elasticity of the lightweight material = 345 kPa; proposed soft zone geometry I as shown in Fig. 6.8(b)) 119
Fig. 6.13. Reduction rates versus modulus of elasticity of lightweight material (E_s): (a) *VAF* and (b) *HAF* (parameter: proposed soft zone geometry I as shown in Fig. 6.8(b)) (continued) 125
Fig. 6.13. Reduction rates versus modulus of elasticity of lightweight material (E_s): (c) deflection and (d) maximum wall stress (σ_{ms}) (parameter: proposed soft zone geometry I as shown in Fig. 6.8(b)) 126
Fig. 7.1. Pressure transfer and shear effect within soil-structure system: (a) embankment installation; (b) trench installation; and (c) imperfect trench installation (F_v = generated friction forces) 130
Fig. 7.2. Effects of foundation stiffness, sidefill treatment and interface conditions for earth loads on the top slab and frictional forces on the sidewall in embankment installation: (a) variation of total vertical earth loads and (b) frictional stresses (in kPa unit) versus interface conditions 132
Fig. 7.3. Variation of shear distributions (in kPa unit) on the sidewall by backfill heights (*H*) (yielding foundation and compacted sidefill) 134
Fig. 7.4. Soil-structure interaction factors for embankment installations: for an yielding foundation (a) top slab and (b) bottom slab (continued) 136
Fig. 7.4. Soil-structure interaction factors for embankment installations: for a unyielding foundation (c) top slab and (d) bottom slab 137
Fig. 7.5. Comparison of soil-structure interaction factors of AASHTO, Kim and Yoo, Tadros et al. and proposed equations on yielding foundation: (a) top slab and (b) bottom slab 138
Fig. 7.6. Notation in imperfect trench installations and geometries of soft zone: (a) notation; (b) soft zone geometry I (proposed); and (c) soft zone geometry II 140
Fig. 7.7. Effects of interface conditions for earth loads on the top slab and frictional forces on the sidewall in imperfect trench installation (yielding foundation and

compacted sidefill): (a) variation of total vertical earth loads and (b) distributions of frictional stresses (in kPa unit) versus interface conditions 141
Fig. 7.8. Earth load reduction rates for the bottom slab versus geometries of soft zone and interface conditions in imperfect trench installations: (a) effects of height of soft zone and (b) effects of width of soft zone (parameters: box size: 3.6 m×3.6 m×360 mm; backfill height= 12 m; yielding foundation and compacted sidefill) 142
Fig. 7.9. Earth load reduction rates for the bottom slab versus modulus of elasticity of lightweight materials in soft zone geometry I: (a) effects of foundation stiffness and sidefill treatment (bonded) and (b) Y,C (Y= yielding foundation; UY= unyielding foundation; C= compacted sidefill; UC= uncompacted sidefill) (continued)..... 144
Fig. 7.9. Earth load reduction rates for the bottom slab versus modulus of elasticity of lightweight materials in soft zone geometry I: (c) Y,UC and (d) (d) UY, C (Y= yielding foundation; UY= unyielding foundation; C= compacted sidefill; UC= uncompacted sidefill) (continued)..... 145
Fig. 7.9. Earth load reduction rates for the bottom slab versus modulus of elasticity of lightweight materials in soft zone geometry I: (e) UY, UC (Y= yielding foundation; UY= unyielding foundation; C= compacted sidefill; UC= uncompacted sidefill) .. 146
Fig. A1.1. Diagrams for coefficient C_d for ditch conduits 169
Fig. A1.2. Diagrams for coefficient C_c for positive projecting conduits..... 171
Fig. A1.3. Diagrams for coefficient C_n for negative projection conduits and imperfect ditch conditions ($p' = 0.5$)..... 172
Fig. A1.4. Diagrams for coefficient C_n for negative projection conduits and imperfect ditch conditions ($p' = 1.0$)..... 173
Fig. A1.5. Diagrams for coefficient C_n for negative projection conduits and imperfect ditch conditions ($p' = 1.5$)..... 174
Fig. A1.6. Diagrams for coefficient C_n for negative projection conduits and imperfect ditch conditions ($p' = 2.0$)..... 175

CHAPTER 1

INTRODUCTION

The behavior of roadway conduits such as concrete, metal and plastic pipes, and concrete box culverts is significantly affected by installation practices. No rigid or flexible pipe products in use today can carry the imposed loads without depending on, at least to some extent, the surrounding soil for support. In the case of round pipes, bedding must be uniform in order to prevent point loads, and the lateral support at the sides of the pipe must restrain displacements. The loads imposed on a roadway conduit are, thus closely related to the installation practices. As the backfill conditions and the installation practices are important for the performance of roadway conduits, it becomes incumbent upon the designer and the contractor to ensure that the backfill conditions and installation schemes specified in the design are strictly adhered to during construction.

Installation standards for roadway conduits have not been thoroughly reviewed nor significantly updated since the work of Marston, Spangler, and others during the first half of the twentieth century (Marston and Anderson 1913; Marston 1930; Spangler 1933; Spangler 1950b). Some of the current installation standards use terminology that is outdated and unsuitable for current construction practice. Bedding conditions presented in current references, such as the ASCE (1970) (American Society of Civil Engineers) and ACPA (American Concrete Pipe Association) (1988; 1994; 2000), continue to

present installation details based on this early work. Recent failures of concrete roadway pipe on a project in Alabama point to either design or construction problems. However, because of the lack of comprehensive forensic engineering analyses conducted on reported failure cases, the current design methods continue to be conservative and, hence, result in installations that are more costly than necessary.

Spangler (1933) realized that the strength of a pipe in an embankment installation is greatly influenced by the bedding quality. Spangler defined four standard bedding types for installation of concrete pipes that were generally similar to the beddings defined earlier by Marston and Anderson (1913) for trench installation of rigid pipes. The current standard installation procedure given in AASHTO LRFD (2004a) (American Association of State Highway and Transportation Officials) replaces the historical beddings of Marston and Spangler and provides a range of soil-structure interaction options.

The loading on deeply buried conduits is primarily affected by soil arching. Soil arching is influenced by several parameters including bedding type, installation method, and conduit stiffness. The detailed discussions of the influences of these parameters on soil arching will be described in each pertinent chapter. The terminology "bedding" used in the buried conduit industry includes not only the soil properties and the compaction rate but also the shape and location of their placement in association to buried pipes as illustrated in Chapter 2. Fig. 1.1 illustrates how relative settlements between soil prisms directly above and adjacent to a buried conduit affect the earth pressure on the conduit. These relative settlements generate frictional stresses that are added to or subtracted from the dead weight of the central prism and affect the resultant load on the pipe, as shown in

Fig. 1.1. When the relative settlement of the soil prism directly above the structure is less than that of the adjacent soil prisms, as usually found in embankment installations in Fig. 1.1(a), the earth load on the pipe is increased by the downward frictional forces exerted on the central soil prism, which is referred to as negative arching (Selig 1972; Vaslestad et al. 1993). Likewise, when the relative settlement of the soil prism directly above the structure is greater than that of the adjacent soil prisms, as depicted in trench installations in Fig. 1.1(b), the layers of soil in the central prism are subjected to a reverse arch shape deformation, and consequently, the earth load on the pipe is reduced by the upward frictional forces exerted on the central soil prism, which is referred to as positive arching.

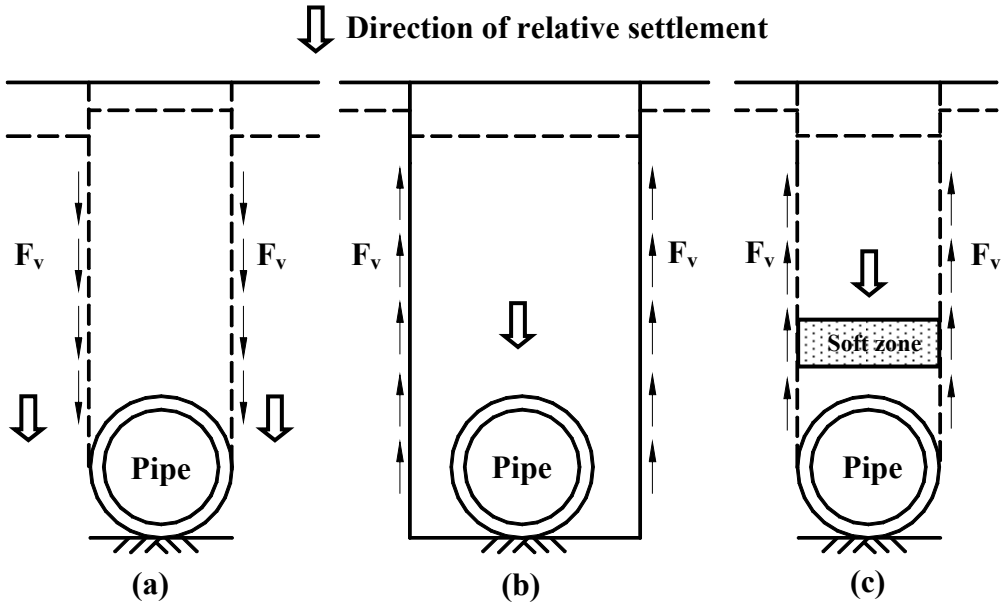

Fig. 1.1. Pressure transfer within a soil-structure system: (a) embankment installation; (b) trench installation; and (c) imperfect trench installation (F_v = generated friction forces or shear stresses)

It is known that soil pressure can be significantly reduced by placing soft lightweight compressible material (referred to lightweight material hereafter), such as baled hay or straw, leaves, compressible soil, or expanded polystyrene above a conduit. These materials induce reverse arching as illustrated in Fig. 1.1(c). The process was called imperfect trench installation (referred to ITI hereafter) by Marston (1922). The ITI method in Fig. 1.1(c) is designed to gain the benefits of a trench installation in an embankment condition. The word "trench" in ITI is in fact a misnomer as there is no trench in the in-situ soil. It is a remnant of terminology used by Marston (1922). When the soft zone induces greater relative settlement within the central soil prisms than that of the adjacent soil prisms, the upward frictional forces similar to those in the trench installations are developed.

Brown (1967) is believed to be the first to analytically quantify the pressure reduction effect of the soft zone by using the finite element method (referred to FEM hereafter). Experimental studies have shown that the predicted earth pressure by Spangler (1950a) for ITI are highly conservative (Sladen and Oswell 1988; Sven and Liedberg 1997; Vaslestad 1990; McAffee and Valsangkar 2005). This is believed to be caused, in part, by using conservative parameters for internal friction, relative settlement ratio, and projection ratio (Tyler 2003). Sladen and Oswell (1988) pointed out the following deficiencies of Spangler's imperfect trench theory:

1) The stiffness of the soft zone was not considered.
2) There were no specific guidelines for the optimum location and geometry of the soft zone.

3) The effects of horizontal stresses on the conduits were not considered.

4) Mechanical properties of the backfill were not considered.

Despite the potential for considerable reductions in earth pressure, ITI has not been widely utilized. There are reservations regarding long-term behavior as well as a lack of reliable information on the mechanical properties of the lightweight materials and the optimum geometry. The ACPA eliminated the imperfect trench method from the 2001 edition of the Concrete Pipe Handbook (ACPA 2001) primarily for these reasons. However, full-scale tests conducted by the Norwegian Road Research Laboratory (Vaslestad et al. 1993) showed that there was no increase in earth pressure after a three-year period. The use of non-biodegradable lightweight materials such as expanded polystyrene, as opposed to baled straw or hay of bygone years, should alleviate concerns for long-term settlement above a pipe. Nevertheless, the effects of time on ITI are still an issue that needs to be resolved as the loss of load reduction over time was not studied in this study. Field test results reported by McAffee and Valsangkar (2005) show that there exists an unmistakable advantage in reducing the vertical earth load on deeply buried conduits of ITI. Therefore, further studies on the behavior of soil-structure interaction associated with ITI remain an attractive challenge.

1.1 Objectives and Scope

The overall objective of this research was to investigate the interactions of soil and buried conduits. The construction materials and installation procedures used significantly affect these interactions. The imposed loading on a conduit is greatly

affected by the relative settlement of the soil prism directly above the conduit. An improved understanding of the fundamentals of the soil-structure interaction is essential to develop technically sound and yet economical design and installation procedures applicable to both designers and contractors.

A specific objective of this paper is to determine an optimum geometry for the soft material zone in ITI for deeply buried conduits by using finite element methods. Finite element analyses were carried out to analyze soil-structure interactions for buried conduits using both ABAQUS (2003) and MSC/NASTRAN (2005). The most commonly used programs for the analysis of roadway conduits, CANDE-89 (Musser 1989; Katona et al. 1976) and SPIDA (Soil-Pipe Interaction Design and Analysis, Heger et al. 1985) were also used to assess the validity of modeling techniques adopted. Accurate determination of the soil pressure associated with various soft materials is essential to designers for selecting conduits with adequate strength for given burial depths and backfill materials available. The effects of bedding and sidefill treatment are also examined for both embankment installations, which are the worst-case vertical load conditions for conduit, and ITI.

The specific tasks accomplished during this research are as follows:

1) Conducted a comprehensive literature search pertinent to research carried out on buried conduits.
2) Compared the results from this study with those from current design methods.
3) Developed optimum geometries of soft zone for ITI for various types of conduits.

4) Developed design guides which included the following items:
   - Predictor equations for the arching factors, deflections, and maximum wall stresses on embankment installation.
   - Predictor equations for the reduction rates of the arching factors, deflections, and maximum wall stresses on ITI.

1.2 Organization

In order to accomplish the research objectives stated above, it was necessary to distinguish four separate subtasks as they are closely related yet exhibit subtle differences reflecting particular characteristics of each conduit as to its construction material and installation processes. Each subtask was basically conducted as an independent investigation with the results from each presented in Chapters 4 through 7. The remainder of this dissertation is presented in the following order:

Chapter 2 presents the current buried structures installation practice based on a review of the technical literature and current standard specifications. Chapter 3 describes the finite element modeling procedures for the soil-structure system. The soil-structure model was simulated with the Duncan soil model and Selig soil parameters. Chapter 4 presents methods of accurately determining the soil pressure exerted on concrete pipes in both embankment installations and ITI. Several design guides in the form of tables and figures were prepared for the selection of concrete pipes. The effect of bedding and sidefill treatment on earth loads is also examined. Chapter 5 discusses methods of accurately determining the soil pressure exerted on corrugated PVC pipes in both

embankment installations and ITI. Several design guides in the form of tables and figures were prepared for the selection of corrugated PVC pipes. The effect of bedding and sidefill treatment on earth loads is also examined. Chapter 6 presents methods of accurately determining the soil pressure exerted on CSP in both embankment installations and ITI. Several design guides in the form of tables and figures were prepared for the selection of CSP. The effect of bedding and sidefill treatment on earth loads is also examined. Included in this chapter is the determination of the elastic buckling strength of the buried CSP based on an iterative finite element analysis. Chapter 7 presents methods of accurately determining the soil pressure exerted on box culverts in both embankment installations and ITI. Several design guides in the form of tables and figures were prepared for the selection of box culverts. The effect of bedding and sidefill treatment on earth loads is also examined. Finally, Chapter 8 presents the summary and conclusions for all studies done and recommendations for future study.

CHAPTER 2

LITERATURE REVIEW

2.1 Introduction

The main role of roadway conduits is to transport water and to be occasionally used as overhead viaducts. The design and construction of buried structures is one of the most important functions undertaken by a public works engineer. The major engineering challenge for a buried structure is the correct understanding of the mechanism by which the structure withstands the earth load imposed on it. The analysis, design, and installation of buried structures thus require an extensive understanding of soil-structure interactions. This chapter presents the current buried structures installation practice based on a review of the technical literature and current standard specifications. A limited survey of selected southern states' current practice is given in Appendix 4.

AASHTO LRFD standard installations that replaced the historical A, B, C, and D bedding (Fig. 2.1) of Marston and Anderson (1913) and Spangler (1933) were developed from a long-range research program by the ACPA in the early 1980s. AASHTO LRFD standard embankment installations shown in Fig. 2.2 were developed from a number of parametric studies using the finite element computer program SPIDA (Heger et al. 1985; ACPA 1989). Loads on buried conduits have shown to be dependent upon installation

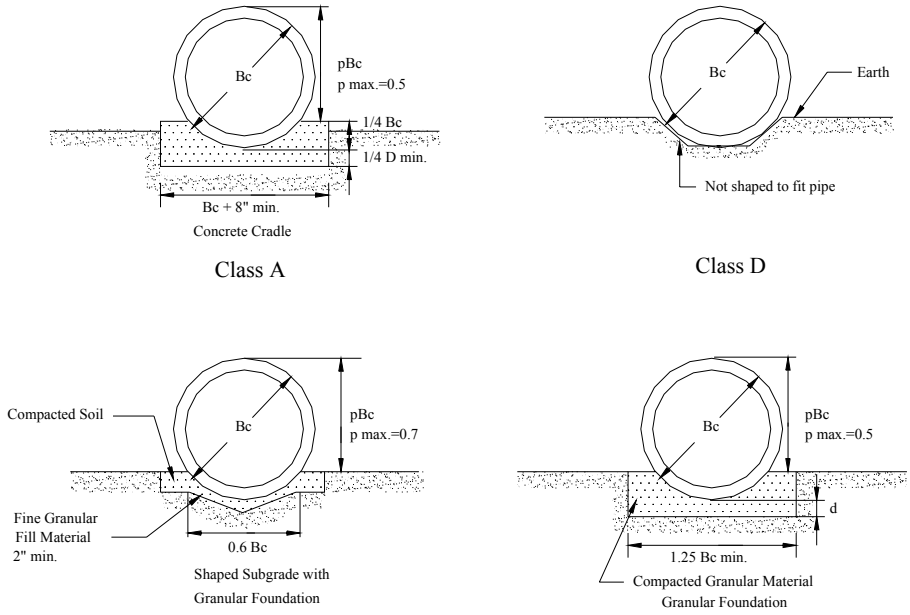

Depth of Bedding
Material Below Pipe

D	d (min.)
27" & smaller	3"
30" to 60"	4"
66" & larger	6"

Legend

Bc = Outside diameter of pipe
H = Backfill cover above top of pipe
D = Inside diameter
d = Depth of bedding material below pipe

Fig. 2.1. Four types of projection bedding for field installation of pipe

conditions. Because of the influence of these installation conditions and the importance of recognizing them when determining loads, installations of buried structures are classified into two broad categories: trench installations and embankment installations. Fig. 2.3 shows various types of conduit installations. Conduit installations are called trench installations when the conduit is located completely below the natural ground surface and the backfill over the conduit is placed between vertical or sloping walls of natural (in-situ or undisturbed) soil extending to the surface (ACPA 1994). Frictional forces between the sides of the trench and the backfill material help to support the weight of the soil overlaying the conduit. Embankment installations refer to those installations where soil is placed in layers above the natural ground (ACPA 1994) as shown in Fig. 2.2. Embankment installations are further subdivided based on their

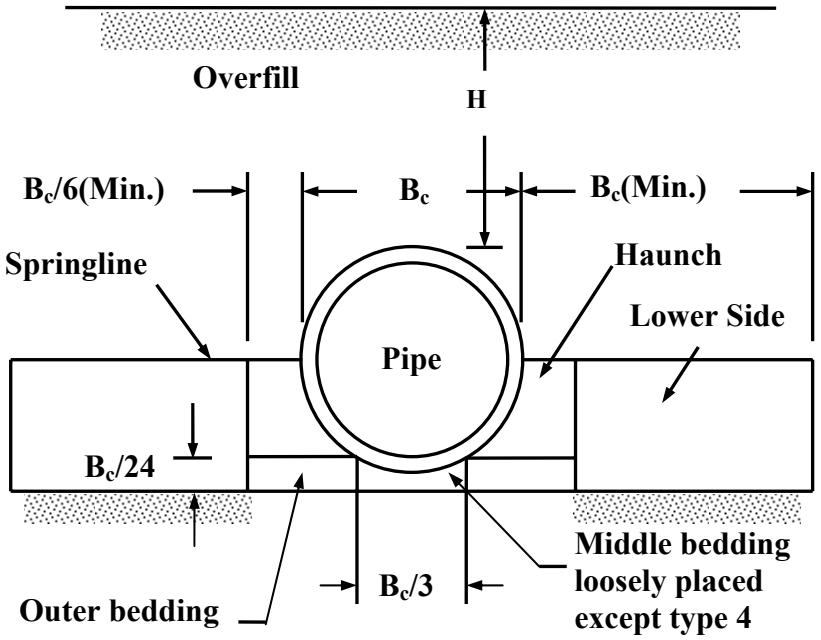

Fig. 2.2. AASHTO standard embankment installations (AASHTO LRFD 2004a)

Table 2.1. Standard Embankment Installation Soils and Minimum Compaction Requirements (AASHTO LRFD 2004a)

Installation Type	Bedding Thickness	Haunch and Outer Bedding	Lower Side
Type 1	B_c/24″ (600 mm) minimum, not less than 3″ (75 mm). If rock foundation, use B_c/12″ (300 mm) minimum, not less than 6″ (150 mm).	95% SW	90% SW, 95% ML or 100% CL
Type 2 (See Note 2.)	B_c/24″ (600 mm) minimum, not less than 3″ (75 mm). If rock foundation, use B_c/12″ (300 mm) minimum, not less than 6″ (150 mm).	90% SW or 95% ML	85% SW, 90% ML or 95% CL
Type 3 (See Note 3.)	B_c/24″ (600 mm) minimum, not less than 3″ (75 mm). If rock foundation, use B_c/12″ (300 mm) minimum, not less than 6″ (150 mm).	85% SW, 90% ML or 95% CL	85% SW, 90% ML or 95% CL
Type 4	No bedding required, except if rock foundation, use B_c/12″ (300 mm) minimum, not less than 6″ (150 mm).	No compaction required except if CL, use 85% CL	No compaction required except if CL, use 85% CL

Notes:

1. Compaction and soil symbols –i.e. “95% SW” refer to SW soil material with a minimum standard proctor compaction of 95%.
2. Soil in the outer bedding, haunch, and lower side zones, except within B_c/3 from the pipe springline, shall be compacted to at least the same compaction as the majority of soil in the overfill zone.
3. Only Type 2 and 3 installations are available for horizontal elliptical, vertical elliptical, and arch pipe.
4. Subtrenches

4.1 A subtrench is defined as a trench with its top below finished grade by more than 0.1H or, for roadways, its top is at an elevation lower than 1 (0.3 m) below the bottom of the pavement base material.

4.2 The minimum width of a subtrench shall be 1.33 B, or wider if required for adequate space to attain the specified compaction in the haunch and bedding zone.

4.3 For subtrenches with walls of natural soil, any portion of the lower side zone in the subtrench wall shall be at least as firm as an equivalent soil placed to the compaction requirements specified for the lower side zone and as firm as the majority of soil in the overfill zone, or shall be removed and replaced with soil compacted to the specified level.

location relative to the original ground level. Conduits founded partially or totally above the original ground level are classified as positive projecting conduits. Conduits founded in a trench excavated below the original ground level beneath the embankment are classified as negative projecting conduits. This is a very favorable method of installing a railway or highway conduit, since the load produced by a given height of fill is generally less than it would be in the case of a positive projecting conduit.

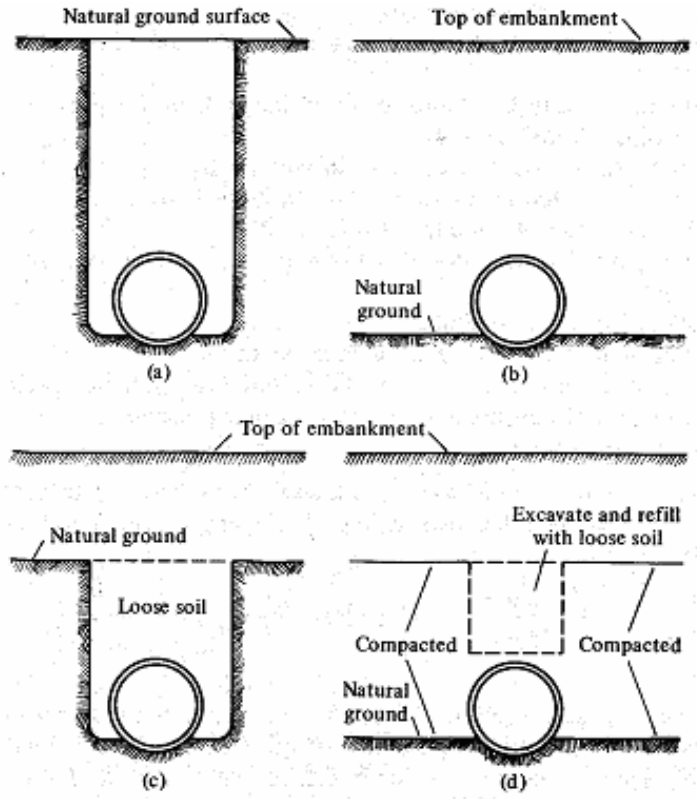

(a) Trench Installation (b) Embankment Installation (Positive Projecting)

(c) Embankment Installation (Negative Projecting) (d) Imperfect Trench Installation

Fig. 2.3. Various types of conduit installations

It has been traditional practice to define total vertical and horizontal earth loads on the pipe in terms of non-dimensional coefficients called the vertical and horizontal arching factors, *VAF* and *HAF*, respectively (ACPA 1994). Traditionally, *VAF* and *HAF* are calculated using Eqs. (2.1) and (2.2).

$$VAF = \frac{W_e}{PL} = \frac{2N_{sp}}{PL} \tag{2.1}$$

$$HAF = \frac{W_h}{PL} = \frac{N_c + N_i}{PL} \tag{2.2}$$

where PL = prism load; W_e = total vertical earth load; W_h = total horizontal earth load; N_{sp} = thrust in the pipe wall at the springline; N_c = thrust in the pipe wall at the crown; and N_i = thrust in the pipe wall at the invert.

2.2 Imperfect Trench Installation

The ITI, sometimes called induced trench installation, attempts to simulate the benefits of a trench installation in an embankment situation. ITI is installed with a compressible inclusion between the top of the conduits and the natural ground surface as shown in Fig. 2.3(d). In traditional ITI, backfill is placed and thoroughly compacted on both sides and for some distance above a projecting embankment conduit. Then a trench is constructed in this compacted fill by removing a prism of soil having the same width as the conduit and refilling with very loose lightweight materials as shown in Fig. 1.1(c). The imperfect trench conduit is a special case that is somewhat similar to the negative projecting conduit, but is even more favorable from the standpoint of reducing the load on the structure (ACPA 1988). Spangler (1950a) applied the approach that he developed

for negative projecting conduits to an installation type developed earlier by Marston and Anderson (1913) to reduce earth loads on the structure in embankment installations.

Modern design specifications have required buried conduits to be placed under increasing fill heights. The failure of buried conduits under these high fill situations can cause significant economic loss and environmental damage. The induced trench installation is used to reduce earth pressures on buried conduits. Induced trench conduits are installed with a lightweight, compressible material in the fill located directly above buried conduits. The compressible layers induce uplift frictional forces created by differential displacements within the backfill that help support the weight of the soil overlying the conduit. The mechanism of forces induced by ITI is shown in Fig. 2.4.

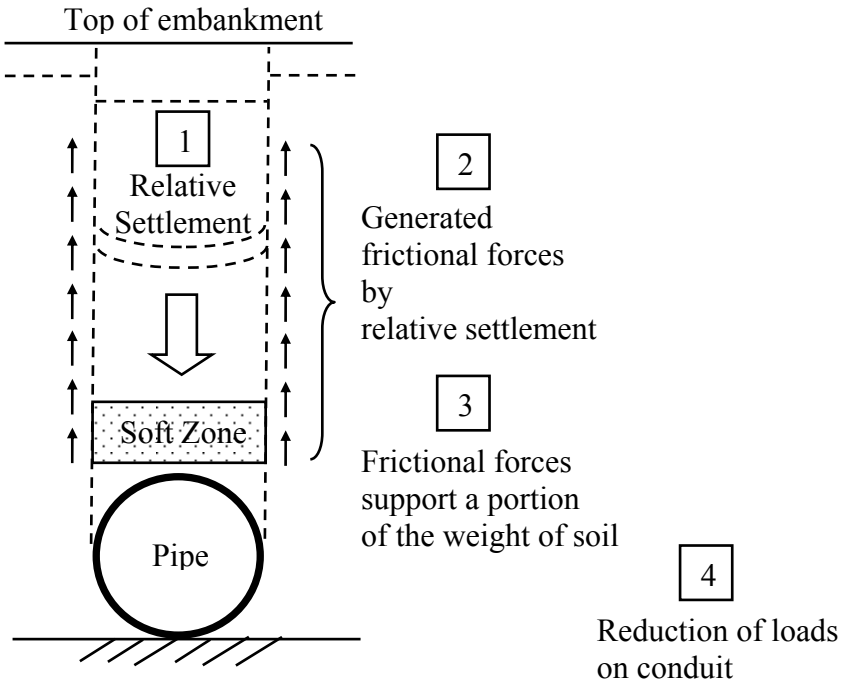

Fig. 2.4. Mechanism of imperfect trench installation

The imperfect trench method of pipe installation was developed by Marston (1922). Spangler (1950a) significantly improved the method. Marston (1930) and Spangler (1950a) quantified the load on conduits installed by imperfect trench conditions by solving differential equations based on the equilibrium conditions of a simplified free body of prisms, and proposed the following equation for predicting loads:

$$W = C_n \gamma B_c^2 \tag{2.3}$$

where C_n = load coefficients and B_c = the out-to-out horizontal span of the conduit. Although graphic illustrations are provided for the computation of coefficients, there exist many practical difficulties as the coefficient proposed contains parameters that cannot be determined readily. These parameters include the settlement ratio represented by Eq. (2.4) and the height of the plane of equal settlement to be determined by a graphical method as shown in Fig. A1.X. Further details on graphic illustrations for C_n are presented in Appendix 1. In order to use the Marston-Spangler equations, it is essential to predetermine the value of the settlement ratio, r_{sd}, defined as follows:

$$r_{sd} = \frac{s_g - (s_d + s_f + d_c)}{s_d} \tag{2.4}$$

where r_{sd} = settlement ratio for imperfect trench conduits; s_g = settlement of surface of compacted soil; s_d = compression of fill in ditch within height; s_f = settlement of flow line of conduit; d_c = deflection of conduit, i.e., shortening of its vertical dimension; and $\left(s_d + s_f + d_c\right)$ = settlement of critical plane. Although the settlement ratio, r_{sd}, is a rational quantity used in the development of the load formula, it is very difficult to predetermine the actual value that will be developed in a specific case. Spangler and

Handy (1982) recommended values of the settlement ratio based on observations of the performance of actual culverts under embankments, as shown in Table A1.2 of Appendix 1. Imperfect trench designs based on the Marston-Spangler theory have generally been successful. However, experimental studies have shown the predicted earth pressure to be highly conservative (Sladen and Oswell 1988; Sven and Liedberg 1997; Vaslestad et al. 1993). This is perhaps attributable, in part, to the conservative parameters used in the development of the design charts (Tyler 2003).

Vaslestad et al. (1993) proposed design equations for determining earth loads on induced trench installations. Earth loads on the conduit are determined by applying an arching factor to the overburden pressure. This arching factor is based on the friction number, S_v, used by Janbu to determine friction on piles (Janbu 1957). Vaslestad's equation for estimating earth pressures on an induced trench culvert is given

$$\sigma_v = N_A \gamma H \tag{2.5}$$

$$N_A = \frac{1 - e^{-2S_V \frac{H}{B}}}{2S_V \frac{H}{B}} \tag{2.6}$$

$$S_V = |\gamma| \tan \rho K_A \tag{2.7}$$

where N_A = arching factor; S_V = Janbu's friction number; B = width of conduit; r = toughness ratio $\left(= \frac{\tan \delta}{\tan \rho} \leq 1 \right)$; $\tan \rho$ = mobilized soil friction; f = degree of soil

mobilization; $\tan\phi$ = soil friction; $K_A = \dfrac{1}{\left[\sqrt{1+\tan^2\rho}+\tan\rho\sqrt{1-\left|1-\left|r\right|\right|}\right]^2}$; and active earth pressure coefficient.

Vaslestad reported that the design method shows good agreement between the earth pressure measured on a full-scale induced trench installation and the results from the finite element analysis program CANDE (Janbu 1957). However, Vaslestad did not include the effect of shear force on the sidefill, foundation characteristics, and sidefill treatment.

ITI procedures have not been improved much since the work of Marston (1913, 1922) and Spangler (1933, 1950a). There has been limited research regarding the quantitative aspect of earth load reduction in ITI. Vaslestad et al.(1993) reported that the Vaslestad equations showed good agreement between earth pressures measured on a full scale ITI and the results from finite element analysis (referred to FEA hereafter) with CANDE-89. Tyler (2003) investigated the effects of a number of variables on earth pressures including the pipe shape, backfill material, as well as the location, width, and stiffness of the soft zone. Tyler (2003) indicated that the soft zone need not be highly compressible or thick to generate significant reduction of earth pressure. Vaslestad and Johansen (1993) and Tyler (2003), however, did not present specific guidelines for optimizing soft zone geometry. Katona (Musser 1989) mentioned that the backpacking material, such as a low density polystyrene foam, can be used to reduce the earth pressure around the pipe (in a qualitative sense), yet he did not present the specifics such as geometries and properties of backpacking. Recently, Yoo et al. (2005) presented

guidelines for optimizing the geometry of the soft zone. The reduction rate, in this study, was defined as follows:

$$R(\%) = 100\left(\frac{X - Y}{X}\right) \tag{2.8}$$

where R = reduction rate; X = maximum values (arching factors, deflections, wall stresses) computed in the embankment installation; and Y = values expected in the ITI.

CHAPTER 3

SOIL-STRUCTURE MODELING

3.1 Introduction

A FEA of a soil-structure system is different from a FEA of a simple, linearly elastic, continuum mechanics problem in several ways. The soil has a nonlinear stress-strain relationship. Therefore, large load increments can lead to significant errors in evaluating stress and strain within a soil mass. In the approximate nonlinear incremental analysis procedures adopted for this study, nonlinear soil properties are simulated by way of the hyperbolic stress-strain relationship. It was also necessary to allow movement between the soil and the walls of the pipe, which necessitated an interface element. As shown by Kim and Yoo (2005) and McVay (1981;1982), the effect of interface behavior was generally insignificant for soil-structure interaction of rigid structures. McVay (1981;1982) also showed that results were reasonable without numerical modeling of the compaction process.

Four widely used computer programs were run, comparatively, for the analysis of buried conduits. ABAQUS (2003) and MSC/NASTRAN (2005) are commercially available general purpose finite element programs. SPIDA (ACPA 1989) and CANDE-

89 (Musser 1989) are the two most commonly used programs for soil-structure interaction analysis.

Although **Article 12.10.2.1**, AASHTO LRFD (2004b) requires that bedding placed under a conduit should be compacted to minimize settlement and control the conduit grade, it was found from FEA that both the loads on the pipe and the bending moments at the invert were reduced when uncompacted (loose) middle bedding was placed as described in Fig. 2.2. McGrath and Selig (1999) also observed this trend. However, the outer bedding, described in Fig. 2.2, should be compacted to provide support to the haunch area of the conduit and to provide an alternate vertical load path around the bottom of the conduit. It has been confirmed in all of the FEA in this study that the haunch area shown in Fig. 2.2 contributes significantly to the support of the earth load. Similar phenomena have been observed by other researchers (McVay 1982; ACPA 1994; McGrath and Selig 1999). Both field tests and computer models show that the bending moments are greater in the case of an uncompacted (or untreated) haunch. In this study, therefore, the installation features described in Fig. 2.2 were included in the numerical modeling. Bedding material should meet the requirement of Article 27.5.2, AASHTO LRFD (2004b). It should be noted, however, that the practice of the mandatory classification of the treated bedding material into three distinct types is problematic. An examination of a series of numerical analysis results (Yoo et al. 2005) reveals that there is no significant difference among types 1, 2, and 3.

3.2 Soil Models and Parameters

Soil stiffness properties are required to analyze soil-structure interaction. Several soil models were investigated to select the soil stiffness property that best depicted the nonlinear soil characteristics.

3.2.1 Duncan Soil Model and Parameters

Kondner (1963) has shown that the nonlinear stress-strain curves for both clay and sand may be approximated by a hyperbola with a high degree of accuracy. This hyperbola can be represented by an equation of the form:

$$(\sigma_1 - \sigma_3) = \frac{\varepsilon}{a + b\varepsilon} \tag{3.1}$$

Where σ_1, σ_3 = the maximum and minimum principal stresses, respectively; ε = the axial strain; and a, b = constants whose values may be determined experimentally. Both of these constants a and b have readily discernible physical meanings. As shown in Figs. 3.1 and 3.2, a is the reciprocal of the initial tangent modulus, E_i, and b is the reciprocal of the asymptotic value of the stress difference which the stress-strain curve approaches at infinite strain $(\sigma_1 - \sigma_3)_{ult}$. The values of the coefficients a and b may be determined readily if the stress-strain data are plotted on transformed axes, as shown in Fig. 3.2. When Eq. (3.1) is rewritten in the following form:

$$\frac{\varepsilon}{(\sigma_1 - \sigma_3)} = a + b\varepsilon \tag{3.2}$$

Here, a and b are the intercept and the slope of the resulting straight line, respectively. By plotting stress-strain data in the form shown in Fig. 3.2, it is straightforward to

determine the values of the parameters a and b corresponding to the best fit between a hyperbola and the test data. It is commonly found that the asymptotic value of $(\sigma_1 - \sigma_3)$ is larger than the compressive strength of the soil by a small amount, because the hyperbola remains below the asymptotic at all finite values of strain. The asymptotic value may be related to the compressive strength by factor, R_f:

$$(\sigma_1 - \sigma_3)_f = R_f (\sigma_1 - \sigma_3)_{ult} \tag{3.3}$$

where $(\sigma_1 - \sigma_3)_f$ = the compressive strength, or stress difference at failure; $(\sigma_1 - \sigma_3)_{ult}$ = the asymptotic value of stress difference; and R_f = the failure ratio, which always has a value less than one. For a number of different soils, the value of R_f has been found to be between 0.75 and 1.00 and is essentially independent of confining pressure. By expressing the parameters *a* and *b* in terms of the initial tangent modulus value and the compressive strength, Eq. (3.1) may be rewritten as

$$(\sigma_1 - \sigma_3) = \frac{\varepsilon}{\left[\frac{1}{E_i} + \frac{\varepsilon R_f}{(\sigma_1 - \sigma_3)_f}\right]} \tag{3.4}$$

This hyperbolic representation of stress-strain curves has been found to be fairly useful in representing the nonlinearity of soil stress-strain behavior (Christian 1982). Except for the case of unconsolidated-undrained tests on saturated soils, both the tangent modulus value and the compressive strength of soils have been found to vary with the confining

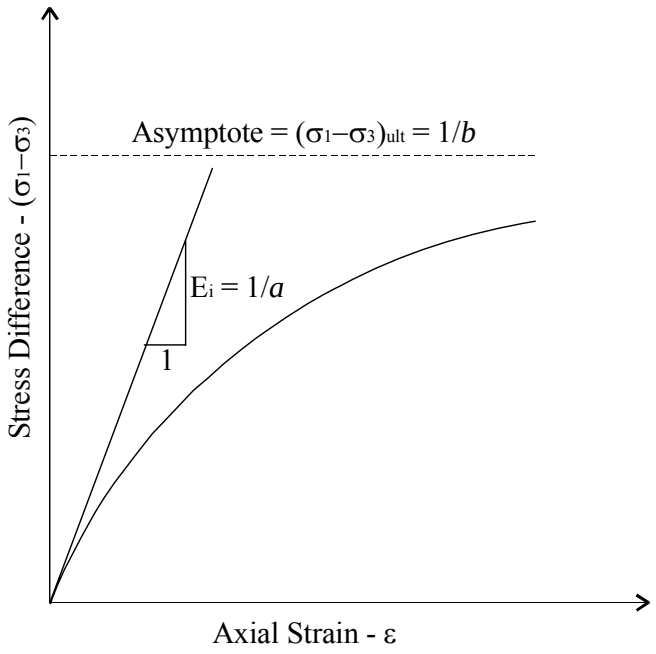

Fig. 3.1. Hyperbolic stress-strain curve

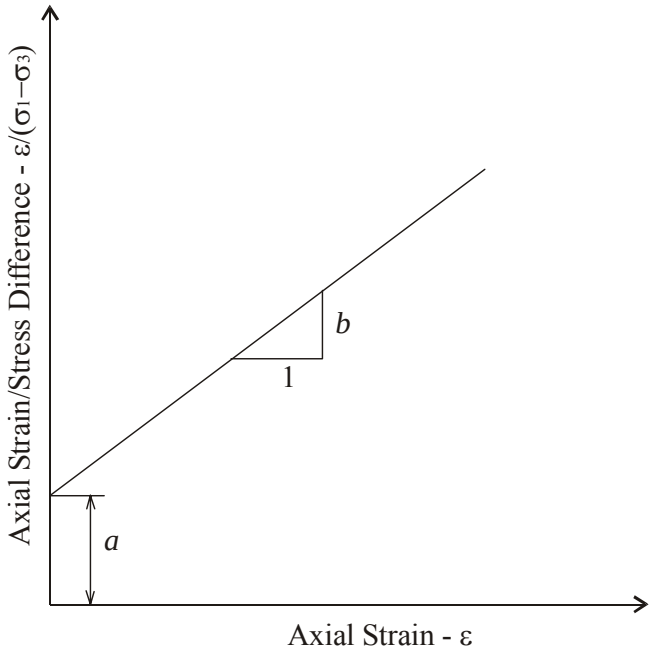

Fig. 3.2. Transformed hyperbolic stress-strain curve

pressure employed in the tests. Experimental studies by Janbu (1963) have shown that the relationship between tangent modulus and confining pressure may be expressed as

$$E_i = K \cdot P_a \left(\frac{\sigma_3}{P_a} \right)^n \tag{3.5}$$

where E_i = the initial tangent modulus; σ_3 = the minimum principal stress; P_a = atmospheric pressure expressed in the same pressure units as E_i and σ_3; K = a modulus number; and n = the exponent determining the rate of variation of E_i with σ_3.

If it is assumed that failure will occur with no change in the value of σ_3, the relationship between compressive strength and confining pressure may be expressed conveniently in terms of the Mohr-Coulomb failure criterion as

$$(\sigma_1 - \sigma_3)_f = \frac{2c\cos\phi + 2\sigma_3 \sin\phi}{1 - \sin\phi} \tag{3.6}$$

where c, ϕ = the Mohr-Coulomb strength parameters. Eqs. (3.5) and (3.6) provide a means of relating stress to strain and confining pressure using the five parameters K, n, c, ϕ, and R_f. Nonlinear, stress-dependent stress-strain behavior may be approximated in finite element analyses by assigning different modulus values to each of the elements into which the soil is subdivided for purposes of analysis. The modulus value assigned to each element is selected on the basis of the stresses or strains in each element. Because the modulus values depend on the stresses, and the stresses in turn depend on the modulus values, it is necessary to perform repeated analyses to ensure that the modulus values and stress conditions correspond for each element in the system.

The stress-strain relationship expressed by Eq. (3.4) may be employed in incremental stress analyses because it is possible to determine the value of the tangent modulus corresponding to any point on the stress-strain curve. If the value of the minimum principal stress is constant, the tangent modulus, E_t, may be expressed as

$$E_t = \frac{\partial(\sigma_1 - \sigma_3)}{\partial \varepsilon} \tag{3.7}$$

Substituting the strain, ε, derived from Eq. (3.4), the initial tangent modulus, E_i, in Eq. (3.4), and the compressive strength, $(\sigma_1 - \sigma_3)_f$, in Eq. (3.6) into the result of the differentiation of Eq. (3.7), the following expression is obtained for the tangent modulus (Duncan and Chang 1970; Wong and Duncan 1974):

$$E_t = \left[1 - \frac{R_f \left(1 - \sin\phi\right)\left(\sigma_1 - \sigma_3\right)}{2c\cos\phi + 2\sigma_3 \sin\phi} \right]^2 K P_a \left(\frac{\sigma_3}{P_a} \right)^n \tag{3.8}$$

For the hyperbolic stress-strain relationships, the same value for the unloading-reloading modulus, E_{ur}, is used for both unloading and reloading. The value of E_{ur} is related to the confining pressure by an equation of the same form as Eq. (3.5)

$$E_{ur} = K_{ur} P_a \left(\frac{\sigma_3}{P_a} \right)^n \tag{3.9}$$

where K_{ur} is the unloading-reloading modulus number. The value of K_{ur} is always larger than the value of K (for primary loading). K_{ur} may be 20% greater than K for stiff soils such as dense sands. For soft soils such as loose sands, K_{ur} may be three times as large as K. The value of the exponent n is nearly unchanged for primary loading and unloading, and in the hyperbolic relationships it is assumed to be the same.

The value of the tangent Poisson's ratio may be determined by analyzing the volume changes that occur during a triaxial test. For this purpose, it is convenient to calculate the radial strains during the test using the equation.

$$\varepsilon_r = \frac{1}{2}(\varepsilon_v - \varepsilon_a) \tag{3.10}$$

where ε_v and ε_a are the volumetric and axial strains. Taking compressive strains as positive, the value of ε_a is positive and the value of ε_r is negative. The value of ε_v may be either positive or negative. If the variation of ε_a versus ε_r is plotted, as shown in Fig. 3.3, the resulting curve can be represented with reasonable accuracy by a hyperbolic equation of the form:

$$\varepsilon_a = \frac{-\varepsilon_r}{\nu_i - d\varepsilon_r} \tag{3.11}$$

Eq. (3.11) may be transformed into Eq. (3.12).

$$-\frac{\varepsilon_r}{\varepsilon_a} = \nu_i - d\varepsilon_r \tag{3.12}$$

As can be seen from Figs. 3.3 and 3.4, the relationship of these parameters can be linearized. In Eq. (3.12), ν_i is the initial Poisson's ratio at zero strain and d is a parameter representing the change in the value of Poisson's ratio with radial strain. For saturated soils under undrained conditions, there is no volume change and ν_i is equal to one half

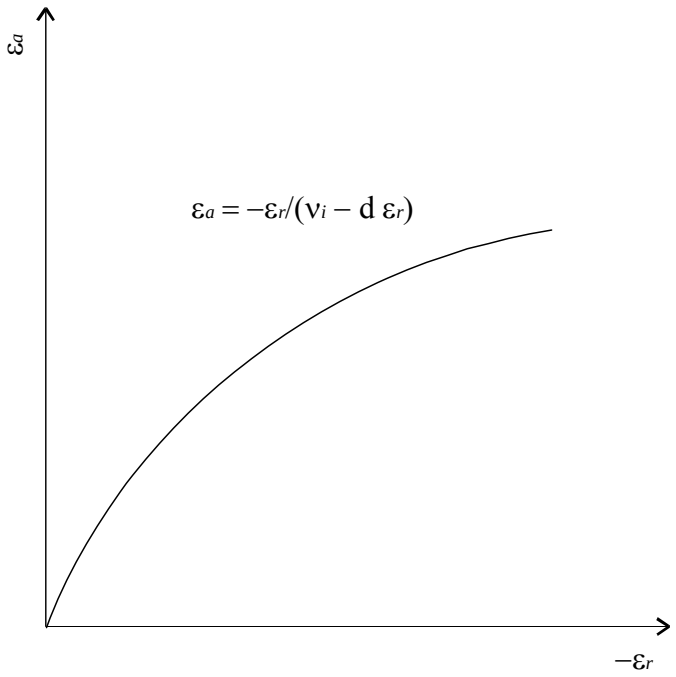

Fig. 3.3. Hyperbolic axial strain-radial strain curve

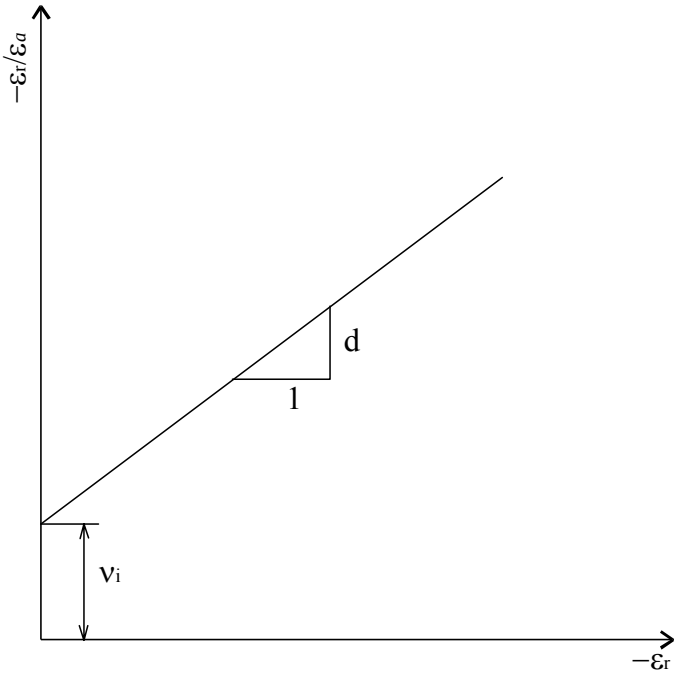

Fig. 3.4. Transformed hyperbolic axial strain-radial strain curve

for any value of confining pressure. This variation of ν_i with respect to σ_3 may be expressed by the equation:

$$\nu_i = G - F \log_{10}\left(\frac{\sigma_3}{P_a}\right) \tag{3.13}$$

where G is the value of ν_i at a confining pressure of one atmosphere, and F is the reduction in ν_i for a ten-fold increase in σ_3. After differentiating Eq. (3.11) with respect to ε_r, substituting Eq. (3.13), and eliminating the strain using Eqs. (3.2) to (3.5), the tangent value of Poisson's ratio may be expressed in terms of the stresses as follows:

$$\nu_t = \frac{G - F\,log\left(\frac{\sigma_3}{P_a}\right)}{\left\{1 - KP_a\left(\frac{\sigma_3}{P_a}\right)^n \left[\frac{d\left(\sigma_1 - \sigma_3\right)\left(1 - sin\,\phi\right)}{2c\,cos\,\phi + 2\sigma_3\,sin\,\phi}\right]\right\}^2} \tag{3.14}$$

where σ_1, σ_3 = maximum and minimum principal stresses, respectively; K = modulus number; n = modulus exponent; c = cohesion intercept; ϕ = friction angle; G, F, d = Poisson's ratio parameters; and P_a = atmospheric pressure. There are nine parameters involved in the hyperbolic stress-strain and volume change relationships, and the roles of these parameters are summarized in Table 3.1.

The nonlinear volume change can also be accounted for by employing the constant bulk modulus instead of Poisson's ratio parameters. The assumption that the bulk modulus of the soil is independent of stress level $(\sigma_1 - \sigma_3)$ and that it varies with confining pressure provides a reasonable approximation to the shape of the volume

change curves. According to the theory of elasticity, the value of the bulk modulus is defined by

$$B = \frac{\Delta\sigma_1 + \Delta\sigma_2 + \Delta\sigma_3}{3\Delta\varepsilon_v} \tag{3.15}$$

Table 3.1. Summary of the hyperbolic parameters

Parameter	Name	Function
K, K_{ur}	Modulus number	Relate E_i and E_{ur} to σ_3
N	Modulus exponent	
C	Cohesion intercept	Relate $(\sigma_1-\sigma_3)$ to σ_3
ϕ	Friction angle	
R_f	Failure ratio	Relates $(\sigma_1-\sigma_3)_{ult}$ to $(\sigma_1-\sigma_3)_f$
G	Poisson's ratio parameter	Value of ν_i at $\sigma_3=p_a$
F	Poisson's ratio parameter	Decrease in ν_i for ten-fold increase in σ_3
D	Poisson's ratio parameter	Rate of increase of ν_t with strain

where B is the bulk modulus, $\Delta\sigma_1$, $\Delta\sigma_2$, and $\Delta\sigma_3$ are the changes in the values of the principal stress, and $\Delta\varepsilon_v$ is the corresponding change in volumetric strain. For a conventional triaxial test, in which the deviator stress $(\sigma_1 - \sigma_3)$ increases while the confining pressure is held constant. Eq. (3.15) may be expressed as:

$$B = \frac{(\sigma_1 - \sigma_3)}{3\varepsilon_v} \tag{3.16}$$

The value of the bulk modulus for a conventional triaxial compression test may be calculated using the value of $(\sigma_1 - \sigma_3)$ corresponding to any point on the stress-strain curve. When values of B are calculated from tests on the same soil specimen at various confining pressures, the bulk modulus will usually be found to increase with increasing confining pressure. The variation of B with confining pressure can be approximated by an equation of the form (Duncan et al. 1980):

$$B = K_b P_a \left(\frac{\sigma_3}{P_a} \right)^m \tag{3.17}$$

where K_b is the bulk modulus number and *m* is the bulk modulus exponent, both of which are dimensionless, and P_a is atmospheric pressure. Experimental studies of this soil model, sometimes called the modified Duncan model, for most soils, has resulted in values of *m* varying between 0.0 and 1.0. If a bulk modulus is known, the tangent Poisson's ratio can be determined from the basic theory of elasticity by the following equation:

$$\nu_t = \frac{1}{2} - \frac{E_t}{6B} \tag{3.18}$$

Although the hyperbolic relationships outlined previously have proven to be quite useful for a wide variety of practical problems, it has some significant limitations. Duncan et al. (1980) outlined the following limitations: 1) Based on the generalized Hooke's law, the relationships are most suitable for analysis of stresses and movements prior to failure. The relationships are capable of accurately predicting nonlinear relationships between loads and movements, and it is possible to continue the analyses up to the stage where there is local failure in some elements. However, once a stage is reached where the behavior of the soil mass is controlled to a large extent by properties assigned to elements which have already failed, the results will no longer be reliable, and they may be unrealistic in terms of the behavior of real soils at and after failure. 2) The hyperbolic relationships do not include volume changes due to changes in shear stress, or shear dilatancy. They may, therefore, be limited with regard to the accuracy with which they can be used to predict deformations in dilatant soils, such as dense sands under low confining pressures. The values of the tangent Poisson's ratio calculated using Eq. (3.7) may result in a value exceeding 0.5 for some combinations of parameter values and stress values, so it needs to be specified to be less than 0.5 in the computer program. 3) The parameters are not fundamental soil properties, but only values of empirical coefficients that represent the behavior of the soil under a limited range of conditions. The values of the parameters depend on the density of the soil, its water content, the range of pressures used in testing, and the drain conditions. In order that the parameters will be representative of the real behavior of the soil under field conditions, the laboratory test conditions must correspond to the field conditions with regard to these factors.

3.2.2 Selig Bulk Modulus and Parameters

Both the Duncan et al. (1980) and Selig (1988) parameters were derived using the same Young's modulus obtained from constant confining pressure triaxial tests. Musser (1989), however, recognized that Selig's model incorporated an alternative method for obtaining the bulk modulus based on a hydrostatic compression test. In this test, the soil specimen is compressed under an increasing confining pressure applied equally in all directions. According to Eq. (3.15), tangent bulk modulus *B* is the slope of the hydrostatic stress-strain curve. Selig observed that the curve relating σ_m and ε_{vol} was found to be reasonably represented by the hyperbolic equation

$$\sigma_m = \frac{B_i \varepsilon_{vol}}{1 - (\varepsilon_{vol} / \varepsilon_u)} \tag{3.19}$$

where B_i = initial tangent bulk modulus, and ε_u = ultimate volumetric strain at large stress. As the tangent bulk modulus B is the slope of the hydrostatic stress-strain curve, σ'_m, it can be determined by differentiating Eq. (3.19) with respect to ε_{vol} and substituting the expression for ε_{vol} obtained by rearranging Eq. (3.19). The result is Selig's bulk modulus given by Eq. (3.20).

$$B = B_i (1 + \sigma_m / (B_i \varepsilon_u))^2 \tag{3.20}$$

To determine the parameters B_i and ε_u, the test results from the left side of Fig. 3.5 are plotted in linearized hyperbolic form as shown in Fig. 3.6. Eq. (3.19) shows a straight line as shown in Fig. 3.6. Once B_i and ε_u are known, the test results can then be represented by Eq. (3.20).

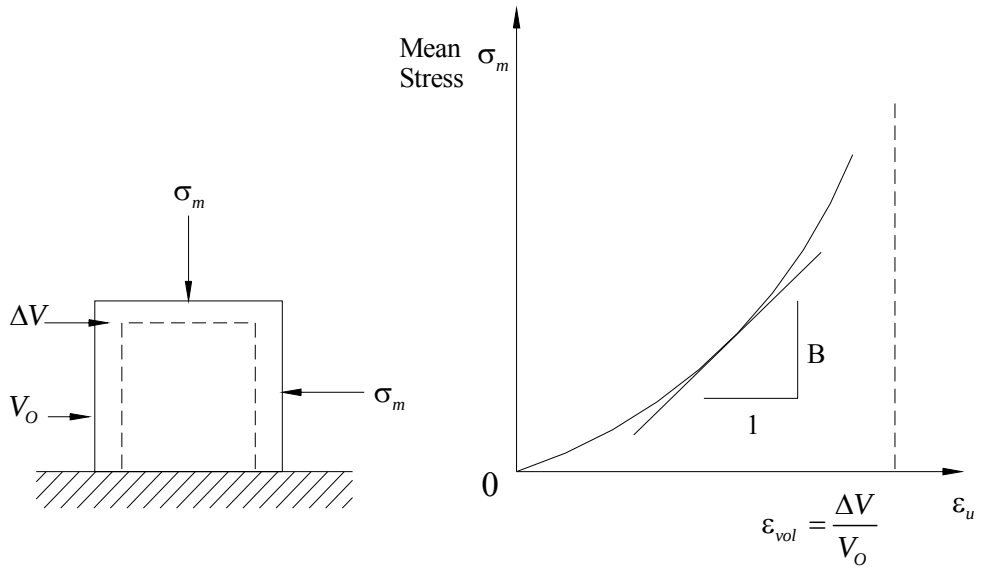

Fig. 3.5. Hydrostatic compression test

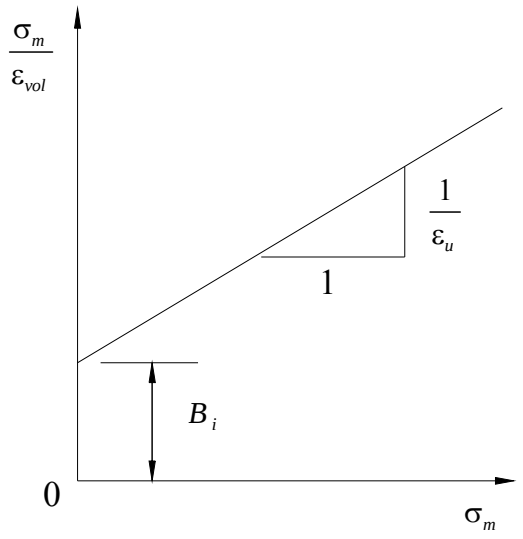

Fig. 3.6. Linear transformation of hyperbola for bulk modulus

Lin (1987) has shown that the hyperbolic formulation for bulk modulus given by Eq. (3.20) better represents soil behavior in a hydrostatic compression test than Duncan's power formulation represented by Eq. (3.17), thus favoring the use of Selig's model.

3.3 Finite Element Modeling

3.3.1 Modeling Techniques

The schematic finite element models 'embankment installation and ITI' are shown in Fig. 3.7. Taking advantage of symmetry, only one-half of the system is included in the model. Experience has shown that lateral boundaries of the model need not be extended further than 3 times the conduit width from the center of the conduit (stipulated to be 2.5 and 3 times the conduit width, respectively, in the current version of SPIDA and CANDE-89). For deep fill heights, the current version of SPIDA and CANDE-89 (Level 2 option) do not permit top boundaries to extend beyond 3 times and 1.5 times, respectively, the conduit width above the crown of the conduit; after which an equivalent overburden pressure is to be used to represent the remaining soil weight. It is further noted that CANDE-89 (Level 2 option) limits the number of beam elements to 10 while SPIDA allows it to be 19. CANDE-89 (Level 3 option) eliminates the mesh limitations imposed in Level 2 analysis. However, the lack of an automatic mesh generation scheme that is available in the lower level options in CANDE-89 makes the input data generation a fairly cumbersome task.

The FEA results in this study also showed that lateral and top boundaries need not

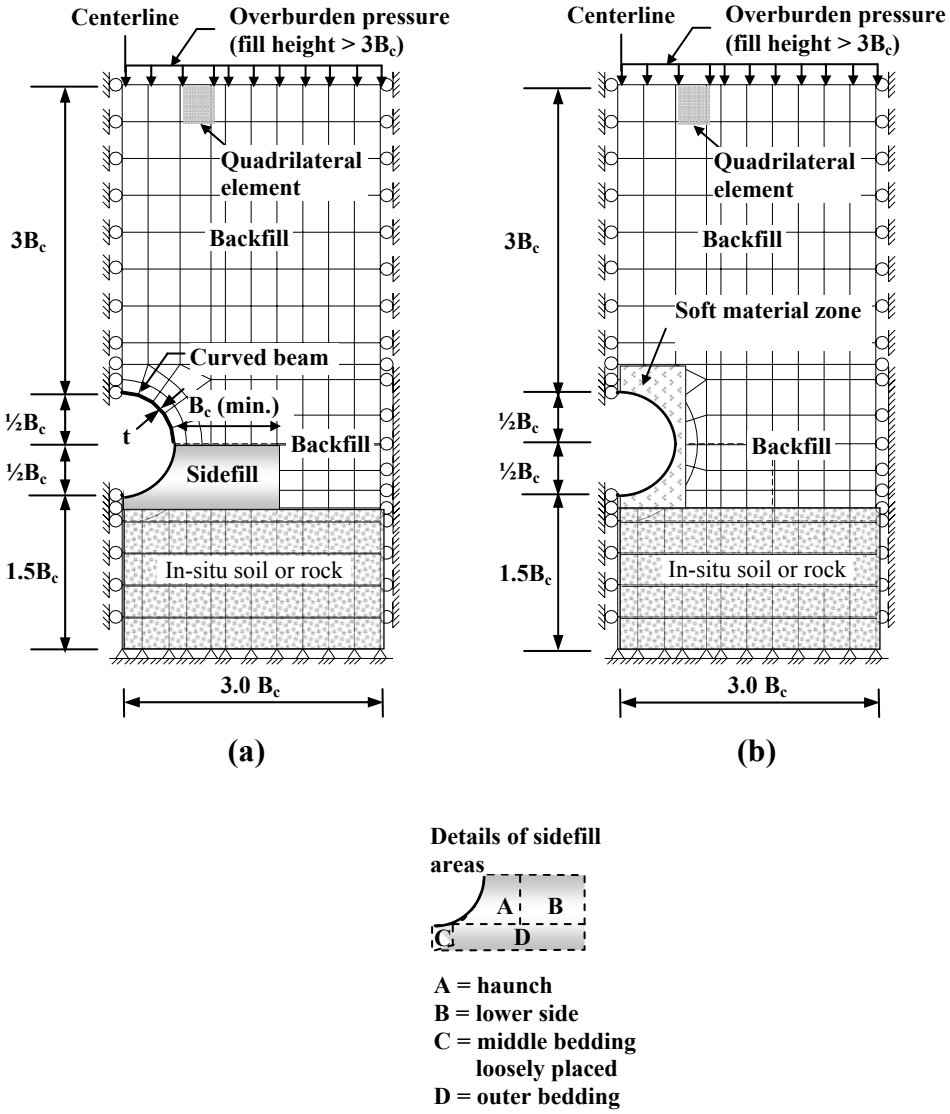

Fig. 3.7. Schematic finite element model: (a) embankment installation and (b) imperfect trench installation (B_c = width of the pipe; t = pipe wall thickness)

be extended beyond 3 times the width of the conduit from the center of the conduit and 3 times the width of the conduit from the crown of the conduit, respectively. A rigid layer was located 1.5 times the width of the conduit below the invert (or bottom) of the conduit since soil beyond this depth did not affect the results. Curved beam elements and straight beam elements are used to model the circular pipes and box culverts, respectively. A plane strain linear elastic element was used for soil. The elastic properties of the soil were described by two stiffness parameters, tangent modulus (E_t) and bulk modulus (B) as defined by Eqs. (3.8) and (3.20), respectively. The unit weight of soil was assumed to be 19 kN/m^3 (120 pcf). Nonlinear soil behavior was approximated by incremental analyses, i.e., by changing soil property values as backfill is placed and compacted. Values of tangent modulus and Poisson's ratio were computed for each layer by using Eqs. (3.21) and (3.22) based on the assumption that soil layers are in principal stress states.

$$\sigma_1^{(i)} = \gamma_i (H_i / 2) + \sum_{j=j+1}^{n} \gamma_j H_j \tag{3.21}$$

$$\sigma_3^{(i)} = K_0 \sigma_1^{(i)} \tag{3.22}$$

where $\sigma_1^{(i)}$ = maximum principal stress in ith layer of soil (numbering commences from the bottom to the top of the backfill); $\sigma_3^{(i)}$ = minimum principal stress in ith layer of soil; H_i = depth of ith soil layer; γ_i = density of ith soil layer; and K_0 = coefficient of lateral earth pressure. These values are substituted for the principal stresses in Eq. (3.8) for the tangent modulus (E_t) and in Eq. (3.20) for the bulk modulus (B) for each layer. Poisson's ratio (ν) is then computed by Eq. (3.18). Soil parameters, such as the internal

friction angle and soil cohesion used in Duncan and Selig's formulations, are available for a variety of soil types in the *Concrete Pipe Technology Handbook* (ACPA 1994) and also in the *CANDE-89 User Manual* (Musser 1989). Although the manual variations of the soil properties for each layer used to simulate the nonlinear behavior of soil in the analysis using ABAQUS and MSC/NASTRAN appears to be haphazard, the numerical results compared with those from SPIDA and CANDE-89 for simple test cases correlate very well. Typical sample comparisons are discussed in detail in the next section 3.3.2. Such time consuming and laborious procedures were dictated by the aforementioned limitations with regard to the backfill height and mesh generation schemes imposed in SPIDA and CANDE-89 for deeply buried conduits.

In the past, materials such as baled hay or straw and sawdust were tried for lightweight materials in the ITI. However, these materials left unanticipated large holes after they rotted away and consequently, the use of ITI methods was perceived to be unreliable despite their theoretical soundness. Because of the availability of modern non-biodegradable materials such as expanded polystyrene blocks (geofoam), polystyrene beads (a.k.a. peanuts), the legitimate concern of the bygone era has been largely overcome. McAffee and Valsangkar (2004) reported experimentally measured modulii of lightweight materials ranging from 345 kPa (50 psi) for geofoam to 2756 kPa (400 psi) for bales of hay. However, Poisson's ratio for geofoam is generally less than 0.1. Based on these two references, values of modulus of elasticity (E_s) of lightweight materials varied between 345 kPa (50 psi) and 2756 kPa (400 psi) and Poisson's ratio (ν) was assumed equal to 0.1 throughout this study.

3.3.2 Verification of Modeling Techniques

In order to assess the validity of the soil modeling techniques adopted, the analytical results from ABAQUS and MSC/NASTRAN, general purpose 3-D finite element codes, were compared with those of SPIDA and CANDE-89, special purpose computer codes.

1) Concrete pipes

The example used is a concrete pipe having an inside diameter of 1.8 m (72 in.) with a backfill height of 6 m (20 ft). The modulus of elasticity, Poisson's ratio, and unit weight of concrete pipe were taken to be 25 GPa (3,600 ksi), 0.20, and 23 kN/m^3 (145 pcf). As shown in Fig. 3.8, the distributions of pressure normal to the pipe surface from ABAQUS and MSC/NASTRAN show excellent agreement with those of SPIDA and CANDE-89. Typical input files of SPIDA and CANDE-89 are presented in Appendices 2 and 3.

2) Corrugated PVC pipes

The analytical results from ABAQUS were compared with those from CANDE-89, MSC/NASTRAN, and field tests of Sargand et al. (2001a; 2001b) at the Ohio Research Institute for Transportation and Environment (ORITE). The corrugated PVC pipe has an inside diameter of 0.76 m (30 in.). The unit weight of backfill materials is 21.2 kN/m^3 (135 pcf) and the fill height is 12.2 m (40 ft). Fig. 3.9 shows the radial

pressure distributions from ABAQUS, MSC/NASTRAN, and CANDE-89 under the full-bonded interface conditions. The maximum radial pressure from ABAQUS shows good agreement with those from CANDE-89 and MSC/NASTRAN with less than 5% difference. For the radial pressure at the pipe crown, data from ABAQUS under the full-bonded interface conditions showed good agreement with that from the field test with less than 10% difference as shown in Fig.3.9.

3) Corrugated Steel Pipes

The example CSP has a diameter of 2 m (78 in.). The unit weight of backfill materials used in this comparison is 18.9 kN/m^3 (120 pcf) and the backfill height (H) is 24.4 m (80 ft). Fig. 3.10 shows the radial pressure distributions from ABAQUS, MSC/NASTRAN, and CANDE-89. The maximum radial pressure from ABAQUS agrees well with those from MSC/NASTRAN and CANDE-89 with less than 7% difference.

The results from ABAQUS, also, were compared with those from field tests and numerical investigation by the Ohio Research Institute for Transportation and the Environment (ORITE) (Sargand and Moreland 2004). Fig. 3.11 shows the construction of the multi-plate corrugated steel pipe. The diameter of pipe was 6.4 m (252 in.). The steel plates were 0.95 cm (0.375 in.) thick and had a 15.24 cm (6 in.) by 5.08 cm (2 in.) corrugation profile. It is noted that slotted joints were developed to relieve thrust stress by circumferential contraction of the plates (Katona and Akl 1987) in deep embankment installations. By reducing the circumferential length of a corrugated metal culvert the

surrounding soil envelope is forced into a compression arch, which in turn carries a greater portion of the soil loading. In essence, this is an indirect imperfect trench installation method by inducing deflection at the crown of the pipe, thereby simulating the positive arching. The joint travel length (JTL), 0.5 in., of the slotted joint was used in the CANDE-89. Fig. 3.12 shows a typical slotted joint. Fig. 3.13 shows that the vertical earth pressures on the crown computed with ABAQUS were relatively close to those from CANDE-89 investigation by Sargand and Moreland (2004). ABAQUS and CANDE-89 had a tendency to overpredict the earth pressures on the crown.

4) Box Culverts

An example was taken from AASHTO M 259 (AASHTO 2002). A single cell box culvert having interior dimensions of 3 m × 3 m and 250 mm thick walls was installed in an embankment condition. The backfill height was 4.9 m. The interface condition between the box culvert and adjacent sidefills was assumed to be full-bonded (frictional coefficient = ∞). As shown in Fig. 3.14, the pressure and frictional force distributions from ABAQUS and MSC/NASTRAN show excellent agreement with those from CANDE-89. The maximum difference was less than 6%. The soil pressure directly above the sidewall was substantially higher than the soil pressure at the center of the top slab, where the largest relative vertical deflection is expected to occur. It appears that the inclusion of reinforced steel in the calculation of the slab stiffness has a negligible effect on the soil pressure distribution, as explained in Article 8.6, ACI (2002).

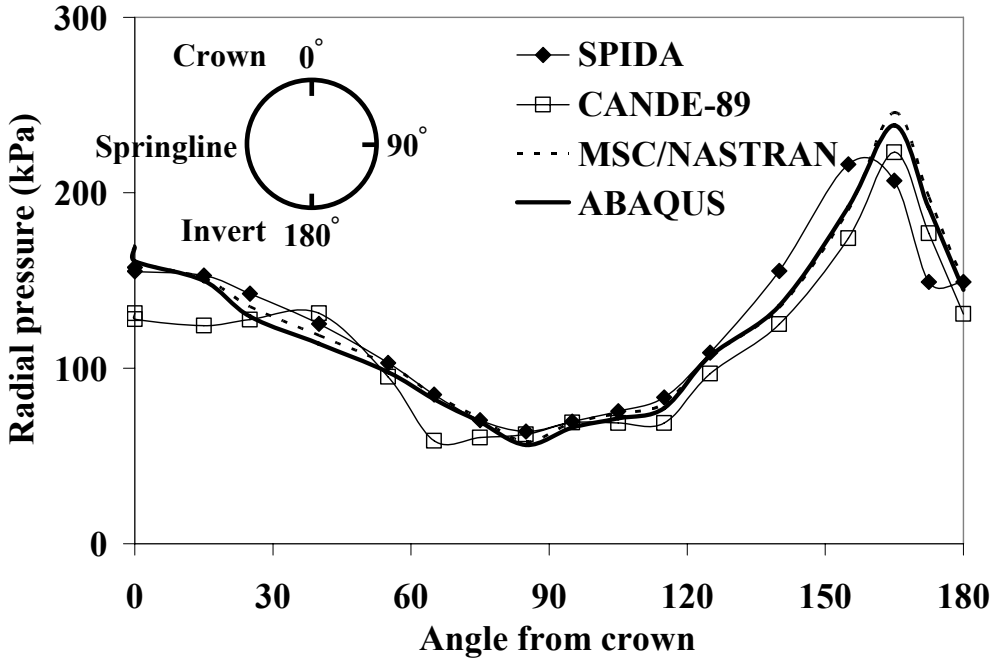

Fig. 3.8. Comparison of radial pressure distributions in AASHTO standard embankment installation (parameters: inside diameter of pipe= 1.8 m; backfill height= 6 m; sidefill= AASHTO type 3)

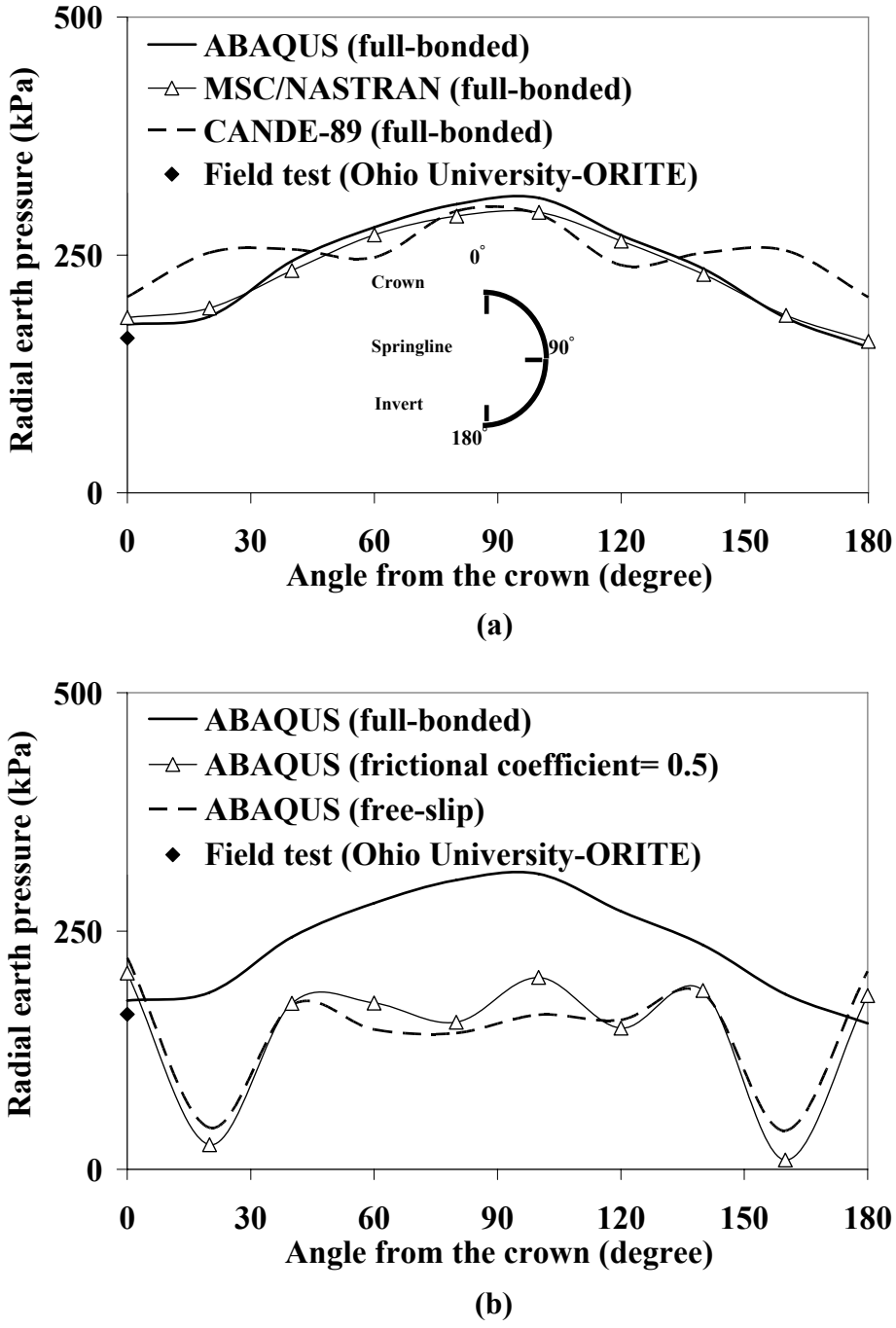

Fig. 3.9. Finite element modeling versus field test by the Ohio Research Institute for Transportation and Environment (ORITE): (a) verification of modeling techniques and (b) effects of interface conditions (parameters: pipe diameter = 0.8 m; fill height = 12 m)

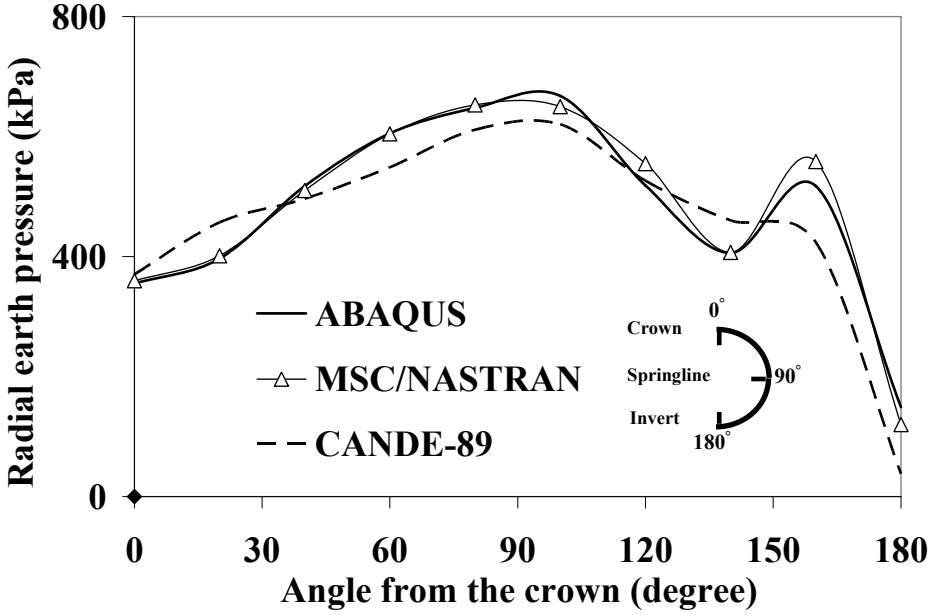

Fig. 3.10. Comparison of radial earth pressures by ABAQUS, MSC/NASTRAN, and CANDE-89 (parameters: pipe diameter = 2 m; fill height = 24.4 m; interface condition= full-bonded)

Fig. 3.11. Multi-plate corrugated steel pipe during construction (Sargand and Moreland 2004)

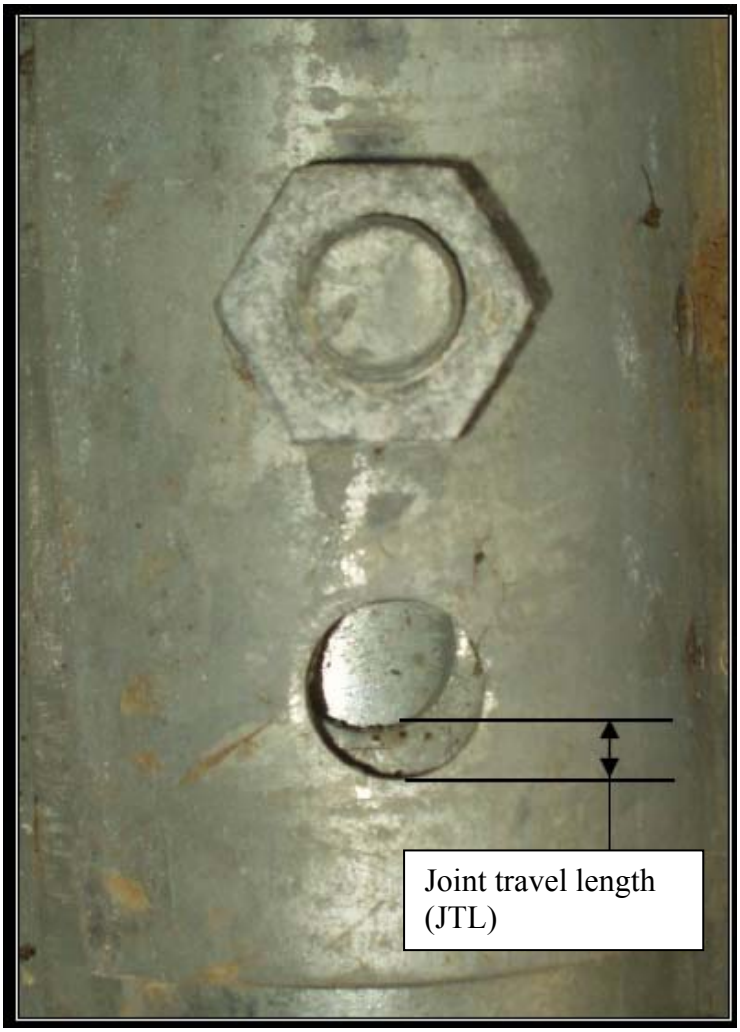

Fig. 3.12. Slotted joint (Sargand and Moreland 2004)

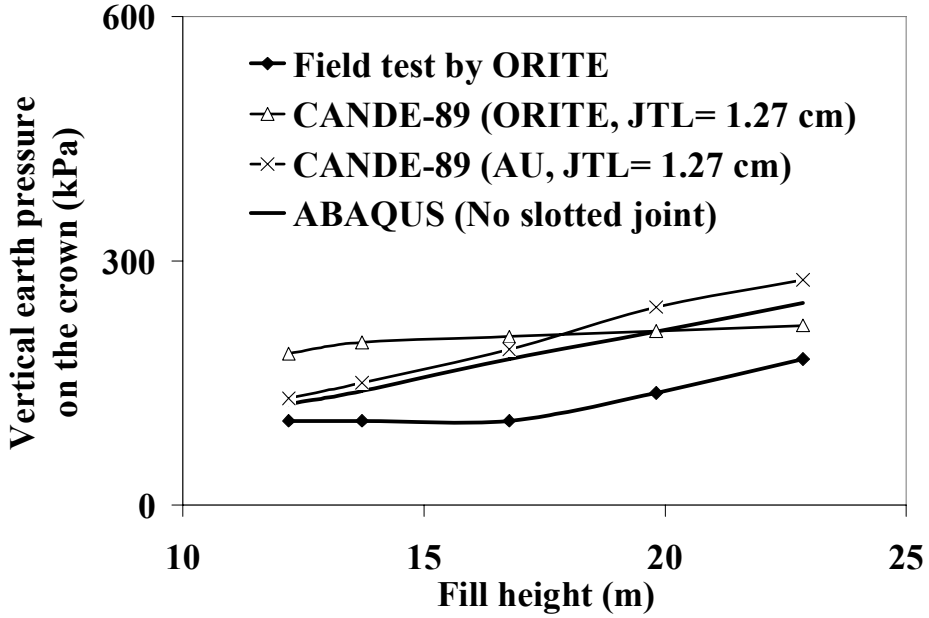

Fig. 3.13. FEM vs. field tests by the Ohio Research Institute for Transportation and the Environment (ORITE) (*D*= 6.4m, JTL= joint travel length, AU= Auburn University)

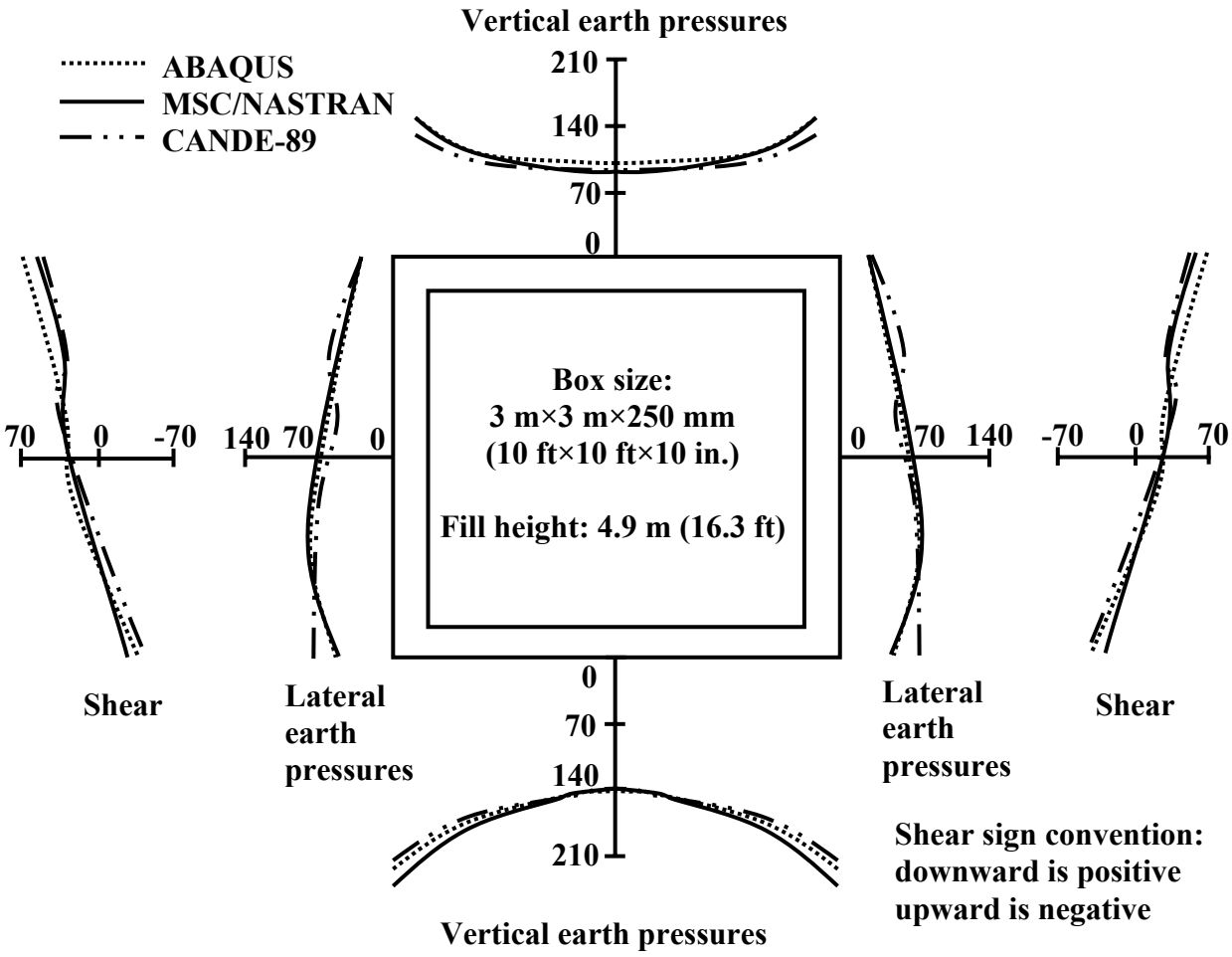

Fig. 3.14. Comparison of earth pressures and shear distributions (in kPa unit) from CANDE-89, ABAQUS, and MSC/NASTRAN

3.4 Optimum Geometry of Imperfect Trench Installations

The single most important original contribution of this study is the discovery of the optimum geometry of the soft material zone in association with ITI of deeply buried conduits. Although the notion of placing lightweight materials above the deeply buried conduits will lessen the earth loads on the conduits by inducing a reverse arching action has existed for nearly the past one hundred years, none has ever successfully come up with an optimum geometry of the soft material zone. Further, no information on the quantitative assessment of the effectiveness of the ITI has been available.

Kim and Yoo (2005) presented an improved geometry for the soft material zone over any existing ones. However, they overlooked an important aspect of the development of unexpectedly large frictional stresses induced by the placement of the soft material zone. It was found during this study that these unexpected frictional stresses can effectively be eliminated by extending the soft material zone down to the bottom level of conduits as illustrated schematically in Fig. 3.7. The effectiveness of the reduction of the earth pressure on the deeply buried conduits installed under the optimum geometry of the ITI is truly outstanding. The highest reduction rate observed during the analysis of over 4,000 hypothetical models is 85% of the anticipated earth pressure for a conduit in ordinary embankment installations. The detailed dimensions of the extended soft material zone geometry are slightly different reflecting the particular characteristics of four major conduits studied in this study. The detailed dimensions and the effectiveness of reducing the unexpected frictional stresses for each of these four major conduits will be described in the subsequent chapters.

CHAPTER 4

SOIL-STRUCTURE INTERACTION FOR DEEPLY BURIED CONCRETE ROUND PIPES

4.1 Introduction

This chapter presents the soil-structure interaction pertinent to deeply buried concrete pipes. The loading on deeply buried concrete pipes is significantly affected by soil arching in addition to the quality of bedding. As mentioned on page 2 of Chapter 1 of this dissertation, Spangler (1933) realized that the required strength of a pipe in an embankment installation is greatly influenced by the quality of its bedding. Spangler's four standard bedding types proposed for the embankment installations were generally similar to those defined earlier by Marston and Anderson (1913) for trench installations. The current American Association of State Highway and Transportation Officials standard installation procedure (AASHTO LRFD 2004a) stipulates improved bedding types beyond those of Marston and Spangler and provides a range of soil-structure interaction options.

Presented in this chapter is a detailed description of the behavior of concrete pipes installed using the embankment installation method and the ITI method. As the primary objective of this study is to define an optimum geometry for the soft material zone in

association with ITI, the detailed dimensions and effectiveness of the round concrete pipes installed under the ITI method are discussed. In order to facilitate the selection of concrete pipes with proper strength for the given burial depth and backfill materials available, an accurate determination of the soil pressure associated with various soft materials is of paramount importance. This chapter also includes the effect of bedding and sidefill treatment on earth loads for both conventional (embankment) and ITI.

4.2 Background

As mentioned earlier, the soil pressure on the deeply buried conduits is primarily affected by soil arching action. In turn, there are three major parameters affecting the soil arching: beddings, installation methods, and stiffness of the structures. The current AASHTO LRFD (2004a) procedure for computing total earth load on a concrete pipe for embankment installations is given by Eq. (4.1). The equation is essentially the same as those proposed by Marston (1913, 1930) and Spangler (1933).

$$W_e = F_e w B_c H \tag{4.1}$$

where W_e = total vertical earth load; F_e= soil-structure interaction factor for embankment installation; w = unit weight of soil; B_c = width of the structure; and H = backfill height.

Fig. 2.2 is the reproduction of AASHTO standard installations replacing the historical A, B, C, and D beddings of Marston and Spangler. AASHTO standard installations differ significantly from Marston and Spangler's theory. Spangler's bedding factor research suffered from some severe limitations. First, for the embankment condition, Spangler developed a general equation for the bedding factor, which partially

included the effects of lateral pressure. For the trench condition, Spangler established conservative fixed bedding factors, which neglected the effects of lateral pressure, for each of the three beddings (ACPA 1996). Second, loads were considered as acting only at the top of the pipe. Third, axial thrust was not considered. The bedding width of test installations was also less than the width designated in his bedding configurations so as to distort the effect of the sidefill. Fourth, standard beddings were developed to fit assumed theories for soil support rather than reflecting the field construction practice. Fifth, bedding materials and compaction levels were not adequately defined. AASHTO standard installations provide the basis for a more rational design and installation method for deeply buried pipes reflecting field construction practice. AASHTO standard installations also have several advantages over historical A, B, C, and D beddings because of the following considerations of practical construction (ACPA 1994):

1) A flat foundation and bedding simplifies construction.
2) Embedment soil cannot be compacted in the lower haunch area up to about 40 degrees from the invert.
3) AASHTO standard installations do permit the use of a range of embedment soils from the best quality granular soils that are easily compacted to various lesser quality soils that may be readily available at a site. Also included is the option to use many native soils without compaction around the pipe for bedding, embedment and backfill.

4) AASHTO standard installations permit the compaction requirements to be limited to those zones around the pipe where the embedment provides beneficial vertical or lateral support to the pipe.

AASHTO standard installations were developed from an ACPA long-range research program on the interaction of buried concrete pipe and soil in the early 1980s. Four AASHTO Standard Installations were produced as a result of numerous parametric studies using the finite element computer program, SPIDA, for the direct design of buried concrete pipe. The SPIDA studies were conducted for positive projection embankment conditions, which are the worst-case vertical load conditions for pipe, and which provide conservative results for other embankment and trench conditions. The parametric studies confirm concepts postulated from past experience and solidified the following procedure for soil-structure interaction (Heger 1988; ACPA 1996):

1) Loosely placed, uncompacted bedding directly under the invert of a pipe significantly reduces pressures on the pipe.
2) The soil in the haunch area from the foundation to the pipe springline provides significant support to the pipe and good compaction reduces earth pressures on the pipe.
3) The compaction level of the soil directly above the haunch, from the pipe springline to the top of the pipe grade level, has negligible effects on earth pressures on the pipe. Compaction of the soil in this area is not necessary unless required for pavement structures above.

4) Installation materials and compaction levels below the springline have a significant effect on strength requirements of the pipes.

This study confirms that the AASHTO standard installations provide an optimum range of soil-pipe interaction characteristics in the embankment installations consolidating the results of various theories and experimental and numerical studies available.

4.3 Soil-Structure Interaction

The primary aim of the soil-structure interaction analyses was to determine the earth load and pressure distribution, which is sensitively affected by bedding and sidefill treatment. As arching factors (vertical and horizontal) are the major parameters in the determination of the earth load exerted on concrete pipes, they were the primary objective of the refined soil-structure interaction analyses in this chapter.

4.3.1 Effects of Bedding and Sidefill Treatment

Distributions of radial pressure on round concrete pipes computed using SPIDA for AASHTO standard embankment installations are shown in Fig. 4.1. As can be seen from the figure, the pressure distributions for AASHTO type 1, 2, and 3 standard embankment installations are fairly close while AASHTO type 4 standard embankment installation exhibits a very sharp pressure increase at the invert. It is recalled that there is little or no control over either materials or compaction of bedding and sidefill for AASHTO type 4 standard embankment installation. The maximum fill height tables generated from both the results from FEA conducted in this study and ACPA show that differences in the maximum earth pressure in the critical haunch area are less than 5% for

pipes installed with AASHTO type 1, 2, and 3 standard embankment installations. Because of the seemingly indiscernible advantage of AASHTO type 1 and 2 standard embankment installations despite the highest construction quality and degree of inspection demanded, only the AASHTO type 3 standard embankment installation will be investigated in all subsequent comparative analyses. This observation has been transmitted to the Alabama Department of Transportation as a suggested revision in its State Specifications. It is noted in Fig. 4.1 that the maximum earth pressure on the pipe for AASHTO type 1, 2, and 3 standard embankment installations occurs at about 25 degrees from the invert. This differs from the Heger pressure distribution presented in AASHTO LRFD (2004a) **Figure 12.10.2.1-1**. The acute pressure increase at the invert for AASHTO type 4 standard embankment installation emphasizes the paramount importance of installing a treated bedding, at least marginally. AASHTO type 3 bedding would fit the bill at the least cost.

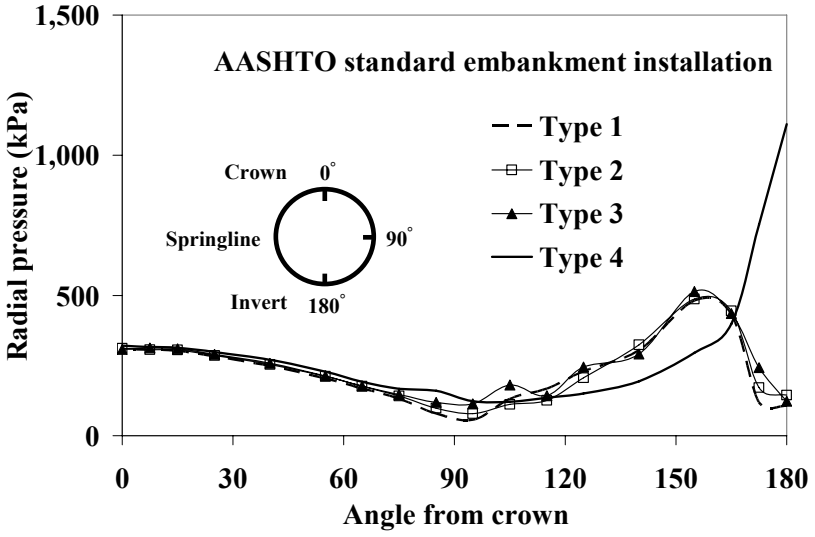

Fig. 4.1. Radial pressure distributions on pipe wall in AASHTO standard embankment installations (parameters: inside diameter of pipe= 1.8 m; backfill height= 12 m)

4.3.2 Arching Factors

For pipe installations with a vertical axis of symmetry, the law of statics (a hoop-tension analogy) requires that the total vertical earth load above the pipe springline be equal to twice the earth load thrust in the pipe wall at the springline. Similarly, the total horizontal earth load on one side of the pipe must be equal to the summation of horizontal thrusts in the pipe wall at the crown and at the invert. When analysis procedures other than FEM are used for buried pipes, it is convenient to define total vertical and horizontal earth loads on the pipe in terms of non-dimensional coefficients called the vertical and horizontal arching factors, *VAF* and *HAF*, respectively (AASHTO LRFD 2004a). The ACPA (1994) introduced the following equations to calculate these coefficients:

$$VAF = \frac{W_e}{PL} = \frac{2N_{sp}}{PL} \tag{4.2}$$

$$HAF = \frac{W_h}{PL} = \frac{N_c + N_i}{PL} \tag{4.3}$$

where PL = prism load; W_e = total vertical earth load; W_h = total horizontal earth load; N_{sp} = thrust in the pipe wall at the springline; N_p = thrust in the pipe wall at the crown; and N_i = thrust in the pipe wall at the invert.

Fig. 4.2 compares the AASHTO arching factors for AASHTO type 3 and 4 standard embankment installations to those developed analytically in this study with SPIDA and MSC/NASTRAN. AASHTO stipulates constant vertical arching factors of 1.4 (AASHTO type 3) and 1.45 (AASHTO type 4) and constant horizontal arching factors of 0.37 (AASHTO type 3) and 0.30 (AASHTO type 4) independent of backfill height. As shown in Fig. 4.2, the *VAF* computed with SPIDA and MSC/NASTRAN is

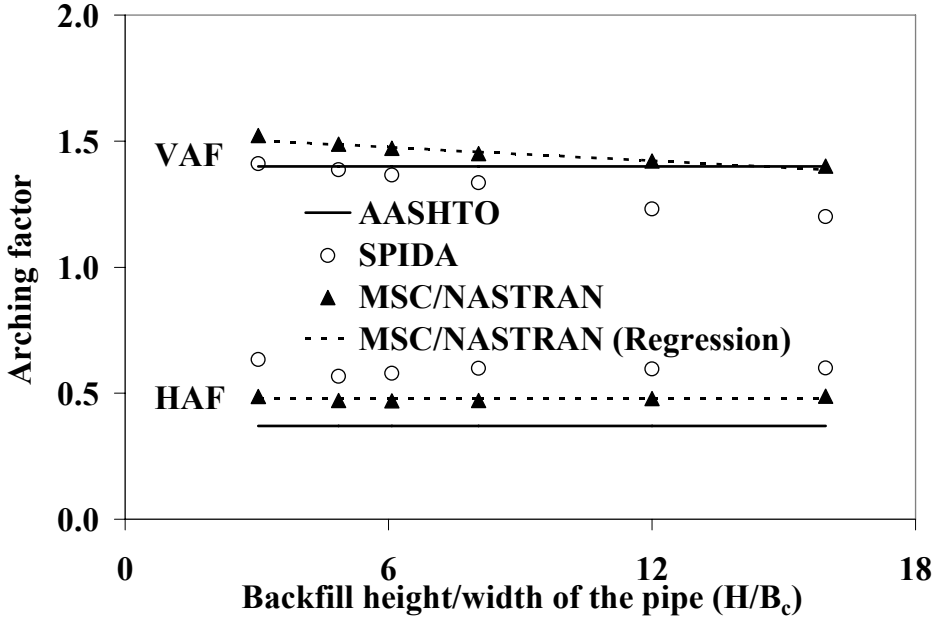

(a)

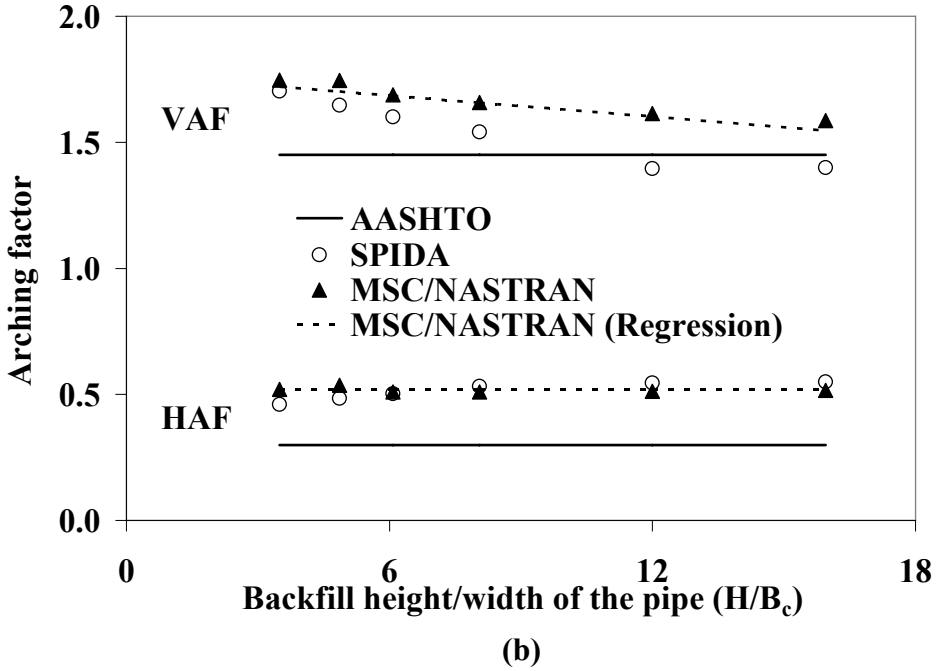

(b)

Fig. 4.2. Vertical arching factor (*VAF*) and horizontal arching factor (*HAF*) versus backfill height: (a) AASHTO type 3 standard embankment installation and (b) AASHTO type 4 standard embankment installation

affected by backfill height. In the case of AASHTO type 4 standard embankment installation, the *VAF* stipulated by AASHTO is approximately 8-17% less than that calculated by MSC/NASTRAN. The constant *HAF* for AASHTO type 3 and type 4 is approximately 23% and 43%, respectively, less than that evaluated by MSC/NASTRAN. This is noted as serious unconservative nature embedded in the current AASHTO stipulations. However, the *HAF* computed with SPIDA and MSC/NASTRAN does not vary appreciably with backfill height. An examination of Fig. 4.2 indicates that an approximate ratio of the vertical arching factors to the horizontal arching factors is 3.0 for type 3 bedding and 3.5 for type 4 in embankment installations.

More than 300 hypothetical models were run in order to collect data to formulate linear regression equations for the vertical arching factors of concrete pipes. Soil properties and compaction rates were varied with each bedding type in addition to backfill heights. An examination of the data collected from the series of model analyses reveals that the soil properties and the compaction rates had insignificant effects on the vertical arching factors, only the backfill height was retained in the recommended *VAF* predictor equations, Eqs. (4.4) and (4.5). The recommended *HAF* are 0.48 and 0.52, respectively, for AASHTO type 3 and type 4 standard embankment installations based on values computed by MSC/NASTRAN. As in the case of AASHTO provision, *HAF* does not vary along the fill height.

$$VAF = -0.009\frac{H}{B_c} + 1.53 \quad \text{for AASHTO type 3} \tag{4.4}$$

$$VAF = -0.014\frac{H}{B_c} + 1.77 \quad \text{for AASHTO type 4} \tag{4.5}$$

4.4 Imperfect Trench Installation

Fig. 4.3(a) shows a schematic for ITI as suggested by Marston (1922) and Spangler (1950a) and used by Vaslestad et al. (1993) and McAffee and Valsangkar (2005) in their field test programs. The geometry of the soft zone is controlled by three parameters: width, W; height, H_s; and the distance from the top of the pipe to the bottom of the soft zone, H'. Other pipe dimensions, B_c and t, were defined earlier in Fig. 3.7.

Based on a large number of parametric studies (over 1,000 cases), soft zone geometry I was identified to be the most effective in reducing the earth pressure. Fig. 4.3(b) describes this optimum geometry for the soft zone designated as geometry I. Vaslestad et al. (1993) also studied improved soft zone geometry, designated as geometry II, illustrated in Fig. 4.3(c). It was found that when soft zone are included, significantly

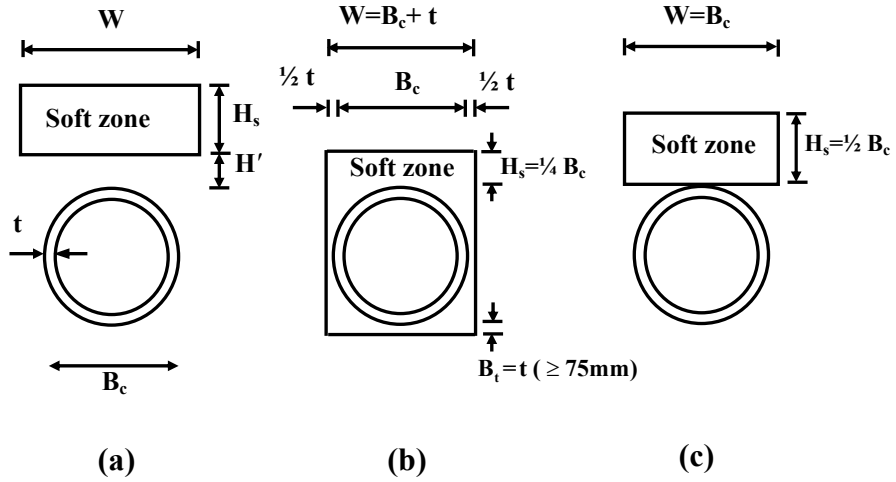

Fig. 4.3. Notation for imperfect trench installations and geometries of soft zone: (a) notation; (b) soft zone geometry I (proposed); and (c) soft zone geometry II (existing) (B_t = thickness of soft material below invert)

different patterns of shear stresses

were developed on the pipe sidewall due to an alteration of the soil movement relative to the pipe. In the case of the embankment installation without the soft zone, a positive frictional force (in the clockwise tangential direction) developed on the concrete pipe above the springline while a negative frictional force (in the counter-clockwise tangential direction) developed below the springline, as illustrated in Fig. 4.4. As these two frictional forces of opposite direction were nearly equal in magnitude, there was no significant axial force increase at the springline. It was discovered during this study that the effect of altered shearing stress pattern in the soft zone geometry II could be accounted for the increment of the axial force along the pipe wall as shown in Fig.4.4. Consequently, the total radial pressure distribution as presented in Fig. 4.5 shows not only high intensity but also significant variations along the pipe perimeter. The magnitude and variation in the total radial pressure is believed to be directly caused by the development of the frictional stress. For the soft zone geometry II, the radial pressure at about 25 degrees from the invert was significantly greater than that at the crown as shown in Fig. 4.5. An examination of Fig. 4.5 reveals that any amount of the earth pressure reduction gained by the soft zone geometry II would be eliminated entirely and then some. One effective measure found to remedy this undesirable frictional stress distribution in association with the soft zone was to extend the soft zone to the bedding as shown in Fig. 4.3(b) for soft zone geometry I. This discovery was largely based on a serendipity thinking process. The dramatic decrease in resulting frictional stress is shown in Fig. 4.4. This, then, results in significant decreases in the radial pressure on the pipe as

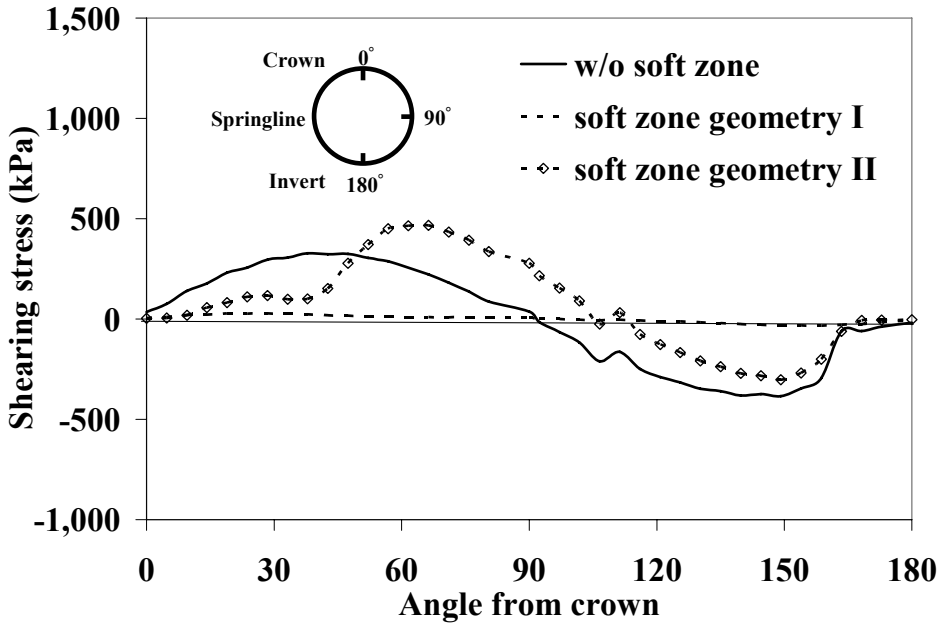

Fig. 4.4. Shearing stress development along the sidewall (parameters: inside diameter of pipe =1.8 m; backfill height=32 m; sidefill= AASHTO type 3)

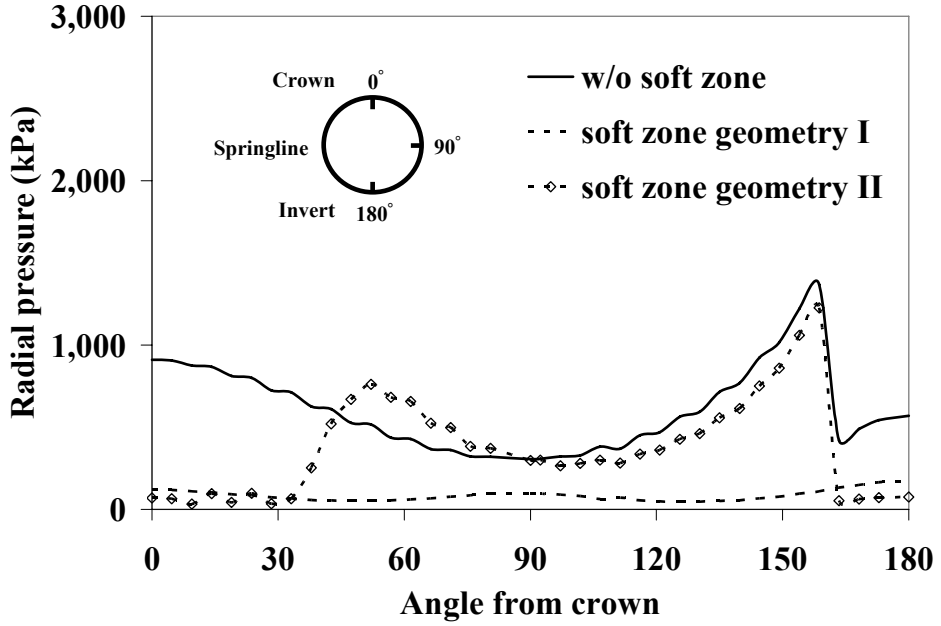

Fig. 4.5. Comparison of radial pressure distributions of embankment installation, soft zone geometry I, and soft zone geometry II (parameters: inside diameter of pipe =1.8 m; backfill height=32 m; sidefill= AASHTO type 3)

shown in Fig. 4.5. The superb reduction in the earth pressure on the pipe for the soft zone geometry I is quite evident.

The optimization of the soft zone geometry is illustrated in Fig. 4.6. It was found that the size of the soft zone affects the earth pressure reduction rates in the determination of *VAF* and *HAF*. As shown in Fig. 4.6(a), the reduction rate, R_v, (to be incorporated in *VAF*) remains virtually unchanged once the height of the soft zone divided by the outside diameter of the pipe reaches 0.25. The reduction rate, R_h, (to be incorporated in *HAF*) exhibits a slightly diminishing trend as the ratio of the height of the soft zone to the width of pipe increases. Fig. 4.6(b) gives the earth load reduction rate as a function of the width of the soft zone. An optimum width is selected to be the outside diameter plus the wall thickness of the pipe for soft zone geometry I as the curves show a typical diminishing return. It is noted that the lightweight material, geofoam (E_s = 345 kPa and ν = 0.1), was used in all model analyses shown in Fig. 4.6. An examination of Fig. 4.6 indicates that an average ratio of the vertical arching factors to the horizontal arching factors is 1.8 in ITI.

As the lightweight materials may take a variety of different forms, such an molded geofoam panels and/or cubes, loose polystyrene peanuts, etc., maintaining the optimum geometry of the soft material zone as shown in Fig. 4.3(b) will require careful construction procedures when loose polystyrene peanuts are used. A pre-molded geofoam appears to be an attractive construction scheme to consider. A few construction schemes have been discussed by Yoo et al. (2005).

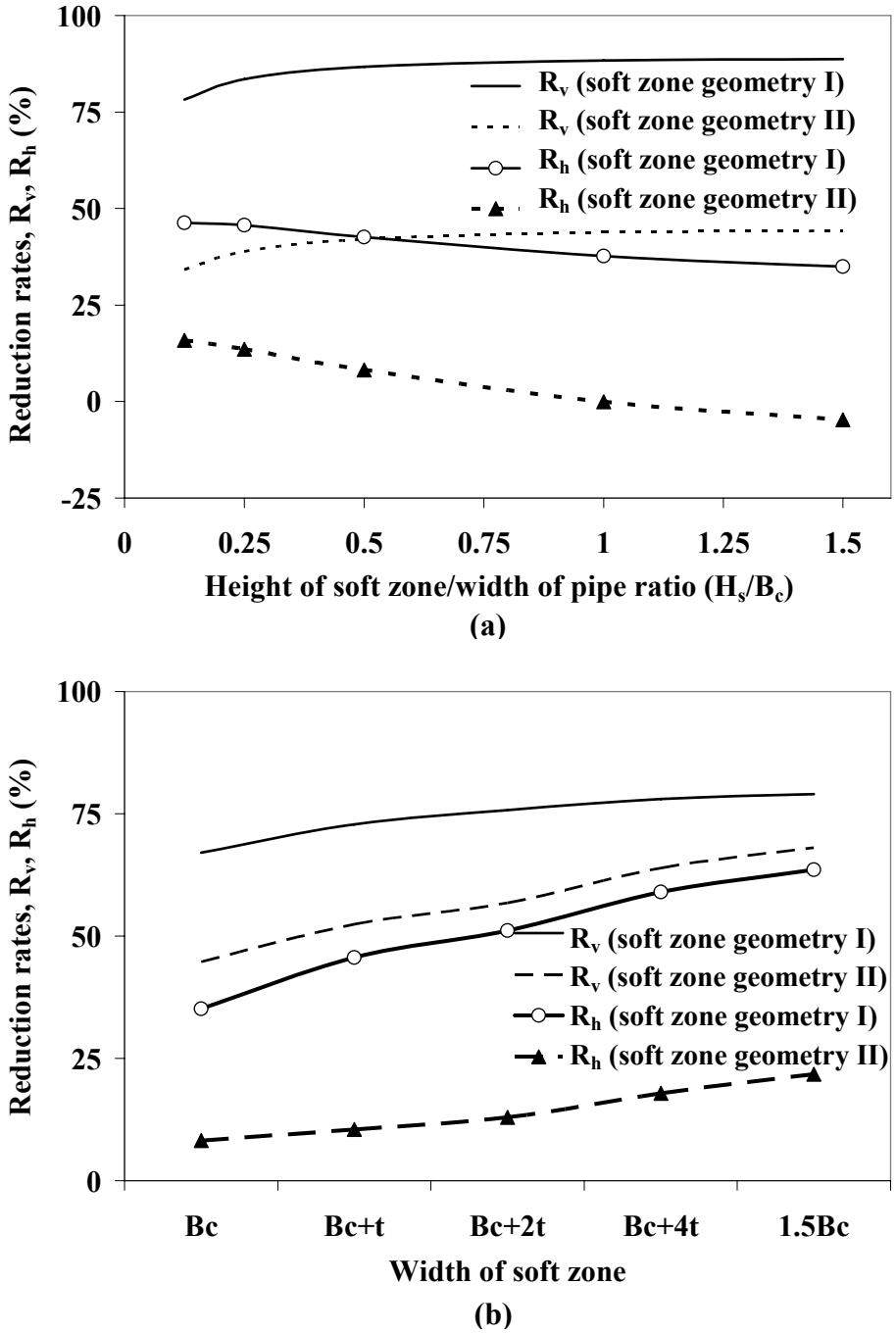

Fig. 4.6. Reduction rates (R_v, R_h) versus soft zone geometry I and geometry II: (a) effects of height of soft zone and (b) effects of width of soft zone (parameters: inside diameter of pipe =1.8 m; backfill height=32 m; sidefill= AASHTO type 3)

4.5 Predictor Equations

The geometry of the soft zone, the ratio of the fill height to the outside diameter of the pipe, and the modulus of elasticity (E_s) and Poisson's ratio of the lightweight materials were considered to be variables affecting the earth load reduction rate for ITI. After the two dominant geometric parameters were identified in Fig. 4.6, the remaining variables were varied. An examination of the analysis results revealed that the ratio of the fill height to the outside diameter of the pipe and Poisson's ratio of the lightweight materials did not greatly affect the earth load reduction rate. Therefore, these two variables were not considered further in the development of predictor equations. The synthesis of the numerical data indicated earth load reduction rates were most sensitive to the modulus of elasticity of the lightweight material. Fig. 4.7 shows the result of the linear regression analyses on the earth load reduction rate. As can be seen from Fig. 4.7, earth load reduction rates decrease as the modulus of elasticity of the lightweight material increases. Fig. 4.7 demonstrates that the lightweight material should be as soft as practically possible provided everything else remains largely unchanged: e.g., cost, the ease of construction, embankment performance.

Predictor equations for earth load reduction rates (R_v and R_h) associated with the optimum soft material zone geometry discovered were derived by a means of a linear regression method. As shown in Eqs. (4.6) and (4.7), the reduction rates are functions of the modulus of elasticity of the lightweight material only. In order to generate Eqs. (4.6) and (4.7), a total of approximately 1,000 models were analyzed.

$$R_v = 95.76 e^{-0.0003\, E_s} \tag{4.6}$$

$$R_h = 55.64\, e^{-0.0004\, E_s} \tag{4.7}$$

where R_v, R_h = vertical and horizontal arching factor reduction rates given in terms of percentage; E_s = modulus of elasticity of lightweight materials. Vertical and horizontal arching factors in ITI, therefore, are proposed to be calculated by Eqs. (4.8) and (4.9).

$$VAF_i = VAF\left(1 - R_v / 100\right) \tag{4.8}$$

$$HAF_i = HAF\left(1 - R_h / 100\right) \tag{4.9}$$

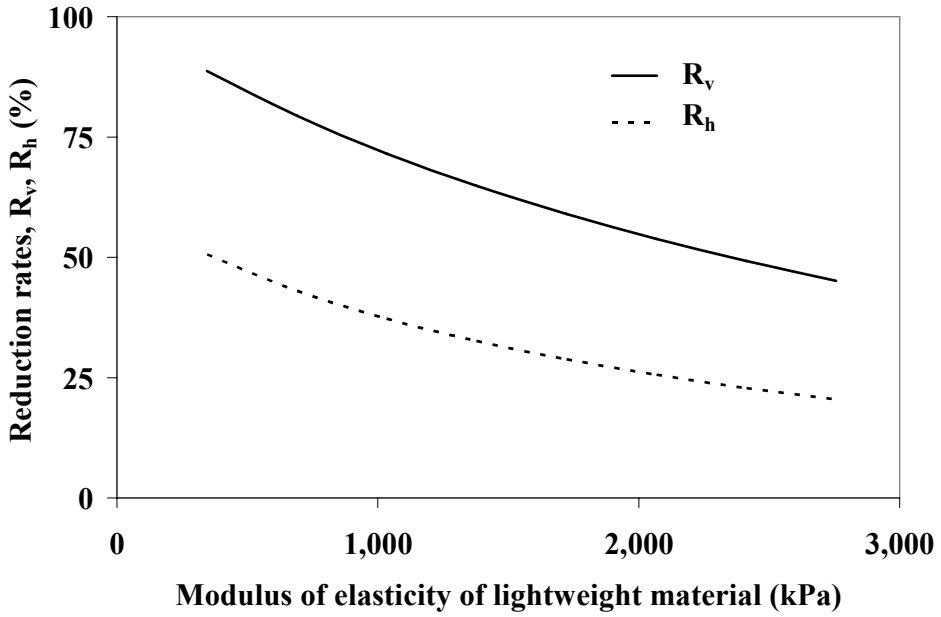

Fig. 4.7. Reduction rates (R_v, R_h) versus modulus of elasticity of material in soft zone geometry I

where VAF_i, HAF_i = vertical and horizontal arching factors in imperfect trench installation; VAF, HAF = vertical and horizontal arching factors given by Eqs. (4.4) and (4.5) and Fig. 4.2 for embankment installations. The reduction rate, R_h, may reach up to

50% of that determined from AASHTO type 3 and type 4 embankment installations as shown in Fig. 4.6(a).

As there are no specific guidelines available regarding Marston and Spangler's approach to the optimum soft zone geometry and material properties, it is not feasible to make a direct comparison of the earth pressure reduction rates. Nevertheless, an attempt was made to determine approximate pressure reduction rates by Marston and Spangler's approach by assuming parameters used in Marston and Spangler comparable to those used in the present study. The earth load reduction rates by Marston and Spangler's approach thus computed are approximately 40% less than those determined from Eqs. (4.6) and (4.7). A detailed description of the Marston and Spangler's approach in the determination of the reduction factors is included in Appendix 1.

4.6 Displacement of Soft Material Zone

Fig. 4.8 shows the profile of the vertical displacement at the top of the soft material zone. It is evident from Fig. 4.8 that the highly effective nature of geofoam (E_s = 345 kPa) for the earth pressure reduction is due to the relatively large displacement of the soft material. In the case of geofoam, the soft zone depth is reduced to one half of the original (unloaded) value.

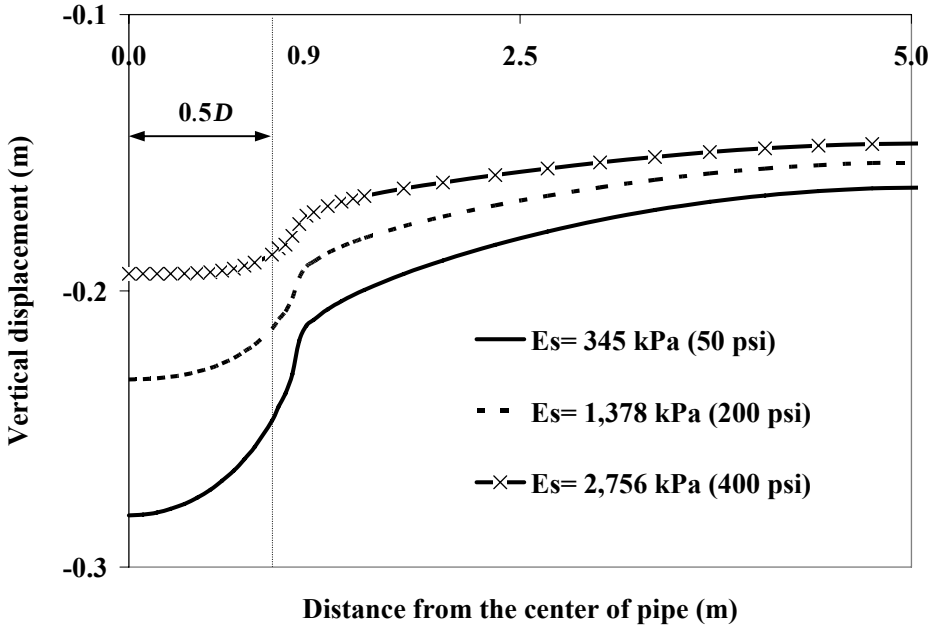

Fig. 4.8. Vertical displacement at the top of the soft material zone versus modulus elasticity of lightweight material (E_s) (parameters: pipe diameter= 1.8 m, fill height= 32 m)

CHAPTER 5

SOIL-STRUCTURE INTERACTION FOR BURIED CORRUGATED PVC PIPES

5.1 Introduction

The use of plastic pipes on federal-aided projects was once prohibited (Civil Connection 2006). As of December 15, 2006, the federal highway administration requires "equal consideration" in the specification of alternate pipe materials including plastic and corrugated aluminum. A few vendors offer a joint less plastic pipe installation for a considerable distance. With these recent developments, it is envisioned that the presence of corrugated PVC pipes in highway drainage structures will be dramatically increased.

Theoretical studies for designing buried flexible pipe were first performed by Spangler (1941). Watkins (1990; 2000) reported that the ratio of the vertical soil pressure to the horizontal soil pressure in flexible pipes is only on the order of 2.0 while it can be as high as 3.5 in rigid pipes in embankment installation. This value is close to that evaluated in Chapter 4 for the ratio of the vertical arching factors to the horizontal arching factors for type 4 bedding in embankment installations. This is the major difference between the behavior of rigid and flexible pipes. The mechanics of induced

small positive arching is illustrated in Fig. 5.1 where the deformation of the flexible pipe causes a redistribution of the earth load from the crown to the sides of the pipe.

This study presents the predictor equations for deflections and maximum wall stress as well as arching factors for the buried corrugated PVC pipes using the FEA for both the embankment installation and ITI. Values from these predictor equations are compared with those evaluated from the currently available predictor equations by AASHTO LRFD (2004a), Spangler (1941), and Burns and Richards (1964) for embankment installations.

The objective of this study to quantify the efficiency of ITI and the soil-structure interaction is extended to corrugated PVC pipes using the FEM. The properties of corrugated PVC pipes used in this study were taken from the AASHTO LRFD (2004a). An optimum geometry for the soft zone developed in Chapter 4 for rigid concrete pipes is re-examined herein whether any minor or major modifications are needed. Predictor

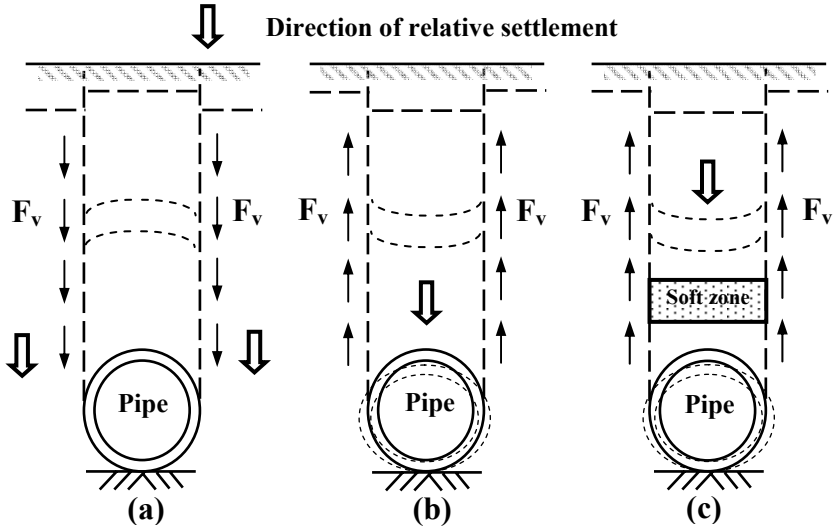

Fig. 5.1. Pressure transfer within a soil-pipe system: (a) rigid pipe in embankment installation; (b) flexible pipe in embankment installation; and (c) rigid or flexible pipe in imperfect trench installation (F_v = generated friction forces or shear stresses)

equations for the reduction rates of arching factors, deflections, and maximum wall stresses are proposed as a function of the modulus of elasticity of the lightweight material.

5.2 Background

5.2.1 Vertical Arching Factors

Burns and Richard (1964) first provided theoretical solutions for vertical load on an elastic circular conduit buried in an isotropic, homogeneous infinite elastic medium, with uniformly distributed pressure acting on horizontal planes at an infinite distance. According to Burns and Richard, *VAF* are as follows:

For full-bond interface

$$VAF = 0.714 - 0.714\left(\frac{S_H - 0.7}{S_H + 1.75}\right) + \left(\frac{1.143 + 0.054 S_B}{2.571 + 0.572 S_H + 0.163 S_B + 0.039 S_B S_H}\right) \tag{5.1}$$

For free-slip interface

$$VAF = 0.81 - 0.714\left(\frac{S_H - 0.7}{S_H + 1.75}\right) + 0.095\left(\frac{27.31 - S_B}{16.81 + S_B}\right) \tag{5.2}$$

where

$$S_H = \frac{M_S R}{E_P A_P} \tag{5.3}$$

$$S_B = \frac{M_S R^3}{E_P I} \tag{5.4}$$

where S_H = hoop stiffness parameter; M_S = one-dimensional constrained soil modulus; R = pipe radius; E_P = modulus of elasticity of pipe material; A_P = area of pipe wall per unit length; S_B = bending stiffness parameter; and I = moment of inertia of cross section of the pipe wall per unit length.

McGrath (1998; 1999) consolidated Burns and Richard equations eliminating the interface parameter. The McGrath equations adopted by AASHTO LRFD (2004a) are as follows:

$$VAF = 0.76 - 0.71\left(\frac{S_H - 1.17}{S_H + 2.92}\right) \tag{5.5}$$

$$S_H = \phi_S \frac{M_S R}{E_P A_P} \tag{5.6}$$

where ϕ_S = resistance factor for soil stiffness (= 0.9).

The AASHTO LRFD equations incorporate only the hoop stiffness parameter (S_H), discarding the bending stiffness (S_B) parameters. However, field tests by Sargand and Masada (2003) showed that elastic solutions for accurately predicting vertical soil pressure at the crown required both hoop stiffness (S_H) and bending stiffness (S_B) parameters.

The constrained soil modulus (M_S) used in the elastic solutions by Burns and Richard and AASHTO LRFD reflects the effect of the change in soil stiffness that takes place with increasing depth of fill. A constrained soil modulus (M_S) can be determined by performing one-dimensional tests on representative soil samples at appropriate strain

levels. Representative constrained soil moduli (M_S) for this study were adopted from Table 12.12.3.4-1, AASHTO LRFD (2004a).

5.2.2 Deflections

Deflection and wall stress are primary performance parameters in the design of corrugated PVC pipe. Deflection is quantified by the ratio of the vertical decrease in diameter (Δ_y) to the pipe diameter (*D*). Spangler (1941; Watkins and Spangler 1958) developed the following semi-empirical Iowa formula for calculating the deflection of flexible pipes under earth load:

$$\frac{\Delta_y}{D}(\%) = \left(\frac{K_b q D_L}{E_P I_P / R^3 + 0.061 E'} \right) \times 100 \tag{5.7}$$

where Δ_y = vertical decrease in diameter; D = pipe diameter; K_b = bedding factor; q = vertical stress (surface stress) on the pipe; D_L = deflection lag factor (dimensionless); and E' = modulus of soil reaction (passive pressure at haunch area). The Spangler equation needs properties such as the bedding factor (K_b), deflection lag factor (D_L), and modulus of soil reaction (E') which are generally determined by tests, and is therefore cumbersome to apply.

Burns and Richard (1964) provided the following theoretical solutions for deflections in addition to Eqs. (5.1) through (5.4) for vertical loads:

For full-bond interface

$$\frac{\Delta_y}{D}(\%) = \frac{q}{4M_s}\left[UF\left(1 - a_0^*\right) + VF\left(1 - a_2^* - 2b_2^*\right)\right] \times 100 \tag{5.8a}$$

For free-slip interface

$$\frac{\Delta_y}{D}(\%) = \frac{q}{4M_s}\left[UF\left(1-a_0^*\right)+\frac{2}{3}VF\left(1+a_2^{**}-4b_2^{**}\right)\right]\times 100 \tag{5.8b}$$

where

$$UF = 2B_k M_s R/(E_p A) \tag{5.8c}$$

$$VF = C_k M_s R^3/(3E_p I) \tag{5.8d}$$

$$a_0^* = \frac{UF-1}{UF+(B_k/C_k)} \tag{5.8e}$$

$$a_2^* = \frac{C_k(1-UF)VF - UF(C_k/B_k)+2B_k}{(1+B_k)VF + C_k(VF+1/B_k)+2(1+C_k)} \tag{5.8f}$$

$$a_2^{**} = \frac{2VF-1+(1/B_k)}{2VF-1+(3/B_k)} \tag{5.8g}$$

$$b_2^* = \frac{(B_k + C_k \times UF)VF - 2B_k}{(1+B_k)VF + C_k(VF+1/B_k)UF + 2(1+C_k)} \tag{5.8h}$$

$$b_2^{**} = \frac{2VF-1}{2VF-1+(3/B_k)} \tag{5.8i}$$

where UF = extensional flexibility ratio; VF = bending flexibility ratio; B_k = nondimensional parameter $=(1+K_s)/2$; C_k = nondimensional parameter $=(1-K_s)/2$; K_s = lateral stress ratio $=\nu/(1-\nu)$; and ν = Poisson's ratio of soil.

5.3 Soil-Structure Interaction

5.3.1 Corrugated PVC Pipe versus Concrete Pipe

Whether a pipe is considered to be flexible or rigid depends on the pipe stiffness relative to the stiffness of the surrounding soil (McGrath 1999). Fig. 5.1 illustrates how the pressure transfer within a soil-structure system is different according to the relative stiffness between the pipe and the surrounding soil. The earth load on a rigid pipe in an embankment installation is larger than the prism load above the pipe. Downward frictional force develops along the sides of the soil prism as differential settlement occurs, as illustrated in Fig. 5.1(a). The earth load on a flexible pipe will be less than the prism load due to the upward frictional force that develops along the sides of the soil prism, as shown in Fig. 5.1(b).

5.3.2 Finite Element Modeling

The PVC has stress-strain relationships that are nonlinear and time dependent. The initial modulus of elasticity (E_{ini} , short-term), minimum 50-year modulus of elasticity (E_{50}, long-term), Poisson's ratio (ν), and unit weight (γ) of PVC materials were taken to be 2.75 GPa (400 ksi), 0.96 GPa (140 ksi), 0.30, and 9.3 kN/m^3 (59 pcf), respectively, from AASHTO LRFD (2004a).

Kim and Yoo (2002; 2005) and McVay (1982) reported that the effect of interface behavior was insignificant for soil-structure interaction of rigid conduits. Sargand et al. (2002) installed and monitored the response of 18 deeply buried thermoplastic pipes. The field study by Sargand et al. (2002) showed that the loads on corrugated PVC pipes

were predicted more closely by the full-bond interface model. As will be shown later, however, the vertical arching factors, *VAF* , of flexible conduits appear to be significantly affected by the assumed interface conditions. In order to clarify the effects of the interface conditions for the corrugated PVC pipes, this study examined three interface conditions: full-bonded (with a coefficient of friction equal to infinity), frictional slip (with a coefficient of friction equal to 0.5), and free-slip (with a coefficient of friction equal to zero).

5.3.3 Effects of Sidefill Material Properties

It is acknowledged and this study confirms that the surrounding sidefill (haunch area and lower side) for a flexible pipe provides considerable support. Therefore, if the sidefill is uncompacted, the support becomes weak. Fig. 5.2 shows that the sidefill of gravelly sand (SW90 or SW95) (gravelly sand compacted to 90% or 95% of maximum density per AASHTO (2002)) is more efficient than that of silty sand (ML90 or ML95) or silty clay (CL90 or CL95) in reducing the earth load on the pipe. This is due to the higher value of the modulus of soil reaction of gravelly sand than that of silty sand and/or silty clay as evidenced in Eq. (5.7). AASHTO LRFD (2004b) specifies gravelly sand of SW90 as a minimum requirement of backfill materials for corrugated PVC pipes.

The numerical analyses in this study were executed using several different compaction values including the SW90. However, in the comparative study with AASHTO LRFD (2004a), analysis data from the AASHTO LRFD compaction rate of SW90 was used.

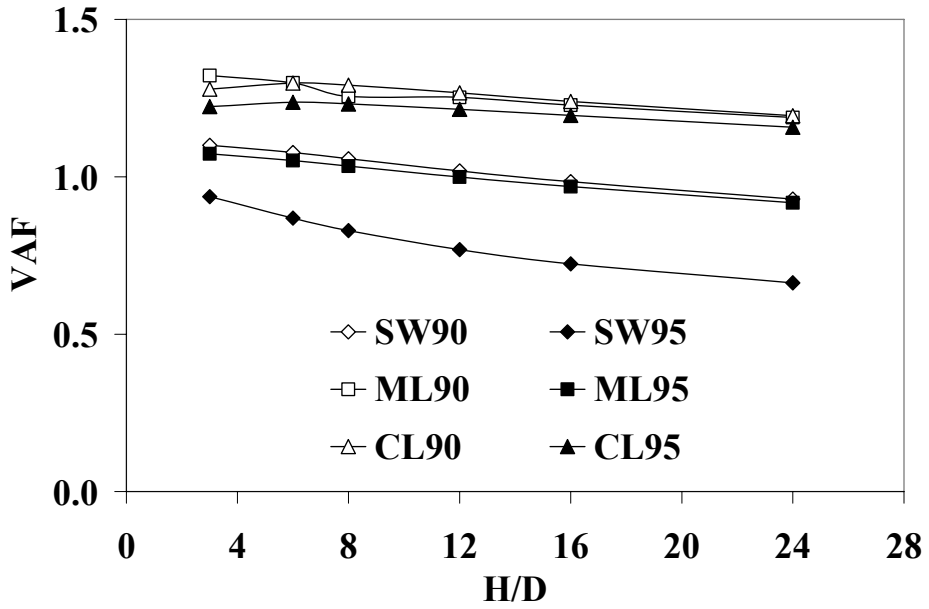

(a)

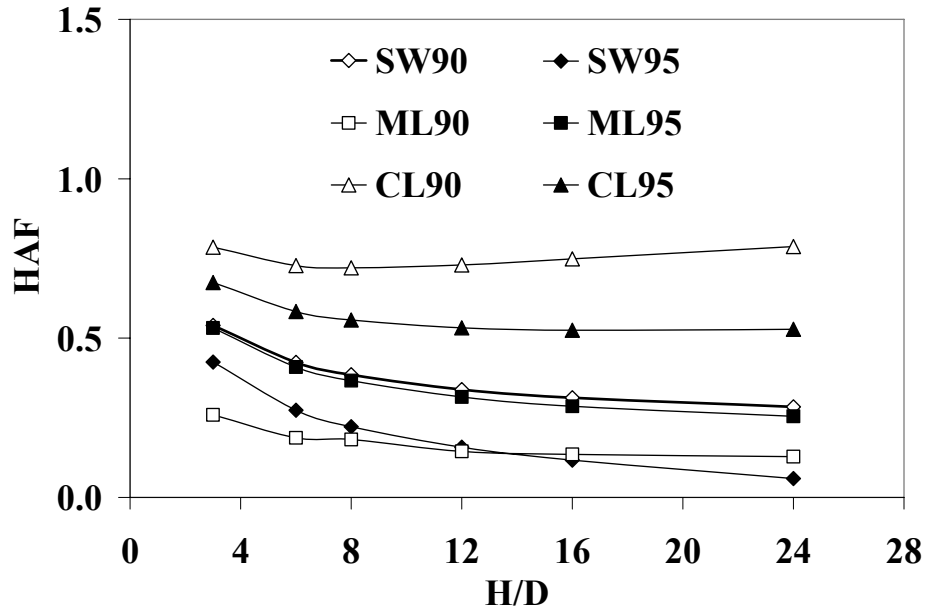

(b)

Fig. 5.2. Effects of the properties of backfill material: (a) *VAF* versus *H/D* and (b) *HAF* versus *H/D*

5.3.4 Effects of Interface Conditions and Time-Dependent Properties

Values determined from FEA were compared (Fig. 5.3) with those obtained from equations by Burns and Richard (1964) and AASHTO LRFD (2004a). Fig. 5.3 shows that the arching factors were affected by *H/D*, interface conditions, and the time-dependent material properties of corrugated PVC pipes. Deflections, however, were hardly affected by interface conditions and time-dependent material properties. Fig. 5.3 indicates the following trends:

1) In the case of *VAF* for short-term properties, the FEA showed that the *VAF* by ABAQUS for the full-bonded interface conditions are in good agreement with those by the AASHTO LRFD equations where the interface conditions were not included. The *VAF* by ABAQUS and AASHTO LRFD range between those by Burns and Richard computed for full-bonded and free-slip interface conditions.
2) In the case of *VAF* for long-term properties, the *VAF* by ABAQUS under full-bonded interface condition are fairly close to those by the Burns and Richard equation under the free-slip interface condition.
3) The *VAF* by ABAQUS decrease slightly as the ratio of the fill height to the pipe diameter (*H/D*) increases.
4) The *VAF* by ABAQUS under frictional slip and free-slip interface conditions are 25% and 45% less, respectively, than those under the full-bonded interface condition. The *VAF* by Burns and Richard under the free-slip interface condition are 26% less than *VAF* under the full-bonded interface condition.

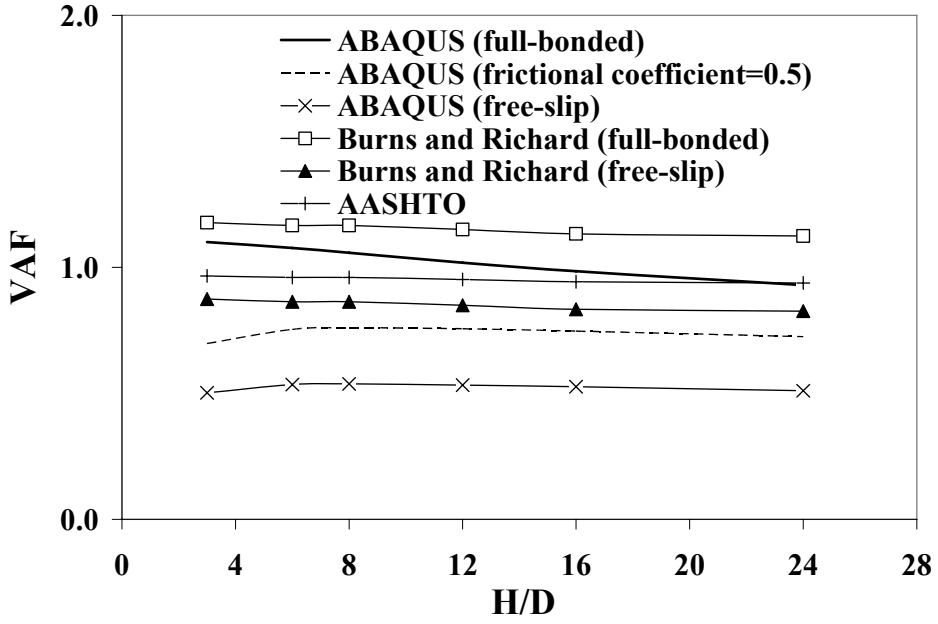

(a)

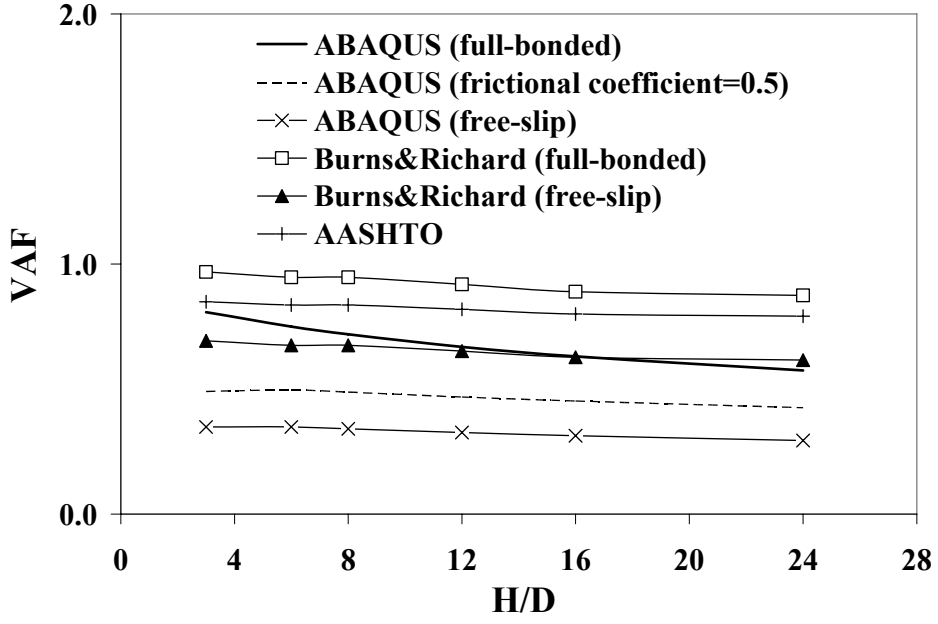

(b)

Fig. 5.3. Finite element analyses versus current design equations: (a) *VAF* versus *H/D* (short-term) and (b) *VAF* versus *H/D* (long-term) (parameters: pipe diameter = 0.6 m) (continued)

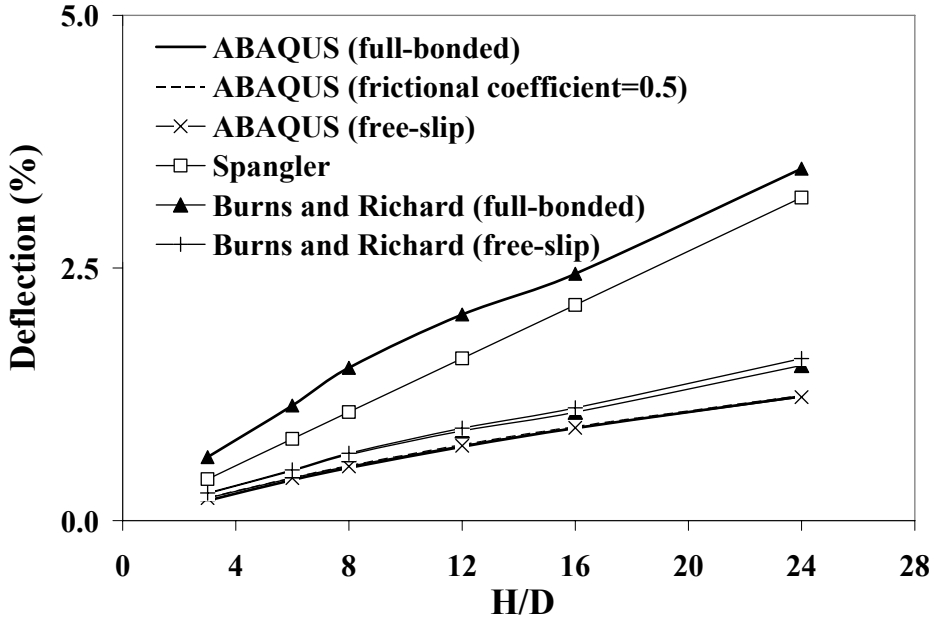

(c)

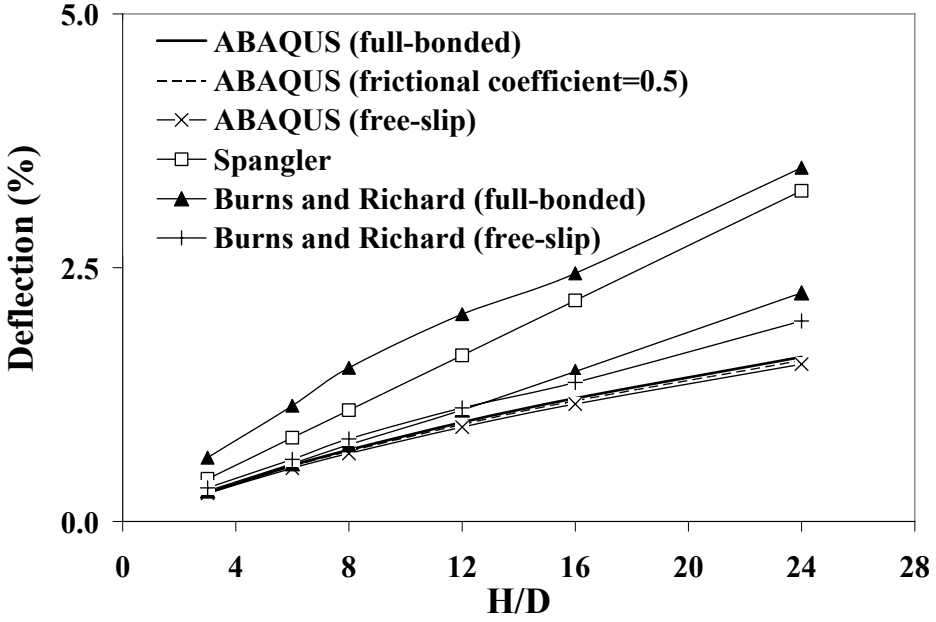

(d)

Fig. 5.3. Finite element analyses versus current design equations: (c) deflection versus *H/D* (short-term) and (d) deflection versus *H/D* (long-term) (parameters: pipe diameter = 0.6 m; deflection lag factor (D_L) = 1; bedding factor (K_b) = 0.1)

Although the interface effect on *VAF* in flexible conduits is fairly significant, the degree of the interface effect cannot be determined by analysis alone. A well-designed field testing program is needed to answer this question. A conservative approach of full bond is an intermediate option.

5) The deflections from ABAQUS were much less than those computed with the Spangler equation (1941) while they were relatively close to those from the Burns and Richard (1964) deflection equations, as shown in Figs. 5.3(c). The results from the ABAQUS and Burns and Richard deflection equations also showed that the interface conditions have insignificant effects on the deflections of corrugated PVC pipes. This observation is attributable to the fact that the deflection is primarily controlled by the earth pressure at the crown, which is not sensitively affected by the interface conditions, while *VAF* in flexible conduits are measured as the sum of the axial stress and the bending stress at the springline where the interface conditions play an important role.

5.4 Imperfect Trench Installation

5.4.1 Optimization of Soft Zone Geometry

The soft zone geometry is controlled by three parameters: width, W; height, H_s; and the distance from the top of the pipe to the bottom of the soft zone, H' (Fig. 5.4(a)). Fig. 5.4(a) shows a schematic for an ITI as suggested by Spangler (1950a) and Vaslestad et al. (1993). Vaslestad et al. (1993) also studied an optimum geometry for ITI as

shown in Fig. 5.4(c) in addition to that shown in Fig. 5.4(a). As was discussed in Chapter 4 of this dissertation, the soft zone geometry II shown in Fig. 5.4(c) incurs an unexpectedly large frictional stress development along the side of the conduit. Based on a large number of parametric studies (over 1,000 cases), soft zone geometry I, as shown in Fig. 5.4(b), was identified to be the most effective in reducing the earth pressure. It is noted that the optimum soft zone geometry I shown in Fig. 5.4(b) differs slightly from that shown in Fig. 4.3(b). As the plastic pipe diameters are relatively small, the minimum thickness of the soft zone at the side and bottom is represented in terms of the pipe diameter, whereas it was specified in terms of the pipe wall thickness in the case of concrete pipes.

Justification for the optimized soft zone geometry I given by Fig. 5.4(b) is given in Fig. 5.5. As shown in Fig. 5.5(a), the reduction rate, R_{ms}, (to be incorporated in maximum wall stress) remains virtually unchanged once the height of the soft zone divided by the outside diameter of the pipe reaches 0.25.

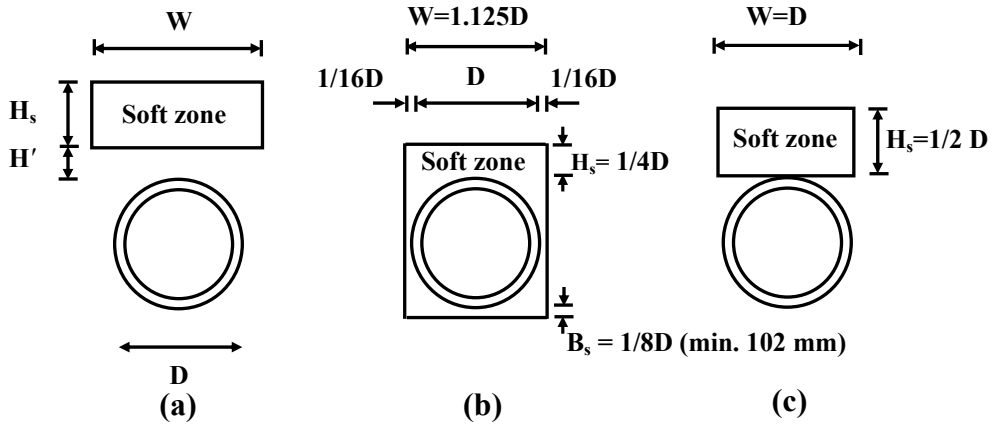

Fig. 5.4. Notation for imperfect trench installations and geometries of soft zone: (a) notation; (b) soft zone geometry I (proposed); and (c) soft zone geometry II (tried by Spangler (1950a) and Vaslestad et al. (1993))

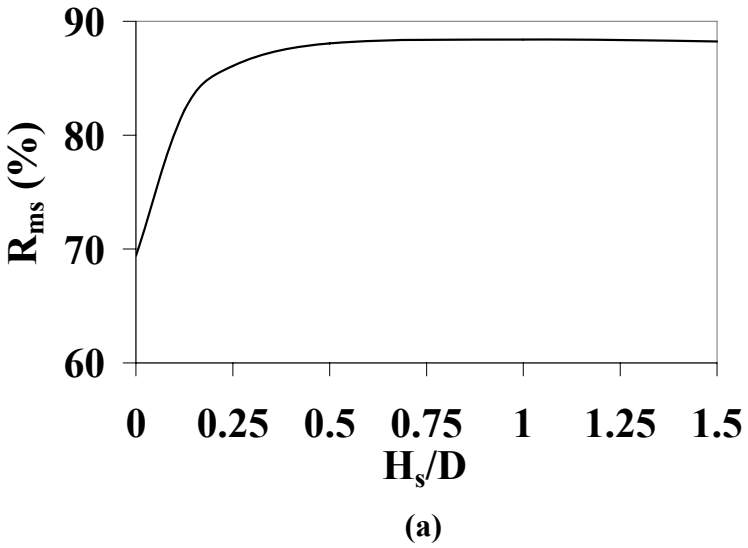

(a)

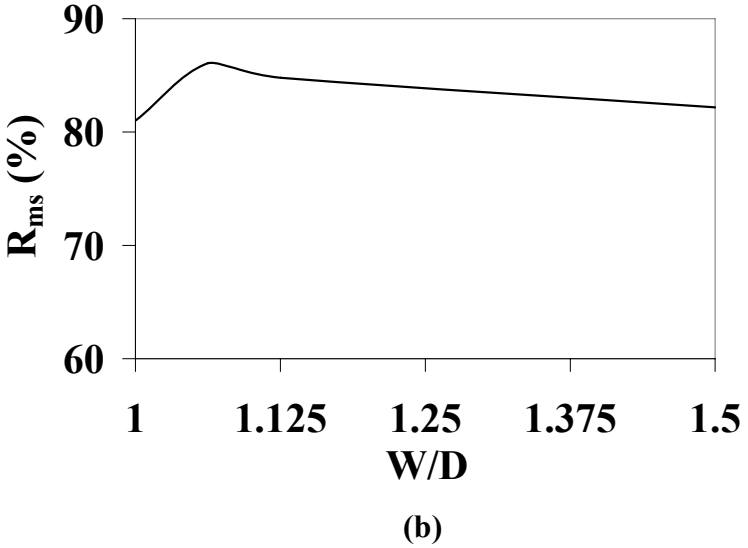

(b)

Fig. 5.5. Optimization process of soft zone geometry I: (a) height of soft zone (H_s) with W / D = 1.125 and B_s / D = 0.125 and (b) width of soft zone (W) with H_s / D = 0.25 and B_s / D = 0.125 (R_{ms} = reduction rate of maximum wall stress) (continued)

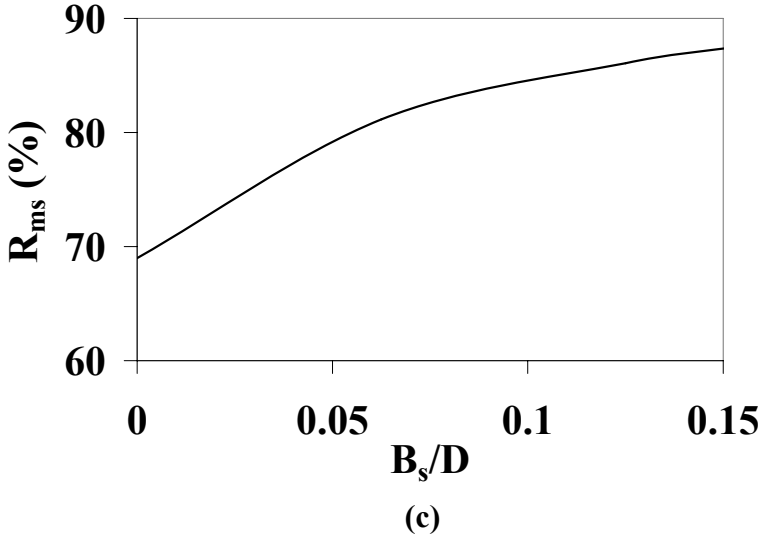

Fig. 5.5. Optimization process of soft zone geometry I: (c) bedding thickness of soft zone (B_s) with $H_s / D = 0.25$ and $W / D = 1.125$ (R_{ms} = reduction rate of maximum wall stress)

Fig. 5.5(b) gives the same reduction rate as a function of the width of the soft zone. As can be seen from Fig. 5.5(b), the maximum reduction rate of the pipe wall stress occurs when the width of the soft material zone is slightly wider than the pipe diameter. This occurrence is due to the loss of lateral support by the sidefill in the case of flexible conduits, thereby increasing the bending moment at springline. It is recalled that the reduction rate continues to increase as the width of the soft zone increases in the case of rigid conduits where lateral support by the sidefill is not important to maintain the conduit geometry. As can be seen from Fig. 5.6(b), there must be a soft material zone around the springline in order to avoid the development of high shear. At the same time, the width of the soft material zone needs to be slightly larger than the diameter as shown in Fig. 5.4(b). An optimum compromise for these seemingly reverse trends is reached when the width of the soft material zone is taken to be the pipe diameter plus 1/8 times the pipe diameter, D. Bedding thickness of 1/8 D is recommended as the curve in Fig. 5.4(c) shows only slightly larger reduction rates (R_{ms}) for the ratio of bedding thickness to pipe diameter (B_s / D) greater than 1/8. Fig. 5.6 shows that the optimum soft zone geometry I is highly effective in reducing the earth pressure on corrugated PVC pipes. As the lightweight material, geofoam (E_s = 345 kPa and ν = 0.1) was used in all model analyses shown in Figs. 5.5 and 5.6.

5.4.2 Imperfect Trench Installation versus Embankment Installation

McAffee and Valsangkar (2005) confirmed higher-than-expected lateral pressures on the pipe with ITI in the case of concrete pipes. Their data show a redistribution of the

earth load from the crown to the sides of the concrete pipe resulting in a slightly higher lateral pressure on the pipe at the springline. As shown in Fig. 5.6(b), it was found that, when soft zones are included, significantly different patterns of shear stresses were developed on the pipe sidewall due to an alteration of the soil movement relative to the pipe. In the case of the embankment installation, a positive frictional force (in the clockwise tangential direction) developed on corrugated PVC pipes above the springline while a negative frictional force (in the counter-clockwise tangential direction) developed below the springline, as shown in Fig. 5.6(b). As these two frictional forces of opposite direction were nearly equal in magnitude, there was no significant axial force increase at the springline of the pipe, as shown in Fig. 5.6(b). It is recalled that the increment of the axial force along the pipe wall is indeed equal to the frictional force developed due to the alteration of soil movement. For soft zone geometry II as shown in Fig. 5.4(c), the radial pressure at about 25 degrees from the invert was significantly larger than that at the crown, as shown in Fig. 5.6(a). One effective measure found to remedy this undesirable frictional stress distribution was to extend the soft zone to the bedding as shown in Fig. 5.4(b). The resulting frictional stress is dramatically decreased as shown in Fig. 5.6(b). This, in turn, significantly decreases the radial pressure on the pipe as shown in Fig. 5.6(a). The superb reduction in the earth pressure on the pipe for the proposed soft zone geometry I is evident.

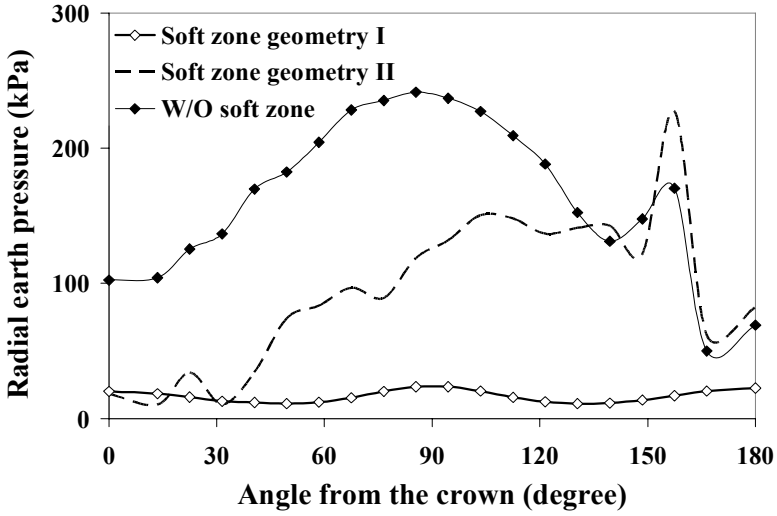

(a)

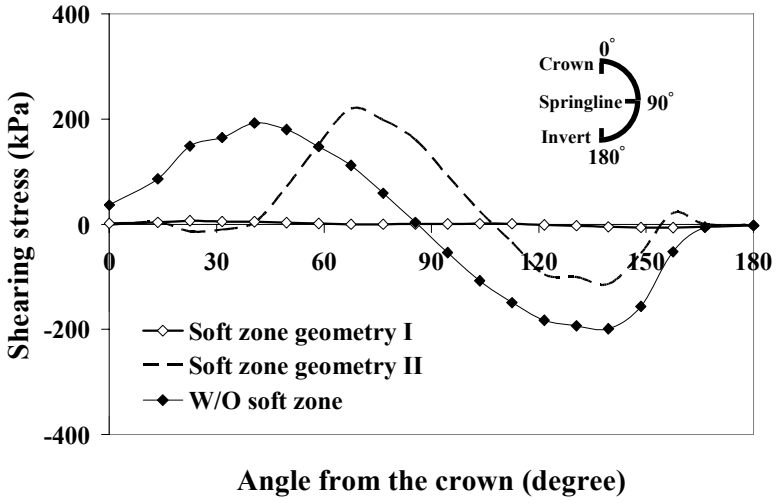

(b)

Fig. 5.6. Imperfect trench installations versus embankment installation: (a) radial earth pressure and (b) frictional stress (parameters: pipe diameter = 0.6 m; short-term material properties; fill height = 15 m; modulus of elasticity of the lightweight material = 345 kPa) (continued)

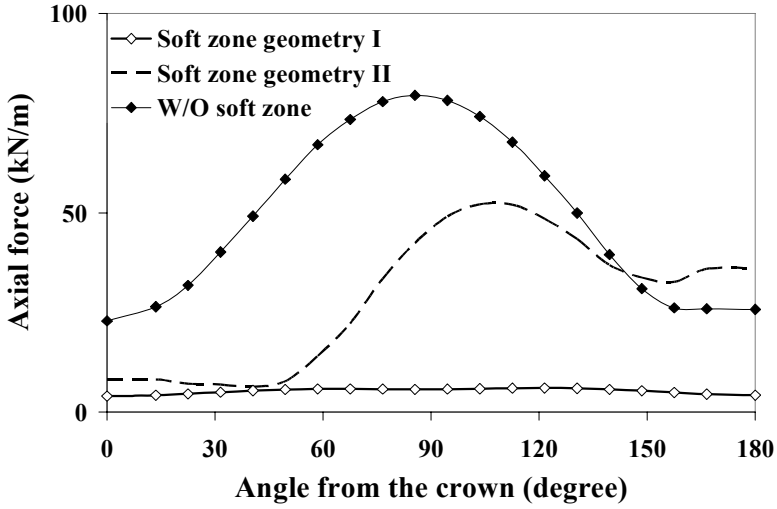

(c)

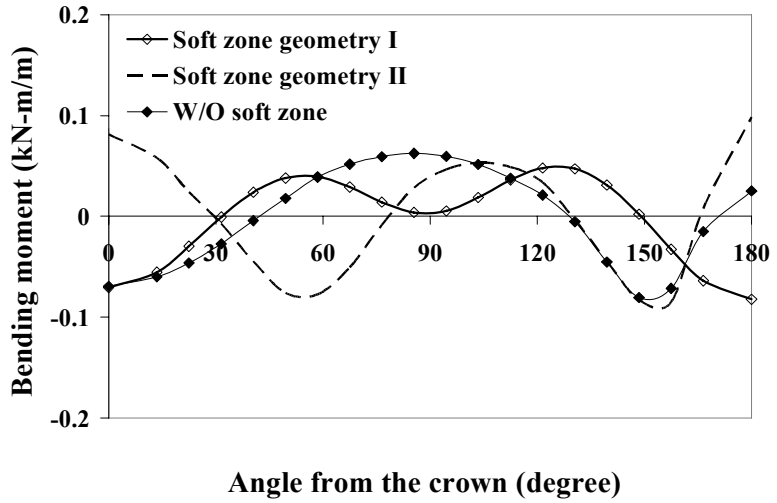

(d)

Fig. 5.6. Imperfect trench installations versus embankment installation: (c) axial force and (d) bending moment (parameters: pipe diameter = 0.6 m; short-term material properties; fill height = 15 m; modulus of elasticity of the lightweight material = 345 kPa) (continued)

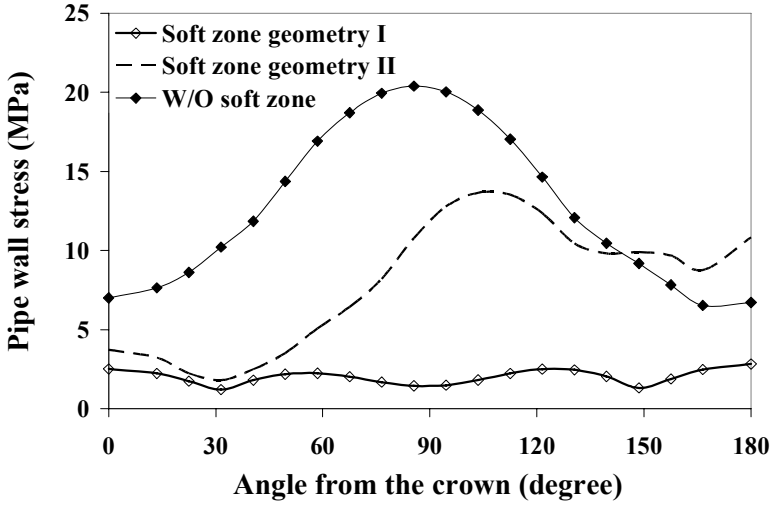

(e)

Fig. 5.6. Imperfect trench installations versus embankment installations: (e) pipe wall stress (parameters: pipe diameter = 0.6 m; short-term material properties; fill height = 15 m; modulus of elasticity of the lightweight material = 345 kPa)

5.5 Predictor Equations

5.5.1 Arching Factor, Deflection, and Maximum Wall Stress

More than 1,000 hypothetical models were run in order to collect data to formulate linear regression equations for the arching factors, deflections, and maximum wall stresses based on the full-bonded interface condition in embankment installations. Fig. 5.7 shows that the arching factors, deflections, and maximum wall stresses are affected by the ratio of the pipe diameter to radius of gyration (*D/r*) and time-dependent material properties as well as *H/D*. Therefore, *H/D*, *D/r*, and time-dependent material properties were retained for recommended arching factors and deflection predictor equations, Eqs. (5.9) through (5.12), based on values computed by ABAQUS. Following **Table A12-13**, AASHTO LRFD (2004a), values of *D/r* were varied between 60 and 100. The *D/r*, however, has insignificant effects on the maximum wall stresses. Hence, *D/r* is excluded from the predictor equation for maximum wall stresses as shown in Eq. (5.12).

$$VAF = \left[-0.008\frac{H}{D} + 1.124 \right] / \left(\frac{D}{77r} \right)^{0.538} \quad \text{for short-term material properties} \qquad (5.9a)$$

$$VAF = \left[-0.011\frac{H}{D} + 0.816 \right] / \left(\frac{D}{77r} \right)^{0.961} \quad \text{for long-term material properties} \qquad (5.9b)$$

$$HAF = 0.744\left(\frac{H}{D} \right)^{-0.310} / \left(\frac{D}{77r} \right)^{0.961} \quad \text{for short-term material properties} \qquad (5.10a)$$

$$HAF = 0.578\left(\frac{H}{D} \right)^{-0.489} / \left(\frac{D}{77r} \right)^{1.782} \quad \text{for long-term material properties} \qquad (5.10b)$$

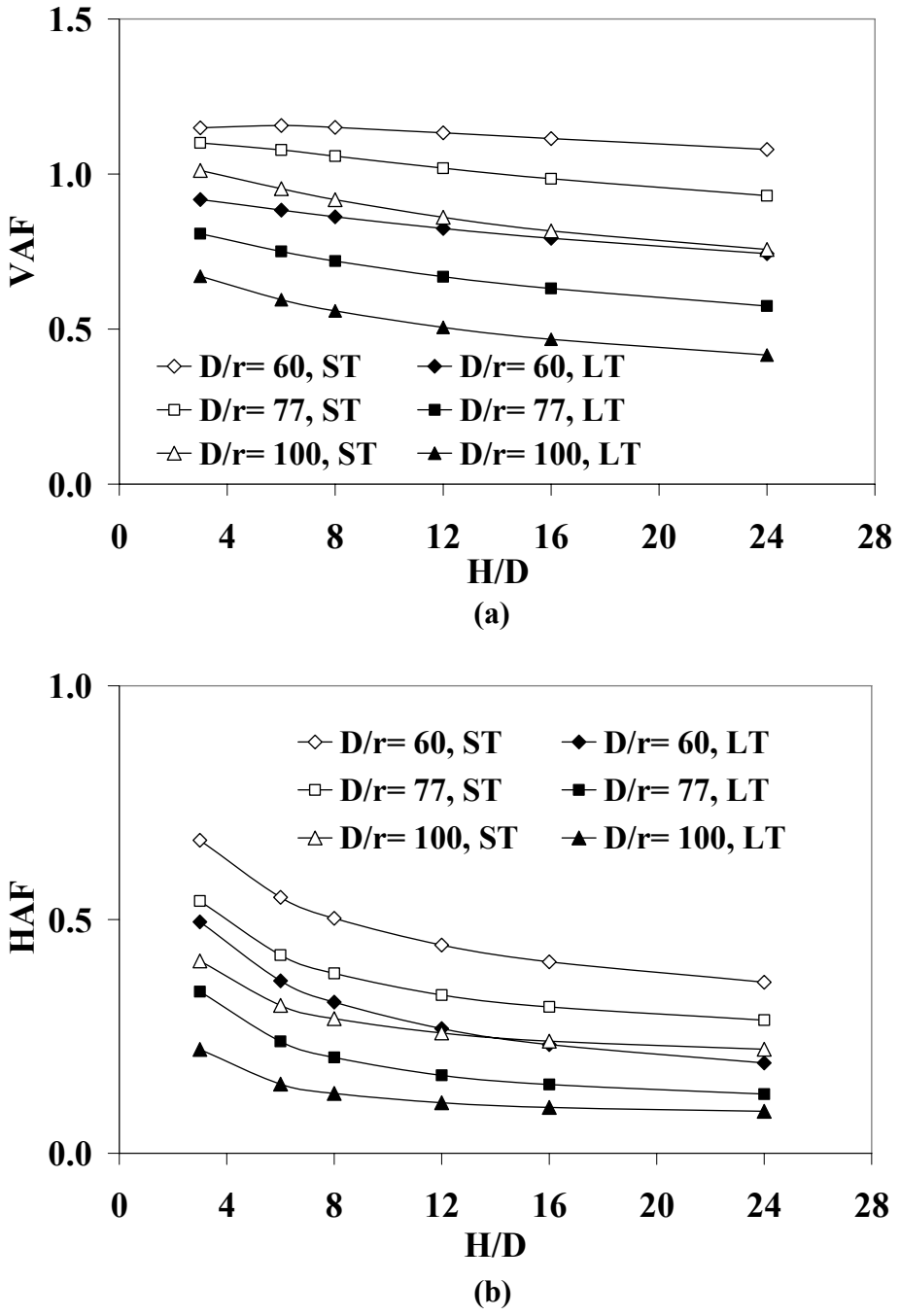

Fig. 5.7. Predictor equations of arching factors, deflection, and soil-structure interaction multiplier (F_{ms}) for maximum wall stress: (a) *VAF* and (b) *HAF* (*D* = pipe diameter; *r* = radius of gyration of corrugation; *ST* = short-term material properties; *LT* = long-term material properties; modulus of elasticity of the lightweight material = 345 kPa) (continued)

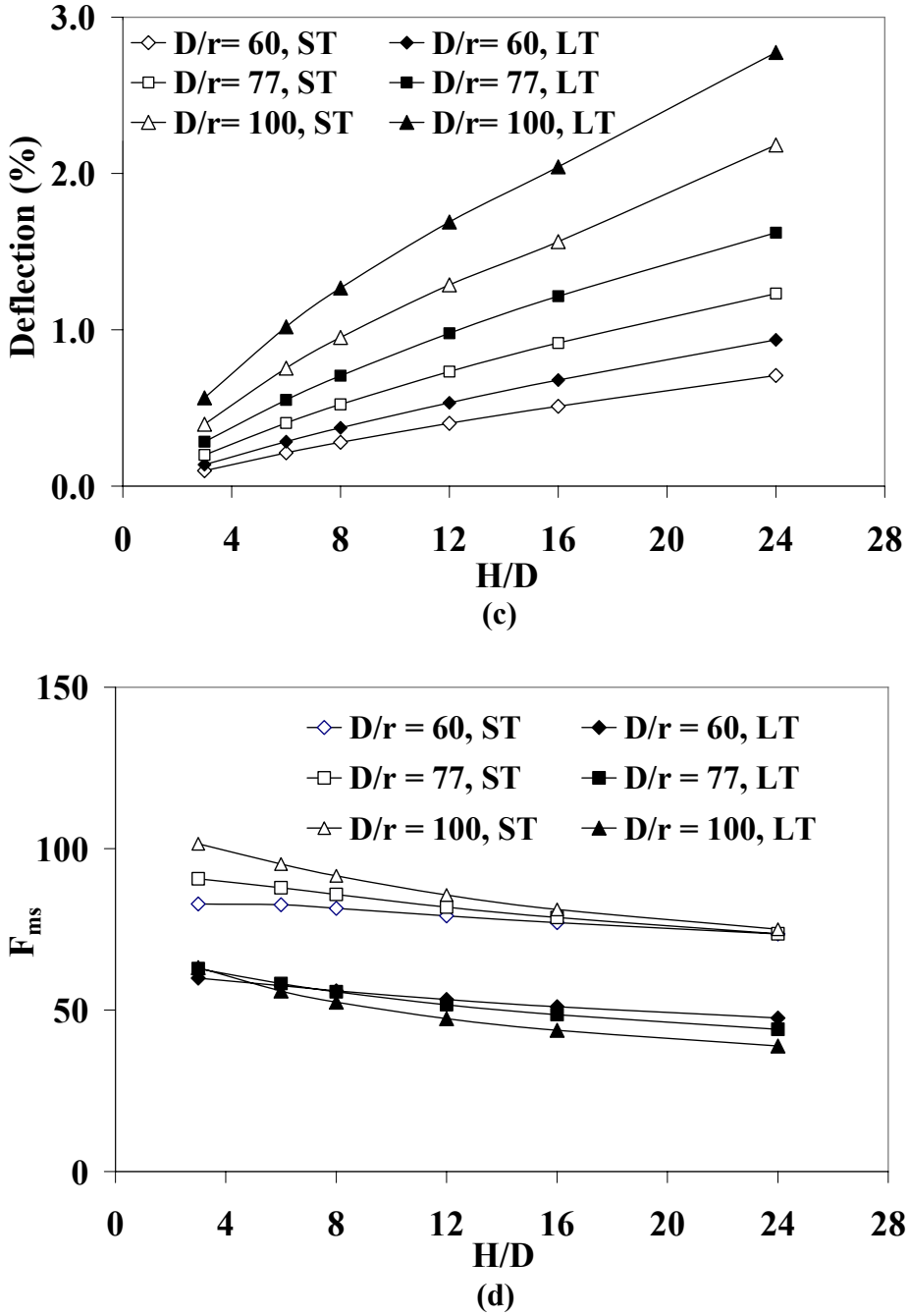

Fig. 5.7. Predictor equations of arching factors, deflection, and soil-structure interaction multiplier (F_{ms}) for maximum wall stress: (c) deflection and (d) F_{ms} (D = pipe diameter; r = radius of gyration of corrugation; *ST* = short-term material properties; *LT* = long-term material properties; modulus of elasticity of the lightweight material = 345 kPa)

$$\frac{\Delta_y}{D}(\%) = \left[0.049\frac{H}{D} + 0.110\right]\left(\frac{D}{77r}\right)^K \quad \text{for short-term material properties} \qquad (5.11a)$$

$$\frac{\Delta_y}{D}(\%) = \left[0.063\frac{H}{D} + 0.110\right]\left(\frac{D}{77r}\right)^K \quad \text{for long-term material properties} \qquad (5.11b)$$

$$K = \left(\frac{H}{D}\right)^{0.33} \qquad (5.11c)$$

$$F_{ms} = \left[-0.82\frac{H}{D} + 92.51\right] \quad \text{for short-term material properties} \qquad (5.12a)$$

$$F_{ms} = \left[-0.87\frac{H}{D} + 63.51\right] \quad \text{for long-term material properties} \qquad (5.12b)$$

where F_{ms} is the soil-structure interaction multiplier for maximum wall stresses. Maximum wall stresses, therefore, are calculated by Eq. (5.13).

$$\sigma_{\max} = F_{ms}\left(\frac{PL}{D}\right) \qquad (5.13)$$

5.5.2 Reduction Rates

It should be noted in Figs. 5.6(c) and 5.6(e) that the reduction rate of maximum wall stresses computed from the combined action of bending moment and axial force is 85%, although the reduction rate of the arching factors computed from the axial force alone reaches up to 92%. This reflects that the reduction rate related to bending moment is only 18%, as shown in Fig. 5.6(d). The geometry of the soft zone, *D/r*, *H/D*, time-dependent material properties, and the modulus of elasticity and Poisson's ratio of the lightweight materials are variables affecting the reduction rates of the arching factors, deflections, and maximum wall stresses in ITI. After the three dominant geometric

parameters of soft zone were identified as shown in Fig. 5.5, the remaining variables were varied in the production run of nearly 1,000 hypothetical models. An examination of the analysis results revealed that *D/r*, *H/D*, and Poisson's ratio of the lightweight materials hardly affect the reduction rate of arching factors, deflections, and maximum wall stresses. Therefore, these three variables were not considered further in the development of predictor equations. The analyses indicated the reduction rates for the arching factors, deflections, and maximum wall stresses were sensitive to the modulus of elasticity of the lightweight material. Time-dependent material properties had insignificant effects on the reduction rates of *VAF* , deflections, and maximum wall stress except those of *HAF* . Fig. 5.8 shows that the reduction rates for the proposed soft zone geometry I decrease as the modulus of elasticity of the lightweight material increases. This demonstrates that the lightweight material should be as soft (low modulus of elasticity) as practically possible.

Based on the data collected from a number of parametric studies, predictor equations for the reduction rates associated with the proposed soft zone geometry I were derived by a means of a linear regression method. It is noted that the modulus of elasticity of the lightweight material is the only variable as given in Eqs. (5.14a) through (5.14e).

$$R_v = \left[-0.015E_s + 91.74\right] \tag{5.14a}$$

$$R_{hs} = \left[7\times10^{-6}E_s{}^2 - 0.047E_s + 96.34\right] \tag{5.14b}$$

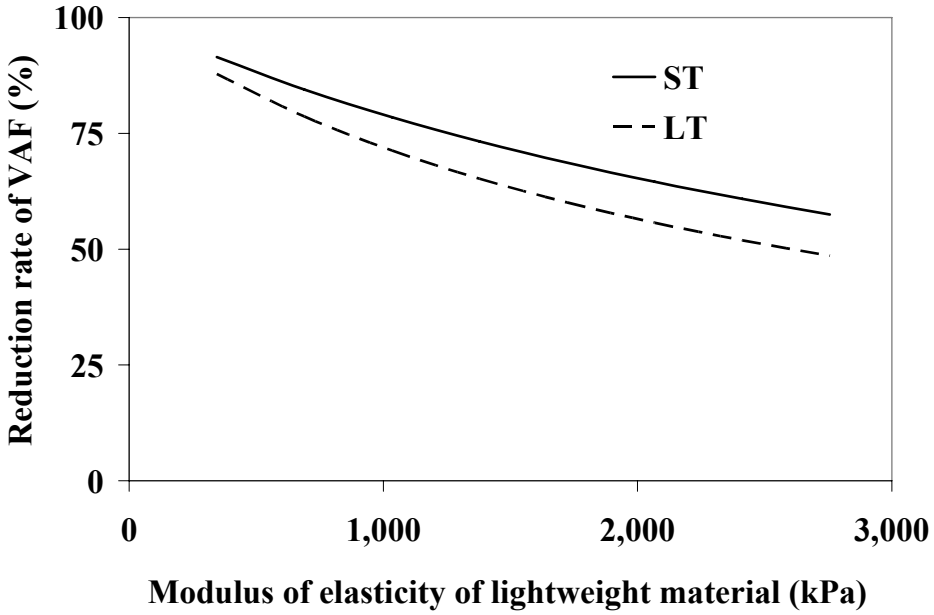

(a)

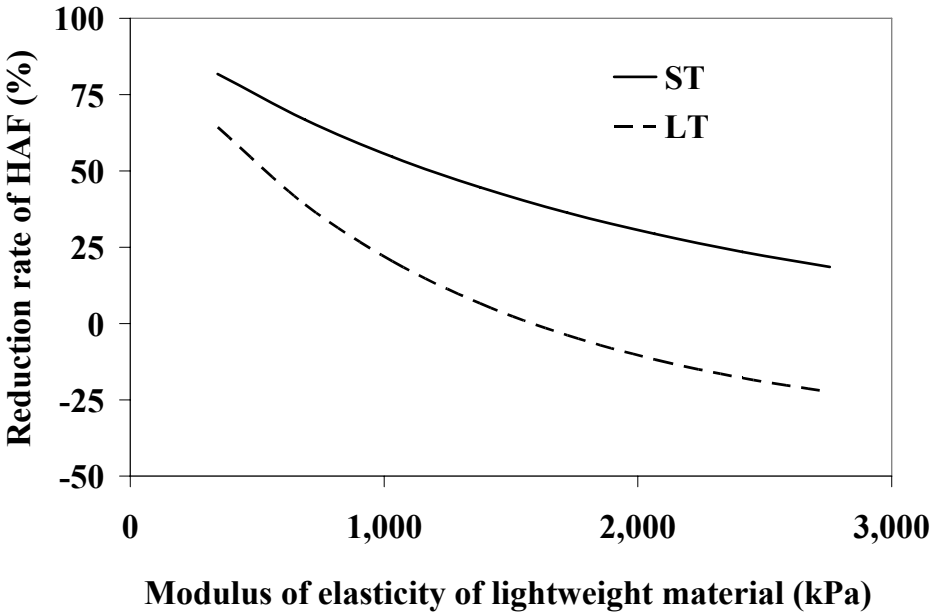

(b)

Fig. 5.8. Predictor equations of reduction rates: (a) *VAF* and (b) *HAF* (*ST* = short-term material properties; *LT* = long-term material properties; σ_{ms} = maximum wall stress) (continued)

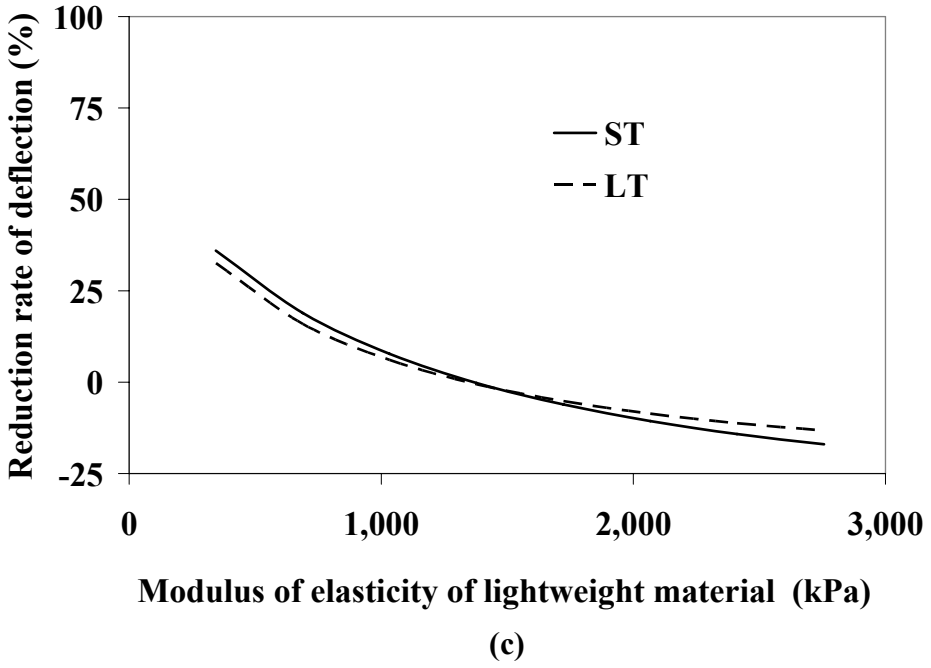

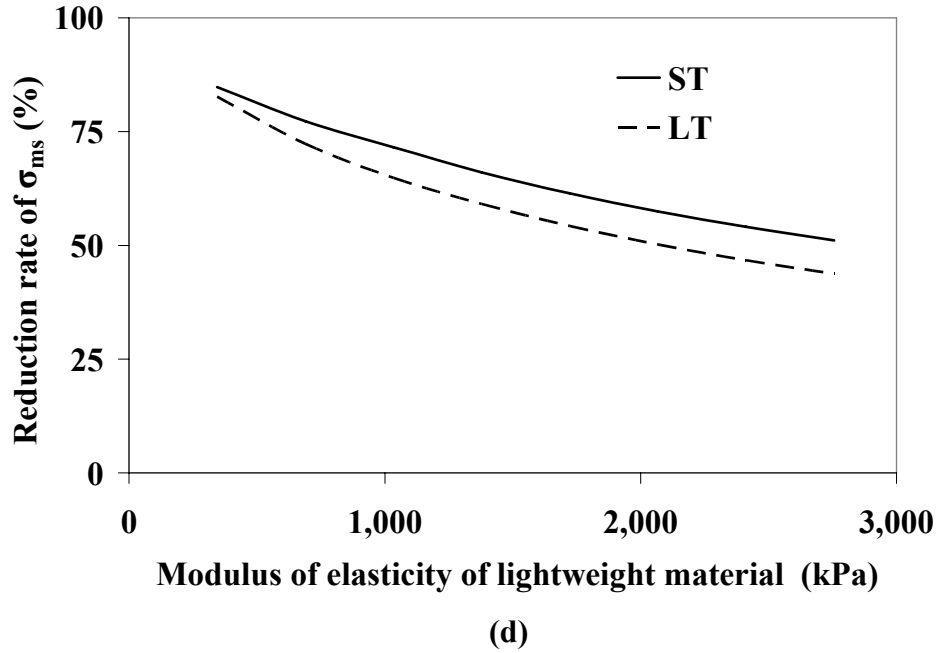

Fig. 5.8. Predictor equations of reduction rates: (c) deflection and (d) maximum wall stress (*ST* = short-term material properties; *LT* = long-term material properties; σ_{ms} = maximum wall stress)

$$R_{hl} = \left[1 \times 10^{-5} E_s^{\,2} - 0.077 E_s + 87.35\right] \tag{5.14c}$$

$$R_d = \left[9 \times 10^{-6} E_s^{\,2} - 0.048 E_s + 49.67\right] \tag{5.14d}$$

$$R_{ms} = \left[-0.015 E_s + 85.08\right] \tag{5.14e}$$

where R_v = vertical arching factor reduction rate (%); E_s = modulus of elasticity of lightweight materials (kPa); R_{hs} = horizontal arching factor reduction rate (%) for short-term material properties; R_{hl} = horizontal arching factor reduction rate (%) for long-term material properties; R_d = deflection reduction rate (%); and R_{ms} = maximum wall stress reduction rate (%).

Arching factors, deflections, and maximum wall stresses in PVC pipes under ITI can now be evaluated incorporating the above equations for various reduction factors and the procedure defined by Eq. (2.8).

CHAPTER 6

SOIL-STRUCTURE INTERACTION FOR BURIED CORRUGATED STEEL PIPES

6.1 Introduction

Spangler (1941) is believed to be the first who studied the behavior of buried metal pipes. As the stiffness of CSP is somewhere between those of rigid concrete pipes and flexible plastic pipes, a corrugated metal pipe may be categorized as semi-flexible (Moore 2000). As a consequence, the mechanics of soil arching for CSP is slightly

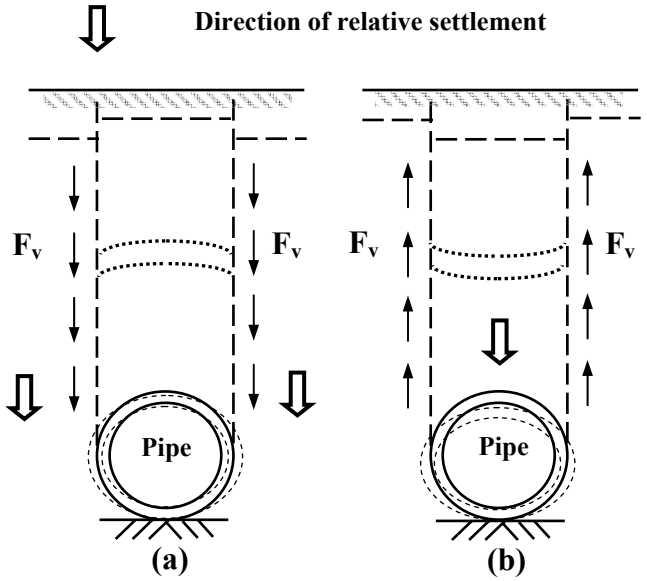

Fig. 6.1. Pressure transfer within a soil-pipe system: (a) corrugated steel pipe in embankment installation and (b) corrugated PVC pipe in embankment installation (F_v = generated friction forces or shear stresses; interface condition= full-bonded)

different from that of rigid or flexible pipes. Although the downward deflection at the top of the CSP, as shown in Fig. 6.1(a), is small, the relative downward deflection of the adjacent backfill soil prism is greater than that of the central soil prism, thereby inducing a negative arching action. This mechanism is similar to the one occurring in a rigid pipe and results in a vertical arching factor greater than one. In the case of truly flexible pipes, the vertical deflection of the central soil prism is greater than the deflection of the adjacent backfill soil prisms, as shown in Fig. 6.1(b), and induces a positive arching action resulting in a vertical arching factor less than one.

As the CSP is frequently made of very thin gauge cold-formed steel sheets, elastic flexural buckling may be an important design parameter. Therefore, it is necessary for designers to be able to assess the buckling strength of CSP. Despite a substantial difference in the buckling strengths of CSP determined by the American Iron and Steel Institute (AISI 1994) and AASHTO LRFD (2004a) procedures, there has been little expressed concern (Brockenbrough 2006). This is perhaps due to the fact that there is another limit imposed by the CSP industry with regard to the maximum slenderness ratio (D/r) of CSP permitted. CSP is rarely designed with $D/r > 294$, where D = diameter of pipe and r = radius of gyration per unit length. This study formulated a new equation for the buckling strength of CSP based on the soil-structure interaction using FEA. The buckling strength computed from the new equation is compared with those determined from AISI and AASHTO LRFD procedures. Predictor equations for arching factors, deflections, maximum wall stresses, and buckling strengths are proposed for embankment installations.

Depending upon the geometry of the soft material zone, the horizontal earth pressure can be significantly increased at the expense of the reduced vertical earth pressure as described in Chapter 5. McAffee and Valsangkar (2005) reported a case study of ITI of rigid pipes in New Brunswick, Canada. They measured earth pressure on a recently constructed concrete pipe and confirmed higher-than-expected lateral earth pressure, almost as high as vertical earth pressure. They concluded that these higher lateral pressures need to be considered in the design of pipes with ITI.

Because corrugated steel pipes are relatively flexible, they induce a small amount of reverse soil arching. Therefore, there has been limited research regarding the effects of ITI on flexible pipes. As part of the overall objective of this study, an investigation of the efficiency of ITI for CSP is made and predictor equations are generated for major design variables including an effective measure to overcome higher-than-expected lateral earth pressures in conventional ITI. After synthesizing and quantifying analytical data collected from some 1,200 hypothetical models, an optimum geometry for the soft zone in ITI is proposed. Predictor equations for the reduction rates of arching factors, deflections, and maximum wall stresses are proposed as a function of the modulus of elasticity of the lightweight material and the pipe slenderness ratio (ratio of the pipe diameter to thickness).

6.2 Background

6.2.1 Vertical Arching Factors

Burns and Richard (1964) provided theoretical solutions for the behavior of (generic) elastic circular conduit deeply buried in an isotropic, homogeneous infinite elastic medium as mentioned earlier in Chapter 5. AISI (1994) provides graphical means to determine the vertical arching factor for CSP. Vertical arching factors of 0.86, 0.75, and 0.65 were given for gravelly sand compacted to 85% (SW85), 90% (SW90), and 95% (SW95). These compaction rates are stipulated in AASHTO T-99 (AASHTO 2002) as the maximum density required.

McGrath (1998; 1999) proposed simplified equations consolidating two separate equations by Burns and Richard for different interface conditions. The McGrath equations adopted by AASHTO LRFD (2004a) were given in Chapter 5.

6.2.2 Deflections

Deflections and wall stresses are primary performance parameters in the design of CSP. The deflection of CSP is defined as the ratio of the vertical decrease in diameter (Δ_y) to the pipe diameter (D). Spangler (1941; Watkins and Spangler 1958) developed the semi-empirical Iowa formula, Eq. (5.7), for calculating the deflection of flexible pipes under the earth load.

McGrath's (1998) proposed the following equation to compute deflections of CSP:

$$\frac{\Delta_y}{D}(\%) = \left(\frac{q}{E_P A_P / R + 0.57 M_s} + \frac{K_B q D_L}{E_P I / R^3 + 0.061 M_s} \right) \times 100 \tag{6.1}$$

The first term in Eq. (6.1) quantifies the effects of hoop compression while the second is Spangler's Iowa formula quantifying the effects of bending deformation.

6.2.3 Buckling

AISI (1994) presents a series of equations for the critical buckling stresses for CSP with backfill compacted to 85% standard AASHTO T-99 density. Details of experiments that are the basis for these equations are summarized in a paper by Watkins and Moser (1969) as follows:

$$f_{cr} = f_y = 227{,}370\,\text{kPa}\ (33{,}000\,\text{psi}) \quad \text{when } \frac{D}{r} < 294 \tag{6.2}$$

$$f_{cr} = 275{,}600 - 0.558\left(\frac{D}{r}\right)^2 \quad \text{when } 294 < \frac{D}{r} < 500 \tag{6.3}$$

$$f_{cr} = \frac{3.4 \times 10^{10}}{\left(\frac{D}{r}\right)^2} \quad \text{when } 500 > \frac{D}{r} \tag{6.4}$$

where f_{cr} = critical buckling stress and f_y = minimum yield point of steel.

On the other hand, AASHTO LRFD (2004a) stipulates the following critical stress formulas to be applied in association with SW90 backfill compaction requirements:

$$f_{cr} = 6.89\left[f_u - \frac{f_u^{\,2}}{48 E_p}\left(kD/r\right)^2 \right] \quad \text{if } D < 0.0254 \frac{r}{k}\sqrt{\frac{24E_p}{f_u}} \tag{6.5}$$

$$f_{cr} = 6.89\left[\frac{12E_p}{\left(kD/r\right)^2} \right] \quad \text{if } D > 0.0254 \frac{r}{k}\sqrt{\frac{24E_p}{f_u}} \tag{6.6}$$

where f_u = specified minimum metal strength, 310 MPa (45,000 psi) and k = soil stiffness factor, 0.22.

6.3 Soil-Structure Interaction

6.3.1 Finite Element Modeling

The modulus of elasticity (E_p), Poisson's ratio (ν), and unit weight (γ) of steel were taken to be 200 GPa (29,000 ksi), 0.30, and 77 kN/m^3 (490 pcf), respectively, from AASHTO LRFD (2004a). In order to clarify the effects of the interface conditions for CSP, this study examined three interface conditions: full-bonded ($\mu = \infty$), frictional slip ($\mu = 0.5$), and free-slip ($\mu = 0$).

6.3.2 Effects of Sidefill Material Properties

The surrounding sidefill for CSP provides considerable support. Therefore, sidefill compaction is critical for CSP performance. Fig. 6.2 shows that the gravelly sand placed at sidefill at a compaction rate of 90 or 95% AASHTO T-99 maximum density (SW90 or SW95) is more efficient than similarly compacted silty sand (ML90 or ML95) or silty clay (CL90 or CL95) placed at sidefill in reducing earth loads on the pipe. This phenomenon is caused by the higher lateral support that the SW sidefill provides due to

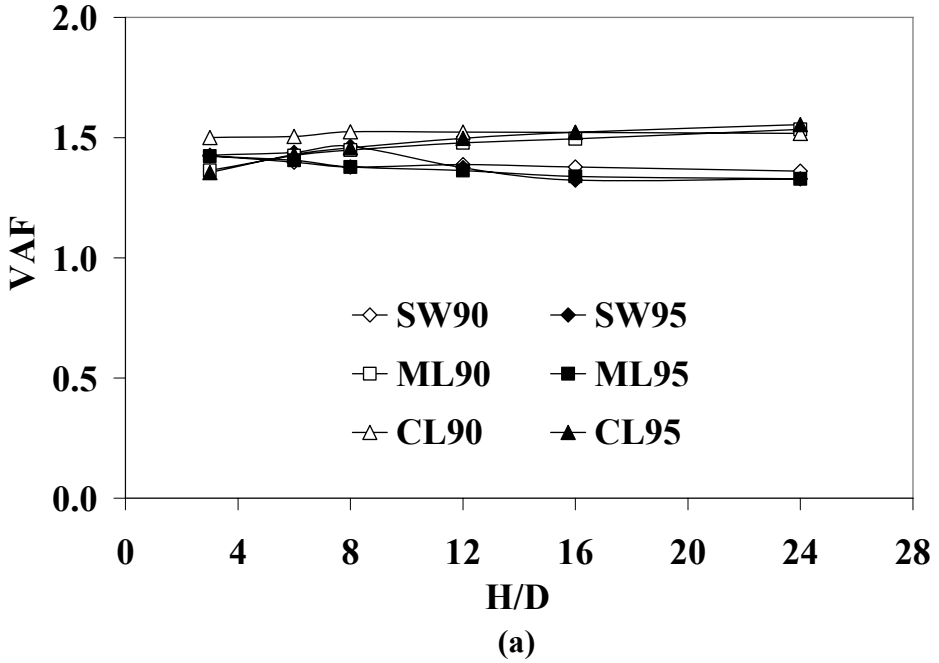

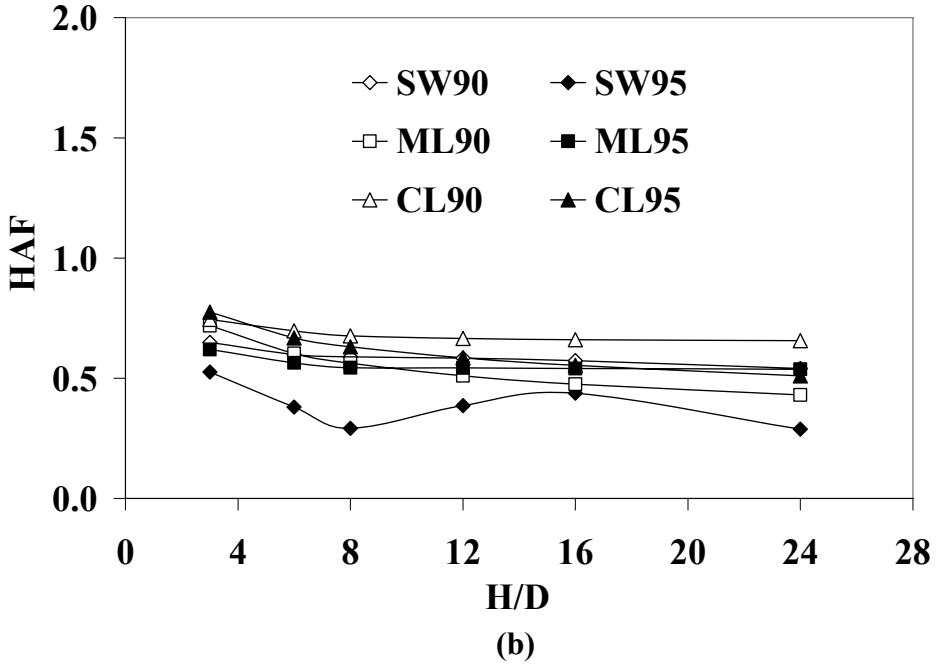

Fig. 6.2. Effects of the properties of backfill material: (a) *VAF* versus *H/D* And (b) *HAF* versus *H/D* (parameter: interface condition= full-bonded)

the higher modulus of soil reaction. AASHTO LRFD (2004b) specifies SW90 as a minimum requirement for CSP sidefill. The analyses were performed with several different soil types and compaction rates, including SW90. However, only the AASHTO LRFD SW90 was used in the analyses that are compared with AASHTO LRFD (2004a) results as shown in Fig. 6.3.

6.3.3 Effects of Interface Conditions

Values determined from FEA were compared with those computed from currently available equations including those from AASHTO LRFD, Burns and Richard, and AISI. Fig. 6.3 shows that vertical arching factors were sensitively affected by interface conditions. With the full-bonded interface condition, *VAF* by ABAQUS are in good

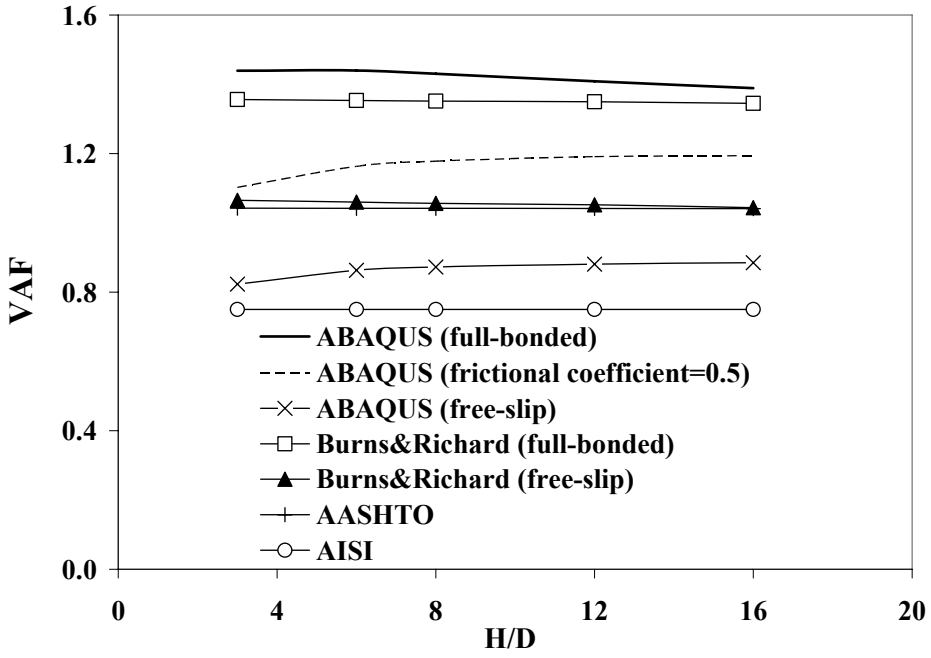

Fig. 6.3. Variations of vertical arching factor (*VAF*)

agreement with those by Burns and Richard (1964). Also, *VAF* by AASHTO LRFD (2004a) and Burns and Richard with the free-slip condition lie between the values computed by ABAQUS for frictional slip and free-slip interface conditions, respectively. *VAF* by AASHTO are close to those by the Burns and Richard equation under the free-slip interface condition. *VAF* determined by ABAQUS for frictional slip and free-slip interface conditions are 18% and 39% smaller, respectively, than those for the full-bonded interface condition. *VAF* computed from the Burns and Richard equation for the free-slip interface condition are 22% smaller than those with the full-bonded interface condition.

Fig. 6.4 illustrates the effects of interface conditions on the total vertical load, W_e, which is transformed into *VAF* defined by Eq. (4.2). As expected, Fig. 6.4 correctly

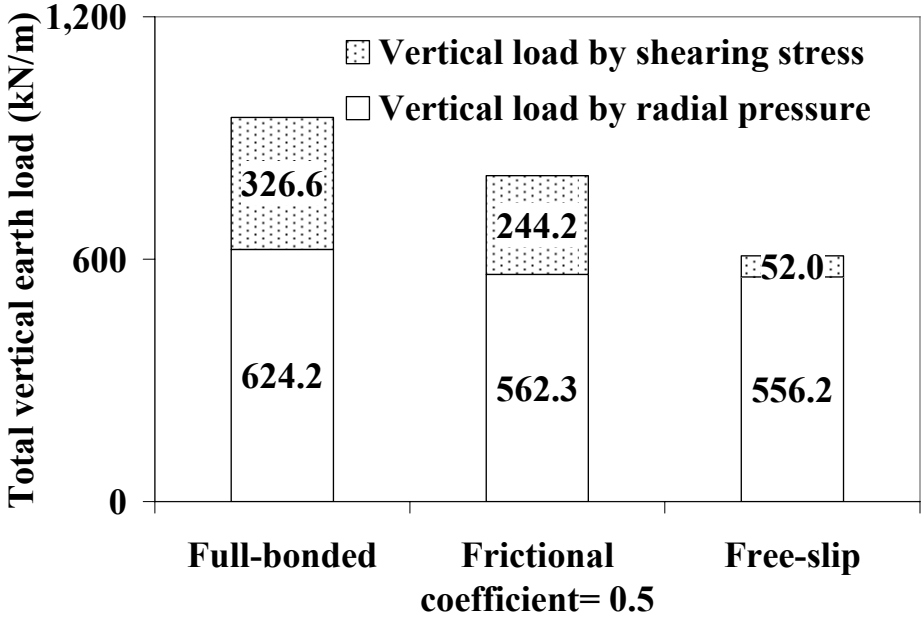

Fig. 6.4. Effects of interface conditions for total vertical earth load (W_e) (parameters: pipe diameter = 2.4 m; fill height = 29 m)

shows that the vertical load resulting from the radial pressure is not very sensitively affected by the interface condition while the vertical load exerted on the CSP due to frictional stress is quite sensitively affected by the interface condition.

It is noted that the dead weight of the CSP is a negligibly small fraction of the total vertical load. Although the effects of interface conditions on *VAF* for CSP are significant (up to 34% of the total vertical load), they cannot be determined rationally by analysis alone. A well-designed field testing program is needed to answer this question. A conservative approach of the full-bonded condition is recommended as an intermediate option.

Fig. 6.5 shows that deflections are not affected very much by interface conditions.

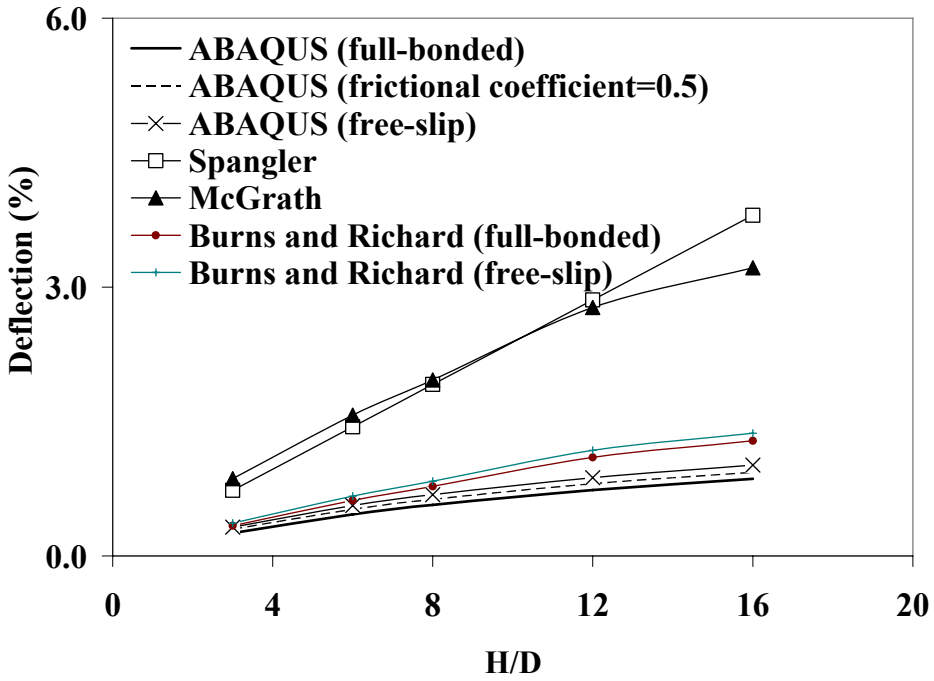

Fig. 6.5. Vertical deflection (parameters: deflection lag factor (D_L) = 1; bedding factor (K_B) = 0.1)

This observation may be attributable to the fact that the vertical load affecting the vertical deflection at the crown is the total earth load above the crown as opposed to the total vertical load computed at the springline shown in Fig. 6.4. Hence, the total vertical load above the crown is not affected by the interface condition. Deflections from ABAQUS were much less than those computed from equations proposed by Spangler (1941), Eq. (5.7) and McGrath (1998), Eq. (6.1). Deflections from Burns and Richard equations, Eq. (5.8a) and Eq. (5.8b), are close to those from ABAQUS. Although the deflection of the CSP rarely controls the design, it may control performance limits (Article 12.12.3.5.4b, AASHTO LRFD 2004a), such as strain limits and reversal of curvature of the pipe. Hence, overestimated deflections from the Spangler and McGrath equations may lead to overly conservative designs.

6.4 Buckling Analyses

The pipe-spring model shown in Fig. 6.6 was developed by placing linear springs below the springline of the CSP to investigate its buckling strength. The spring constants

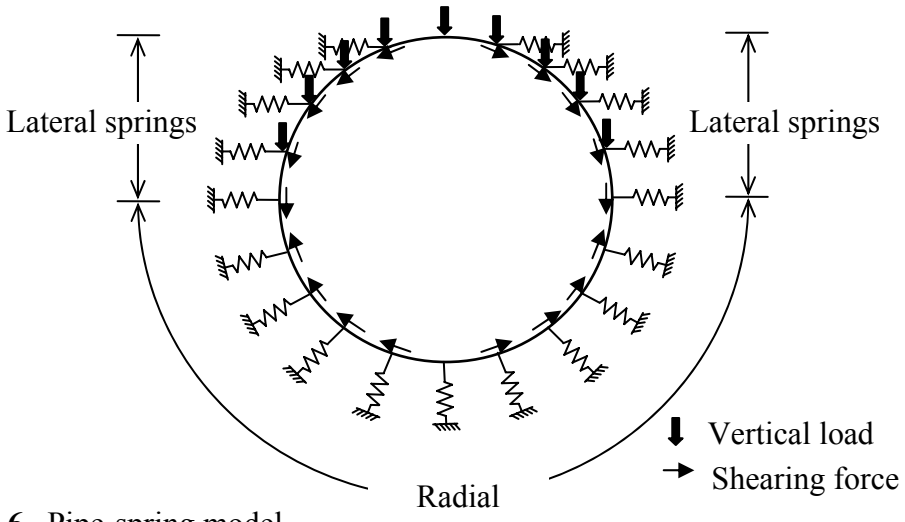

Fig. 6.6. Pipe-spring model

used in the above pipe-spring model were determined by a trial and error process from a series of soil-structure analyses. Equilibrium was checked at each loading. Each trial loading consists of variable frictional forces on the entire surface of the pipe such that they maintain symmetry with respect to the vertical axis. Each trial loading also includes vertical load representing the burial depth at each node above the springline. It is noted that additional lateral springs were needed above the springline to correctly model the soil-structure interaction as shown in Fig. 6.6. These additional lateral springs were needed to correctly simulate the bending moment in the region between the crown and the springline to those developed in the soil-pipe system. It is noted that the bending moment in the region between the invert and the springline is properly accounted for by the presence of the radial springs modeled as shown in Fig. 6.6.

Fig. 6.7 shows comparatively the critical buckling stresses determined from AASHTO LRFD (2004a), AISI (1994), and the pipe-spring model developed herein. The critical buckling stresses determined from the pipe-spring model are in reasonably good agreement with those from AISI. AASHTO LRFD (2004a) yields values considerably greater than the pipe-spring model. The following equations for critical buckling stresses of CSP were derived using data from pipe-spring models with linear regression. It is recalled that the pipe slenderness ratio is not to exceed 294 according to the industry self-imposed limitation (Brockenbrough 2006). Fig. 6.7 clearly shows that the buckling strength determined from AASHTO LRFD (2004a) is considerably greater than that from the pipe-spring model. Although the buckling strength determined from the pipe-spring model is fairly close to that obtained from AISI (1994), the buckling strength from the

pipe-spring model is 7.3% smaller than that from AISI at the upper limit of the industry-imposed slenderness ratio, thereby indicating the unconservative nature of the buckling strength by existing procedures.

$$f_{cr} = f_y = 227{,}370\,\text{kPa}\ \left(33{,}000\,\text{psi}\right) \quad \text{when } \frac{D}{r} \le 343 \tag{6.7a}$$

$$f_{cr} = \alpha \frac{E_p}{\left(D/r\right)^2} \quad \text{when } \frac{D}{r} > 343 \tag{6.7b}$$

$$\alpha = 0.27\left(D/r\right) + 14.94 \quad \text{for SW85} \tag{6.8a}$$

$$\alpha = 0.30\left(D/r\right) + 34.23 \quad \text{for SW90} \tag{6.8b}$$

$$\alpha = 0.20\left(D/r\right) + 114.08 \quad \text{for SW95} \tag{6.8c}$$

where α = dimensionless coefficient.

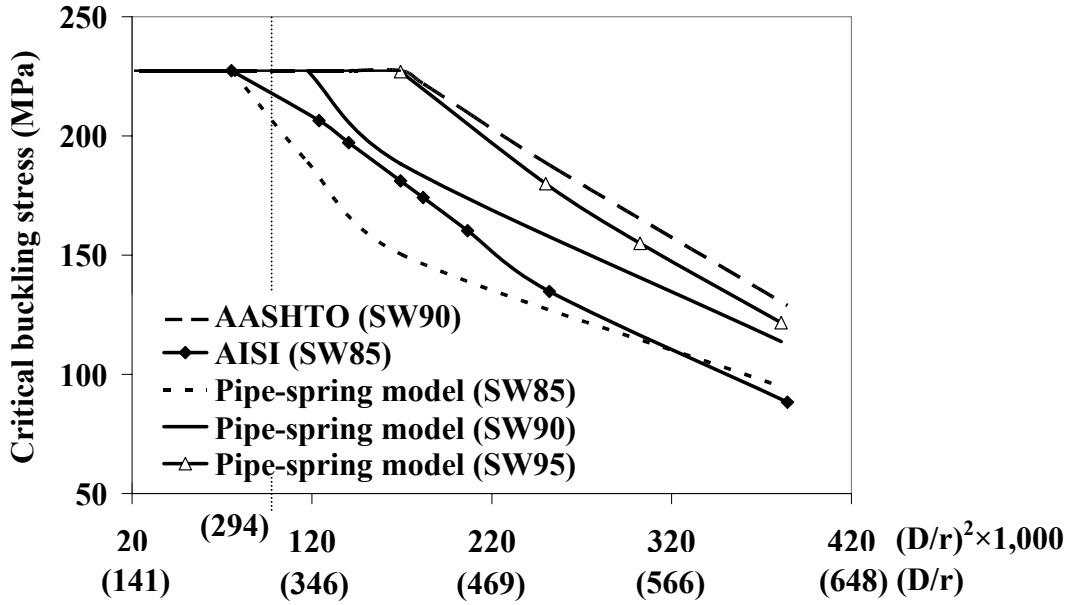

Fig. 6.7. Comparison of critical buckling stresses between AASHTO, AISI, and pipe-spring model (D = pipe diameter; r = radius of gyration of corrugation)

6.5 Imperfect Trench Installation

6.5.1 Optimization of Soft Zone Geometry

As mentioned earlier in the previous chapters, the soft zone geometry is controlled by three parameters: width, *W*; height, H_s; and the distance from the top of the pipe to the bottom of the soft zone, H', as shown in Fig. 6.8(a). Fig. 6.8(c) shows the soft zone geometry suggested by Spangler (1950a) and Vaslestad et al. (1993) where H'=0. In the previous two chapters, it has been demonstrated that the soft zone geometry I similar to that shown in Fig. 6.8(b) is found to be the most efficient one. Based on a large number of parametric studies (over 1,200 cases), the proposed soft zone geometry I shown in Fig. 6.8(b) is shown to be most effective in reducing earth pressure. What is noted herein is that the thickness of the soft zone at the sidewall and bottom is expressed slightly differently than those shown in Figs. 4.3(b) and 5.4(b). It is noted that the sidewall thickness for CSP is fixed at 76 mm (3 in.) and the thickness at the bottom is specified at 1/8 times the diameter of the CSP.

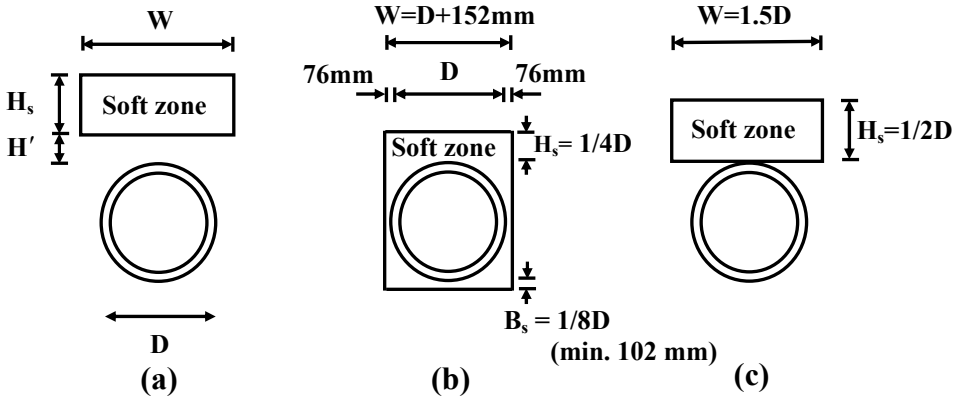

Fig. 6.8. Notation for imperfect trench installations and geometries of soft zone: (a) notation; (b) soft zone geometry I (proposed); and (c) soft zone geometry II

Unlike the case of corrugated PVC pipes where the slenderness ratio, *D/r*, varies in a narrow range, 60 - 100, the slenderness ratio of CSP varies in a wide range, 154-411. Therefore, it became necessary to include the slenderness ratio as a variable in the optimization process given in Fig. 6.9 in addition to the abovementioned three major parameters. It becomes evident from Fig. 6.9 that the optimum soft zone geometry I given in Fig. 6.8(b) is indeed most effective. As shown in Fig. 6.9(a), the reduction rate (R_{ms}) remains virtually unchanged once the height of the soft zone (H_s) divided by the pipe diameter (D) of the pipe reaches 0.25. The optimum bedding thickness of the soft material zone below invert, B_s, is found to be 1/8 times the pipe diameter as the reduction rates (R_{ms}) shown in Fig. 6.9(b) do not improve much beyond the above optimum value. Fig. 6.9(c) gives the variation of the reduction rate as a function of the width of the soft zone, *W*. As shown in Fig. 6.9(c), the maximum reduction rate occurs when the width of the soft zone is taken to be the pipe diameter plus 1/32 times the pipe diameter. It is noted that the reduction rate actually decreases as the width of the soft material zone is increased as shown in Fig. 6.9(c). This is caused by the loss of lateral support due to the presence of wider soft sidefill, thereby increasing the bending moment at the springline (induced as a result of wider lateral deformation of the pipe). In order to facilitate the installation (constructibility) of the soft zone (preferably 76 mm on each side as a minimum), an optimum width of the soft zone was taken to be the pipe diameter plus 152 mm (6 in.) regardless of the pipe diameter for the soft zone as shown in Fig. 6.8(b). Fig. 6.10 shows that the optimum soft zone geometry I is highly effective in

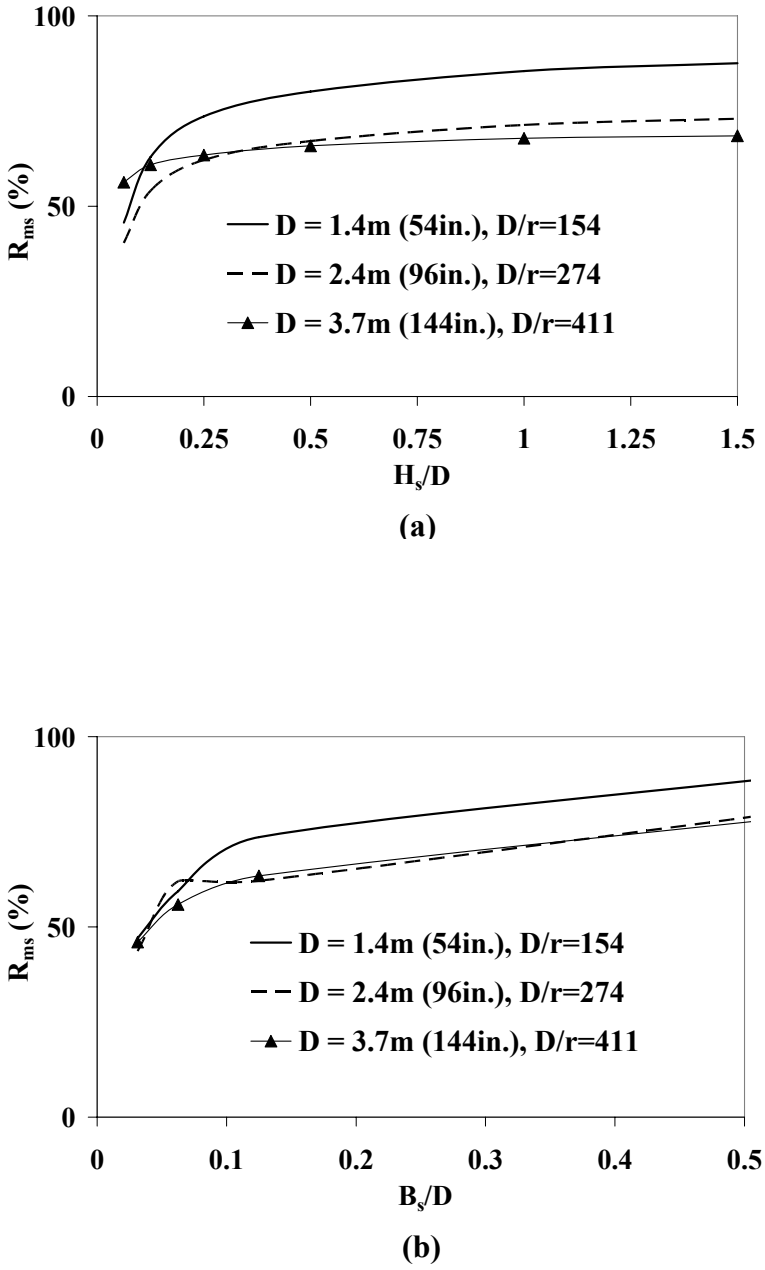

Fig. 6.9. Optimization process of soft zone geometry I: (a) height of soft zone (H_s) with W= D +152mm and B_s/D= 0.125 and (b) thickness of soft zone below invert (B_s) with H_s/D= 0.25 and W= D +152mm (R_{ms} = reduction rate of maximum wall stress; modulus of elasticity of the lightweight material = 345 kPa) (continued)

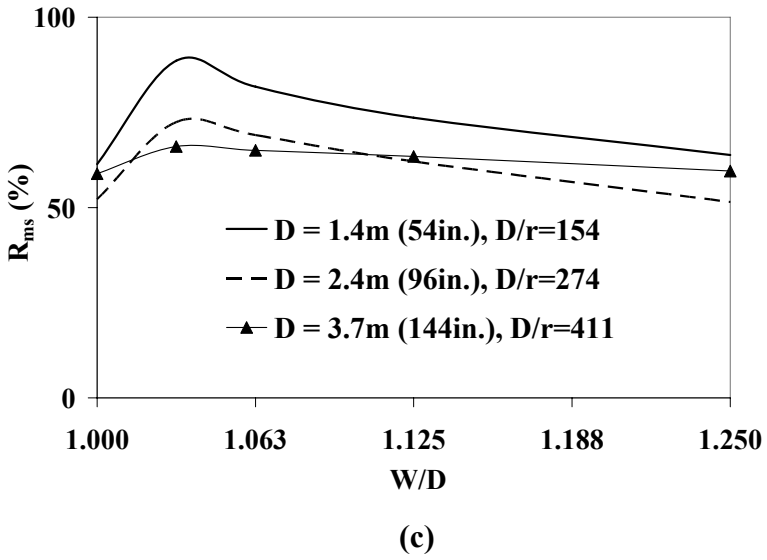

Fig. 6.9. Optimization process of soft zone geometry I: (c) width of soft zone (*W*) with H_s/D= 0.25 and B_s/D= 0.125 (R_{ms} = reduction rate of maximum wall stress; modulus of elasticity of the lightweight material = 345 kPa)

reducing the earth pressure on CSP. Geofoam (E_s = 345 kPa and ν = 0.1) was used as the lightweight material in all model analyses shown in Figs. 6.9 through 6.11.

6.5.2 Imperfect Trench Installation versus Embankment Installation

Higher-than-expected lateral pressure, encountered by McAffee and Valsangkar (2005) when the soft zone is placed only at the top of the pipe as shown in Fig. 6.8(c), occurs due to a redistribution of the load from the crown to the sides of the pipe and the resulting development of undesirable shear stresses . This is confirmed in Fig. 6.10(a). Fig. 6.10(b) shows that when a soft zone is installed, significantly different patterns of shear stresses developed on the pipe sidewall due to an alteration of the soil pressure distribution as compared to the embankment installation.

In the case of embankment installations, a positive frictional force (in the clockwise tangential direction) develops above the springline while a negative frictional force (in the counter-clockwise tangential direction) develops below the springline. As these two frictional forces of opposite direction were nearly equal in magnitude, there was no significant axial force increase at the springline and the bottom of the pipe, as shown in Fig. 6.10(b). For the soft zone geometry II as shown in Fig. 6.8(c), the radial pressure at about 25 degrees from the invert became significantly larger than that at the crown, as shown in Fig. 6.10(a). It is noted herein that the development of frictional forces affect the radial forces on the pipe indirectly due to the relationship of the pressure versus hoop tension. This undesirable frictional stress distribution was practically eliminated by extending the soft zone to the bedding as shown in Fig. 6.8(b). The

resulting frictional stresses are dramatically decreased as shown in Fig. 6.10(b). This, in turn, significantly decreases the radial earth pressure on the pipe as shown in Fig. 6.10(a). As mentioned earlier, the effectiveness of the proposed optimum soft zone geometry I is the most significant contribution of this study. With this effective elimination of the undesirable development of the frictional forces comparatively shown in Fig. 6.4 and Fig. 6.11, the pipe wall stress as the main design criterion is reduced significantly, as shown in Fig. 6.10(e).

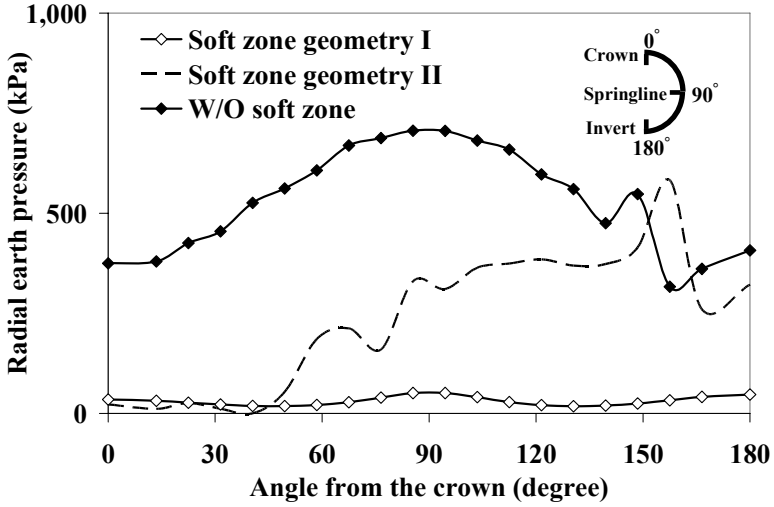

(a)

Fig. 6.10. Imperfect trench installations versus embankment installations: (a) radial earth pressure (parameters: pipe diameter = 2.4 m; fill height = 29 m; modulus of elasticity of the lightweight material = 345 kPa) (continued)

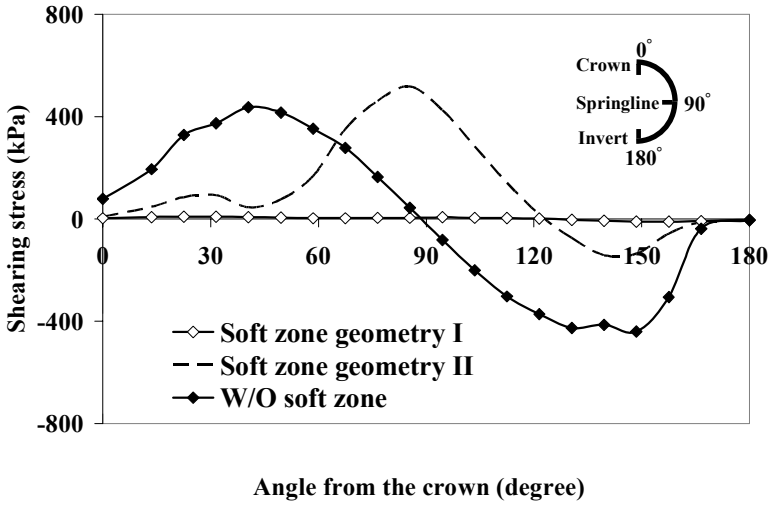

(b)

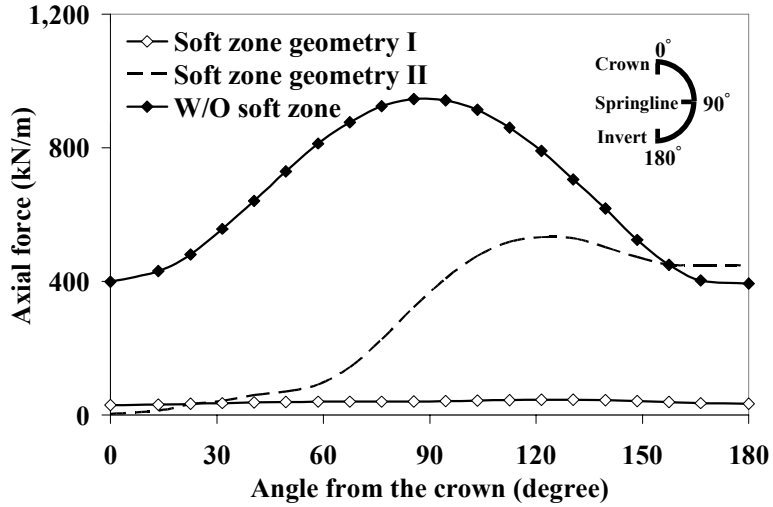

(c)

Fig. 6.10. Imperfect trench installations versus embankment installations: (b) frictional stress and (c) axial force (parameters: pipe diameter = 2.4 m; fill height = 29 m; modulus of elasticity of the lightweight material = 345 kPa) (continued)

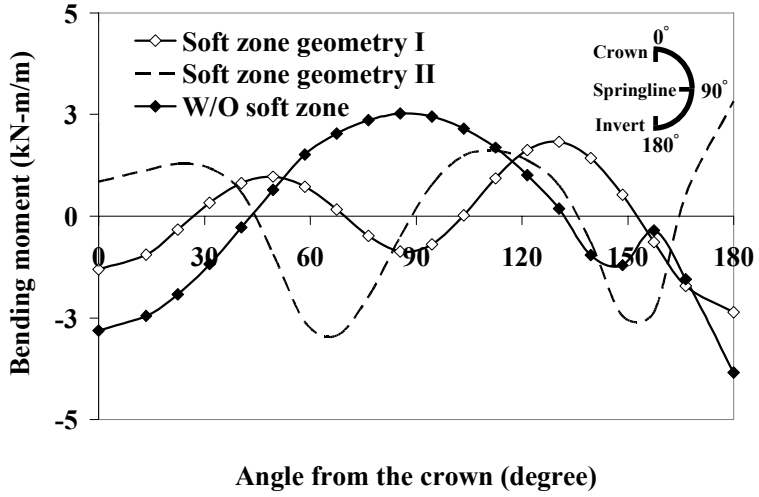

(d)

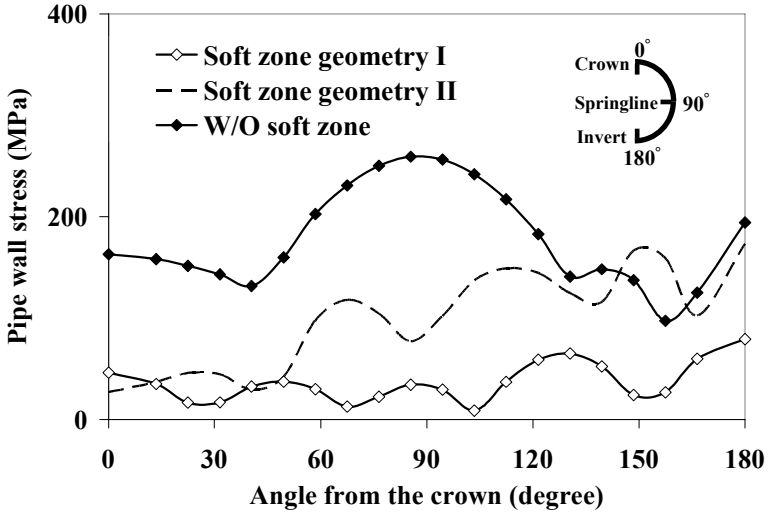

(e)

Fig. 6.10. Imperfect trench installations versus embankment installation: (d) bending moment and (e) pipe wall stress (parameters: pipe diameter = 2.4 m; fill height = 29 m; modulus of elasticity of the lightweight material = 345 kPa)

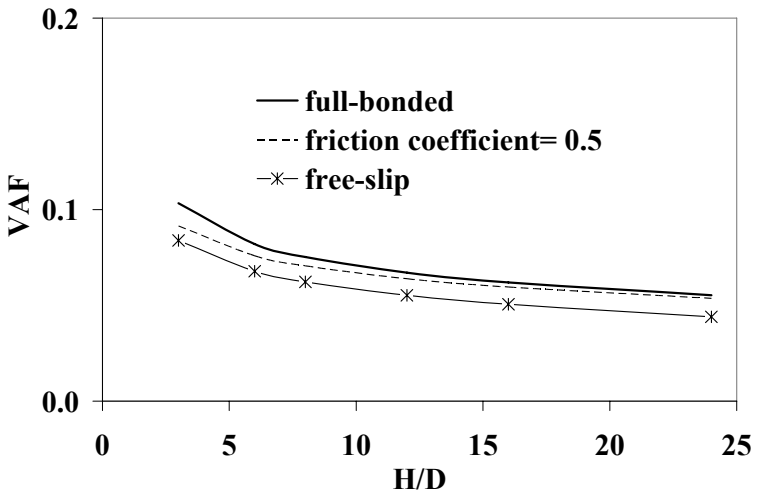

(a)

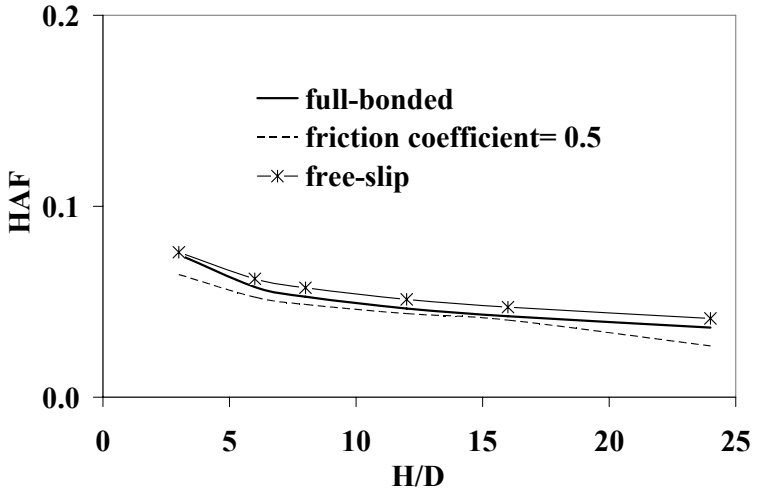

(b)

Fig. 6.11. Effects of interface properties in ITI: (a) *VAF* versus *H/D* and (b) *HAF* versus *H/D* (parameters: modulus of elasticity of the lightweight material = 345 kPa; proposed soft zone geometry I as shown in Fig. 6.8(b)) (continued)

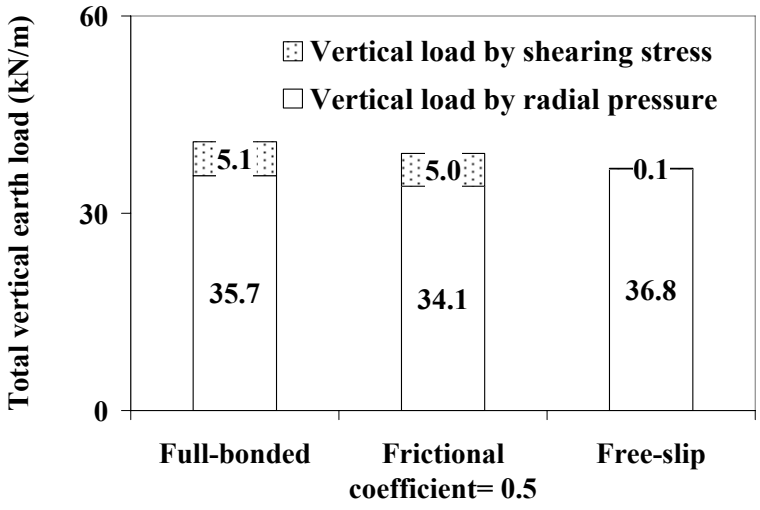

(c)

Fig. 6.11. Effects of interface properties in ITI: (c) total vertical earth load (W_e) versus interface properties for pipe diameter = 2.4 m and fill height = 29 m (parameters: modulus of elasticity of the lightweight material = 345 kPa; proposed soft zone geometry I as shown in Fig. 6.8(b))

6.6 Predictor Equations

6.6.1 Arching Factor, Deflection, and Maximum Wall Stress

More than 1,200 hypothetical models were run in order to generate data to develop equations for arching factors, deflections, and maximum wall stresses. The full-bonded interface condition was assumed conservatively and linear regression techniques were used to develop equations. Following **Tables 2.6** and **HC-3**, AISI (1994), values of *D/r* were varied between 154 and 411. Fig. 6.12 shows that arching factors for buried CSP are hardly affected by *H/D* or *D/r*. Therefore, *VAF* and *HAF* were recommended to be 1.4 and 0.6, respectively, regardless of *H/D* or *D/r*, for SW90. These are significantly higher values as compared with those determined from AASHTO LRFD (2004a) and AISI (1994). It is recalled that these arching factors are greatly affected by the interface conditions as shown in Fig. 6.3. It appears from Fig. 6.3 that arching factors computed from AASHTO LRFD and AISI procedures are rather close to those determined from ABAQUS assuming a free-slip interface condition, which would seem unconservative. It is recalled that Sargand et al. (2002) showed that the earth loads on corrugated PVC (flexible pipe) were predicted more closely by the full-bonded interface model as discussed earlier.

Deflections, as shown in Fig. 6.12(c), are affected by *H/D* and *D/r*, and the following equation was developed for deflection:

$$\frac{\Delta_y}{D}(\%) = \left(0.087\frac{H}{D} + 0.167\right)\left(\frac{D}{274r}\right) \tag{6.9}$$

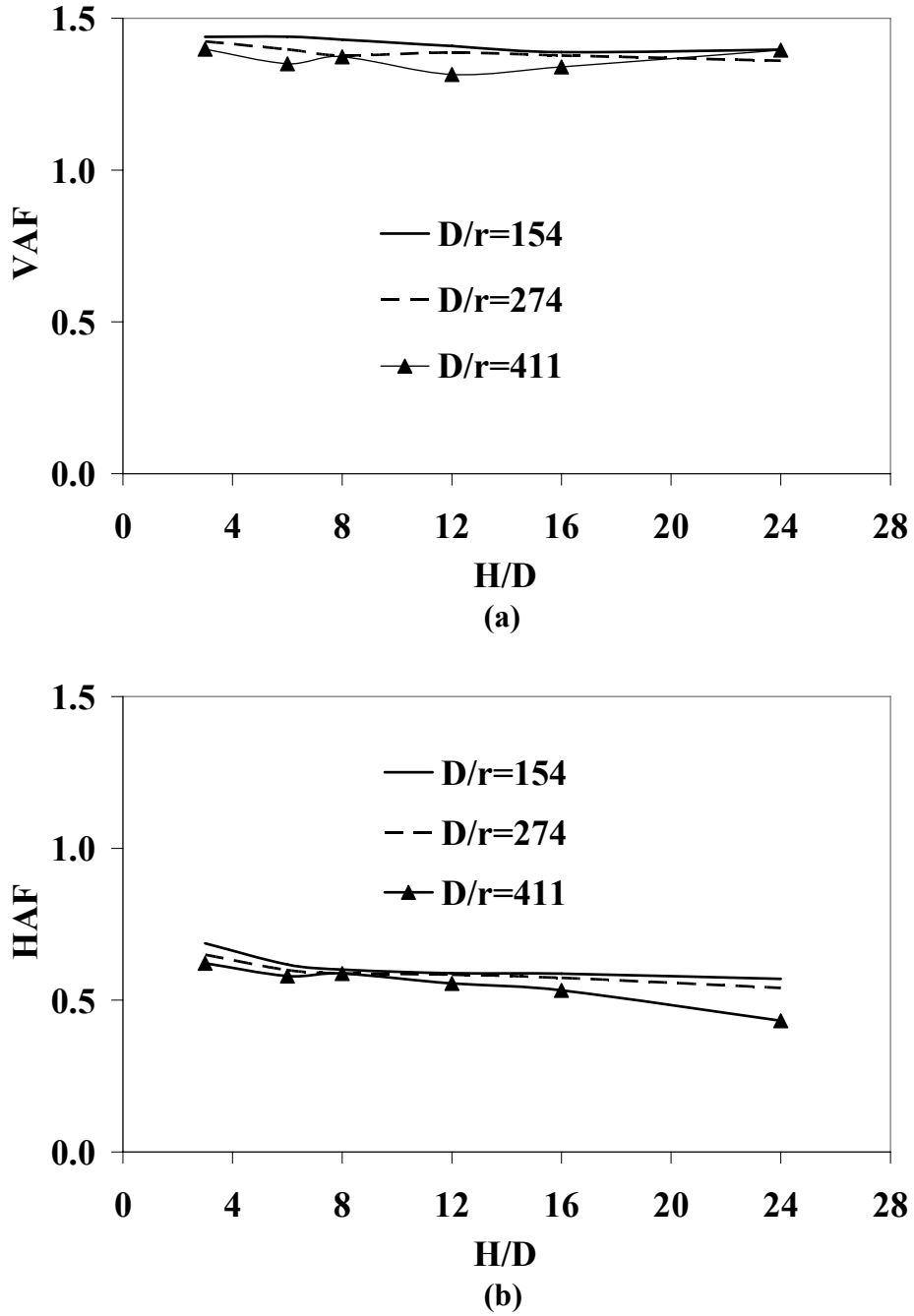

Fig. 6.12. Arching factor, deflection, and soil-structure interaction multiplier (F_{ms}) for maximum wall stress versus *H/D*: (a) *VAF* and (b) *HAF* (*D* = pipe diameter; *r* = radius of gyration of corrugation; interface condition= full-bonded) (continued)

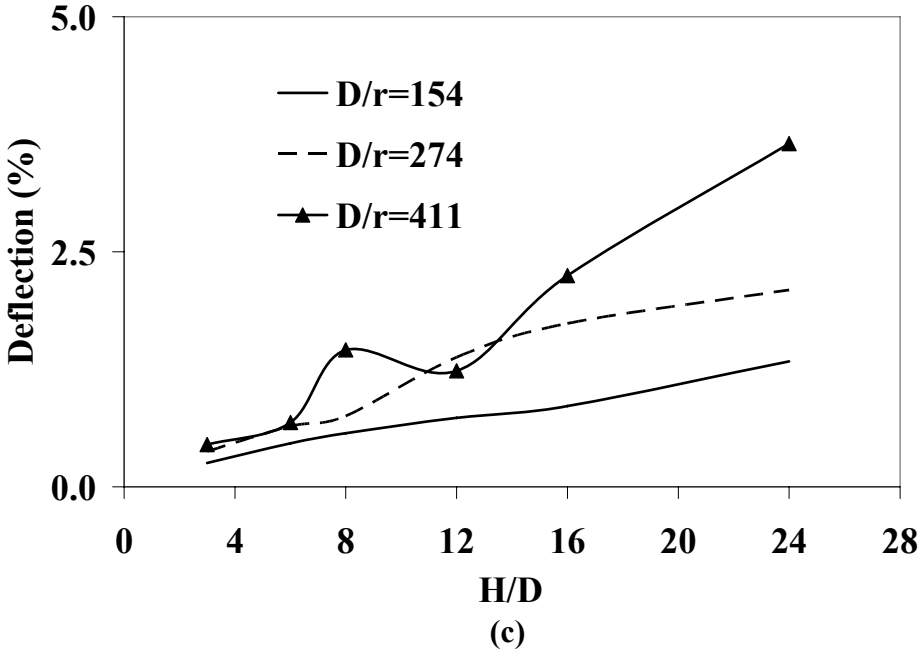

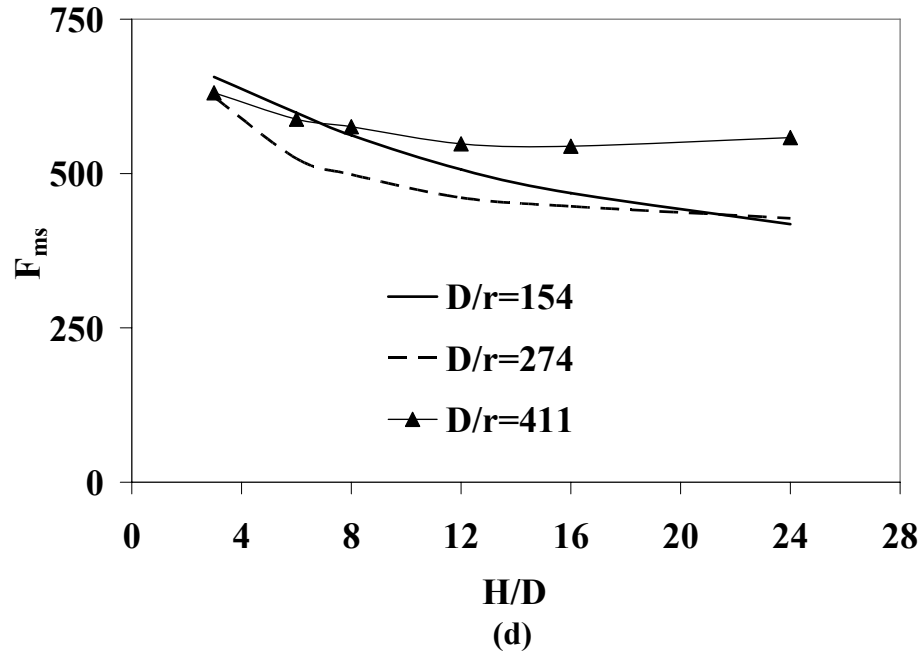

Fig. 6.12. Arching factor, deflection, and soil-structure interaction multiplier (F_{ms}) for maximum wall stress versus *H/D*: (c) deflection and (d) soil-structure interaction multiplier (F_{ms}) (*D* = pipe diameter; *r* = radius of gyration of corrugation; interface condition= full-bonded)

Fig. 6.12(d) introduces a parameter, F_{ms}, to be incorporated into a procedure to determine the wall stress as the main design criterion. As can be seen from Fig. 6.12(d), the parameter is not affected very much by *H/D* and *D/r*. A value of 575 for F_{ms} appears to be a reasonably conservative value to be used for all ranges of *H/D* and *D/r*. Maximum wall stresses ($\sigma_{\max}$), therefore, can be calculated as follows:

$$\sigma_{\max} = F_{ms}\left(\frac{PL}{D}\right) = 575\left(\frac{PL}{D}\right) \tag{6.10}$$

6.6.2 Reduction Rates

The geometry of the soft zone, H/D, D/r, and the modulus of elasticity and Poisson's ratio of the lightweight materials are variables affecting the reduction rates of the arching factors, deflections, and maximum wall stresses in ITI. After the three dominant geometric parameters of the soft zone (height, bedding thickness, width) were identified as shown in Fig. 6.9, the remaining variables were varied in the production run of nearly 1,200 hypothetical models. An examination of the analysis results revealed that H/D and Poisson's ratio of the lightweight materials do not very much affect the reduction rate of arching factors, deflections, and maximum wall stresses. Therefore, these two variables were not considered further in the development of predictor equations. As shown in Fig. 6.13, D/r has moderate effects on the reduction rates for horizontal arching factors, deflections, and maximum wall stresses except vertical arching factors. The analyses indicated that the reduction rates for the arching factors, deflections, and maximum wall stresses were very sensitive to the modulus of elasticity

of the lightweight material. Fig. 6.13 shows that these reduction rates decrease as the modulus of elasticity of the lightweight material increases as was the case in two previous chapters. This demonstrates that the lightweight material should be as soft (low modulus of elasticity) as practically possible, contrary to Tyler (2003), who erroneously discounted the importance of the properties of the soft materials.

Eqs. (6.11) through (6.18) are the reduction rates to be incorporated into the predictor equations for CSP in ITI. These equations have been formulated by linear regression analyses based on data collected over 1,200 hypothetical models.

$$R_v = \left(-0.010E_s + 97.08\right) \tag{6.11}$$

$$R_h = \left(-0.015E_s + 95.34\right) \quad \text{for } D/r \le 274 \tag{6.12}$$

$$R_h = \left(-0.015E_s + 95.34\right) + \left(\frac{D/r}{274}\right)^{\beta_1} \quad \text{for } D/r > 274 \tag{6.13}$$

$$\beta_1 = E_s^{0.26} \tag{6.14}$$

$$R_d = \left(7\times10^{-6}E_s^{\,2} - 0.047E_s + 81.79\right) \quad \text{for } D/r \le 274 \tag{6.15}$$

$$R_d = \left(7\times10^{-6}E_s^{\,2} - 0.047E_s + 81.79\right) - \left(\frac{D/r}{274}\right)^{\beta_2} \quad \text{for } D/r > 274 \tag{6.16}$$

$$\beta_2 = E_s^{0.30} \tag{6.17}$$

$$R_{ms} = \left(7\times10^{-6}E_s^{\,2} - 0.045E_s + 86.48\right)\left(\frac{274}{D/r}\right)^{0.3} \tag{6.18}$$

where R_v = vertical arching factor (*VAF*) reduction rate (%); E_s = modulus of elasticity of lightweight materials (kPa); R_h = horizontal arching factor (*HAF*) reduction rate (%); β_1 ,

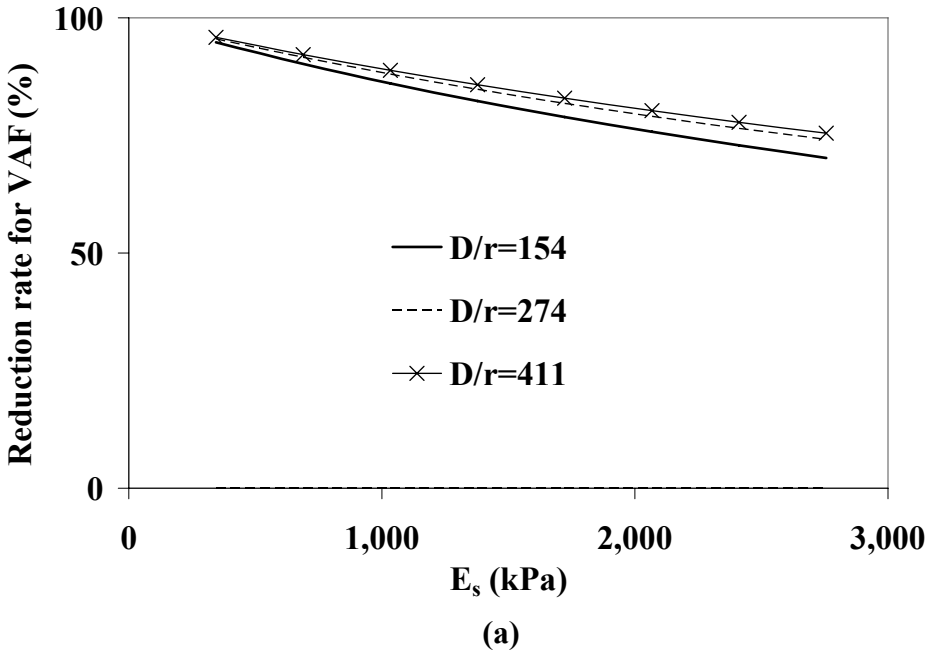

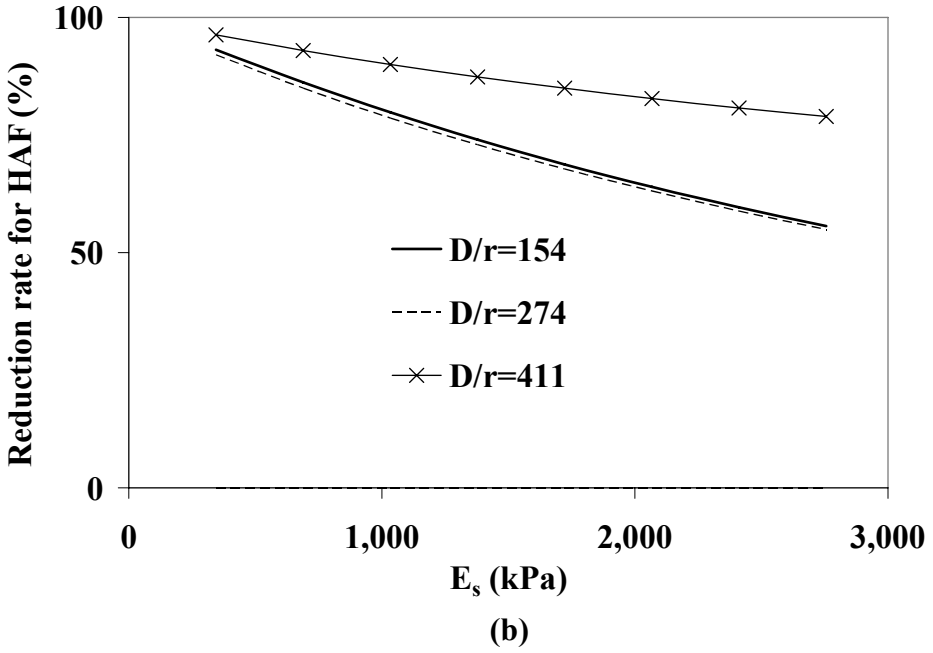

Fig. 6.13. Reduction rates versus modulus of elasticity of lightweight material (E_s): (a) *VAF* and (b) *HAF* (parameter: proposed soft zone geometry I as shown in Fig. 6.8(b)) (continued)

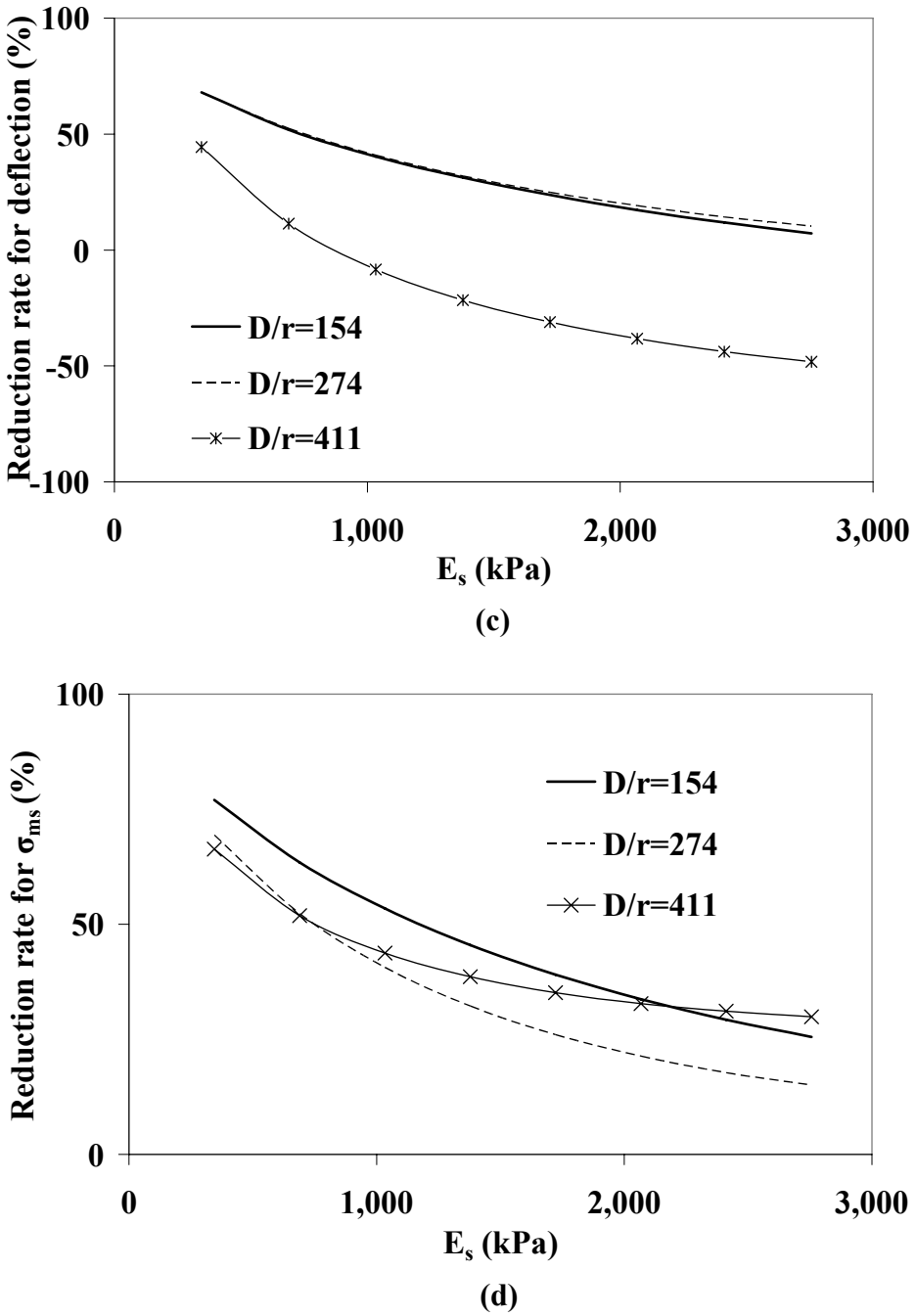

Fig. 6.13. Reduction rates versus modulus of elasticity of lightweight material (E_s): (c) deflection and (d) maximum wall stress (σ_{ms}) (parameter: proposed soft zone geometry I as shown in Fig. 6.8(b))

β_2 = nondimensional parameters; R_d = deflection reduction rate (%); and R_{ms} = maximum wall stress reduction rate (%). It is noted that an appropriate conversion factor must be incorporated in the above equations when the unit of E_s is different from kPa. It is noted in Figs. 6.10(c) and 6.10(e) that the reduction rate of the arching factors related to axial force alone reaches up to 95%, and the reduction rate of maximum wall stresses related to the combined action of bending moment and axial force is 69%. This reflects the fact that the reduction rate related to the bending moment is only 38%, as shown in Fig. 6.10(d). The reason for such a small reduction has been explained earlier (loss of lateral support).

Arching factors, deflections and maximum wall stresses in CSP under ITI (represented by *Y* in Eq. (2.8)) can now be evaluated incorporating the same for the embankment installations (represented by *X* in Eq. (2.8)).

CHAPTER 7

SOIL-STRUCTURE INTERACTION FOR BURIED BOX CULVERTS

7.1 Introduction

The possibility of reducing earth pressure on deeply buried concrete box culverts by the ITI method has been contemplated during the last several decades. There have been limited research results published primarily regarding the qualitative aspect of load reduction in ITI. It was found during the course of this study that significant frictional forces develop along the sidewalls of box culverts and adjacent sidefills in ITI. As a result, the earth pressure exerted at the bottom of a culvert can be significantly higher than the sum of the earth load at the top plus the dead weight of the culvert. The current AASHTO LRFD (2004a) provisions do not consider these frictional forces that develop along the side of the culvert. This practice is justified in the case of culverts under embankment installation as will be discussed later, but the undesirable development of the frictional forces along the sides of culverts cannot be neglected in ITI, as their effect can be quite significant.

Recently, Yoo et al. (2005) discovered that, although ITI reduces earth pressures on the top and bottom slabs, downward frictional force on the sidewalls increases the

pressure on the bottom slab beyond the sum of the pressure on the top slab and the dead weight of the structure.

7.2 Background

The current AASHTO LRFD (2004a) procedure for computing the total earth load for culverts in embankment installations is given by Eqs. (7.1) and (7.2). These equations are essentially the same as those proposed by Marston and Anderson (1913) and subsequently modified by Marston (1930).

$$W_e = F_e w B_c H \tag{7.1}$$

$$F_e = 1 + 0.20\frac{H}{B_c} \tag{7.2}$$

where W_e is the total earth load, F_e is the soil-structure interaction factor for embankment installations that shall not exceed 1.15 in compacted fill nor 1.40 in uncompacted fill, w is the unit weight of soil, B_c is the width of the structure, and H is the backfill height.

Katona and Vittes (1982) stated that soil shear traction produces a significant downward force that must be accounted for by increased pressure on the bottom slab in embankment installations. Tadros et al. (1989) proposed pressure formulas for the top, the sidewall, and the bottom of positive projection box culverts by using CANDE-1980, a special-purpose finite element program. Eqs. (7.3) through (7.5) were proposed for silty-clay by Tadros et al. Tadros et al. (1989) considered the effect of frictional forces in the pressure equation for the bottom slab, but the effects of sidefill treatment were not considered.

$$P_T = (0.047 + 0.919 \times 10^{-4} H)(w)(H) \tag{7.3}$$

$$P_S = (0.029)(w)(H) \tag{7.4}$$

$$P_B = P_T + \frac{(57 + 8.02H_c)(2H_c)}{B_c} \tag{7.5}$$

where P_T is the pressure on the top slab, P_S is the pressure on the sidewall, P_B is the pressure on the bottom slab, H is the fill height above the point considered, w is the unit weight of soil, H_c is the height of the box culverts, and B_c is the width of the box culverts.

Kim and Yoo (2005) recently proposed equations for estimating earth pressure on the top slab for positive projection box culverts as shown in Fig. 7.1(a). However, Kim and Yoo did not consider the effect of frictional forces on the sidewalls for earth pressure on the bottom slab.

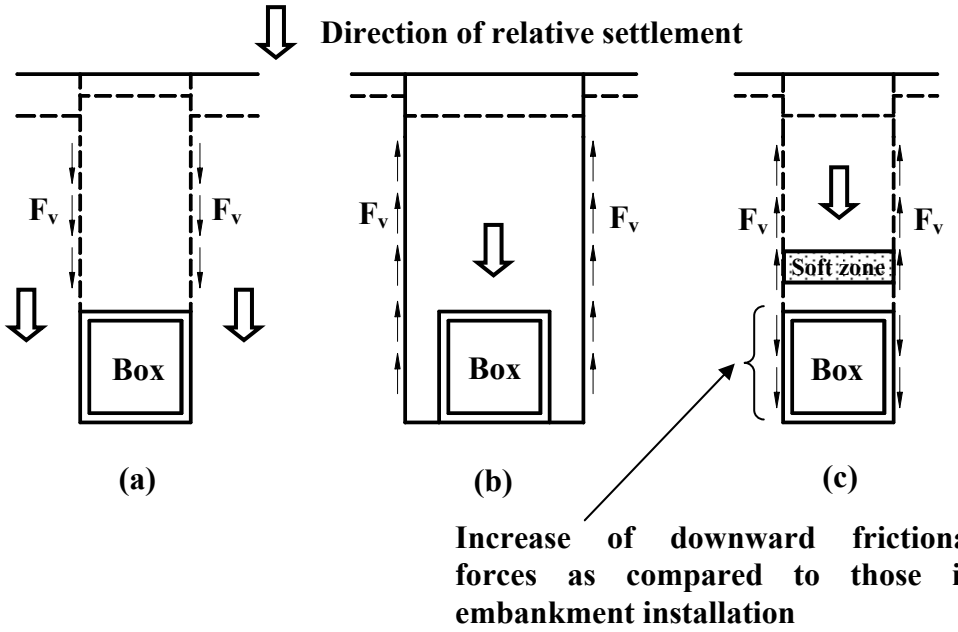

Fig. 7.1. Pressure transfer and shear effect within soil-structure system: (a) embankment installation; (b) trench installation; and (c) imperfect trench installation (F_v = generated friction forces)

Eqs. (7.6) and (7.7) proposed by Kim and Yoo (2005) indicate that the soil-structure interaction factor for embankment installations, F_e , for computing earth load on the top slab is a function of the foundation stiffness. Concrete box culverts are most likely to be installed on a yielding foundation unless a solid rock layer is encountered immediately under the concrete box culverts.

$$F_e = 1.047H^{0.055} \text{ on yielding foundation} \tag{7.6}$$

$$F_e = 1.200H^{0.059} \text{ on unyielding foundation} \tag{7.7}$$

The focus of this study is to present the effects of frictional forces acting on the sidewalls of buried box culverts as determined with FEA and detailed soil modeling. These frictional forces have different magnitudes and patterns depending on the installation type: embankment installation or ITI. Optimum geometries for the soft zone in ITI and the earth load reduction rates from numerous parametric studies will be presented.

7.3 Soil-Structure Interaction

7.3.1 Effects of Foundation Stiffness, Sidefill Treatment, and Interface Condition

The results of FEA show that the magnitude of the total load on the bottom slab always exceeds the sum of top earth load and dead load of the structure due to the net downward frictional force on the sidewalls. Fig. 7.2 shows the total vertical earth load acting on the bottom slab as the sum of the earth load on the top slab, the frictional force on the sidewalls, and the dead load of the structure in a number of different combinations

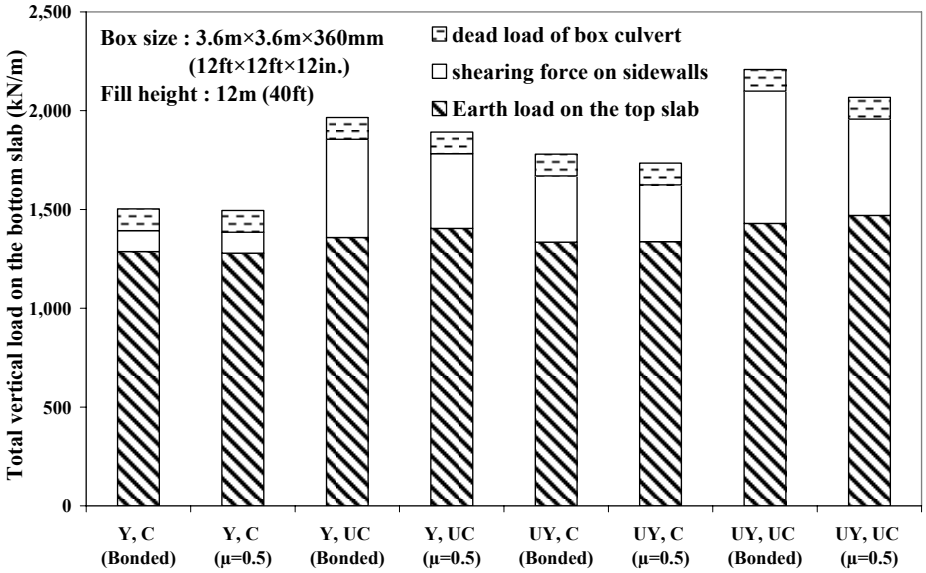

(a)

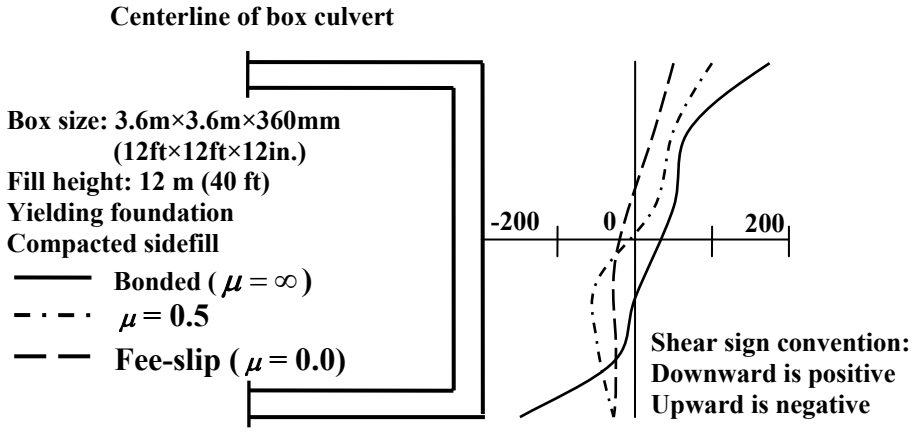

(b)

Fig. 7.2. Effects of foundation stiffness, sidefill treatment and interface conditions for earth loads on the top slab and frictional forces on the sidewall in embankment installation: (a) variation of total vertical earth loads and (b) frictional stresses (in kPa unit) versus interface conditions

of foundation stiffness, sidefill treatment, and interface conditions (coefficients of friction).

The contribution of the frictional force to the total vertical load on the bottom slab, as shown in Fig. 7.2(a), amounts to 7 - 19% and 25 - 30% for compacted and uncompacted sidefills, respectively. Fig. 7.2(a) also shows that the frictional forces on the sidewalls are smaller for the combination of compacted sidefill and yielding foundation than for the combination of uncompacted sidefill and unyielding foundation.

Although the magnitude of the frictional force varies as interface conditions vary, as shown in Fig. 7.2(b), the net downward frictional forces for specific foundation and sidefill conditions are not greatly affected by interface conditions. The computed differences in the total earth load at the bottom slab between bonded and frictional slip (with a coefficient of friction equal to 0.5) cases are less than 5%. Hence, the interface elements between the box culvert and adjacent sidefills in embankment installations were not considered further in this study. The frictional force on the sidewalls develops due to relative slips between the box culvert sidewalls and adjacent soil. As demonstrated in Figs. 7.2(b) and 7.3, the direction of the frictional force reverses in the middle of the wall, i.e., the frictional force acts downward at the top slab level but it acts upward at the bottom slab level. Fig. 7.3 shows that the net downward frictional forces do not differ very much, although the magnitude of the frictional forces on the sidewalls increases with backfill height.

7.3.2 Soil-Structure Interaction Factors

The soil-structure interaction factor, F_e, given in Eq. (7.2) does not recognize the contribution of the frictional force developed along the sidewall of the box culvert. The pressure on the bottom slab, according to AASHTO, is computed by summing the earth pressure at the top slab and dead load of the structure and may lead to an unconservative design. Therefore, F_e including frictional force effects should be used to compute design loadings of box culverts. Soil-structure interaction factors, developed with different computer programs, as a function of the ratio of the fill height to culvert width are plotted in Fig. 7.4 for yielding and unyielding foundations. Eqs. (7.14) and (7.15) were derived based on analytical values by a means of regression.

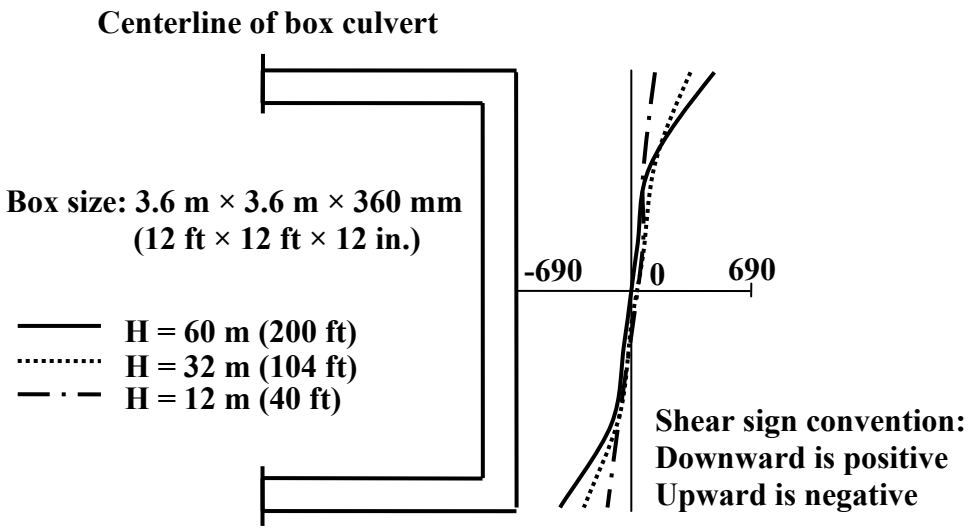

Fig. 7.3. Variation of shear distributions (in kPa unit) on the sidewall by backfill heights (H) (yielding foundation and compacted sidefill)
Earth pressure on the top slab:

$$F_e = -0.005\left(H / B_c\right) + 1.304 \quad \text{on compacted sidefill} \tag{7.14a}$$

$$F_e = -0.012\left(H / B_c\right) + 1.407 \quad \text{on uncompacted sidefill} \tag{7.14b}$$

Earth pressure on the bottom slab:

$$F_e = 0.004\left(H / B_c\right)^2 - 0.105\left(H / B_c\right) + 2.105 \quad \text{on compacted sidefill} \tag{7.15a}$$

$$F_e = 0.006\left(H / B_c\right)^2 - 0.175\left(H / B_c\right) + 2.685 \quad \text{on uncompacted sidefill} \tag{7.15b}$$

Fig. 7.4 shows proposed F_e for earth pressure along with values computed by various computer programs. Proposed values are in good agreement with those computed by MSC/NASTRAN. The noticeable differences in the soil-structure interaction factors between proposed values and those predicted by CANDE-89 under option level 2 may be attributable to the fact that the current version of CANDE-89 limits the maximum backfill height to be 1.5 times the culvert height and any fill height beyond this limit is to be treated by considering equivalent overburden pressure at the top.

Fig. 7.5(a) shows that the soil-structure interaction factor for the top slab, computed with several methods, is independent of fill height. The soil-structure interaction factor evaluated with Eqs. (7.3) through (7.5) suggested by Tadros et al. (1989) increases as the fill height increases, which is contrary to established reasoning. Kim and Yoo (2005) showed that the compacted fill along the sides of the box section did not appear to significantly affect F_e for the top slab. In the case of the bottom pressure, however, F_e was affected by the compactness of sidefill. As expected, compacted

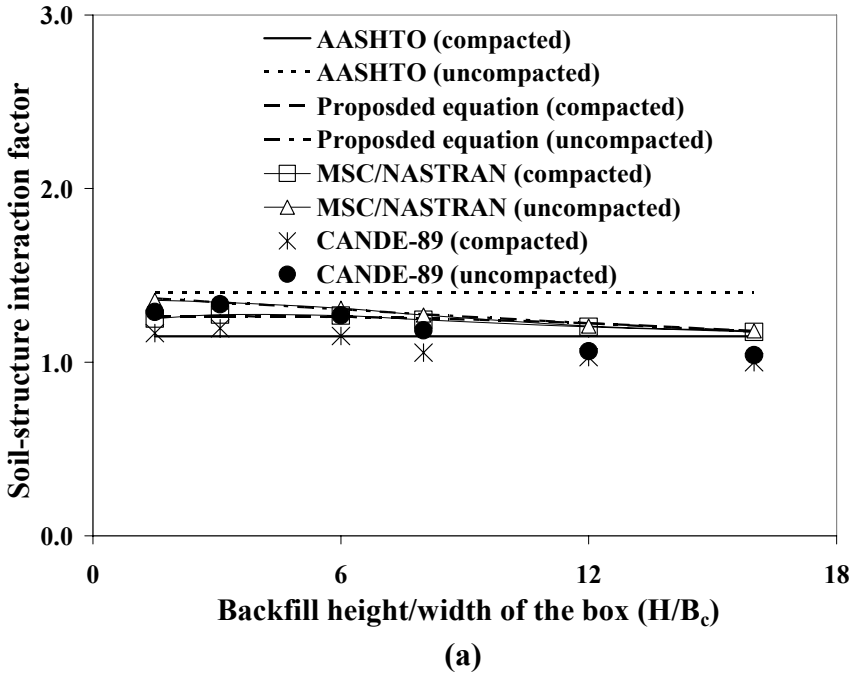

(a)

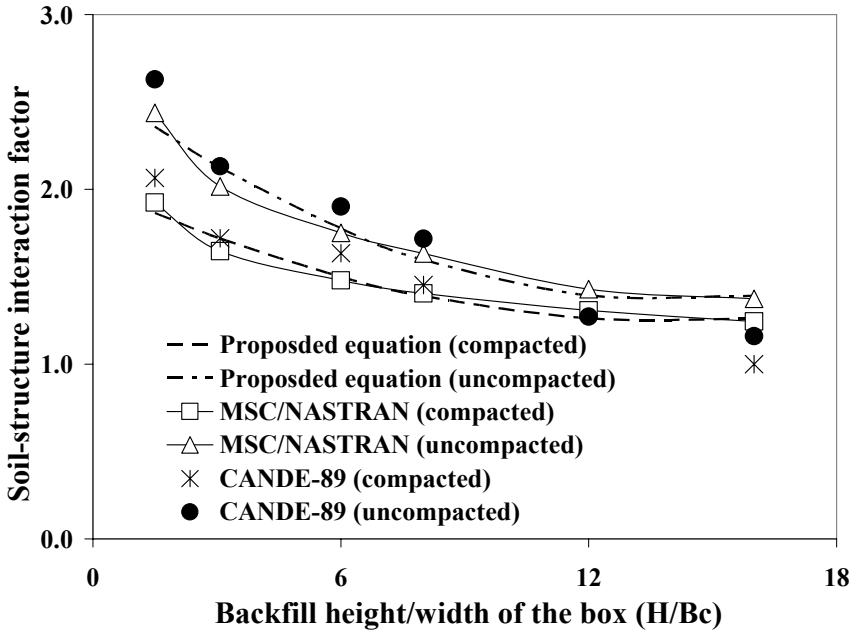

(b)

Fig. 7.4. Soil-structure interaction factors for embankment installations: for an yielding foundation (a) top slab and (b) bottom slab (continued)

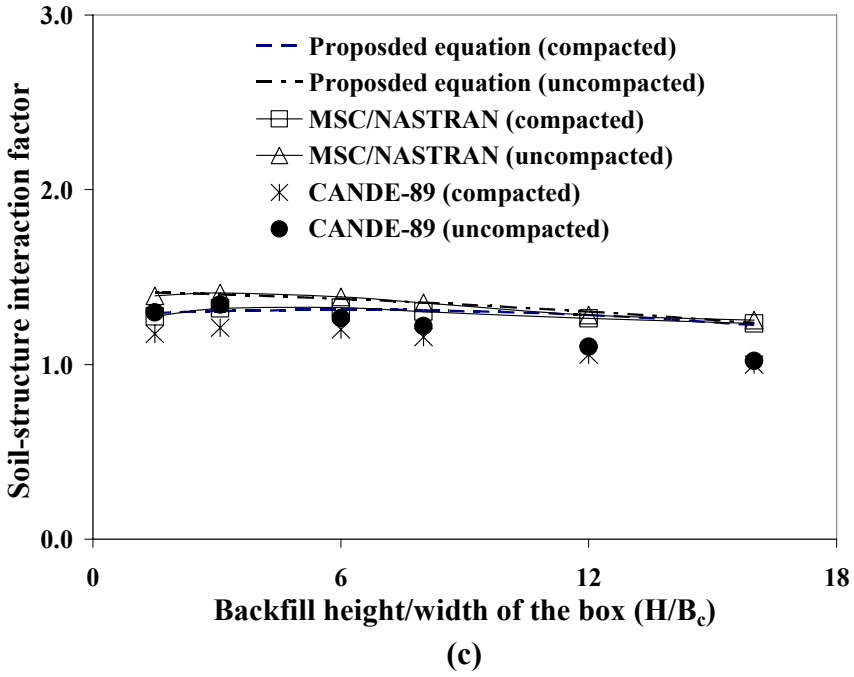

(c)

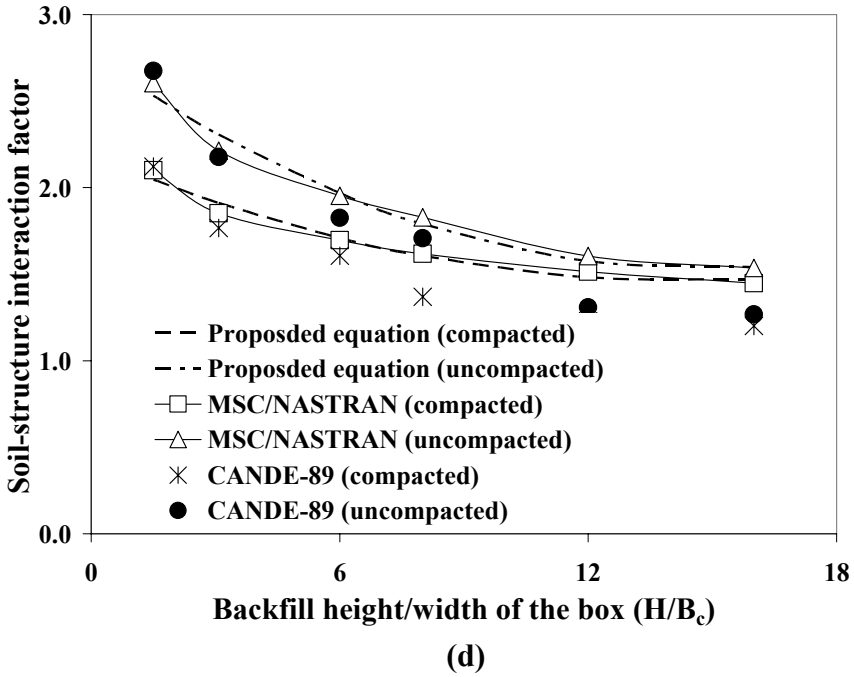

(d)

Fig. 7.4. Soil-structure interaction factors for embankment installations: for a unyielding foundation (c) top slab and (d) bottom slab

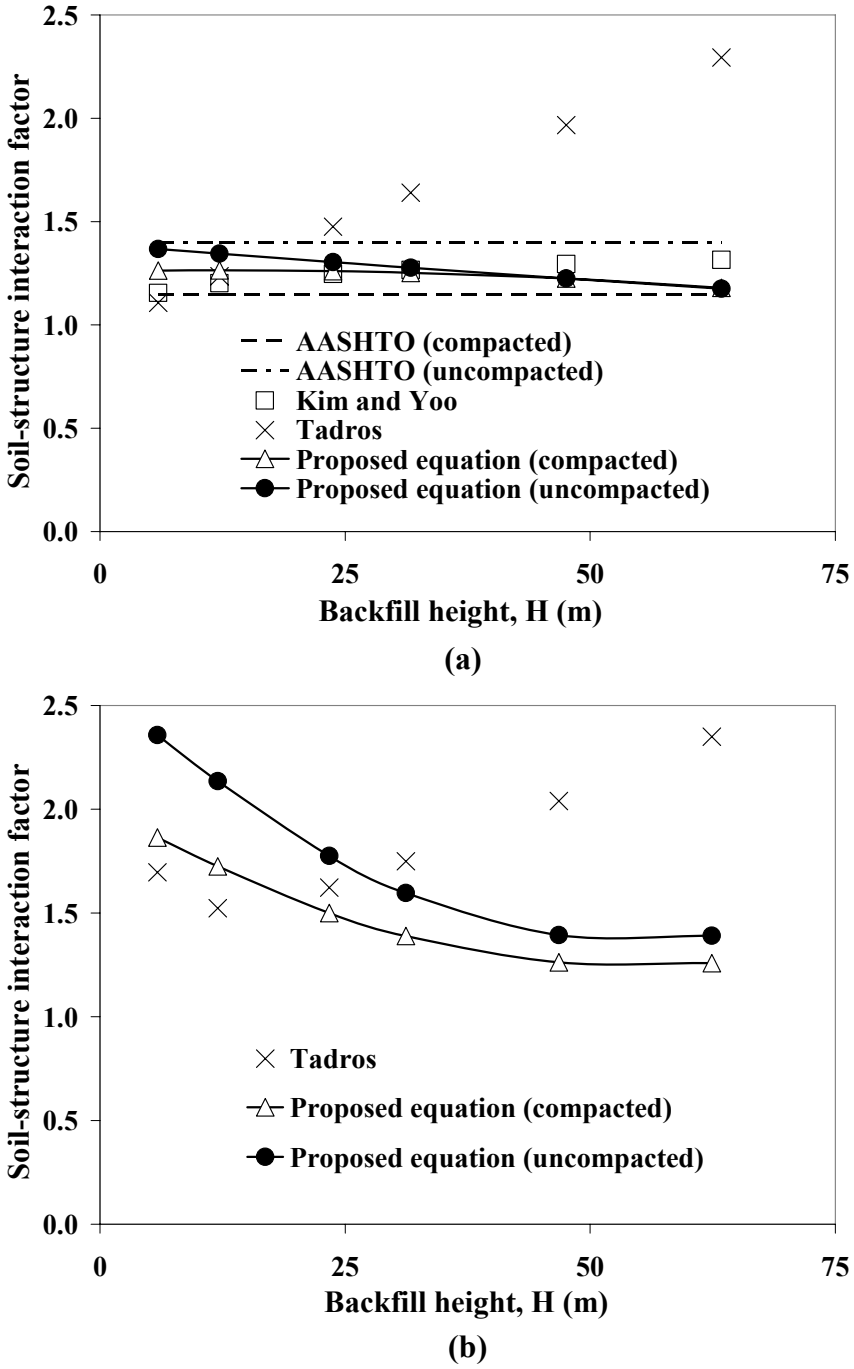

Fig. 7.5. Comparison of soil-structure interaction factors of AASHTO, Kim and Yoo, Tadros et al. and proposed equations on yielding foundation: (a) top slab and (b) bottom slab

sidefills tend to reduce the relative slippage between the adjacent soils along the sidewall and thereby reduce the frictional force developed.

7.4 Imperfect Trench Installation

7.4.1 Effects of Soft Zone Geometry and Interface Conditions

The geometry of the soft zone is also found to be controlled by three parameters: width, W; height, H_s; and the distance from the top of the culvert to the bottom of the soft zone, H'. Marston (1922), Spangler (1950a), and Vaslestad et al. (1993) proposed the traditional ITI geometry shown in Fig. 7.6(a). Kim and Yoo (2005) analyzed the specific ITI, depicted as soft zone geometry II in Fig. 7.6(c). They found that, compared to conventional embankment installation, the earth load on the top slab was reduced. It was found later during this study that significant frictional forces developed on the sidewalls which were transferred to the bottom slab. This observation led to the discovery of the soft zone geometry I in Fig. 7.6(b), where a layer of soft material is placed on the culvert sidewalls. Fig. 7.7(a) compares the effects of soft zone geometries I and II. It is informative to compare the total vertical load and the frictional force developed in conventional embankment installations. It is evident in Fig. 7.7(a) that the total load on the bottom slab is considerably less for geometry I than for geometry II. This is due primarily to reduced sidewall frictional forces.

The distribution of frictional force on culvert sidewalls for soft zone geometries I and II are compared in Fig. 7.7(b). There is no reversal in sign of the frictional force near the culvert mid-depth in ITI as compared to those shown in Figs. 7.2(b) and 7.3 for

embankment installations. Fig. 7.7 shows that sidewall frictional forces are directly related to the interface condition for the geometry II. The placement of the soft zone at the sidewalls of the culvert in the geometry I considerably reduced the development of the frictional forces.

A series of numerical investigations resulted in the optimum geometry for the soft zone shown in Fig. 7.6(b). The thickness of the soft zone along the sidewall of the culvert greater than the thickness of the culvert wall did not result in further reduction of the frictional force as shown in Fig. 7.8(b). Fig. 7.7 demonstrated that the soft zone geometry I reduces the developing large frictional forces. Consequently, it is more effective in reducing earth pressure on the bottom slab than the soft zone geometry II. It appears from Fig. 7.7(a) that the difference in frictional forces developed between the two simulated interface conditions, i.e., full-bonded ($\mu = \infty$) and free-slip ($\mu = 0.0$) for the soft zone geometry I is 66%.

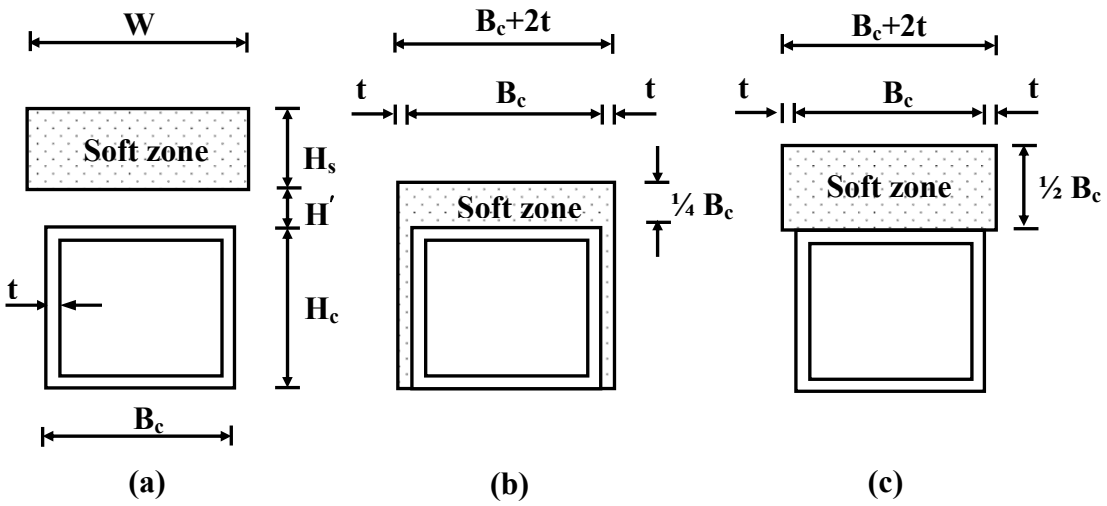

Fig. 7.6. Notation in imperfect trench installations and geometries of soft zone: (a) notation; (b) soft zone geometry I (proposed); and (c) soft zone geometry II

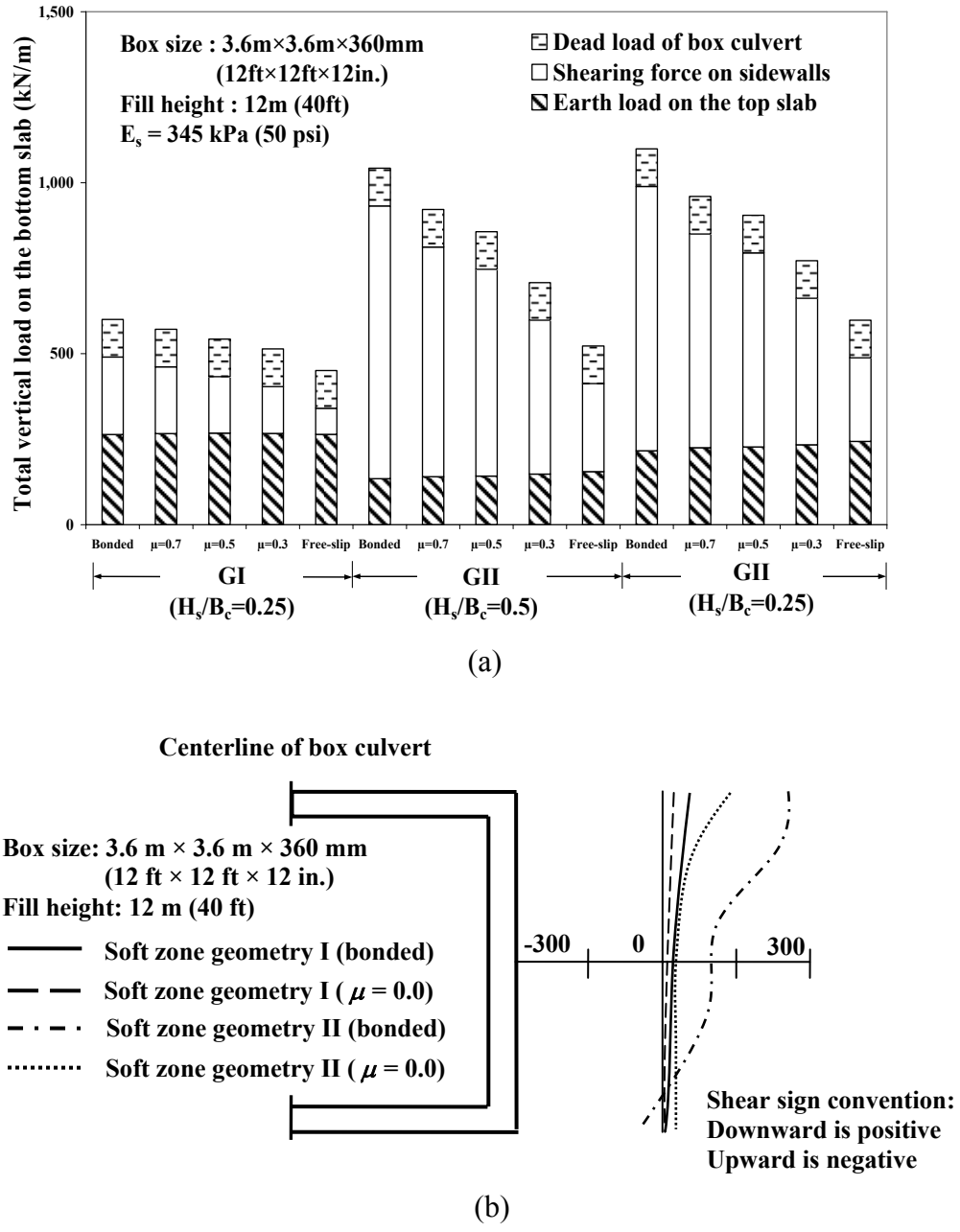

Fig. 7.7. Effects of interface conditions for earth loads on the top slab and frictional forces on the sidewall in imperfect trench installation (yielding foundation and compacted sidefill): (a) variation of total vertical earth loads and (b) distributions of frictional stresses (in kPa unit) versus interface conditions

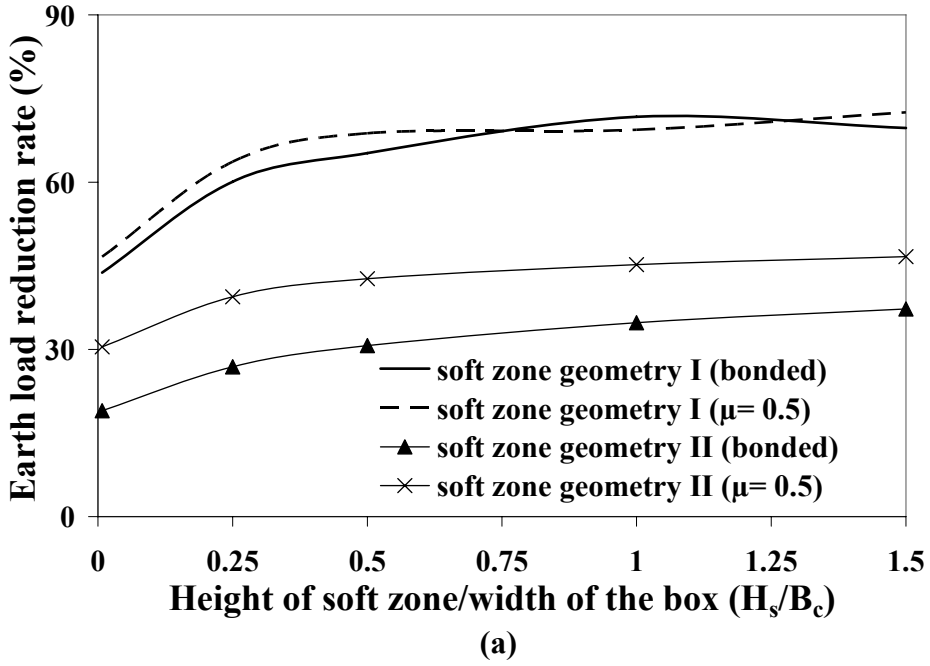

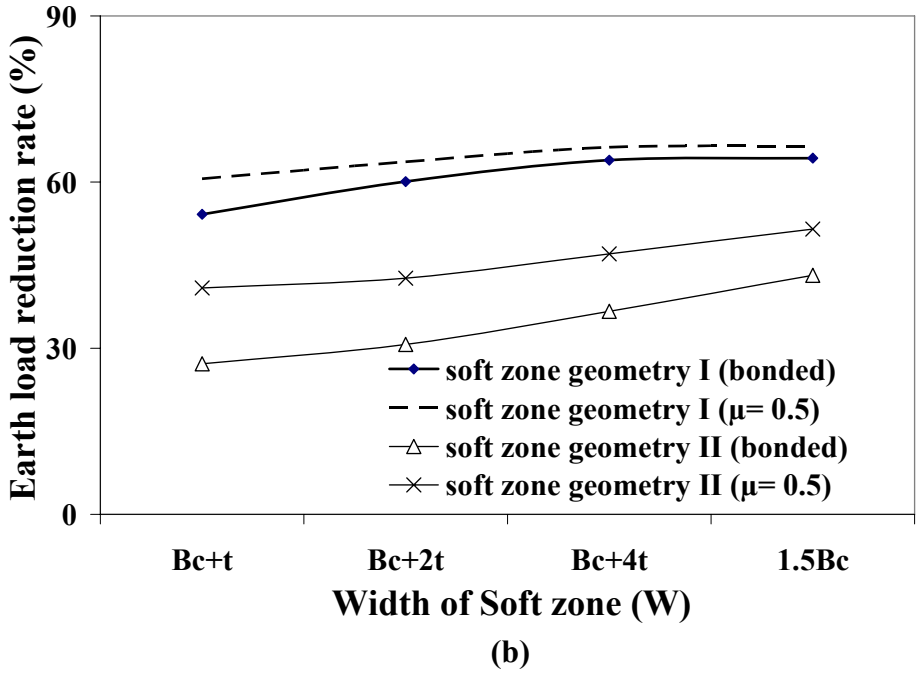

Fig. 7.8. Earth load reduction rates for the bottom slab versus geometries of soft zone and interface conditions in imperfect trench installations: (a) effects of height of soft zone and (b) effects of width of soft zone (parameters: box size: 3.6 m×3.6 m×360 mm; backfill height= 12 m; yielding foundation and compacted sidefill)

It is noted in Fig. 7.7(a) that the contribution of the frictional force to the total earth pressure is relatively small in the soft zone geometry I. Although the total difference in frictional forces which developed following two extreme cases of the friction coefficient for the soft zone geometry I is 66%, it amounts to 25% difference in the total vertical earth pressure. The 25% difference is, therefore, considered to be non-negligible in the design of ITI.

7.4.2 Predictor Equations

The geometry of the soft zone, interface condition, ratio of the fill height to the width of the box culvert, and modulus of elasticity and Poisson's ratio of the lightweight materials are variables affecting the earth load reduction rate for ITI. After the optimum geometric parameters were identified in Fig. 7.8, the remaining variables not related to the geometry of the optimum soft zone, such as the ratio of the fill height to the width of the box culvert, and modulus of elasticity (E_s) and Poisson's ratio of the soft material, were analyzed. An examination of the analysis results revealed that the ratio of the fill height to the width of the box culvert and Poisson's ratio of the lightweight materials did not affect the earth load reduction rate very much. The analysis results indicated that the modulus of elasticity of the lightweight material is a major parameter affecting the earth load reduction rate as can be seen from Fig. 7.9. As the interface condition has a considerable effect on the total earth load on the bottom slab, its effect was incorporated in the proposed equations of the earth load reduction rate. Eqs. (7.16a) through (7.16l)

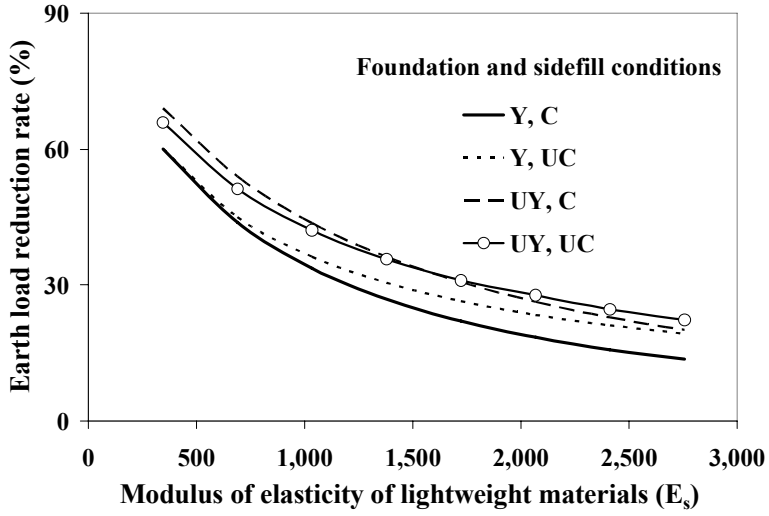

(a)

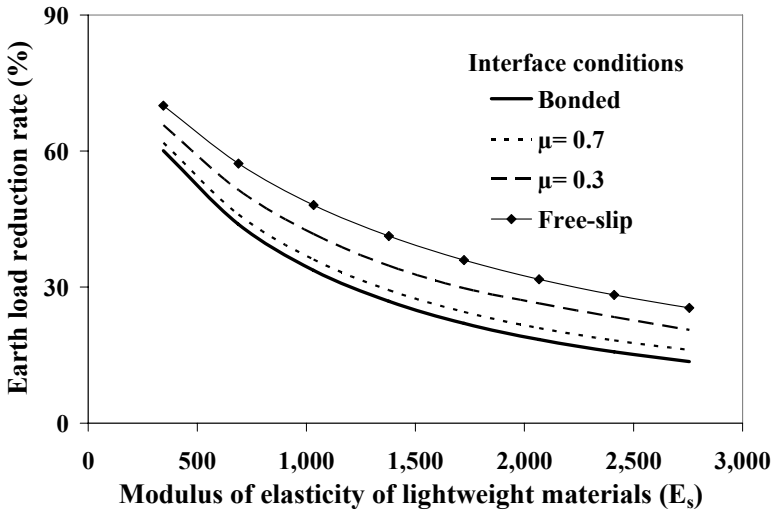

(b)

Fig. 7.9. Earth load reduction rates for the bottom slab versus modulus of elasticity of lightweight materials in soft zone geometry I: (a) effects of foundation stiffness and sidefill treatment (bonded) and (b) Y,C (Y= yielding foundation; UY= unyielding foundation; C= compacted sidefill; UC= uncompacted sidefill) (continued)

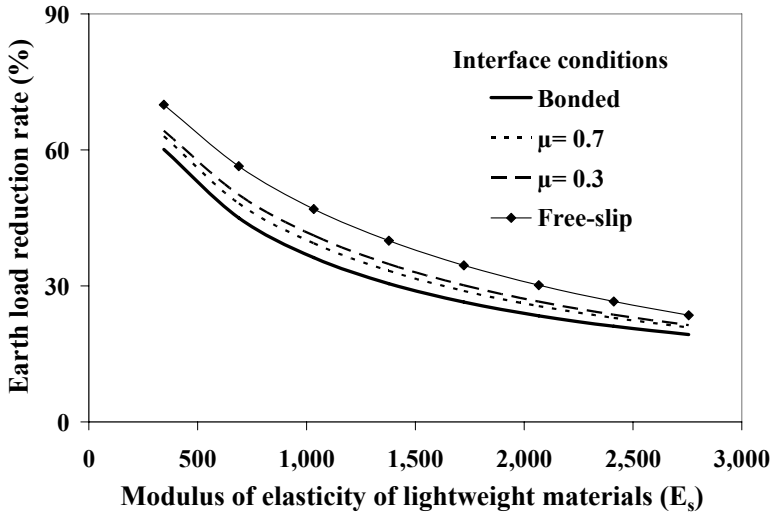

(c)

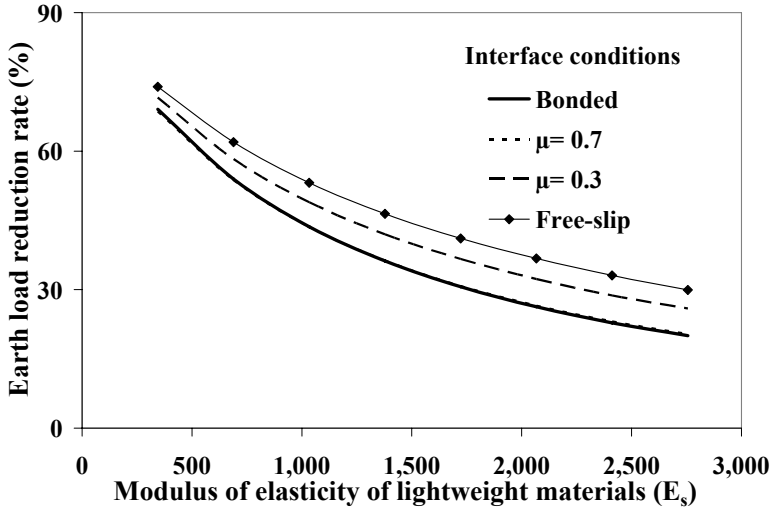

(d)

Fig. 7.9. Earth load reduction rates for the bottom slab versus modulus of elasticity of lightweight materials in soft zone geometry I: (c) Y,UC and (d) (d) UY, C (Y= yielding foundation; UY= unyielding foundation; C= compacted sidefill; UC= uncompacted sidefill) (continued)

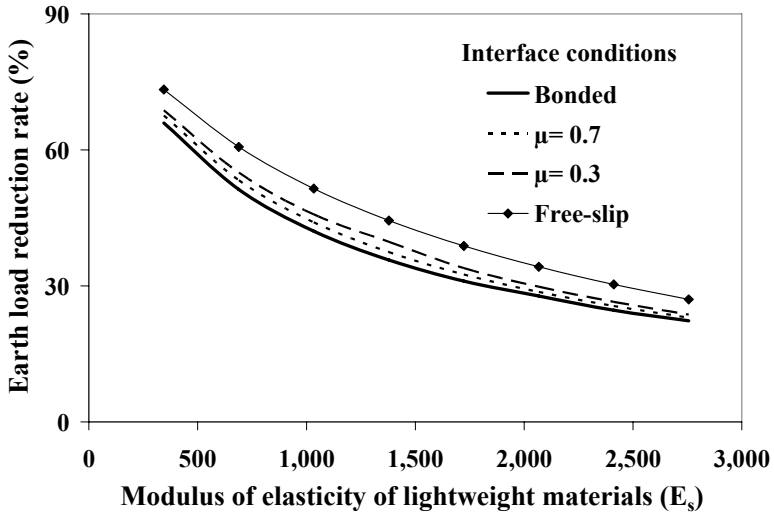

(e)

Fig. 7.9. Earth load reduction rates for the bottom slab versus modulus of elasticity of lightweight materials in soft zone geometry I: (e) UY, UC (Y= yielding foundation; UY= unyielding foundation; C= compacted sidefill; UC= uncompacted sidefill)

were formulated for earth load reduction rates for the bottom slab in the soft zone geometry I based on linear regression on data collected from several hundred hypothetical models. It is of interest to note that a lightweight material such as baled hay having a high value of modulus of elasticity close to that of loosened soil ($E_s = 3{,}445$ kPa) reduces the total earth load only 20%.

For yielding foundation and compacted sidefill:

$$R = 66.46\, e^{-0.0006\, E_S} \qquad \text{for full-bonded } (\mu = \infty) \qquad (7.16a)$$

$$R = 66.46\, e^{-0.0006\, E_S}\ \mu^{-0.0517} \qquad \text{for frictional slip } (\mu = 0.3 \text{ - } 0.7) \qquad (7.16b)$$

$$R = 76.04\, e^{-0.0004\, E_S} \qquad \text{for free-slip } (\mu = 0.0) \qquad (7.16c)$$

For yielding foundation and uncompacted sidefill:

$$R = 61.94\, e^{-0.0005\, E_S} \qquad \text{for full-bonded } (\mu = \infty) \qquad (7.16d)$$

$$R = 61.94\, e^{-0.0005\, E_S}\ \mu^{-0.0808} \qquad \text{for frictional slip } (\mu = 0.3 \text{ - } 0.7) \qquad (7.16e)$$

$$R = 76.67\, e^{-0.0004\, E_S} \qquad \text{for free-slip } (\mu = 0.0) \qquad (7.16f)$$

For unyielding foundation and compacted sidefill:

$$R = 76.37\, e^{-0.0005\, E_S} \qquad \text{for full-bonded } (\mu = \infty) \qquad (7.16g)$$

$$R = 76.37\, e^{-0.0005\, E_S}\ \mu^{-0.0131} \qquad \text{for frictional slip } (\mu = 0.3 \text{ - } 0.7) \qquad (7.16h)$$

$$R = 79.88\, e^{-0.0004\, E_S} \qquad \text{for free-slip } (\mu = 0.0) \qquad (7.16i)$$

For unyielding foundation and uncompacted sidefill:

$$R = 69.48\, e^{-0.0004\, E_S} \qquad \text{for full-bonded } (\mu = \infty) \qquad (7.16j)$$

$$R = 69.48\, e^{-0.0004\, E_S}\ \mu^{-0.0574} \qquad \text{for frictional slip } (\mu = 0.3 \text{ - } 0.7) \qquad (7.16k)$$

$$R = 80.40\, e^{-0.0004\, E_S} \qquad \text{for free-slip } (\mu = 0.0) \qquad (7.16l)$$

where R is the earth load reduction rate (%), E_s is the modulus of elasticity of lightweight materials (kPa), and μ is the coefficient of friction. Soil-structure interaction factors in ITI represented as soft material geometry I, therefore, are to be calculated by Eq. (7.17).

$$F_{ei} = F_e (1 - R/100) \tag{7.17}$$

where F_{ei} is the soil-structure interaction factor in ITI, and F_e is the soil-structure interaction factor given by Eqs. (7.14) and (7.15) for embankment installation.

7.4.3 Height of Soft Zone

As can be seen from Figs. 7.7 and 7.8(a), the total earth pressure at the bottom level of the culvert for the geometry II is slightly reduced (on the average, 5-6%) in the case when the thickness of the soft zone is equal to 0.5 times the exterior width of the culvert as compared to the same in the case when the thickness of the soft zone is equal to 0.25 times the exterior width of the culvert. The difference in the total earth pressure at the bottom level of the culvert for geometry I is even smaller than that observed in geometry II. From the cost-benefit consideration, this is perceived to be the typical case of diminishing return. Hence, the height of the soft zone was taken to be 0.25 times the exterior width of the culvert. It is noted that Fig. 7.8(b) and all the values used in the computation of reduction rates of the total earth load in rounded pipes reported in Chapters 4, 5, and 6 were generated using the height of the soft zone for geometry II to be twice the height for geometry I. This was done intentionally to compensate for any uneven/unfavorable conditions in comparison. For example, the extension of the soft

zone all the way down to the bottom level of the conduits on both sides in geometry I would indeed require additional material as compared to the case in geometry II.

CHAPTER 8

SUMMARY AND CONCLUSIONS

8.1 Summary and Conclusions

The single most important accomplishment of the study is the discovery of the optimum soft zone geometry I to be incorporated into the ITI of deeply buried conduits. Although Brown (1967) first introduced the possibility of numerically assessing the effectiveness of ITI, and Kim and Yoo (2002) extended this concept considerably, no one has ever recognized the development of fairly high intensity frictional forces on the sides of the conduits in ITI as a result of altered soil movements around it. How to effectively reduce the undesirable frictional forces during the course of this study by extending the soft zone all the way to the bottom level of the conduit was discovered. As a consequence, this research demonstrates the phenomenal earth load reduction capability (up to 85%) by the introduction of the optimum soft zone geometry I. The optimum soft zone geometry can be applied to any deeply buried conduits with minor adjustment. Conduits studied in this research include round concrete pipes, corrugated PVC pipes, corrugated steel pipes, and box culverts. Although the optimum soft zone geometry I is applicable to all of the conduits mentioned here, there are a few subtleties representing particular characteristics of each conduit that require additional attention. Presented are

some of the highlights of these observations and precautionary measures needed in dealing with each conduit.

Concrete Pipes

1) The maximum earth pressure on a pipe installed with the AASHTO type 1, 2, or 3 standard embankment installations occurs at about 25 degrees from the invert. This differs markedly from the Heger pressure distribution presented in Figure 12.10.2.1-1, AASHTO LRFD (2004). The acute pressure increase at the invert for AASHTO type 4 standard embankment installation emphasizes the importance of treating the bedding material, at least marginally, to achieve the beneficial effect of the haunch in AASHTO type 3 standard embankment installation.
2) Vertical arching factors for buried concrete pipes are affected by backfill height as well as installation practices for bedding and sidefill. AASHTO, however, stipulates constant vertical and horizontal arching factors independent of backfill height. In the case of AASHTO type 4 standard embankment installation, the *VAF* stipulated by AASHTO is approximately 8-17% less than that calculated by MSC/NASTRAN. The constant *HAF* of AASHTO type 3 and type 4 is approximately 23% and 43%, respectively, less than that evaluated by MSC/NASTRAN. However, the *HAF* computed with SPIDA and MSC/NASTRAN do not vary appreciably with backfill height.

3) This study showed that the modulus of elasticity (E_s) of lightweight materials in the soft zone is the single most important factor affecting the earth load reduction rate in the ITI.

Corrugated PVC Pipes

1) It has been shown that the interface effect on *VAF* in flexible conduits is not negligible as in the case of rigid conduits. However, the degree of the interface effect cannot be determined by analysis alone, although the analysis procedure used in this study demonstrates that any interface effect including in-between condition can be reflected. A well-designed field testing program is needed to answer this question; however, a conservative approach of full bond interface model is an intermediate option.
2) The deflections from ABAQUS were much less than those computed from Spangler equation (1941) while they were relatively close to those from the Burns and Richard (1964) deflection equations. The results from the ABAQUS and Burns and Richard deflection equations, also, showed that the interface conditions have insignificant effects on the deflections of corrugated PVC pipes. This observation appears valid as the primary parameter affecting the deflection of flexible PVC pipes is the earth load at the crown which does not vary much depending upon the interface conditions.
3) The reduction rate of the arching factors related to axial force alone reaches up to 92%, while the reduction rate of maximum wall stresses related to the combined action of bending moment and axial force is 85% as the reduction rate related to

bending moment is only 18%. This is due to the fact that the maximum bending moment at the springline is not significantly reduced because of the horizontal movement of the flexible pipe aided by the presence of soft zone that was needed to minimize the frictional forces.

Corrugated Steel Pipes

1) The arching factors for buried CSP are not affected very much by the pipe slenderness ratio, *D/r*, and the ratio of fill height-to-diameter, *H/D*. Therefore, the current practice of specifying constant values for *VAF* and *HAF* by AASHTO LRFD and AISI is justified. However, their *VAF* (AASHTO LRFD=1.1, AISI=0.75) appear to be quite unconservative. Further, they do not specify *HAF* at all. It has been found that *VAF* and *HAF* need to be 1.4 and 0.6, respectively, for SW90.
2) The constant arching factors and the simplified predictor equations for the deflections at the crown and the maximum wall stresses, Eqs. (6.9) and (6.10), do not require the value of the constrained soil modulus (M_S) as in other existing predictor equations by Burns and Richard (1964) and/or AASHTO LRFD (2004a).
3) The interface effect on *VAF* of CSP in embankment installation is not negligible as in the case for rigid conduits.
4) The elastic buckling strengths of the buried CSP were carried out on the pipe-spring model. The elastic buckling strengths from the pipe-spring model are in good agreement with those computed from the AISI procedure. AASHTO LRFD (2004a) gave critical stresses greater than those from the pipe-spring model.

Box Culverts

1) Total vertical earth loads on the bottom slab of box culverts are computed as the sum of the earth load on the top slab, the frictional force on the sidewalls, and the dead load of the structure. Numerical analyses carried out on deeply buried box culverts in embankment installations show that the frictional force developed between the sidewall of the culvert and adjacent soil sidefill amounts up to 7 – 19% and 25 – 30% of the total vertical load on the bottom slab for compacted and uncompacted sidefills, respectively. Current AASHTO equations that do not consider the shear effect are unconservative.
2) Fairly high intensity of frictional force is developed along the sidewall of culverts in ITI primarily due to the additional shear transmitted from the central soil prism immediately above the structure as a result of reverse arching action. The frictional force for the total vertical load on the bottom slab in ITI amounts up to 77 – 79% for compacted sidefill and 80 – 81% for uncompacted sidefill.
3) The interface conditions of the box culvert-soil system were also found to have a significant effect on the total earth pressure of ITI at the bottom slab depending upon the coefficient of friction assumed.

It is hoped that an innovative understanding of the soil-structure interaction for deeply buried conduits and other findings presented in this study will find their way into improved specifications in the near future. As the economic impact appears to be huge,

immediate implementation of these findings by designers and contractors is particularly urgent for conduits buried under several hundred feet of fill.

8.2 Recommendations for Future Study

Field experimental studies of deeply buried roadway conduits would be desirable in order to calibrate the results of the FEA and verify the validity and reasonableness of the assumptions of the physical behavior of the soil-structure interaction and material properties and characterization adopted in this study. In light of the importance of the interface condition between the exterior wall of the conduits and the backfill soil on the behavior of the soil-structure interaction, particularly in ITI, a detailed experimental study on this topic is urgently needed. Information on the properties and behavior, particularly the long-term effect and potential environmental degradation, of the soft materials envisioned for ITI would be a welcome addition.

REFERENCES

AASHTO (2002). *AASHTO standard specifications for transportation materials and methods of sampling and testing*, 22nd. American Association of State Highway and Transportation Officials, Washington, DC.

AASHTO (2004a). *AASHTO LRFD Bridge Design Specifications*, 3rd ed., American Association of State Highway and Transportation Officials, Washington, DC.

AASHTO (2004). *LRFD Bridge Construction Specifications*, 2nd ed. American Association of State Highway and Transportation Officials, Washington, DC.

ABAQUS User's manual. (2003). Habbitt, Karlsson and Sorensen, Inc., Pawtucket, RI.

ABAQUS Theory manual. (2003). Habbitt, Karlsson and Sorensen, Inc., Pawtucket, RI.

ACI (2002). Building Code Requirements for Structural Concrete (ACI 318-02) and Commentary (ACI 318R-02), Second Printing, American Concrete Institute, Michigan.

ACPA (1988). *Concrete Pipe Handbook*, Third Printing, American Concrete Pipe Association, Irving, TX.

ACPA (1989). *SPIDA users instructions micro computer version 3c*. American Concrete Pipe Association, Vienna, VA.

ACPA (1994). *ACPA Concrete Pipe Technology Handbook*. Second Printing, American

Concrete Pipe Association, Vienna, VA.

ACPA (1996). Standard Installations and Bedding Factors for the Indirect Design Method. *Design Data 40*, American Concrete Pipe Association, Vienna, VA.

ACPA (2000). *Concrete Pipe Design Manual*, Thirteenth Printing, American Concrete Pipe Association, Vienna, VA.

ACPA (2001). *ACPA Concrete Pipe Handbook*. American Concrete Pipe Association, Vienna, VA.

AISI (1994). *Handbook of Steel Drainage & Highway Construction Products*, 5th. American Iron and Steel Institute, Washington, DC.

ASCE Manual of Practice No.37. (1970). Design and Construction of Sanitary and Storm Sewers, American Society of Civil Engineers (ASCE), New York, NY.

Brockenbrough, R.L. (2006). A personal correspondence (e-mail, June 29, 2006) to Yoo, C.H., Department of Civil Engineering, Auburn University, Auburn, AL.

Brown, C.B. (1967). *Forces on Rigid Culverts Under High Fills. J. Struct. Div*., ASCE, 93(5), 195-215.

Burns, J. Q., and Richard, R. M. (1964). Attenuation of Stresses for Buried Cylinders. In *Proc.*, *Symposium on Soil-Structure Interaction*, University of Arizona Engineering Research Laboratory, Tucson.

Christian, J.T. (1982). "The Application of Generalized Stress-Strain Relations." *Proceeding of the Symposium on Limit Equilibrium, Plasticity and Generalized Stress-Strain Applications in Geotech. Eng.,* ASCE Annual Convention and Exposition, Hollywood, FL.

Civil Connection. (2006). "FHWA Broadens Allowable Pipe Choices." On-line version at http//www.news.cenews.com, December 26, 2006.

Duncan, J.M., Byne, P., Wong, K.S., and Mabry, P. (1980). "Strength, Stress-Strain and Bulk Modulus Parameters for Finite Element Analyses of Stresses and Movement in Soil Masses." *UCB/Gt/80-01*, Univ. of California, Berkeley, CA.

Duncan, J.M., and Chang, C.Y. (1970). "Nonlinear Analysis of Stress and Strain on Soils." J. Soil Mech. and Found. Div., ASCE, 96(5), 1629-1653.

Heger, F.J. (1988). "New Installation Designs for Buried Concrete Pipe." *Proceedings of Pipeline Infrastructure,* ASCE, 117-135.

Heger, F.J., Liepins, A.A., and Selig, E.T. (1985). "SPIDA: An Analysis and Design System for Buried Concrete Pipe." Advances in Underground Pipeline Engineering – *Proceeding of the International Conference*, ASCE, 143-154.

Janbu, N. (1957). Earth pressure and bearing capacity calculations by generalized procedure of slices, Proc.4.Int.Conf.SMFE, London, Vol. 2, 207-212.

Janbu, N. (1963). Soil Compressibility as Determined by Oedometer and Triaxial Tests, European Conference on Soil Mechanics & Foundations Engineering, Wiesbaden, Germany Vol. 1, 19-25.

Kang, J., Parker, F., and Yoo, C.H. (2007). Soil-structure interaction for deeply buried corrugated steel pipes. Part I: Embankment installation. Engineering Structures.

Katona, M.G., Akl, A.Y. (1987). Design of buried culverts with stress-relieving joints. Transportation Research Record; 1129: 39-54.

Katona, M.G., Vittes, P.D. (1982). Soil-structure analysis and evaluation of buried box-

culvert Designs. Transportation Research Record; 878: 1-7.

Katona, M.G., Smith, J.M., Odello, R.S., and Allgood, J.R. (1976). CANDE-a modern approach for the structural design and analysis of buried culverts. Report FHWA-RD-77-5, FHWA, U.S. Department of Transportation.

Kim, K., and Yoo, C.H. (2002). Design Loading for Deeply Buried Box Culverts, Highway Research Center, Auburn University, AL.

Kim, K., and Yoo, C.H. (2005). "Design Loading for Deeply Buried Box Culverts." *J. Geotech. Geoenviron. Eng.*, ASCE, 131(1), 20-27.

Kondner, R.L. (1963). "Hyperbolic Stress-Strain Response: Cohesive Soils." *J. Soil Mech. Found. Div.*, ASCE, 98(1), 115-143.

Lin, R-S.D. (1987). "Direct Determination of Bulk Modulus of Partially Saturated Soils." *Project Report ACP87-341P,* M.S. Degree, University of Massachusetts, Amherst, MA.

Marston, A. (1922). "Second Progress Report to the Joint Concrete Culvert Pipe Committee." Iowa Engineering Experimental Station, Ames, IA.

Marston A. (1930). The theory of external loads on closed conduits in the light of the latest experiments. *Bulletin 96*. Iowa Engineering Experiment Station, Ames, IA.

Marston, A., and Anderson, A. O. (1913). The theory of loads on pipes in ditches and tests of cement and clay drain tile and sewer pipes. *Bulletin 31*, Iowa Engineering Experiment Station, Ames, IA.

McAffee, R.P., and Valsangkar, A.J. (2004). "Geotechnical Properties of Compressible Materials Used for Induced Trench Construction." *J. Testing and Evaluation*,

32(2), 143-152.

McGrath, T.J., and Selig, E.T. (1999). "Pipe Interaction with the Backfill Envelope." *Report FHWA-RD-98-191*, Federal Highway Administration, U.S. Department of Transportation.

McAffee, R. P., and Valsangkar, A. J. (2005). Performance of an Induced Trench Installation. In *Transportation Research Record: Journal of the Transportation Research Board, No. 1936*, TRB, National Research Council, Washington, DC, 230-237.

McGrath, T. J. (1998). *Design Method for Flexible Pipe*. A Report to the AASHTO Flexible Culvert Liaison Committee, Simpson Gumpertz & Heger Inc.

McGrath, T. J. (1999). Calculating Loads on Buried Culverts Based on Pipe Hoop Stiffness. In *Transportation Research Record: Journal of the Transportation Research Board, No. 1656*, TRB, National Research Council, Washington, DC, 73-79.

McVay, M. C. (1982). *Evaluation of Numerical Modeling of Buried Conduits*, PhD Dissertation, Dept of Civil Engineering, University of Massachusetts, Amherst, Massachusetts.

McVay, M.C., and Selig, E.T. (1981). Soil Model and Finite Element Boundary Studies, Report No. ACP81-283I, Dept. of Civil Engineering, University of Massachusetts, Amherst, Mass.

McVay, M. C. (1982). "Evaluation of Numerical Modeling of Buried Conduits." PhD Dissertation, Dept of Civil Engineering, University of Massachusetts, Amherst,

MA.

Moore, I. D. (2000). Buried Pipes and Culverts. Geotechnical and Geoenvironmental Engineering Handbook, 18: 541-567.

MSC/NASTRAN 2005 Release Guide. (2005). The MacNeal-Schwendler Corp., Los Angeles, CA.

Musser, S.C. (1989). "*CANDE-89 User Manual*." *FHWA-RD-89-169*. Federal Highway Administration, U.S. Department of Transportation.

Sargand, S. M., and Masada, T. (2003). Soil Arching over Deeply Buried Thermoplastic Pipe. In *Transportation Research Record: Journal of the Transportation Research Board,No. 1849*, TRB, National Research Council, Washington, DC, 109-123.

Sargand, S. M., Hazen, G. A., and Masada, T. (2000). *Field Verification of Structural Performance of Thermoplastic pipe Under Deep Backfill Conditions*. Draft Final Report. Ohio Department of Transportation; FHWA, U.S. Department of Transportation.

Sargand, S. M., Masada, T., and Schehl, D. J. (2001). Soil Pressure Measured at Various Fill Heights Above Deeply Buried Thermoplastic Pipe. In *Transportation Research Record: Journal of the Transportation Research Board, No. 1770*, TRB, National Research Council, Washington, DC, 227-235.

Sargand, S. M., Hazen, G. A., White, K., and Moran, A. (2001). Time-Dependent Deflection of Thermoplastic Pipes Under Deep Burial. In *Transportation Research Record: Journal of the Transportation Research Board, No. 1770*, TRB,

National Research Council, Washington, DC, 236-242.

Sargand, S.M., Hazen, G.A., and Masada, T. (2002). Field Verification of Structural Performance of Thermoplastic pipe Under Deep Backfill Conditions. Draft Final Report Ohio Department of Transportation; FHWA, U.S. Department of Transportation.

Sargand, S.M., and Moreland, A. Experimental and Numerical Investigation of A Deeply Buried Corrugated Steel Multi-Plate Pipe. Final Technical Report. Ohio Department of Transportation; FHWA, U.S. Department of Transportation; 2004.

Selig, E.T. (1972). "Subsurface soil-structure interaction: A synopsis."*Highw. Res. Rec*., 413, 1-4.

Selig, E.T. (1988). "Soil Parameters for Design of Buried Pipelines." In *Pipeline Infrastructure:* Proc., Pipeline Infrastructure Conference, ASCE, NY.

Sladen, J.A., and Oswell, J.M. (1988). "The Induced Trench Method – A Critical Review and Case History." *Can. Geotech. J*., 25, 541-549.

Spangler, M.G. (1933). "The supporting Strength of Rigid Pipe Culverts." *Bulletin 112*, Iowa State College, IA.

Spangler, M. G. (1941). The Structural Design of Flexible Culverts. *Iowa State College Bulletin 30*, Vol. XI.

Spangler, M.G. (1950a). "A Theory of Loads on Negative Projecting Conduits." *Proceedings of the Highway Research Board*, 30, Transportation Research Board, Washington, DC, 153-161.

Spangler, M. G. (1950b). Field Measurements of the Settlement Ratios of Various

Highway Culverts, Bulletin 171, Iowa Engineering Experiment Station, Ames, Iowa.

Spangler, M. G., and Handy, R.L. (1982). *Soil Engineering*, 4th Ed., Harper and Row, NY.

Sven, N., and Liedberg, D. (1997). "Load Reduction on A Rigid Pipe Pilot Study of A Soft Cushion." Transportation Research Record, 1594, 217-223.

Tadros, M.K., Benak, J.V., and Gilliland, M.K. (1989). Soil pressure on box culverts. ACI Structural Journal, 86(4): 439-450.

Tyler, M. (2003). "Earth Pressures on Induced Trench Conduits." MS Thesis, Dept of Civil Engineering, University of New Brunswick, Canada.

Vaslestad, J. (1990). "Soil Structure Interaction of Buried Culverts." PhD thesis, The Norwegian Institute of Technology, Norway.

Vaslestad, J., Johansen, T.H., and Holm, W. (1993). "Load reduction on rigid culverts beneath high fills: long term behavior." *Transportation Research Record,* 1415, Transportation Research Board, Washington, DC, 58-68.

Watkins, R. K. (1990). Plastic Pipes Under High Landfills. *Buried Plastic Pipe Technology*, ASTM STP 1093, 379-392.

Watkins, R. K., and Spangler, M. G. (1958). Some Characteristics of the Modulus of Passive Resistance of Soil: A Study in Similitude. Presented at the 37th Annual Meeting of Highway Research Board, Washington DC.

Watkins, R.K., and Moser, R.P. (1969). The structural performance of buried corrugated steel pipes. Utah State University, Logan, Utah and American Iron and Steel

Institute, Washington, DC.

Watkins, R. K., and Anderson, L. R. (2000). Structural Mechanics of Buried Pipes, CRC Press LLC, Boca Raton, FL.

Wong, K.S., and Duncan, J.M. (1974). Hyperbolic Stress-Strain Parameters for Nonlinear Finite Element Analysis of Stresses and Movements in Soil Masses, Report No. TE-74-3, University of California, Berkeley, California.

Yoo, C.H., Parker, F., and Kang, J. (2005). "Bedding and Fill Heights for Concrete Roadway Pipe and Box Culverts." Final Report, *ALDOT Project No. 930-592*, Highway Research Center, Auburn University, AL.

APPENDICES

APPENDIX 1

MARSTON AND SPANGLER' S THEORY

The Marston theory of loads on buried conduits was developed near the beginning of the twentieth century. M.G. Spangler presented three bedding configurations and used the concept of a bedding factor to relate the supporting strength of buried pipe to the strength obtained in a three-edge bearing test (ACPA 1996). Spangler's theory proposed that the bedding factor for a particular pipeline and, consequently, the supporting strength of the buried pipe, is dependent on two installation characteristics: the width and quality of the contact between the pipe and bedding and the magnitude of the lateral pressure and the portion of the vertical height of the pipe over which it acts.

The soil around the conduit was initially divided into prisms by imaginary vertical lines that extend from either side of the conduit to the top of the embankment. The load equations were derived based on an analysis of the forces acting on a thin slice of soil located within the interior prism.

Earth loads on the buried conduits were predicted by applying a factor to the weight of soil overlaying the pipe. The load factor was calculated based on frictional forces that were assumed to develop along these vertical planes. The frictional forces were considered to be generated by differential settlements between the prism of soil

directly above the pipe and those on either side. The direction of these shear forces could increase or decrease the load on the pipe depending upon the direction of the differential settlement between the two prisms, as shown in Fig. 1.1. Greater settlement above the conduit resulted in earth pressures that were less than the overburden. Earth pressures greater than the overburden pressure occurred when greater settlements occurred in the exterior prisms.

Marston (1930) and Spangler (1950b) quantified the load on conduits installed by different construction conditions by solving differential equations based on the equilibrium conditions of a simplified free body of prisms, and proposed equations for predicting loads on conduits due to earth fill as follows:

$W = C_d \gamma B_d^2$ for ditch conduits (A1.1)

$W = C_c \gamma B_c^2$ for positive projecting conduits (A1.2)

$W = C_n \gamma B_c^2$ for imperfect ditch conduits (A1.3)

$W = C_n \gamma B_d^2$ for negative projecting conduits (A1.4)

where C_d, C_c, and C_n = load coefficients; B_d = the horizontal width of ditch; and B_c = the out-to-out horizontal span of the conduit. Although graphical diagrams are provided for the computation of coefficients, there exist still many practical difficulties because the load coefficients proposed contain certain parameters that cannot be determined readily, such as the settlement ratio and the height of the plane of equal settlement. Graphical diagrams for C_d, C_c, and C_n are presented in Figs. A1.1, A1.2, and A1.3. For load coefficients, C_c, in Fig. A1.2, the rays are straight lines that can be represented by

equations when the value of H/B_c exceeds the limits of the diagram. These equations are given in Table A1.1. Symbols used in Figs. A1.1 through A1.6 are defined as follows:

H = height of fill above top of conduit,

B_d = horizontal width of ditch at top of conduit,

B_c = out-to-out horizontal span of conduit,

K = ratio of active lateral unit pressure to vertical and sides of ditch,

μ = $\tan\phi$ = coefficient of internal friction of fill material,

μ' = $\tan\phi'$ = coefficient of friction between fill material and sides of ditch,

p = projection ratio, the vertical distance from the natural ground surface to the top of the structure divided by the structure height, and

p' = projection ratio in negative projection or imperfect ditch installation, the depth of the ditch divided by its width.

As mentioned in Chapter 2, it is difficult to predetermine the actual value of the settlement ratio, r_{sd}, pertinent to a specific case. Spangler and Handy (1982) presented the recommended values of the settlement ratio based on field observations of the performance of actual culverts under embankments, as shown in Table A1.2.

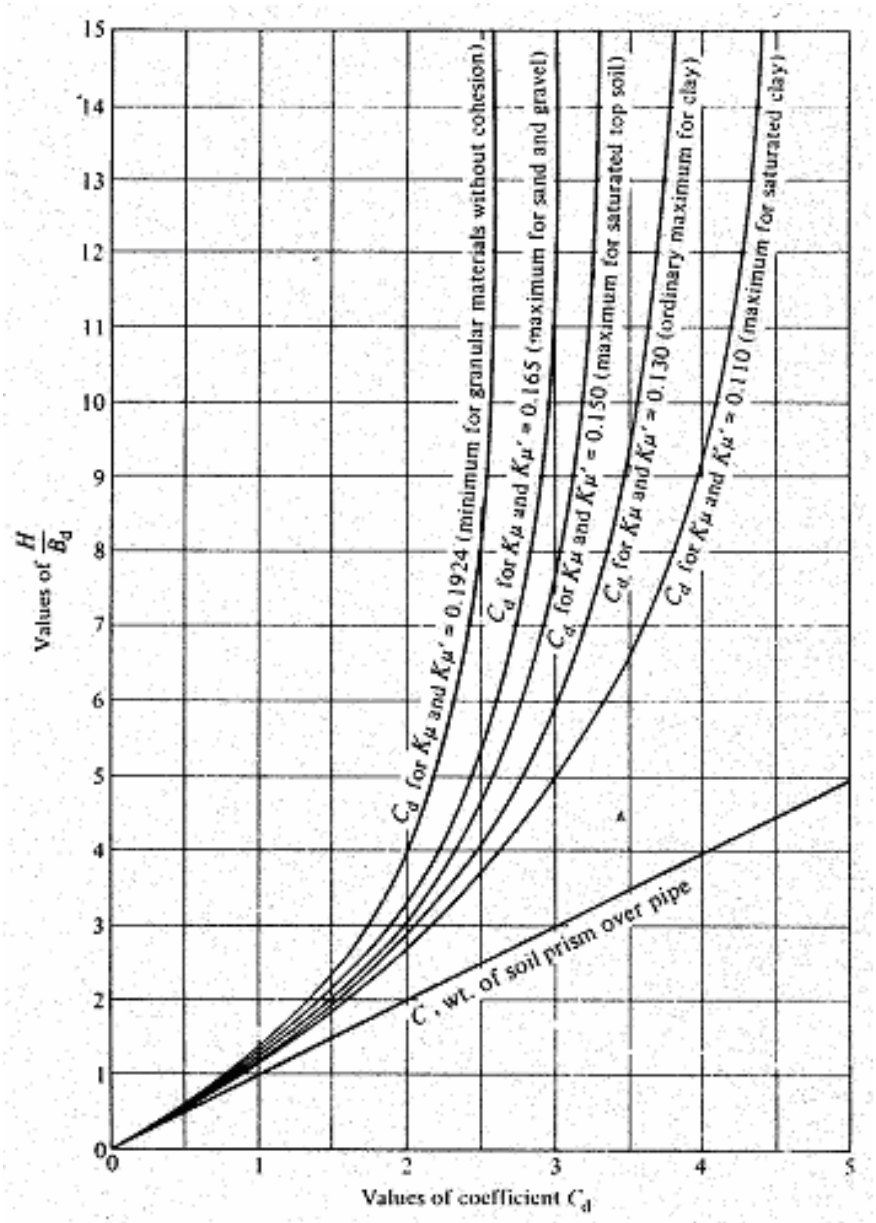

Fig. A1.1. Diagrams for coefficient C_d for ditch conduits

Table A1.1. Values of C_c in terms of H/B_c

Incomplete Projection Condition $K\mu = 0.19$		Incomplete Ditch Condition $K\mu = 0.13$	
$r_{sd}p$	Equation	$r_{sd}p$	Equation
+0.1	$C_c = 1.23\ H/B_c - 0.02$	–0.1	$C_c = 0.82\ H/B_c + 0.05$
+0.3	$C_c = 1.39\ H/B_c - 0.05$	–0.3	$C_c = 0.69\ H/B_c + 0.11$
+0.5	$C_c = 1.50\ H/B_c - 0.07$	–0.5	$C_c = 0.61\ H/B_c + 0.20$
+0.7	$C_c = 1.59\ H/B_c - 0.09$	–0.7	$C_c = 0.55\ H/B_c + 0.25$
+1.0	$C_c = 1.69\ H/B_c - 0.12$	–1.0	$C_c = 0.47\ H/B_c + 0.40$
+2.0	$C_c = 1.93\ H/B_c - 0.17$		

Table A1.2. Design values of settlement ratio

Conditions	Settlement Ratio
Rigid culvert on foundation of rock or unyielding soil	+1.0
Rigid culvert on foundation of ordinary soil	+0.5 ~ +0.8
Rigid culvert on foundation of material that yields with respect to adjacent natural ground	~ +0.5
Flexible culvert with poorly compacted side fills	-0.4 ~ 0.0
Flexible culvert with well-compacted side fills	-0.2 ~ +0.2

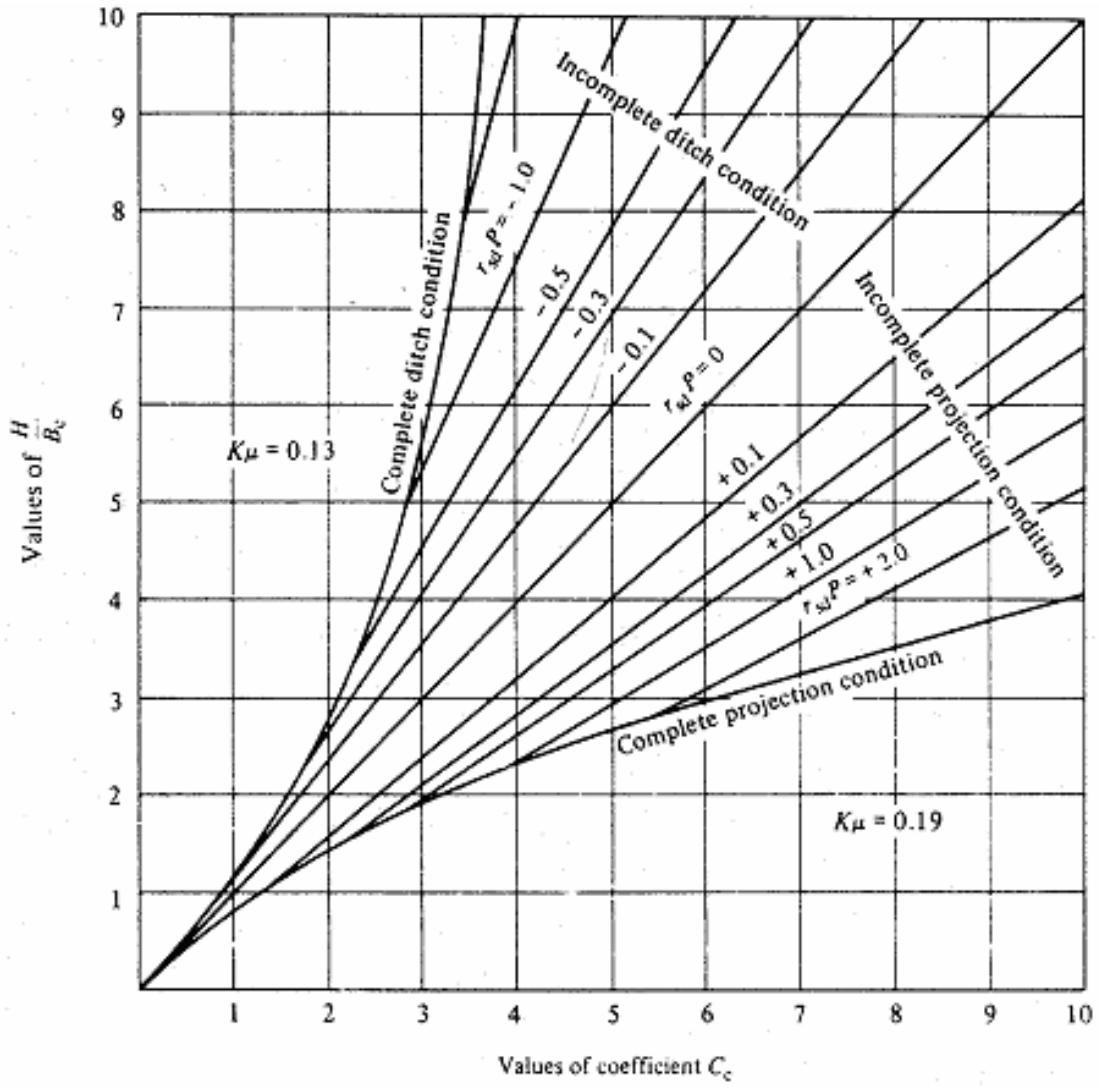

Fig. A1.2. Diagrams for coefficient C_c for positive projecting conduits

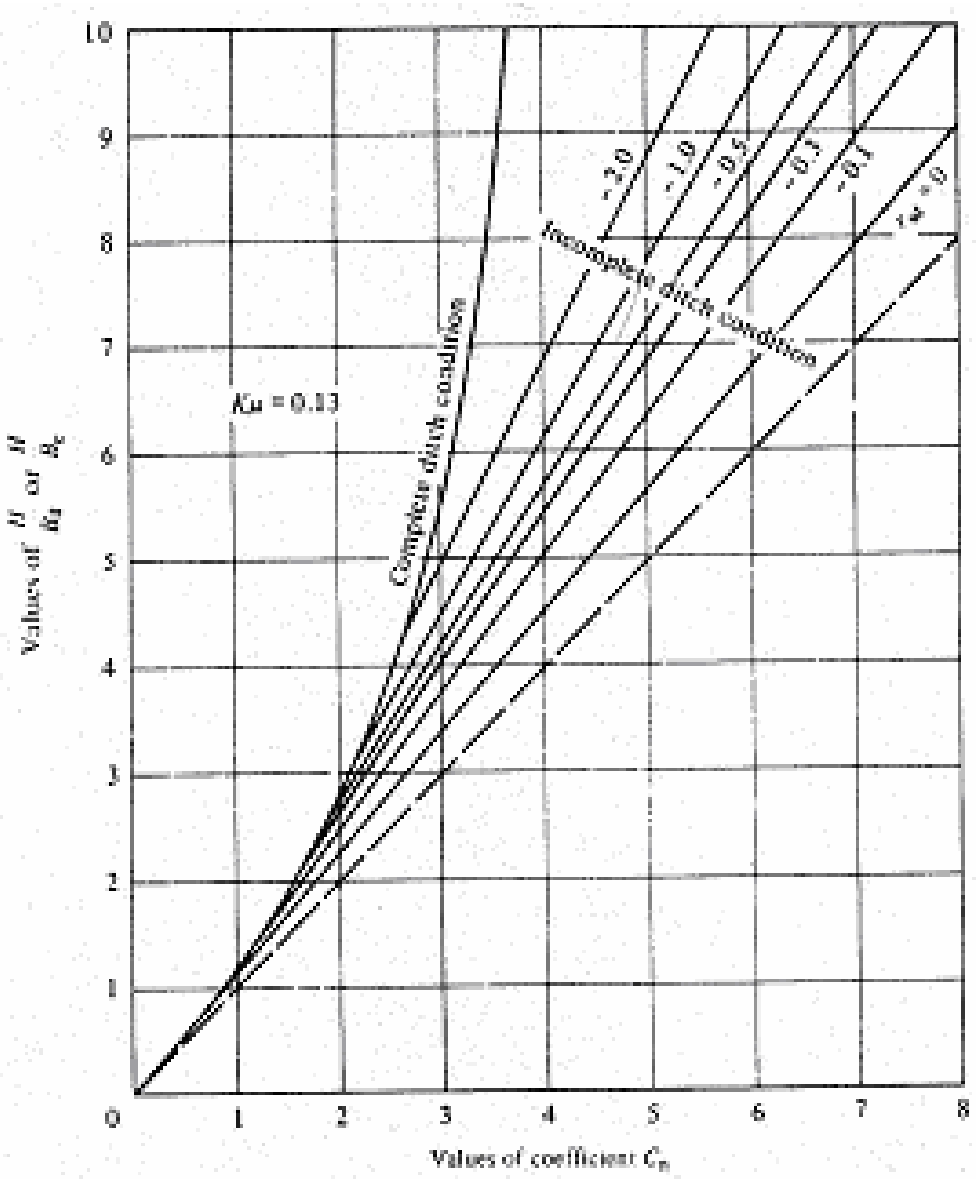

Fig. A1.3. Diagrams for coefficient C_n for negative projection conduits and imperfect ditch conditions ($p' = 0.5$)

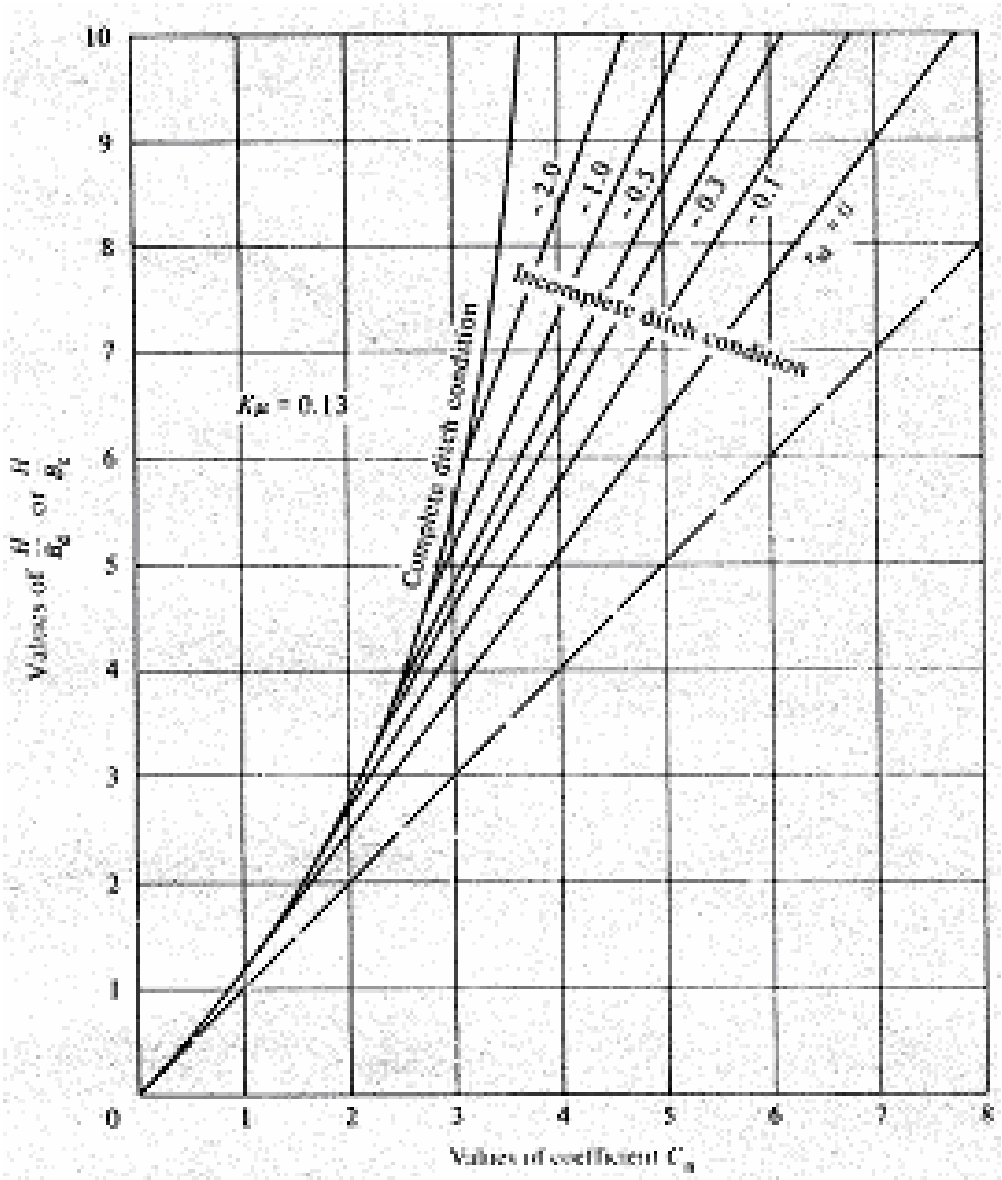

Fig. A1.4. Diagrams for coefficient C_n for negative projection conduits and imperfect ditch conditions ($p' = 1.0$)

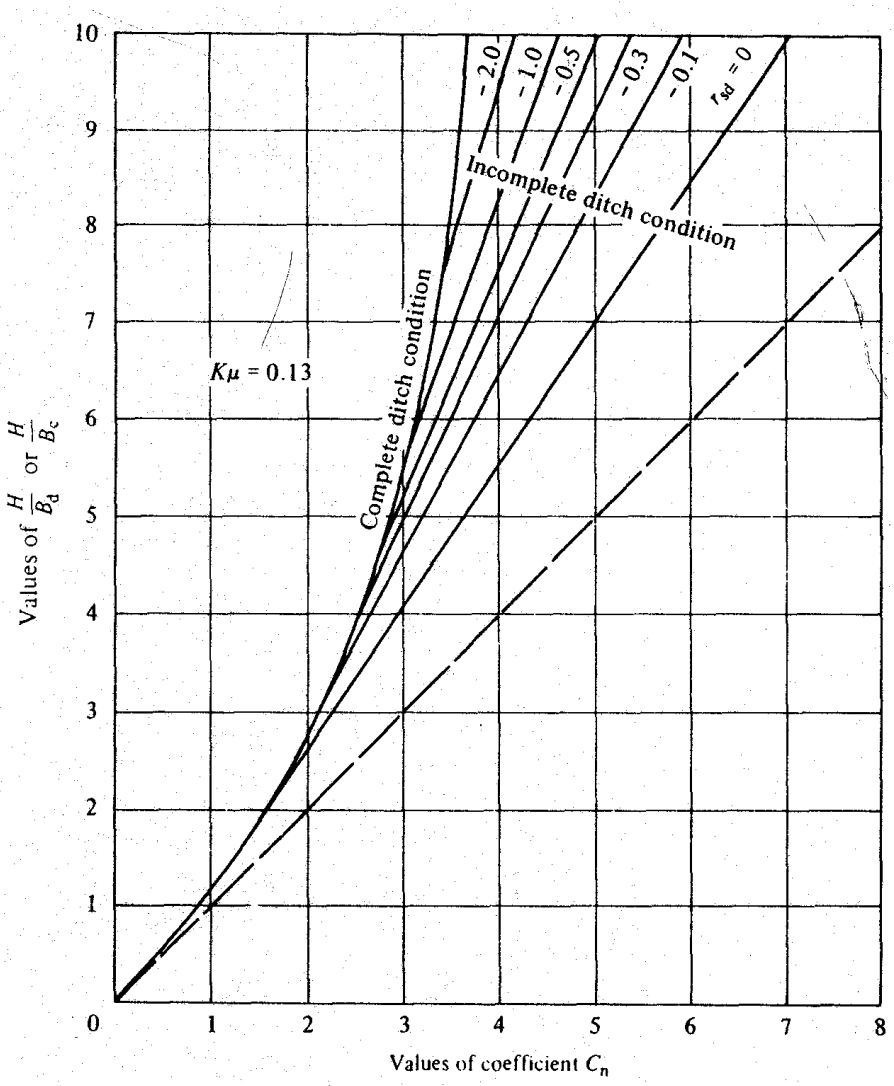

Fig. A1.5. Diagrams for coefficient C_n for negative projection conduits and imperfect ditch conditions ($p' = 1.5$)

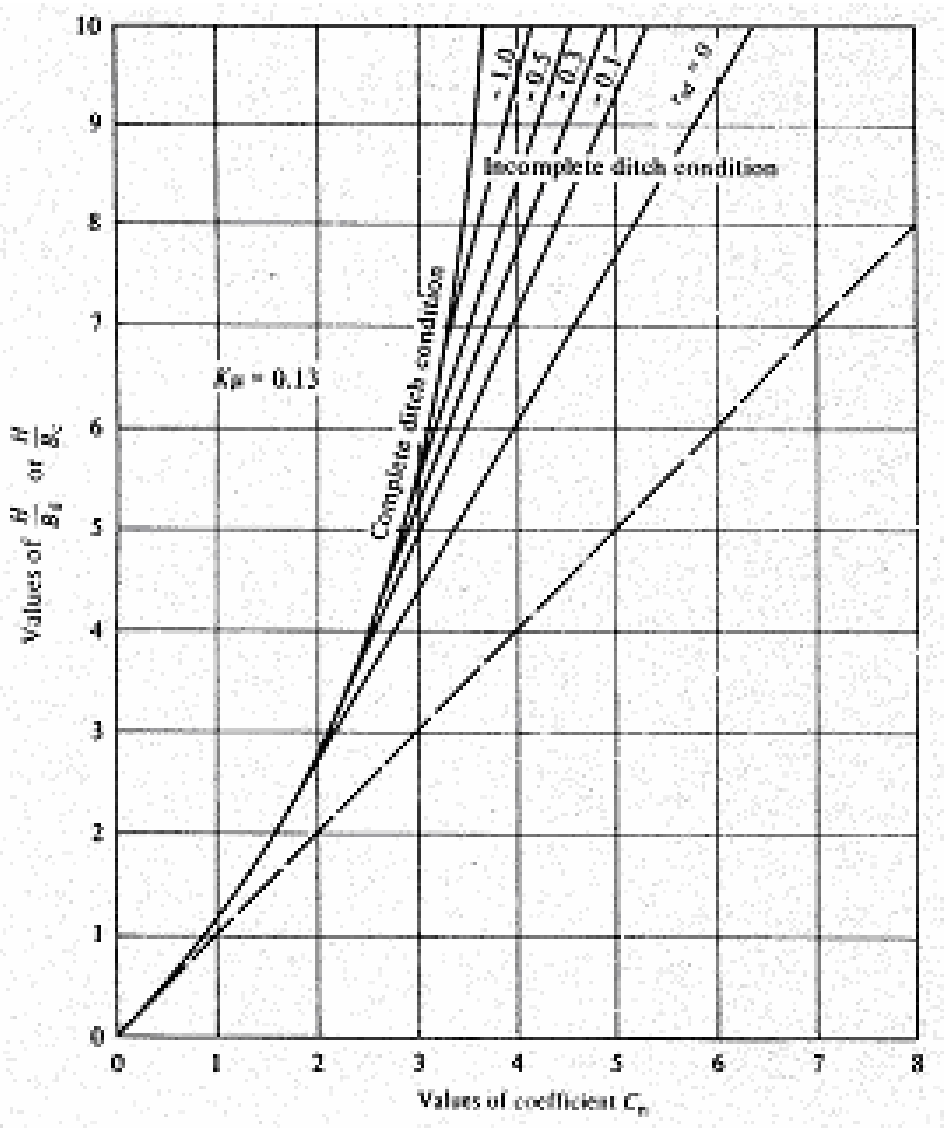

Fig. A1.6. Diagrams for coefficient C_n for negative projection conduits and imperfect ditch conditions ($p' = 2.0$)

APPENDIX 2

TYPICAL INPUT FOR SPIDA

Example 1

Conduit	Installation type	Sidefill
Concrete Round Pipe	Embankment	TREATED

****

TITLE EMBANKMENT

TITLE PIPE 72 INCH WALL B

TITLE FILL HEIGHT 32 FT COVER

TITLE TREATED SIDEFILL

TITLE CIRCULAR PLUS ELLIPTICAL CAGE

PIPE 72.0 7.0

CAGEC 0.48 0.37 1.0 1.0 2.0 2.0 3

CAGEE 0.51 1.0 1.0 2.0 3 12.5

MATERIAL 65.0 6.0

INSTALL 0 32.0 12.0 12.0

MESH 0.15 0.17 0.17 0.83

ZONES 1 11 1

ZONES 18 25 0

ZONES 19 25 0

ZONES 20 25 0

ZONES 21 25 0

ZONES 22 25 0

ZONES 23 25 0

ZONES

PROPERTY 31 3 2

PROPERTY 21 25 2

PROPERTY 33 25 5

PROPERTY 23 25 5

PROPERTY 41 25 7

PROPERTY 51 25 3

PROPERTY 57 25 2

PROPERTY 62 25 2

PROPERTY 67 25 2

PROPERTY 72 25 2

PROPERTY 28 25 2

PROPERTY 38 25 2

PROPERTY 48 25 2

PROPERTY 54 25 2

PROPERTY 59 25 2

```
PROPERTY     64     25      2
PROPERTY     69     25      2
PROPERTY     74     25      2
PROPERTY    125     25      6
PROPERTY    135     25      6
PROPERTY    145     25      6
PROPERTY    155     25      6
PROPERTY    165     25      6
SOIL          4 0.06940   200.0    0.26    0.89    18.4    0.10     3.5    32.0
          0.0     0.9
SOIL         25 0.06940   120.0    0.45    1.00    21.1    0.13     9.0    15.0
          4.0     0.8
SOIL         22 0.0694    450.0    0.35    0.80    12.7    0.08     0.0    38.0
          2.0     0.9
SOIL          1 0.0694    640.0    0.43    0.75    40.9    0.05     0.0    42.0
          4.0     1.1
SOIL         21 0.0694    950.0    0.60    0.70    74.8    0.02     0.0    48.0
          8.0     1.3
SOIL         23 0.0694    440.0    0.40    0.95    48.3    0.06     4.0    34.0
          0.0     1.2
SOIL         26 0.0694     50.0    0.60    0.90    13.0    0.15     6.0    18.0
          8.0     0.5
```

```
SOIL        29 0.0057     35.0    0.55    0.70    1.00    0.50     0.0    44.0
           1.0     0.7
SOIL        28 0.0009      5.0    0.08    0.70    0.12    1.0      0.0    44.0
           1.0     0.7
FACTORS     1.0     1.0     1.0    1.00    1.00    1.00     1.0     1.0     1.0
PRINTB        1    32.0
PRINT         1       1
END
```

Example 2

Conduit	Installation type	Sidefill
Concrete Round Pipe	Imperfect Trench, Geometry I	TREATED

```
**************************************************************************
TITLE   IMPERFECT TRENCH
TITLE   72 INCH WALL B
TITLE    FILL HEIGHT 32 FT COVER
TITLE    UNTREATED sidefill
TITLE   CIRCULAR PLUS ELLIPTICAL CAGE
PIPE       72.0     7.0
CAGEC      0.48    0.37     1.0     1.0     2.0     2.0     3
CAGEE      0.51     1.0     1.0     2.0      3    12.5
MATERIAL    65.0     6.0
INSTALL       0    51.0          12.0    12.0
MESH       0.25    0.17    0.17    0.83
ZONES         1      11       1
ZONES        18      25       0
ZONES        19      25       0
ZONES        20      25       0
ZONES        21      25       0
```

ZONES 22 25 0

ZONES 23 25 0

ZONES

PROPERTY 31 3 2

PROPERTY 21 25 2

PROPERTY 33 25 5

PROPERTY 23 25 5

PROPERTY 41 25 7

PROPERTY 51 25 3

PROPERTY 57 25 2

PROPERTY 62 25 2

PROPERTY 67 25 2

PROPERTY 72 25 2

PROPERTY 28 25 2

PROPERTY 38 25 2

PROPERTY 48 25 2

PROPERTY 54 25 2

PROPERTY 59 25 2

PROPERTY 64 25 2

PROPERTY 69 25 2

PROPERTY 74 25 2

PROPERTY 105 29 6

```
PROPERTY    115     29      6
PROPERTY    125     29      6
PROPERTY    135     25      6
PROPERTY    145     25      6
PROPERTY    155     25      6
PROPERTY    165     25      6
SOIL         4 0.06940   200.0    0.26    0.89    18.4    0.10    3.5    32.0
         0.0     0.9
SOIL        25 0.06940   120.0    0.45    1.00    21.1    0.13    9.0    15.0
         4.0     0.8
SOIL        22 0.0694    450.0    0.35    0.80    12.7    0.08    0.0    38.0
         2.0     0.9
SOIL         1 0.0694    640.0    0.43    0.75    40.9    0.05    0.0    42.0
         4.0     1.1
SOIL        21 0.0694    950.0    0.60    0.70    74.8    0.02    0.0    48.0
         8.0     1.3
SOIL        23 0.0694    440.0    0.40    0.95    48.3    0.06    4.0    34.0
         0.0     1.2
SOIL        26 0.0694     50.0    0.60    0.90    13.0    0.15    6.0    18.0
         8.0     0.5
SOIL        29 0.000520   35.0    0.55    0.70    1.00    0.50    0.0    44.0
         1.0     0.7
```

```
SOIL        28 0.0009     5.0    0.08    0.70    0.12    1.0     0.0    44.0
          1.0     0.7
FACTORS     1.0     1.0     1.0    1.00    1.00    1.00     1.0     1.0     1.0
PRINTB        1    51.0
PRINT         1       1
END
```

Example 3

Conduit	Installation type	Sidefill
Concrete Round Pipe	Embankment	UNTREATED

```
**********************************************************************
TITLE   EMBANKMENT
TITLE   72 INCH WALL B
TITLE    21 FT COVER
TITLE    UNTREATED sidefill
TITLE   CIRCULAR PLUS ELLIPTICAL CAGE
PIPE       72.0     7.0
CAGEC      0.48    0.37     1.0     1.0     2.0     2.0     3
CAGEE      0.51     1.0     1.0     2.0      3    12.5
MATERIAL    65.0     6.0
INSTALL       0    21.0          12.0    12.0
MESH       0.17    0.17    0.17    0.83
ZONES         1      11       1
ZONES        18      25       0
ZONES        19      25       0
ZONES        20      25       0
ZONES        21      25       0
ZONES        22      25       0
```

ZONES 23 25 0

ZONES

PROPERTY 31 11 2

PROPERTY 21 11 2

PROPERTY 33 11 8

PROPERTY 23 11 8

PROPERTY 41 11 1

PROPERTY 42 26 6

PROPERTY 51 26 3

PROPERTY 57 26 2

PROPERTY 62 26 2

PROPERTY 67 26 2

PROPERTY 72 26 2

PROPERTY 28 26 2

PROPERTY 38 26 2

PROPERTY 48 26 2

PROPERTY 54 26 2

PROPERTY 59 26 2

PROPERTY 64 26 2

PROPERTY 69 26 2

PROPERTY 74 26 2

PROPERTY 125 25 6

```
PROPERTY    135     25      6
PROPERTY    145     25      6
PROPERTY    155     25      6
PROPERTY    165     25      6
SOIL        29 0.07233   170.0    0.37    1.07    32.5    0.09    11.0    12.0
        0.0     1.0
SOIL         4 0.06940   200.0    0.26    0.89    18.4    0.10     3.5    32.0
        0.0     0.9
SOIL        25 0.06940   120.0    0.45    1.00    21.1    0.13     9.0    15.0
        4.0     0.8
SOIL        22 0.0694    450.0    0.35    0.80    12.7    0.08     0.0    38.0
        2.0     0.9
SOIL         1 0.0694    640.0    0.43    0.75    40.9    0.05     0.0    42.0
        4.0     1.1
SOIL        21 0.0694    950.0    0.60    0.70    74.8    0.02     0.0    48.0
        8.0     1.3
SOIL        23 0.0694    440.0    0.40    0.95    48.3    0.06     4.0    34.0
        0.0     1.2
SOIL        26 0.0694     50.0    0.60    0.90    13.0    0.15     6.0    18.0
        8.0     0.5
FACTORS     1.0     1.0     1.0    1.00    1.00    1.00     1.0     1.0     1.0
PRINTB      1    21.0
```

```
PRINT     1     1
END
```

Example 4

Conduit	Installation type	Sidefill
Concrete Round Pipe	Imperfect Trench, Geometry Ii	UNTREATED

****

TITLE IMPERFECT TRENCH, GEOMETRY II

TITLE 72 INCH WALL B

TITLE 21 FT COVER

TITLE UNTREATED sidefill

TITLE CIRCULAR PLUS ELLIPTICAL CAGE

PIPE 72.0 7.0

CAGEC 0.48 0.37 1.0 1.0 2.0 2.0 3

CAGEE 0.51 1.0 1.0 2.0 3 12.5

MATERIAL 65.0 6.0

INSTALL 0 21.0 12.0 12.0

MESH 0.25 0.042 0.083 1.50

ZONES 1 11 1

ZONES 18 25 0

ZONES 19 25 0

ZONES 20 25 0

ZONES 21 25 0

ZONES 22 25 0

ZONES 23 25 0

ZONES

PROPERTY 31 11 2

PROPERTY 21 11 2

PROPERTY 33 11 8

PROPERTY 23 11 8

PROPERTY 41 26 7

PROPERTY 51 26 3

PROPERTY 57 26 2

PROPERTY 62 26 2

PROPERTY 67 26 2

PROPERTY 72 26 2

PROPERTY 28 26 2

PROPERTY 38 26 2

PROPERTY 48 26 2

PROPERTY 54 26 2

PROPERTY 59 26 2

PROPERTY 64 26 2

PROPERTY 69 26 2

PROPERTY 77 29 2

PROPERTY 82 29 2

PROPERTY 87 29 2

PROPERTY 92 29 3

PROPERTY 98 29 4

PROPERTY 105 29 7

PROPERTY 115 29 7

PROPERTY 125 25 6

PROPERTY 135 25 6

PROPERTY 145 25 6

PROPERTY 155 25 6

PROPERTY 165 25 6

SOIL 29 0.07233 170.0 0.37 1.07 32.5 0.09 11.0 12.0
0.0 1.0

SOIL 4 0.06940 200.0 0.26 0.89 18.4 0.10 3.5 32.0
0.0 0.9

SOIL 25 0.06940 120.0 0.45 1.00 21.1 0.13 9.0 15.0
4.0 0.8

SOIL 22 0.0694 450.0 0.35 0.80 12.7 0.08 0.0 38.0
2.0 0.9

SOIL 1 0.0694 640.0 0.43 0.75 40.9 0.05 0.0 42.0
4.0 1.1

SOIL 21 0.0694 950.0 0.60 0.70 74.8 0.02 0.0 48.0
8.0 1.3

```
SOIL        23 0.0694    440.0    0.40    0.95    48.3    0.06     4.0    34.0
          0.0     1.2
SOIL        26 0.0694     50.0    0.60    0.90    13.0    0.15     6.0    18.0
          8.0     0.5
FACTORS      1.0     1.0     1.0    1.00    1.00    1.00     1.0     1.0     1.0
PRINTB         1    21.0
PRINT          1       1
END
```

APPENDIX 3

TYPICAL INPUT FOR CANDE-89

Example 1

Conduit	Installation type	Foundation	Sidefill
Box Culverts	Embankment	Yielding	TREATED

```
**************************************************************************
ANALYS 2 CONCRE BOX CULVERTS 7FT TIMES 7FT 8IN                          2
-1.0      8.0       STD  3    0.0001
5000.0    3600000.0 0.25      145.0
8.0       8.0       8.0       8.0       8.0
0.018     0.034     0.035     0.015     0.565     1.0
EMBA      EMBANKMENT
2    2    3    10   46.0      46.0      18.0      120.0              8.0
 1   3    130.0     INSITU (NO 11)
     1.0       1
100.0     50.0      0.01      350.0     0.01      0.01
453.0     0.014
 2   3    120.0     BEDDING (NO 25)
```

1.0 1

9.0 15.0 4.0 120.0 0.45 1.0

53.0 0.092

L3 3 120.0 FILL (NO 25)

0.5 1

9.0 15.0 4.0 120.0 0.45 1.0

21.0 0.13

STOP

Example 2

Conduit	Installation type	Foundation	Sidefill
Box Culverts	Imperfect Trench, Geometry I	Yielding	TREATED

****

ANALYS 2 CONCRE BOX CULVERTS 7FT TIMES 7FT 8IN 2

-1.0 8.0 STD 3 0.0001

5000.0 3600000.0 0.25 145.0

8.0 8.0 8.0 8.0 8.0

0.018 0.034 0.035 0.015 0.565 1.0

EMBA IMPERFECT TRENCH .

MOD

2 2 3 10 46.0 46.0 18.0 120.0 8.0

0 8 0

111 4

112 4

113 4

114 4

121 4

122 4

123 4

```
124                    4
 1   3    130.0     INSITU (NO 11)
    1.0       1
100.0     50.0      0.01      350.0     0.01      0.01
453.0     0.014
 2   3    120.0     BEDDING (NO 25)
    1.0       1
9.0       15.0      4.0       120.0     0.45      1.0
53.0      0.092
 3   3    120.0     FILL (NO 25)
    0.5       1
9.0       15.0      4.0       120.0     0.45      1.0
21.0      0.13
L4   3    10.0      SOFT (NO 29)
    0.5       1
0.0       44.0      1.0       35.0      0.1       1.0
1.0       0.5
STOP
```

APPENDIX 4

SURVEY RESULTS

Neighboring States' Procedures for Construction Practice on Buried Concrete Pipes

A. Questionnaires
Symbols

E: Positive Projection Embankment Installation
N: Negative Projection Embankment Installation
T: Trench Installation
I: Imperfect Trench Installation
J: Jacked or Tunneled Soil Load

1. Do your state′s design specifications for buried culverts include the following installation method? If yes, how many standard bedding and backfill types (as classified in AASHTO Standard Specifications for Highway Bridges: Division II, Sec.27) are permitted for each installation type?

	N	Y	Number of Types
Positive Projection Embankment Installation (E)	☐	☐	( )
Negative Projection Embankment Installation (N)	☐	☐	( )
Trench Installation (T)	☐	☐	( )
Imperfect Trench Installation (I)	☐	☐	( )
Jacked or Tunneled Soil Load (J)	☐	☐	( )
Any others:			

2. Which design criteria are adopted or referred to for the design of each installation type stipulated in your state′s specifications for buried concrete culvert systems?

	E	N	T	I	J
AASHTO Direct Design Methods (SIDD)	☐	☐	☐	☐	☐

AASHTO Indirect Design Methods	☐	☐	☐	☐	☐
Marston/Spangler design procedures	☐	☐	☐	☐	☐
State′s own procedures (in-house)	☐	☐	☐	☐	☐
Others:					

3. If the Direct Design Method is used, what computer software or approximate methods are used for soil-structure interaction analyses?

4. Which procedure is used to determine the earth load and live load transmitted to culvert structures in each installation type?

	E	N	T	I	J
Heger Pressure Distribution	☐	☐	☐	☐	☐
ACPA Concrete Pipe Design Manual	☐	☐	☐	☐	☐
Marston/Spangler design criteria	☐	☐	☐	☐	☐
State′s own procedures (in-house)	☐	☐	☐	☐	☐
Others					

5. Which tests are required by your state′s specifications to ensure an acceptable level of quality control in workmanship and materials during construction?

Soil Density
Line and Grade
Visual Inspection
Infiltration
Exfiltration
Air Testing
Vacuum Testing
Joint Testing Air

6. If the Imperfect Trench Installation method is used, do your state′s specifications include provisions for the size and location of the "soft" material zone relative to the concrete pipe?

7. What are your state's specifications for the "soft" material used in the Imperfect Trench Installation?

B. Survey Results

5 states' results are shown in the following table. Most states allow not only their own design criteria (in-house) but also old Marston and Spangler's theory in 1930's.

Item	Arkansas	Georgia	Tennessee	North Carolina	Mississippi
Installation (No. of Types)	E(3), T(3)	T(1), I(1), J(1)	E(1), N(1), T(1), J(1)	T(2)	T(?),I(?),J(?)
Design Criteria	State's Own	Marston and Spangler	Marston and Spangler	State's Own	AASHTO Indirect Design
Imperfect Trench	N/A	State's Own	N/A	N/A	State's Own

APPENDIX 5

SPECIAL HIGHWAY DRAWINGS OF ALDOT PROJECT 930-592

DESIGN PROCEDURE

(SEE GENERAL NOTE 5)

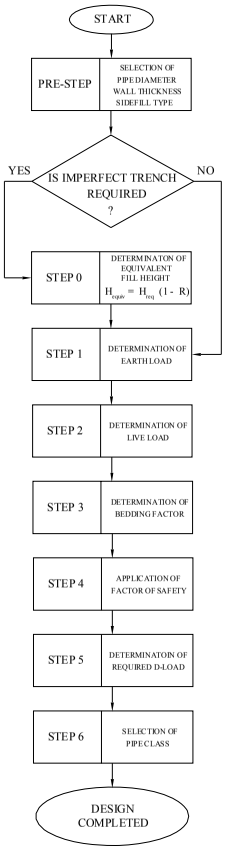

NOTATIONS:

- R = REDUCTION RATE
- H_{equiv} = EQUIVALENT FILL HEIGHT, ft
- H_{req} = REQUIRED FILL HEIGHT, ft
- W_E = TOTAL VERTICAL EARTH LOAD, lb/ft
- W_h = TOTAL HORIZONTAL LOAD, lb/ft
- PL = PRISM LOAD, lb/ft
- VAF = VERTICAL ARCHING FACTOR, $\frac{W_E}{PL}$
- HAF = HORIZONTAL ARCHING FACTOR, $\frac{W_h}{PL}$
- w = UNIT WEIGHT OF SOIL, pcf
- H = HEIGHT OF FILL ABOVE TOP OF PIPE, ft
- Bc = OUT-TO-OUT HORIZONTAL SPAN OF PIPE, ft
- FS = FACTOR OF SAFETY
- BF = BEDDING FACTOR
- Bi = PIPE INSIDE DIAMETER, ft
- E_S = MODULUS OF ELASTICITY OF SOFT MATERIALS, psi
- D-Load = $\frac{W_E \times FS}{BF \times Bi}$, lb/ft/ft
- t = PIPE WALL THICKNESS, in.

DESIGN EXAMPLES

(SEE GENERAL NOTE 5)

PRE-STEP

GIVEN: PIPE INSIDE DIAMETER=144 in., CONCRETE PIPE
WALL THICKNESS: 12 in.
SIDEFILL: TREATED
EARTH FILL: 86 ft OF 120 pcf OVERFILL
MODULUS OF ELASTICITY OF SOFT MATERIAL : 100 psi

FIND: REQUIRED PIPE STRENGTH IN TERMS OF 0.01 in. D-LOAD

	EMBANKMENT	IMPERFECT TRENCH
STEP 0	N/A	FOR TREATED SIDEFILL $R = 0.958\, e^{-0.0021\, Es}$ $= 0.958\, e^{-0.0021\,(100)}$ $= 0.776$ $H_{equiv} = H_{req}(1 - R)$ $= 86\ (1 - 0.776)$ $= 19$ ft
STEP 1	$PL = w\,[\,H + Bc\,(4 - \pi)/8\,]\,Bc$ $= 120\,[\,86 + 14\,(4 - \pi)/8\,]\,14$ $= 147{,}004$ lb/ft $W_E = VAF \times PL$ $= 1.40 \times 147{,}004$ $= 205{,}806$ lb/ft	$PL = w\,[\,H + Bc\,(4 - \pi)/8\,]\,Bc$ $= 120\,[\,19 + 14\,(4 - \pi)/8\,]\,14$ $= 34{,}444$ lb/ft $W_E = VAF \times PL$ $= 1.40 \times 34{,}444$ $= 48{,}221$ lb/ft
STEP 2	THE LIVE LOAD IS NEGLIGIBLE AT DEPTHS OF OVER 10 ft.	THE LIVE LOAD IS NEGLIGIBLE AT DEPTHS OF OVER 10 ft.
STEP 3	THE BEDDING FACTOR IS 2.2 FROM TABLE.	THE BEDDING FACTOR IS 2.2 FROM TABLE.
STEP 4	THE FACTOR OF SAFETY IS 1.0 IF 0.01 in. CRACK STRENGTH IS TO BE USED.	THE FACTOR OF SAFETY IS 1.0 IF 0.01 in. CRACK STRENGTH IS TO BE USED.
STEP 5	$D\text{-LOAD} = \frac{W_E \times FS}{BF \times Bi} = \frac{(205{,}806)(1)}{(2.2)(12)} = 7{,}796$ lb/ft/ft	$D\text{-LOAD} = \frac{W_E \times FS}{BF \times Bi} = \frac{(48{,}221)(1)}{(2.2)(12)} = 1{,}827$ lb/ft/ft
STEP 6	SPECIAL DESIGN IS NEEDED AS THE D-LOAD EXCEEDS 3,000 lb/ft/ft.	SELECT PIPE CLASS IV FOR D-LOAD = 1,827 lb/ft/ft

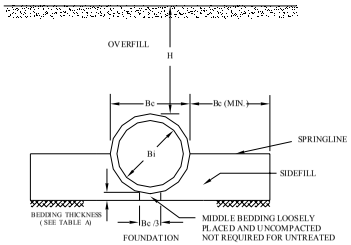

EMBANKMENT INSTALLATION

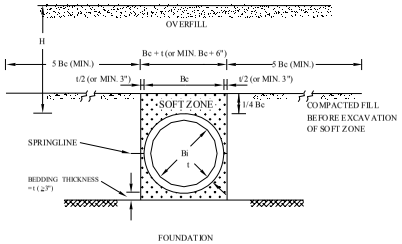

IMPERFECT TRENCH INSTALLATION

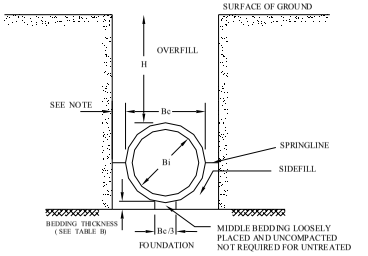

NOTE : CLEARANCE BETWEEN PIPE AND TRENCH WALL SHALL BE ADEQUATE TO ENABLE COMPACTION IF CL, BUT NOT LESS THAN 1'- 6".

TRENCH INSTALLATION

BEDDING FACTOR (BF)

Pipe I.D.(in.)	TREATED	UNTREATED
12	2.5	1.7
36	2.3	1.7
72	2.2	1.7
96	2.2	1.7
144	2.2	1.7

ARCHING FACTOR

SIDE FILL	VAF	HAF
TREATED	1.40	0.37
UNTREATED	1.45	0.30

REDUCTION RATE, R (%)

SIDE FILL	R
TREATED or UNTREATED	$R = 0.958\, e^{(0.0021\, Es)}$

SOFT MATERIALS

MATERIAL	DENSITY (pcf)	Es (psi)
EPS-GEOFOAM	0.9	34
STRAW BALES	9.3	35

NOTE: FOR CONSERVATIVE DESIGN, Es = 100 psi WAS USED IN MAXIMUM FILL HEIGHTS WITH IMPERFECT TRENCH INSTALLATIONS.

MAXIMUM FILL HEIGHTS

(WITHOUT IMPERFECT TRENCH INTALLATION)

UNIT: ft

WALL B*	TREATED SIDEFILL				UNTREATED SIDEFILL			
	CLASS OF PIPE				CLASS OF PIPE			
PIPE I.D. (in.)	II	III	IV	V	II	III	IV	V
12	11	15	22	33	5	7	12	20
24	11	15	22	33	6	8	13	21
36	10	14	21	33	6	8	13	21
60	10	14	21	32	6	8	13	21
72	9	13	20	32	6	8	13	21
84	9	13	20	32	6	8	13	21
108	9	13	20	32	6	8	13	21
132	9	13	20	32	6	8	13	21
144	9	13	20	32	6	8	13	21

MAXIMUM FILL HEIGHTS

(WITH IMPERFECT TRENCH INTALLATION)

UNIT: ft

WALL B*	TREATED SIDEFILL				UNTREATED SIDEFILL			
	CLASS OF PIPE				CLASS OF PIPE			
PIPE I.D. (in.)	II	III	IV	V	II	III	IV	V
12	49	67	98	147	22	31	54	89
24	49	67	98	147	27	36	58	94
36	45	63	94	147	27	36	58	94
60	45	63	94	143	27	36	58	94
72	40	58	89	143	27	36	58	94
84	40	58	89	143	27	36	58	94
108	40	58	89	143	27	36	58	94
132	40	58	89	143	27	36	58	94
144	40	58	89	143	27	36	58	94

* WALL B REFERS TO AASHTO M 170 FOR WALL THICKNESSES OF ROUND CONCRETE ROADWAY PIPES.

SOILS AND MINIMUM COMPACTION REQUIREMENTS

A. EMBANKMENT INSTALLATIONS

TYPE	BEDDING THICKNESS	SIDEFILL COMPACTION
TREATED	Bc/24" MIN., NOT LESS THAN 3". IF ROCK FOR FOUNDATION USE Bc/12" MIN., NOT LESS THAN 6"	85% SW, 90% ML OR 95% CL
UNTREATED	NO BEDDING REQUIRED EXCEPT IF ROCK FOUNDATIONS USE Bc/12" MIN., NOT LESS THAN 6"	NO COMPACTION REQUIRED EXCEPT IF CL, USE 85%

B. TRENCH INSTALLATION

TYPE	BEDDING THICKNESS	SIDEFILL COMPACTION
NO ADVANTAGE OF TREATED SIDEFILL	Bc/24" MIN., NOT LESS THAN 3". IF ROCK FOR FOUNDATION USE Bc/12" MIN., NOT LESS THAN 6"	NO COMPACTION REQUIRED EXCEPT IF CL, USE 85%

GENERAL NOTES

1. THIS DRAWING AND MAXIMUM FILL HEIGHT TABLES ARE INTENDED FOR USE IN DESIGN AND CONSTRUCTION OF ROUND CONCRETE ROADWAY PIPE.
2. THIS DRAWING AND MAXIMUM FILL HEIGHT TABLES CONFORM TO THE SPECIAL PROVISIONS FOR SECTIONS 530 AND 850 IN ALDOT STANDARD SPECIFICATIONS (2002).
3. MAXIMUM FILL HEIGHTS SHOWN IN TABLES ARE FROM TOP OF PIPE TO TOP OF BASE COURSE.
4. MAXIMUM FILL HEIGHT TABLES ARE BASED ON A SOIL WEIGHT OF 120 pcf AND EMBANKMENT INTSALLATION.
5. FURTHER DETAILS ARE AVAILABLE IN THE FINAL REPORT, ALDOT PROJECT, 930-592.
6. TREATED INTALLATION MEANS THAT THE SIDEFILL IS COMPACTED AS SPECIFIED.
7. UNTREATED INSTALLATION MEANS THAT THERE ARE NO REQUIREMENTS FOR SIDEFILL COMPACTOIN.

- SPECIFICATION -
CURRENT ALABAMA DEPARTMENT OF TRANSPORTATION

DESIGN PROCEDURE

(SEE GENERAL NOTE 3)

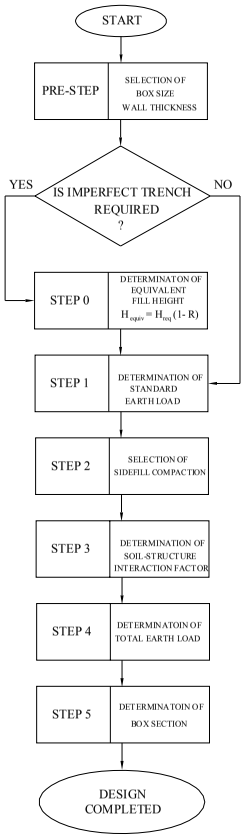

DESIGN EXAMPLES

(SEE GENERAL NOTE 3)

PRE-STEP

GIVEN: 12 ft BY 12 ft BY 12 in. PRECAST CONCRETE BOX SECTION
FOUNDATION: YIELDING
SIDEFILL: TREATED
EARTH FILL: 100 ft OF 110 pcf OVERFILL
MODULUS OF ELASTICITY OF SOFT MATERIAL : 100 psi

FIND: TOTAL EARTH LOAD IN lb/ft

STEP	EMBANKMENT	IMPERFECT TRENCH
STEP 0	N/A	FOR TREATED SIDEFILL AND YIELDING FOUNDATION $R = 0.7334\ e^{-0.0041\ Es}$ $= 0.7334\ e^{-0.0041\ (100)}$ $= 0.487$ $H_{equiv} = H_{req}(1- R)$ $= 100\ (1-0.487) = 52'$
STEP 1	$W = w\ Bc\ H$ $= (110)[12+2(12)/12]\ (100)$ $= 154{,}000$ lb/ft	$W = w\ Bc\ H$ $= (110)[12+2(12)/12]\ (52)$ $= 80{,}080$ lb/ft
STEP 2	SELECT TREATED SIDEFILL	SELECT TREATED SIDEFILL
STEP 3	IN CASE OF INCLUDING SHEAR $Fe1 = 1.823\ (100/14)^{-0.136} = 1.40$ FOR ONLY TOP PRESSURE $Fe1 = -0.009(100/14)^2 + 0.109(100/14) + 1.131$ $= 1.45$, CONTROLS	IN CASE OF IMPERFECT TRENCH, BOTTOM PRESSURE IS ALWAYS MAXIMUM. ∴ Fe1 INCLUDING SHEAR IS USED. $Fe1 = 1.823\ (100/14)^{-0.136}$ $= 1.40$
STEP 4	$We = Fe1\ w\ Bc\ H$ $= (1.45)(110)[12+2(12)/12](100)$ $= 223{,}300$ lb/ft	$We = Fe1\ w\ Bc\ H$ $= (1.40)(110)[12+2(12)/12](52)$ $= 112{,}112$ lb/ft
STEP 5		

REINFORCING STEEL AREAS ARE DETERMINED ON THE ELASTIC METHOD OF STRUCTURAL ANALYSIS AND THE ULTIMATE STRENGTH METHOD OF REINFORCED CONCRETE DESIGN IN ACI 318-02.

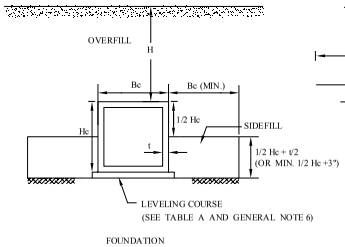

EMBANKMENT INSTALLATION

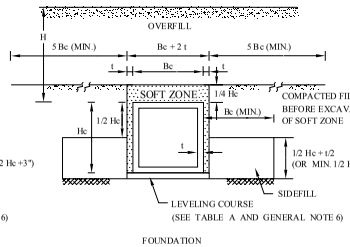

IMPERFECT TRENCH INSTALLATION

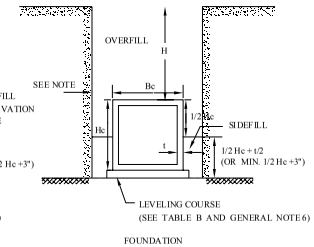

NOTE: CLEARANCE BETWEEN BOX AND TRENCH WALL SHALL BE ADEQUATE TO ENABLE COMPACTION IF CL, BUT NOT LESS THAN 1'-6".

TRENCH INSTALLATION

SOILS AND MINIMUM COMPACTION REQUIREMENTS

A. EMBANKMENT AND IMPERFECT TRENCH INSTALLATIONS

TYPE	LEVELING COURSE BEDDING THICKNESS	SIDEFILL COMPACTION
TREATED	USE t / 2 MIN. NOT LESS THAN 3" IN YIELDING OR UNYIELDING FOUNDATION.	85% SW, 90% ML 0R 95% CL
UNTREATED	USE t / 2 MIN. NOT LESS THAN 3" IN YIELDING OR UNYIELDING FOUNDATION.	NO COMPACTION REQUIRED EXCEPT IF CL, USE 85%

B. TRENCH INSTALLATION

TYPE	LEVELING COURSE BEDDING THICKNESS	SIDEFILL COMPACTION
NO ADVANTAGE OF TREATED SIDEFILL	USE t / 2 MIN. NOT LESS THAN 3" IN YIELDING OR UNYIELDING FOUNDATION.	NO COMPACTION REQUIRED EXCEPT IF CL, USE 85%

SOFT MATERIALS

MATERIAL	DENSITY (pcf)	Es (psi)
EPS-GEOFOAM	0.9	34
STRAW BALES	9.3	35

EQUATIONS FOR REDUCTION RATE (R)

SIDE FILL	FOUNDATION	REDUCTION RATE, R
TREATED	YIELDING	$0.7334\ e^{-0.0041\ Ib}$
	UNYIELDING	$0.6488\ e^{-0.0037\ Ib}$
UNTREATED	YIELDING	$0.8212\ e^{-0.0032\ Ib}$
	UNYIELDING	$0.7193\ e^{-0.0030\ Ib}$

NOTE: EQUATIONS FOR R ARE BASED ON THE BOTTOM PRESSURE.

GENERAL NOTES

1. THIS DRAWING IS INTENDED FOR USE IN DESIGN AND CONSTRUCTION OF BOX CULVERTS.
2. THIS DRAWING CONFORMS TO THE SPECIAL PROVISION FOR SECTION 524 IN ALDOT STANDARD SPECIFICATIONS (2002).
3. FURTHER DETAILS ARE AVAILABLE IN THE FINAL REPORT, ALDOT PROJECT, 930-592.
4. TREATED INSTALLATION MEANS THAT THE SIDEFILL IS COMPACTED AS SPECIFIED.
5. UNTREATED INSTALLATION MEANS THAT THERE ARE NO REQUIREMENTS FOR SIDEFILL COMPACTION.
6. THE REQUIREMENTS FOR LEVELING COURSE APPLY TO BOTH CAST-IN-PLACE BOX CULVERTS AND PRECAST BOX CULVERTS.

- SPECIFICATION -
CURRENT ALABAMA DEPARTMENT OF TRANSPORTATION

NOTATIONS:

- R = REDUCTION RATE
- H_{equiv} = EQUIVALENT FILL HEIGHT, ft
- H_{req} = REQUIRED FILL HEIGHT, ft
- W = STANDARD EARTH LOAD, lb/ft
- W_e = TOTAL EARTH LOAD, lb/ft
- $Fe1$ = SOIL-STRUCTURE INTERACTION FACTOR FOR EMBANKMENT INSTALLATION
- $Fe2$ = SOIL-STRUCTURE INTERACTION FACTOR FOR TRENCH INSTALLATION
- w = UNIT WEIGHT OF SOIL, pcf
- H = HEIGHT OF FILL ABOVE TOP OF BOX, ft
- Bc = OUT-TO-OUT HORIZONTAL SPAN OF BOX, ft
- Es = MODULUS OF ELASTICITY OF SOFT MATERIALS, psi
- Cd = LOAD COEFFICIENT
- Bd = HORIZONTAL WIDTH OF TRENCH AT TOP OF BOX CULVERTS, ft
- t = WALL AND SLAB THICKNESS, in.

SOIL-STRUCTURE INTERACTION FACTOR

	EMBANKMENT INSTALLATION		TRENCH INSTALLATION
SIDE FILL	INCLUDING SHEAR EFFECT	TOP PRESSURE ONLY	TOP PRESSURE ONLY
TREATED	$Fe1 = 1.823\ (H/Bc)^{-0.136}$	$Fe1 = -0.009\ (H/Bc)^2 + 0.109(H/Bc) + 1.131$	$Fe2 = \frac{C_d B_d^2}{H\ Bc}$
UNTREATED	$Fe1 = 2.803\ (H/Bc)^{-0.169}$	$Fe1 = -0.007\ (H/Bc)^2 + 0.077(H/Bc) + 1.357$	

NOTE: FOUNDATION CONDITIONS, YIELDING OR UNYIELDING, DO NOT SIGNIFICANTLY AFFECT Fe1 OR Fe2.

APPENDIX 6

SPECIAL HIGHWAY DRAWING OF HIGHWAY RESEARCH CENTER, AUBURN UNIVERISITY

CORRUGATED PVC PIPES

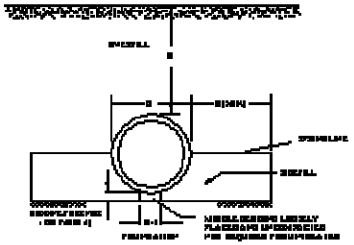

EMBANKMENT INSTALLATION

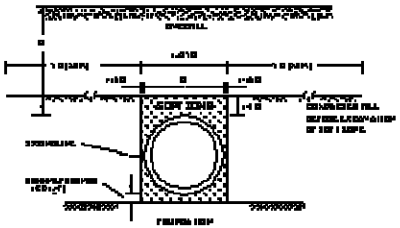

IMPERFECT TRENCH INSTALLATION

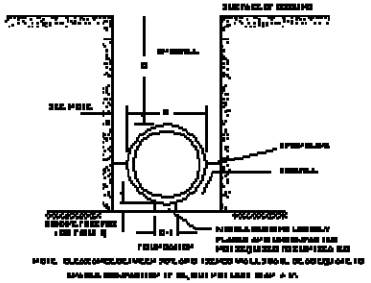

TRENCH INSTALLATION

CORRUGATED STEEL PIPES

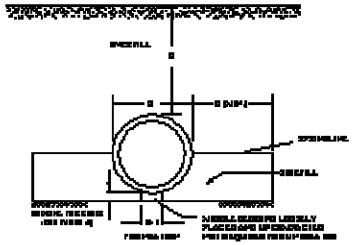

EMBANKMENT INSTALLATION

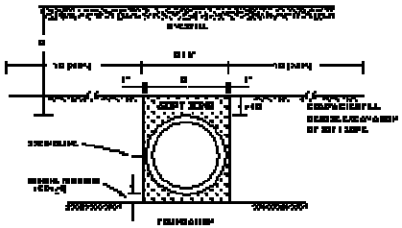

IMPERFECT TRENCH INSTALLATION

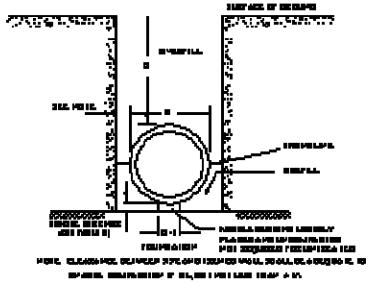

TRENCH INSTALLATION

SOILS AND MINIMUM COMPACTION REQUIREMENTS

A. EMBANKMENT INSTALLATION

TYPE		

B. TRENCH INSTALLATION

TYPE		

GENERAL NOTES

1. FURTHER DETAILS ARE AVAILABLE IN THE ADDENDUM OF THE ROAD DESIGN MANUAL, ALDOT DESIGN, 1998.

HIGHWAY RESEARCH CENTER AT AUBURN UNIVERSITY

APPENDIX 7

VERTICAL STRESS DISTRIBUTIONS OF SOIL ABOVE THE STRUCTURE

A. Concrete Pipe

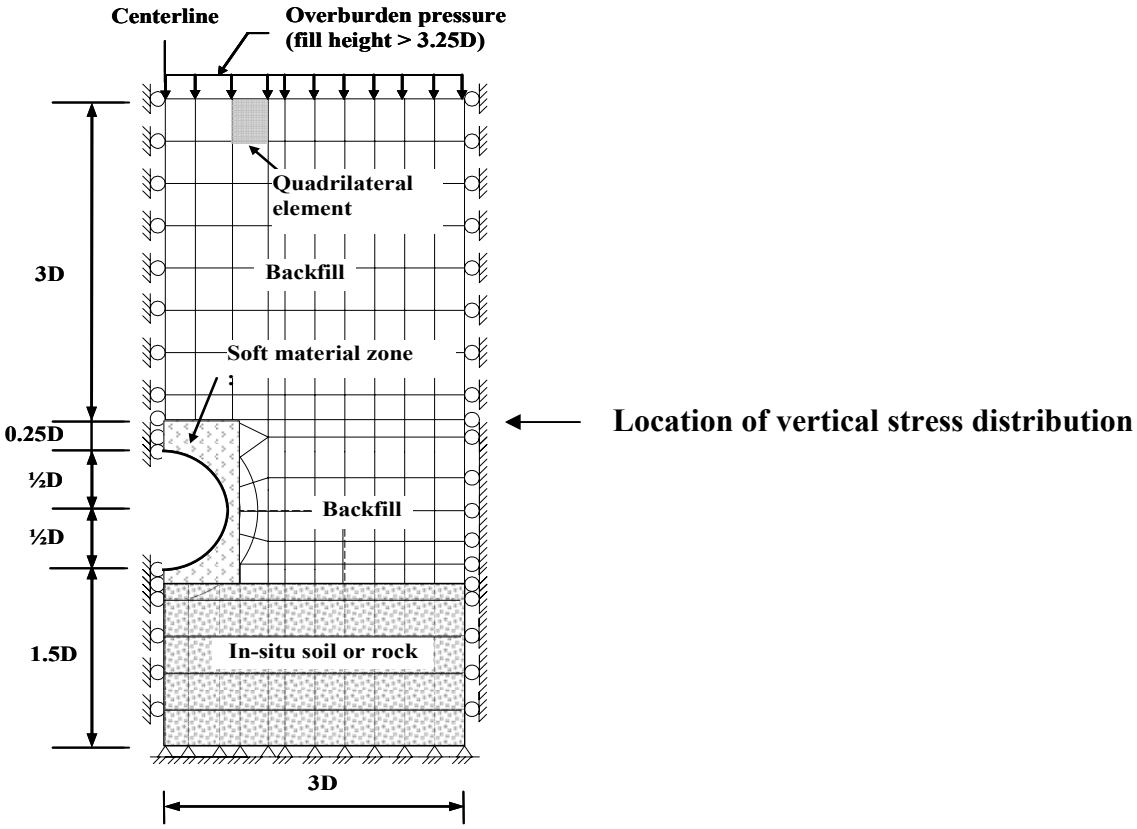

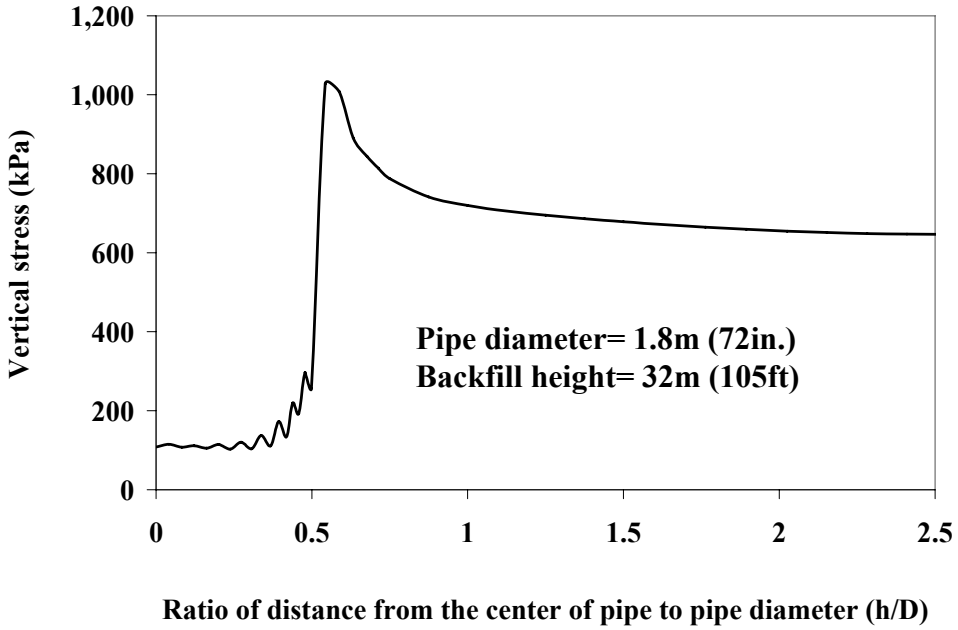

B. Corrugated PVC Pipe

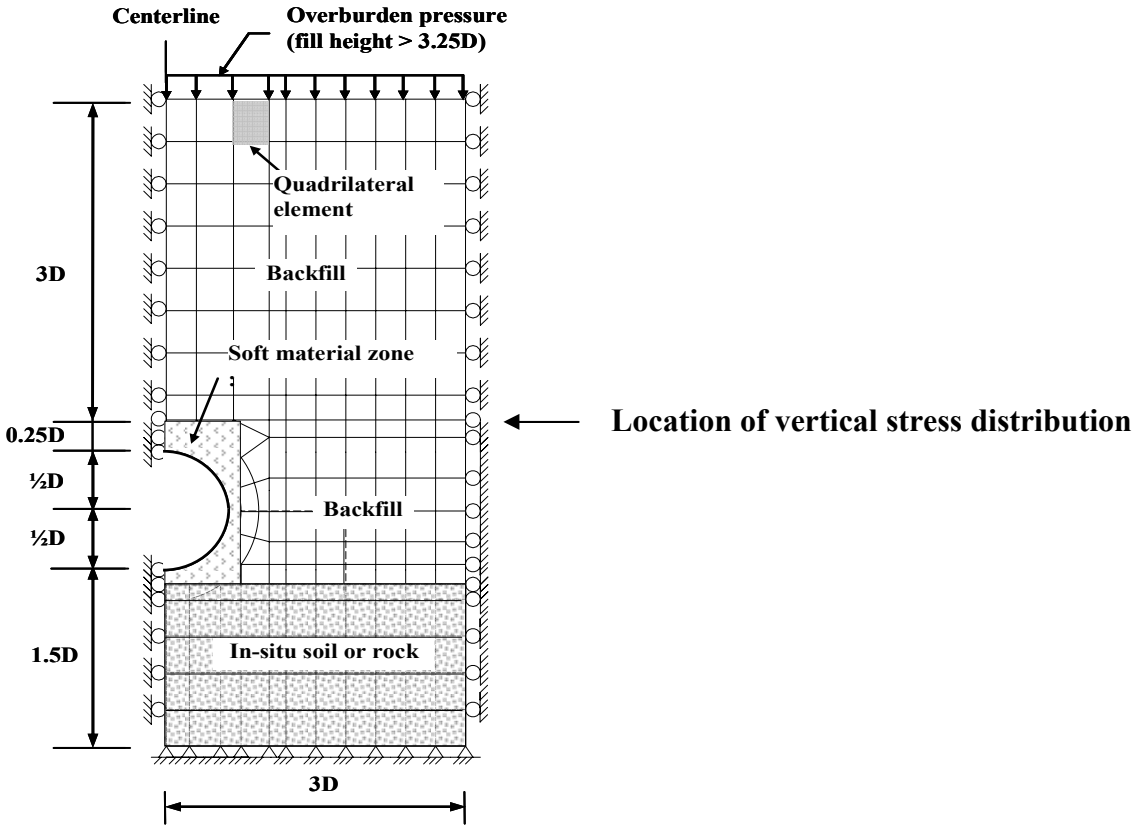

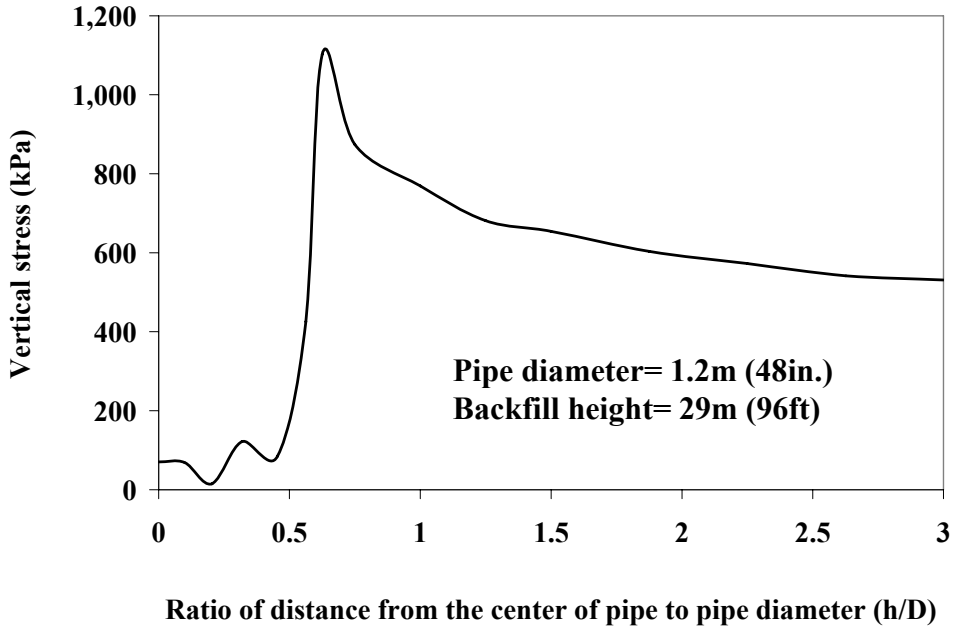

C. Corrugated Steel Pipe

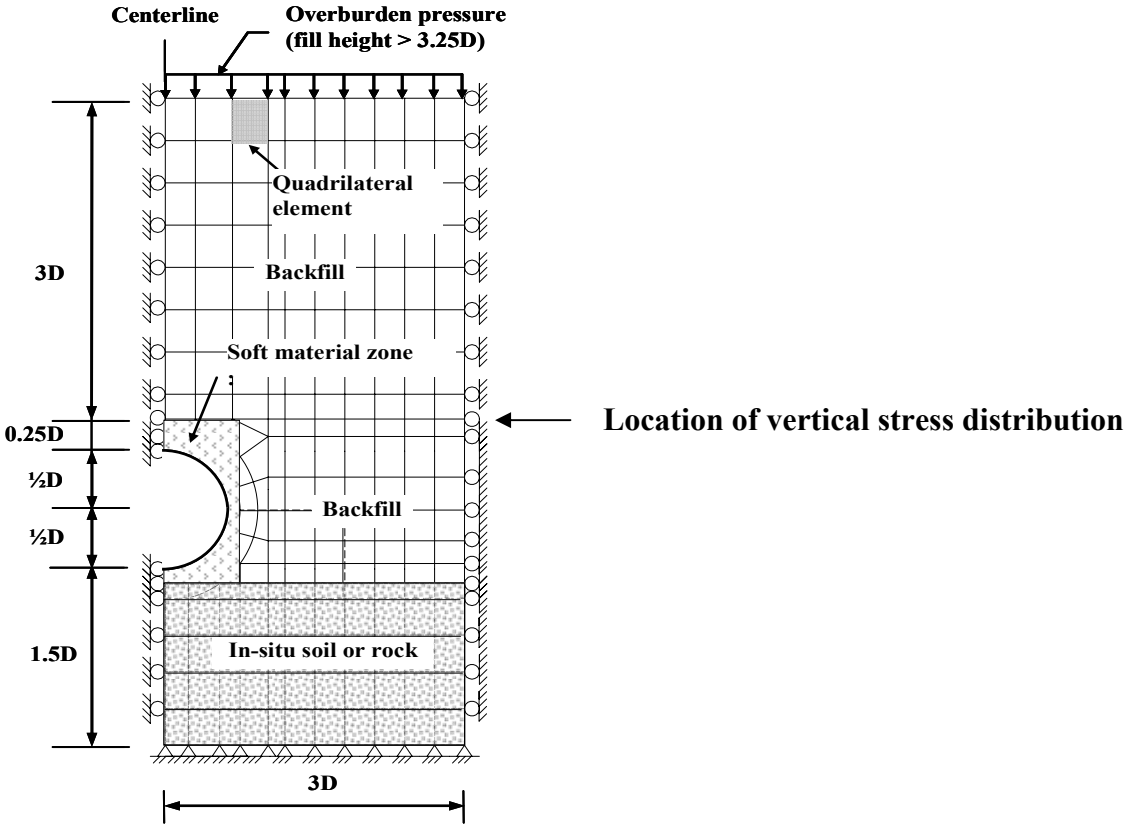

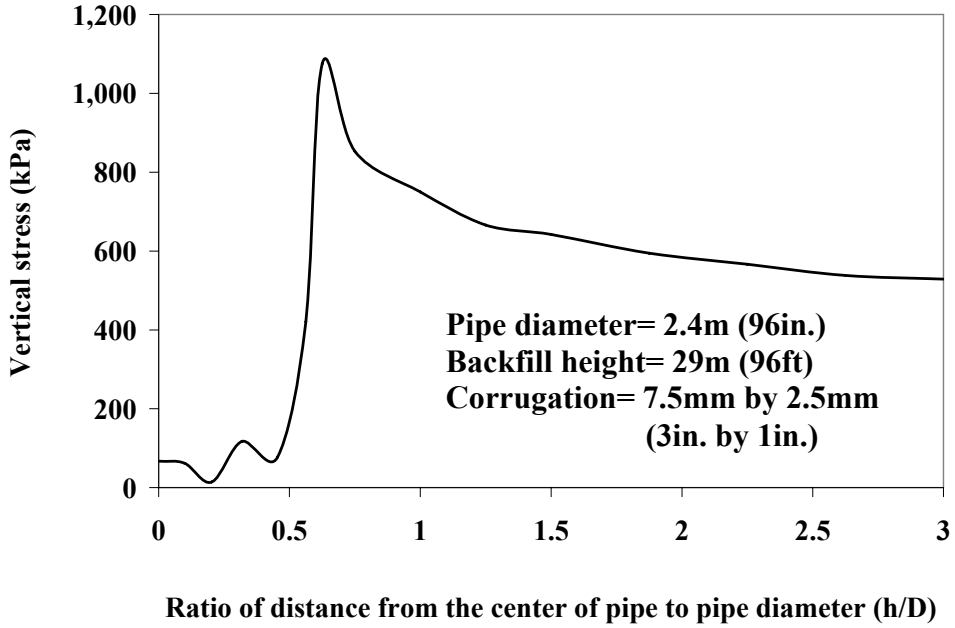
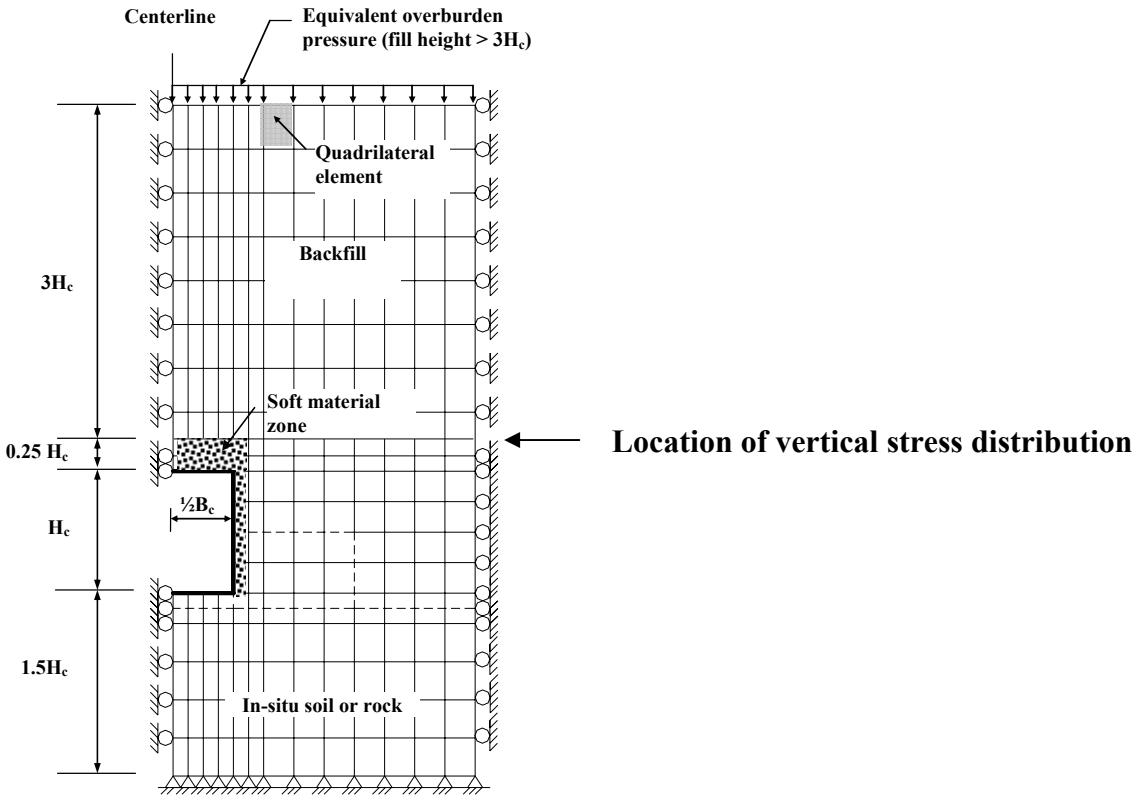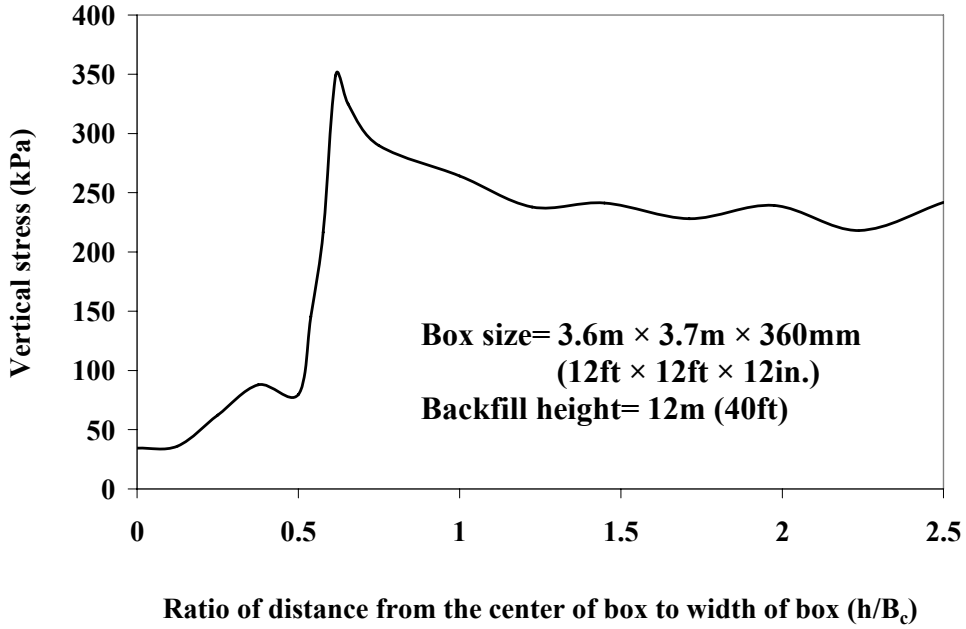
D. Box Culvert